AWARD NUMBER: W81XWH-15-1-0389

TITLE: Theranostics Targeting Metastatic Breast Cancer

PRINCIPAL INVESTIGATOR: Kevin Burgess

CONTRACTING ORGANIZATION: Texas A&M University
College Station, TX 77845

REPORT DATE: October 2016

TYPE OF REPORT: Annual

PREPARED FOR: U.S. Army Medical Research and Materiel Command
Fort Detrick, Maryland 21702-5012

DISTRIBUTION STATEMENT: Approved for Public Release;
Distribution Unlimited

The views, opinions and/or findings contained in this report are those of the author(s) and should not be construed as an official Department of the Army position, policy or decision unless so designated by other documentation.

REPORT DOCUMENTATION PAGE

Form Approved
OMB No. 0704-0188

Public reporting burden for this collection of information is estimated to average 1 hour per response, including the time for reviewing instructions, searching existing data sources, gathering and maintaining the data needed, and completing and reviewing this collection of information. Send comments regarding this burden estimate or any other aspect of this collection of information, including suggestions for reducing this burden to Department of Defense, Washington Headquarters Services, Directorate for Information Operations and Reports (0704-0188), 1215 Jefferson Davis Highway, Suite 1204, Arlington, VA 22202-4302. Respondents should be aware that notwithstanding any other provision of law, no person shall be subject to any penalty for failing to comply with a collection of information if it does not display a currently valid OMB control number. **PLEASE DO NOT RETURN YOUR FORM TO THE ABOVE ADDRESS.**

1. REPORT DATE	2. REPORT TYPE	3. DATES COVERED
October 2016	Annual	30 Sep 2015 - 29 Sep 2016

4. TITLE AND SUBTITLE

Theranostics Targeting Metastatic Breast Cancer

5a. CONTRACT NUMBER

5b. GRANT NUMBER
W81XWH-15-1-0389

5c. PROGRAM ELEMENT NUMBER

6. AUTHOR(S)
Kevin Burgess

E-Mail: burgess@tamu.edu

5d. PROJECT NUMBER

5e. TASK NUMBER

5f. WORK UNIT NUMBER

7. PERFORMING ORGANIZATION NAME(S) AND ADDRESS(ES)

Texas A&M University
College Station, TX
77845

8. PERFORMING ORGANIZATION REPORT NUMBER

9. SPONSORING / MONITORING AGENCY NAME(S) AND ADDRESS(ES)

U.S. Army Medical Research and Materiel Command
Fort Detrick, Maryland 21702-5012

10. SPONSOR/MONITOR'S ACRONYM(S)

11. SPONSOR/MONITOR'S REPORT NUMBER(S)

12. DISTRIBUTION / AVAILABILITY STATEMENT

Approved for Public Release; Distribution Unlimited

13. SUPPLEMENTARY NOTES

14. ABSTRACT

This application is designed to impact three of the overarching challenges identified for this award type: (i) revolutionary treatment regimes replacing drugs that have life-threatening toxicities with safe and effective interventions; (ii) elimination of mortality associated with metastatic breast cancer; and, (iii) distinguishing aggressive breast cancer from indolent forms, to avoid over-diagnosis and treatment. Overall, this work addresses issues that relate to: (i) revolutionary treatment regimes replacing drugs that have life-threatening toxicities with safe and effective interventions; (ii) elimination of mortality associated with metastatic breast cancer; and, (iii) distinguishing aggressive breast cancer from indolent forms, to avoid over-diagnosis and treatment.

15. SUBJECT TERMS

16. SECURITY CLASSIFICATION OF:			17. LIMITATION OF ABSTRACT	18. NUMBER OF PAGES	19a. NAME OF RESPONSIBLE PERSON
a. REPORT	b. ABSTRACT	c. THIS PAGE			USAMRMC
Unclassified	Unclassified	Unclassified	UU	111	19b. TELEPHONE NUMBER *(include area code)*

Table of Contents

Page

Theranostics Targeting Metastatic Breast Cancer

A. Introduction (1paragraph)

The emphasis of this first year of the award, as planned, has been on synthetic chemistry to obtain materials to test in histology, PET (positron emission tomography) and PDT (photodynamic therapy) studies. We have been successful in preparing samples for the testing studies that begin in year 2. However, as anticipated, the synthetic chemistry work was not without problems and must continue and adapt to overcome challenges that now become evident. For instance, one of the molecules first prioritized, compound **1**, was prepared, but only after a great deal of effort; in retrospect it is now clear that this compound has stability issues that make it hard to make, and inappropriate for further studies. Another target compound (**2**) was then prepared, much more efficiently than the first because it does not have stability issues, and because of the experience we gained from making the first target. This compound has poor solubility characteristics despite the fact that it contains two sulfonic acid groups and may required delivery in micelles; this is something that could not have been predicted until the compound was made. Both structures **1** and **2** are based on the aza-BODIPY dye fragment; as a back-up we have also initiated work on a compound based on a different-dye type, *eg* compound **3**. The original proposal outlined plans to add cytotoxic entities other than PDT agents; for this we entered into a collaboration with a biotechnology company who have provided us a small sample of the previous, highly cytotoxic, compound maytensin A. We have also prepared an agent intended solely for PET, *ie* compound **4**; this takes advantage of very recent advances in the field that enable more efficient capture of $^{18}F^-$ than was possible before, via so-called "Perrin capture agents.

B. Keywords (limit to 20 words)

reagents for histology of $TrkC^+$ tumors • photodynamic therapy (PDT) • positron emission tomography (PDT)

C. Accomplishments

What were the major goals of the project?

1 Design and synthesis of second-generation fluorescent, PDT and PET/PDT agents *that absorb >700 nm*, bind TrkC, are localized in $TrkC^+$ cells, generate singlet oxygen under conditions for PDT, and have $TrkC^+$ selective photocytoxicities.

begins in year 1 and continues throughout grant period (about 40 % of total work required achieved this year)

2 Validation of a fluorescent form of one of these agents in histochemistry for diagnosis of patients with $TrkC^+$-expressing tumors.

year 2 and then continues throughout grant period

3 Validation of the iodinated second-generation agent PET imaging human breast cancer tumors in mice, and ablation of these tumors via PDT. This study will involve determination of toxicity *in vivo*, pharmaco-kinetics and -dynamics (using PET) to ascertain distribution and clearance of the labels.

only in years 2 and 3

What was accomplished under these goals?

Synthesis Of Compound **1**

Compound **1** was a structure in the original proposal.

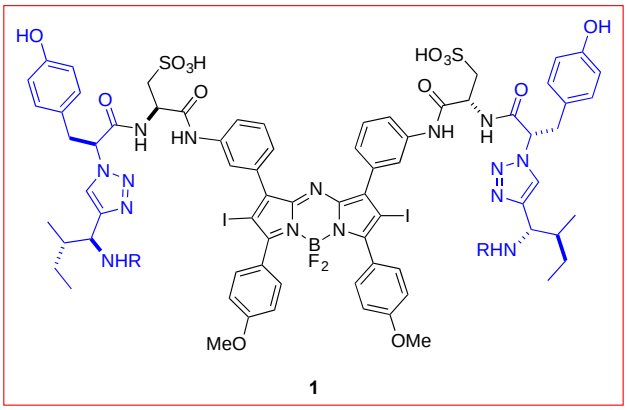

1

Compound **1** was prepared via the following route.

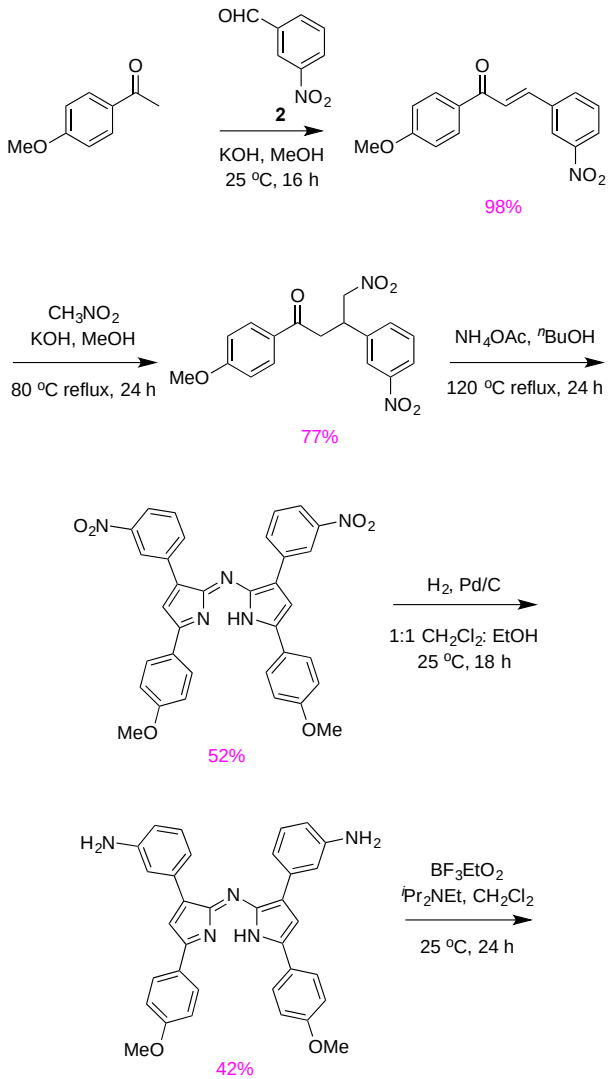

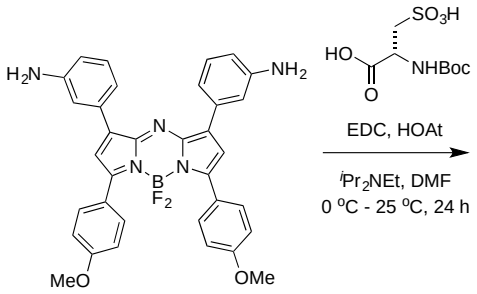
EDC, HOAt
iPr2NEt, DMF
0 °C - 25 °C, 24 h

46%

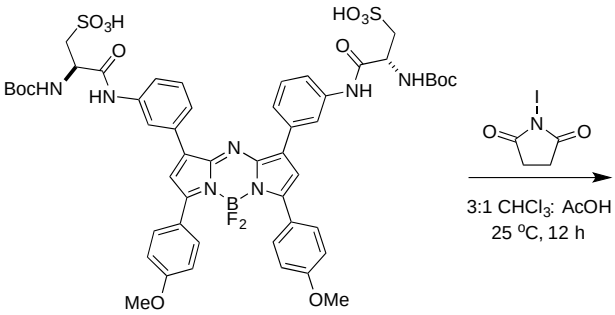
3:1 CHCl3: AcOH
25 °C, 12 h

62%

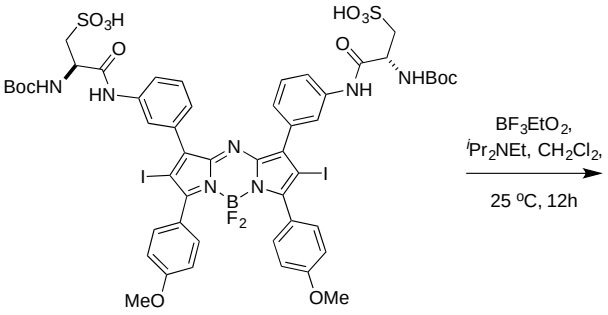
BF3EtO2,
iPr2NEt, CH2Cl2,
25 °C, 12h

66%

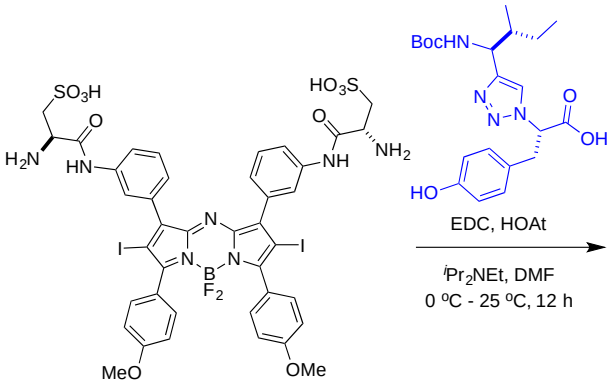
EDC, HOAt
iPr2NEt, DMF
0 °C - 25 °C, 12 h

87%

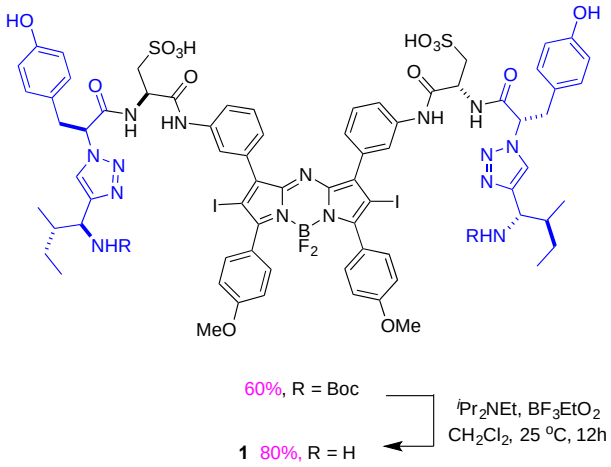

As proposed, the control compound **1'** (bearing an isomeric sequence that does *not* bind TrkC) was prepared from an intermediate in the above sequence, *ie* via this route.

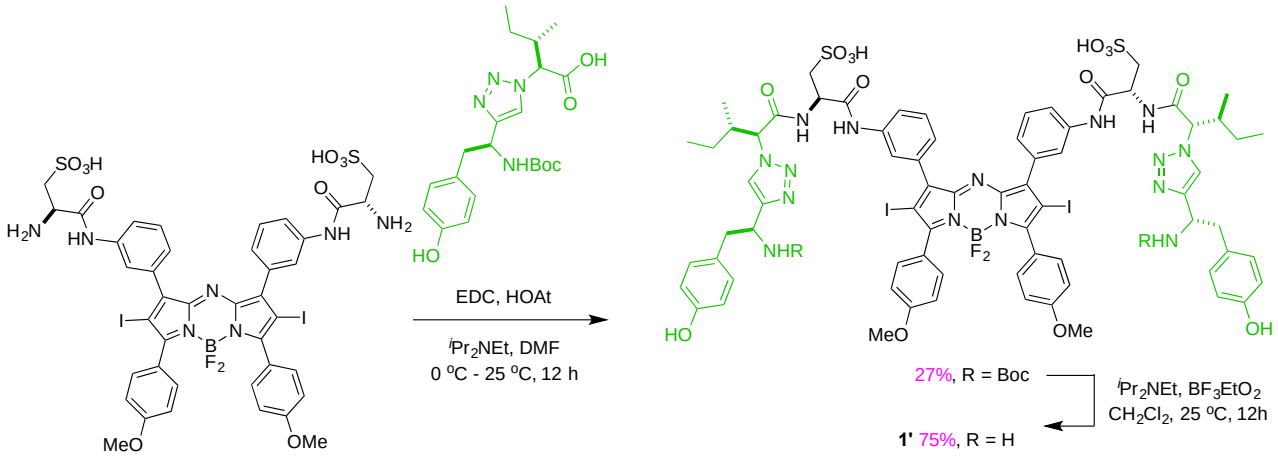

The photocytotoxicity of compound **1** on TrkC$^+$ cells was determined to be 1.2 μM, whereas little photocytotoxicity was observed for TrkC$^-$ cells (Figure 1). The control compound **1'** was not toxic on the same TrkC$^+$ stable transfectant cells but, surprisingly, it did show some photocytotoxicity on mouse 4T1 breast cancer cells.

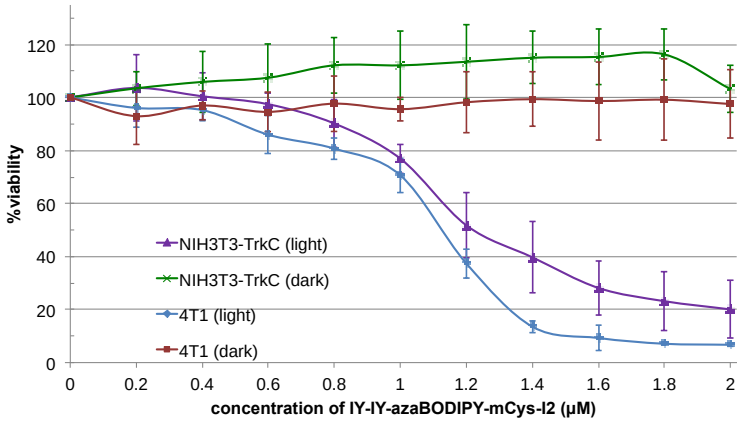

Figure 1. Cytotoxicity of **1** on TrkC expressing cells in light and dark.

Part of the revised SOW was to determine the maximum tolerated dose of compound **1**. We did this: >40 mg/Kg (23 micromole/Kg) in mice.

Many photophysical properties of **1** were determined too, but these studies were curtailed as it became clear that the iodine atoms in **1** are labile, *ie* this compound is insufficiently stable for high yield synthesis and presumably not *in vivo* either. Consequently, we moved on to target **2**.

Synthesis Of Compound **2**

Compound **2** was conceived from a very recent literature reports on a similar structure without targeting groups. That compound was reported to have favorable photophysical properties, good PDT properties, *and* the PDT effect was enhanced in the slightly acidic media of cancer cells. Our design **2** is similar, but with an extra attachment point for targeting groups.

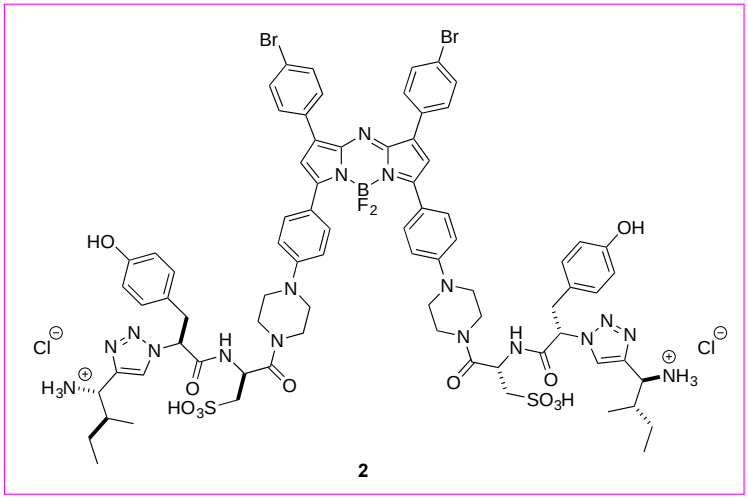

2

Compound **2** was prepared via the following route:

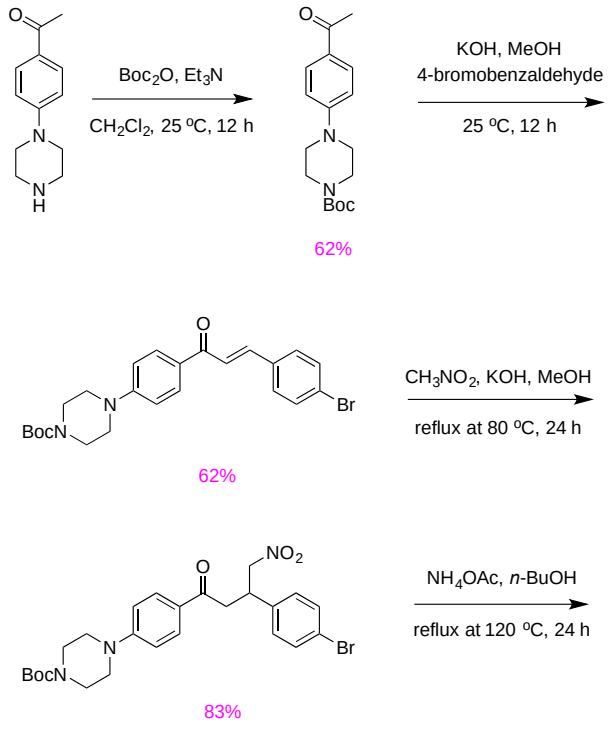

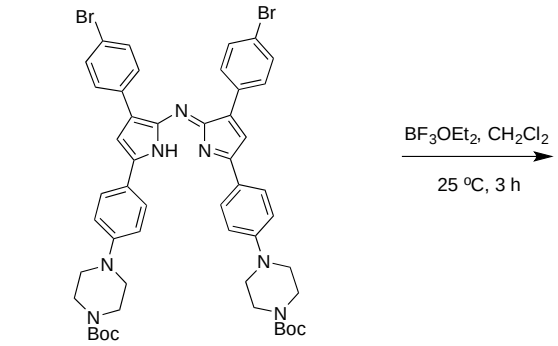
Br
Br
N
NH
N
N
N
N
Boc
Boc
BF3OEt2, CH2Cl2
25 °C, 3 h

54%

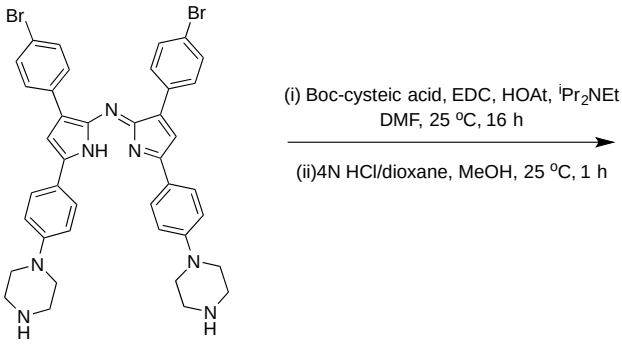
Br
Br
N
NH
N
N
N
N
H
H
(i) Boc-cysteic acid, EDC, HOAt, iPr2NEt
DMF, 25 °C, 16 h
(ii)4N HCl/dioxane, MeOH, 25 °C, 1 h

87%

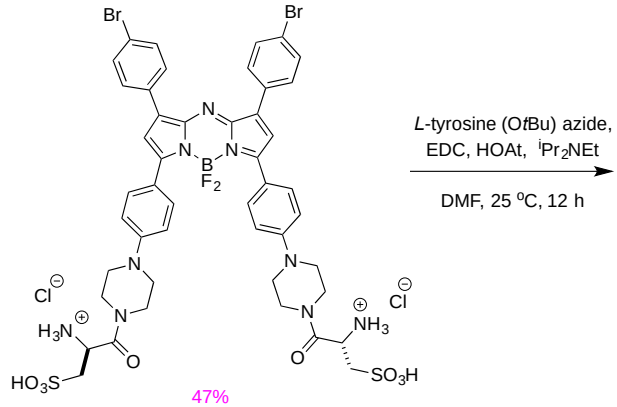
Br
Br
N
N
B
F2
N
N
N
N
Cl
H3N
O
HO3S
NH3
Cl
O
SO3H
L-tyrosine (OtBu) azide,
EDC, HOAt, iPr2NEt
DMF, 25 °C, 12 h

47%

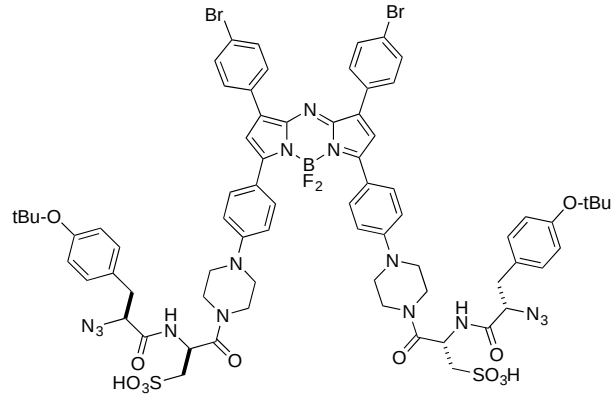
Br
Br
N
N
B
F2
N
N
tBu-O
N3
H
N
O
O
HO3S
N
N
O-tBu
N3
H
N
O
O
SO3H

85%

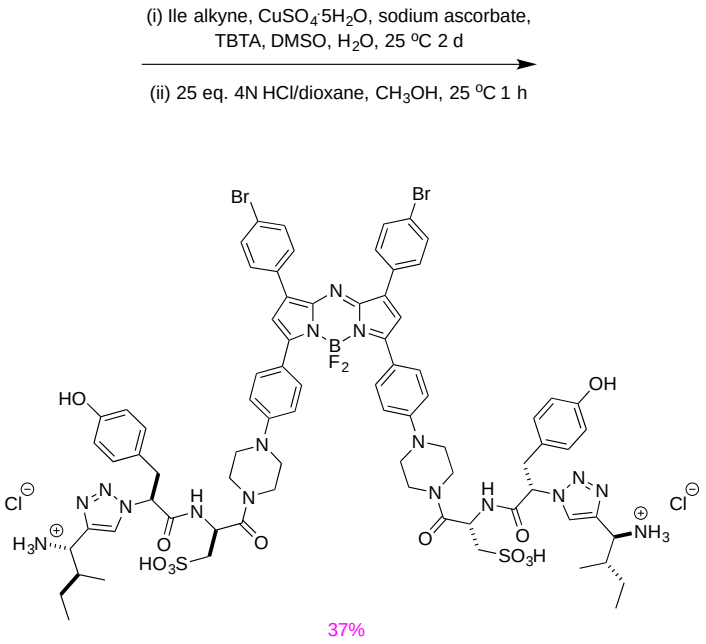

We are still working with compound **2** though its solubility is a concern. As a back-up plan this material may be formulated as a micelle and tested in cellular studies.

Targeted PET Label **4**

In the last two years, fluoride capture agents pioneered by Perrin have been tested in other laboratories and found to be highly efficient ^{18}F capture agents.

Part of our back-up plans was to prepare a targeted PET agent **4**. This is not a theranostic, it does not have optical imaging or PDT characteristics, but it is probably the simplest probe imaginable for imaging TrkC$^+$ metastatic tumors.

The synthesis of **4** is not shown here, but it is considerably shorter than those described above, so not too many resources were spent on this project. This compound is currently with our collaborator, Dr Li, awaiting her second year funding to initiate PET studies.

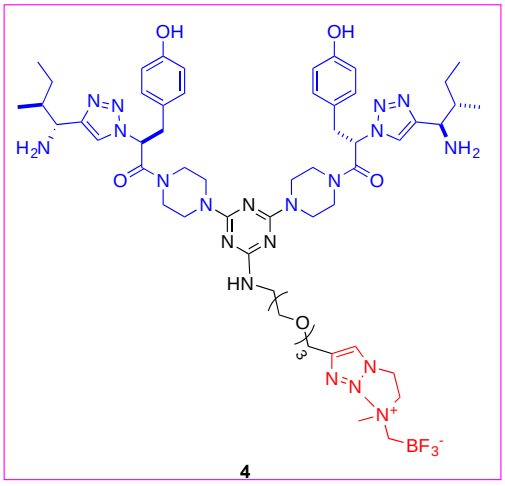

What opportunities for training and professional development has the project provided?

Two graduate students and one postdoctoral research associate were supported on this project.

How were the results disseminated to communities of interest?

I presented the following presentations:

Active Targeting of Cancer Cells, Georgia State University, Atlanta, Georgia, September 2015.

Small Molecules that Bind Proteins, University of Regensburg, Regensburg, GERMANY, June 2016.

Active Targeting of Cancer Cells, Masaryk University, CZECH REPUBLIC, May 2016.

What do you plan to do during the next reporting period to accomplish the goals?

During the next reporting period we will:

(i) initiate *in vivo* studies (PDT and PET) on some of the compounds already prepared; and,

(ii) continue the synthetic studies to produce agents with superior solubility and PDT characteristics.

D. Impact

What was the impact on the development of the principle(s) of the project?

At this early stage, the impact is mostly on improvement of the chemical design of the agents being developed. For instance, we have learned that aza-BODIPY dyes have many desirable properties, but they can be unstable when substituted with iodine at a certain position, and solubilities can be an issue. Consequently, we revised our plans that use aza-BODIPYs and have introduced a back-up option.

What was the impact on other disciplines?

Too early to impact other disciplines.

What was the impact on technology transfer?

A patent application is still in process for the IY-IY targeting groups.

What was the impact on society beyond science and technology?

Too early to impact society outside science, but eventually the goal of this work is to produce a lead compound that will be iteratively improved to form a “theranostic” for diagnosis, imaging, and therapy.

E. Changes/Problems

Changes in approach and reasons for change

Compounds **1** and **2** are both based on azaBODIPY dyes. Since their properties so far have not been ideal, our plan is to broaden the scope of our work so that we are no longer 100% dependent on the azaBODIPY framework.

It recently came to our attention that cyanine dyes with combinations of trimethylammonium and sulfonic acid groups are water soluble, have superb optical characteristics, and can be functionalized. We have embarked on a plan to do this. This work is at an early stage, but our initial target is compound **5**.

Compound **5** is anticipated to have appropriate optical and PET properties. We will introduce bromine atoms in a modified synthesis to induce PD properties.

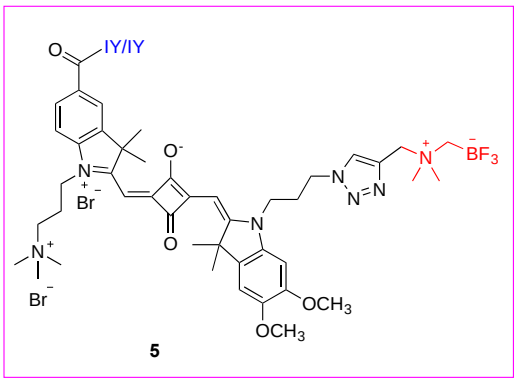

5

Actual or anticipated problems or delays and actions or plans to resolve them

Problems are nearly always encountered in chemical syntheses, but we have anticipated the obvious weak links and constantly consider alternative routes.

If the solubility of compound **2** is insufficient, we plan to deliver it in a micellular system.

Changes that had a significant impact on expenditures

Postdoctoral salaries are more than before as a result of the new labor laws. This will be a problem going forward, but it has not been a problem so far.

Significant changes in use or care of human subjects, vertebrate animals, biohazards, and/or select agents

none

Significant changes in use of care of human subjects

n/a

Significant changed in use of care of vertebrate animals

none

Significant changes in use of biohazards and/or select agents

none

F. Products

Publications, conference papers, and presentations

Small Molecules for Active Targeting in Cancer, C. S. Kue, A. Kamkaew, K. Burgess, L. V. Kiew, L. Y. Chung, H. B. Lee, *Med. Res. Rev.,* 2016, 36, 494-575. (DOI:10.1002/med.21387)

Anthranilic Acid-containing Cyclic Tetrapeptides: At the Crossroads of Conformational Rigidity and Synthetic Accessibility, D. Xin, K. Burgess, *Org. Biomol. Chem.*, 2016, **14**, 5049-5058. PMID: 27173439 (DOI: 10.1039/C6OB00693K)

Heterogeneous Phase Transfer Catalysis in Solid Phase Syntheses of Anth-Cyclic Tetrapeptides, D. Xin, K.-Y. Wong, K. Burgess, *J. Org. Chem.*, 2016, **81**, 8077-8081.

Active Targeting of Cancer Cells, Georgia State University, Atlanta, Georgia, September 2015.

Small Molecules that Bind Proteins, University of Regensburg, Regensburg, GERMANY, June 2016.

Active Targeting of Cancer Cells, Masaryk University, CZECH REPUBLIC, May 2016.

Websites or other Internet sites

none

Technologies or techniques

Only the novel syntheses already described.

Inventions, patent application, and/or licenses

A patent application covering the targeting ligands is still in progress.

Other Products

none

G. Participants & Other Collaborating Organizations

What individuals have worked on the project?

Name: Zhengyang Jiang

Project Role: graduate student at TAMU

ORCID ID: 0000-00002-1725-2883

Nearest person month worked: 12 months.

Contribution: Mr. Jiang prepared the original aza-BODIPY lead compound and tests of its photophysical properties; resynthesis on a scale sufficient for in vivo toxicity studies; and, initiated synthesis of second BODIPY lead compound.

Name: Syed Usama

Project Role: graduate student at TAMU

ORCID ID: 0000-0002-7487-1568

Nearest person month worked: 3 months.

Contribution: Mr. Usama performed the syntheses of new targeted agents designed for PET and optical imaging based on cyanine dyes.

Name:Dr. Jaya Shrestha

Project Role: postdoctoral associate at TAMU

ORCID ID: 0000-0002-1357-0251

Nearest person month worked: 2 months

Contribution: Dr. Shrestha initiated a synthesis of a new potential lead compound based on squariene dye framework.

Has there been a change in the active other support of the PD/PI(s) or senior/key personnel?

None

What other organizations were in involved as partners?

None yet, but Dr Li's role as co-PI at Methodist is about to begin.

Special Reporting Requirements

none

H. Appendices (attached journal articles, reprints, CV, patent applications)

Small Molecules for Active Targeting in Cancer

Chin S. Kue,[1] *Anyanee Kamkaew,*[2] *Kevin Burgess,*[2] *Lik V. Kiew,*[1] *Lip Y. Chung,*[3] *and Hong B. Lee*[3]

[1]Department of Pharmacology, Faculty of Medicine, University of Malaya, 50603 Kuala Lumpur, Malaysia
[2]Department of Chemistry, Texas A & M University, Box 30012, College Station, TX 77842
[3]Department of Pharmacy, Faculty of Medicine, University of Malaya, 50603 Kuala Lumpur, Malaysia

Published online in Wiley Online Library (wileyonlinelibrary.com).
DOI 10.1002/med.21387

Abstract: For the purpose of this review, active targeting in cancer research encompasses strategies wherein a ligand for a cell surface receptor expressed on tumor cells is used to deliver a cytotoxic or imaging cargo. This area of research is more than two decades old, but in those 20 and more years, how many receptors have been studied extensively? What kinds of the ligands are used for active targeting? Are they mostly naturally occurring molecules such as folic acid, or synthetic substances developed in campaigns for medicinal chemistry efforts? This review outlines the most important receptor or ligand combinations that have been used in active targeting to answer these questions, and therefore to address the most important one of all: is research in active targeting affording diminishing returns, or is this an area for which the potential far exceeds progress made so far? © 2016 Wiley Periodicals, Inc. Med. Res. Rev., 36, No. 3, 494–575, 2016

Key words: drug delivery; active targeting; cancer therapeutics; cancer imaging; small-molecule ligands

1. INTRODUCTION

A. Specific Aims of This Review

Effective cancer treatment hinges around (i) early diagnosis, (ii) location of the primary tumor and metastases, (iii) killing cancer cells as effectively as possible while minimizing toxicity to the patient (i.e., optimizing therapeutic index), and (iv) high accumulation in tumor lesion. Drug targeting can be used to address all four issues (i) to (iv), to overcome some limitations of conventional nontargeted approaches. There are generally two types of drug targeting to deliver therapeutic cargoes to tumor sites.[1] *Passive targeting* is based on enhanced permeability and retention (EPR, discussed in Section 2) effect using big, usually polymeric molecules

Correspondence to: Hong B. Lee, Department of Pharmacy, Faculty of Medicine, University of Malaya, 50603 Kuala Lumpur, Malaysia. E-mail: hongboonlee@um.edu.my.

Additional corresponding author: Burgess Kevin, Department of Chemistry, Texas A & M University, Box 30012, College Station, TX 77842. E-mail: burgess@chem.tamu

© 2016 Wiley Periodicals, Inc.

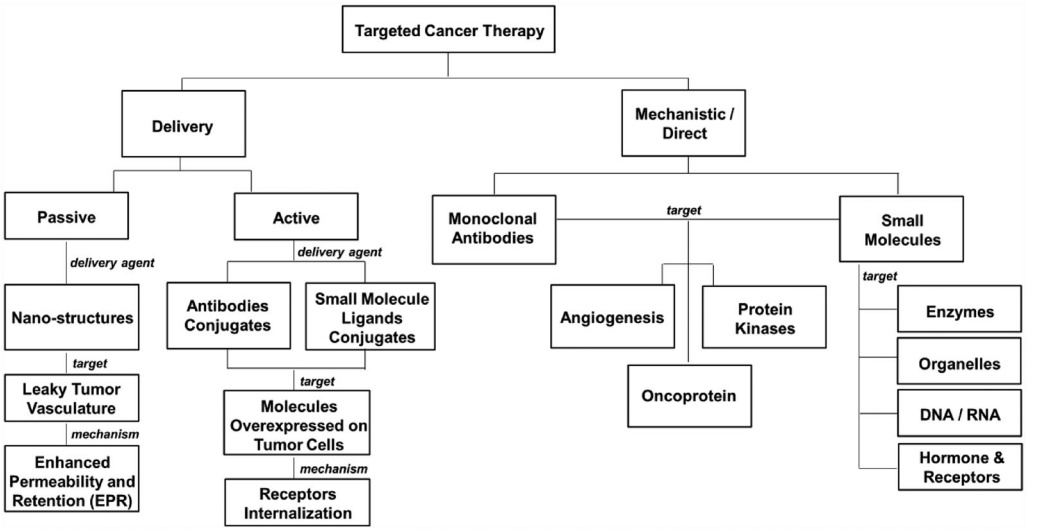

Figure 1. Different targeting strategies for anticancer therapeutics.

as carriers. *Active targeting* is based on targeting moieties such as ligands and antibodies (Figure 1). These targeting methods are different from *mechanistic or direct targeting* strategies that employ monoclonal antibodies (mAbs) or small-molecule compounds to bind to surface proteins or to interfere in biochemical pathways that are upregulated in cancer. Mechanistic targeting is illustrated in Figure 1 and examples for each target have been extensively reviewed.[2,3] Unfortunately, many mechanistically targeted chemotherapeutic agents have limitations such as toxicities to the heart, skin, and gastrointestinal tract[4]; low accumulation in tumor lesion[5]; and resistance in cancer cells.[6]

Active targeting of anticancer therapeutics may increase their affinities and endocytic internalization in tumors.[7,8] These linked targeting moieties may selectively bind to surface molecules (proteins, sugars, or lipids), perturbing tumor accumulation and residence time.[9–11] Indeed, many of the small molecules in mechanistic/direct targeting have been used either as delivery agents (e.g., probestin for CD13) or cargoes (e.g., mitogen-activated protein kinase kinase [MEK] kinase) in active targeting (Section 4).

This review on small molecules for active targeting is to identify the following:

1. their potential in oncology;
2. the most significant obstacles that must be overcome to realize this potential;
3. illustrative types of cargoes that can be used for imaging and for chemotherapeutics;
4. strategies for joining active targeting agents and cargoes to form conjugates;
5. illustrative entities that have been used for targeting, and what they interact within tissue; and,
6. state-of-the-art small-molecule active targeting strategies with respect to particular cancer types.

Finally, we are intrigued by successful strategies used to investigate targeting cancer with small-molecule agents. Highlighted here are approaches and important data that should be collected, and in what order, to validate targeting approaches.

B. Significance

Diagnosis of cancer types typically involves treating biopsied material with a targeting agent conjugated to a fluorescent dye; if the tissue stains this implies that cancer type expresses whatever the agent bound. Most often, the targeting agent is an mAb (histochemistry). Small-molecule alternatives to mAbs can have advantages in terms of cost and reagent stabilities in diagnoses, but the most significant unmet need for small-molecule active targeting agents is in imaging and chemotherapy.

Imaging usually involves injection of a conspicuous spectroscopic probe into a subject, then observing regions of interest. Magnetic resonance (MR), positron emission tomography (PET), and optical probes are most common in imaging. Probes must preferentially accumulate in the tissue of interest to be of value, though they can work if the probe accumulated everywhere else but the region of interest. Preferential accumulation of a probe relative to nontargeted agents tends to facilitate greater resolution and sensitivity.

Chemotherapy of cancer requires destroying tumor tissue, or at least restricting its growth and metastatic spread. Compounds with potent cytotoxicities have no use as medicines if they cause intolerable side effects or death. Consequently, therapeutic index tends to be more important than absolute toxicity in cancer chemotherapy[12], where:

$$\text{Therapeutic index} = \frac{\text{Toxic dose}}{\underset{\textit{In general}}{\text{Therapeutic dose}}} \quad \frac{\text{Lethal dose}_{50}}{\underset{\textit{In animals}}{\text{Effective dose}_{50}}} \quad \frac{\text{Tolerated dose}_{50}}{\underset{\textit{In humans}}{\text{Effective dose}_{50}}}.$$

Pharmaceuticals that are actively targeted can have enhanced therapeutic indices because their concentrations proximal to tumors are increased, and/or their accumulation in healthy tissue is decreased over a suitable time frame. There are distinct advantages to using the same active targeting entity for histochemical diagnosis, imaging, and chemotherapy because in those cases positive staining characterizes one property of the tumor, and it also indicates the active targeting agent used has potential to deliver imaging and chemotherapeutic agents in vivo because of that property[13]. Unfortunately, state-of-the-art oncology has not arrived at that level yet. Most current standards of care involve various agents for staining tissue biopsy samples, imaging and therapeutic agents that are not actively targeted, or feature different targeting entities. The "holy grail" is to use exactly the same substance to diagnose, image, and treat; this is the intention behind the design of theranostics (chimeras of therapeutics and diagnostics).

Various building blocks for active targeting, imaging, and therapy are available, so formation of theranostics can be achieved by joining these together. It is relatively easy to do this, particularly if the fragments are not covalently bound to each other but are simply captured into nanoparticle, polymeric, or liposome constructs. However, unless the stance of the drug regulatory agencies changes, constructs such as these are unlikely to be approved for use in human subjects because they are essentially mixtures. Even if regulatory agencies would overlook the complexity and potential batch-to-batch variability problems, one pivotal issue related to distribution in vivo remains. Actively targeted constructs should preferentially accumulate in the tumor tissue. Size matters for ease of penetration into tumors, and the ideal size is usually small. For these reasons, discrete small-molecule theranostics can have significant advantages over nanoparticle, polymeric, or liposome constructs[14].

This review focuses on small molecules used for active targeting, excluding peptides longer than five-mers. It does not cover nanoparticle, polymer, or liposome constructs, even if small-molecular targeting groups have been attached, because pharmacokinetic and pharmacodynamic issues favor small-size agents for targeting tumors.

2. PHARMACOKINETIC AND PHARMACODYNAMIC ISSUES GOVERNING DELIVERY INTO TUMORS

A. Enhanced Permeation and Retention, and Tumor Back Pressure

Rapid growth of solid tumors is often constrained by availability of oxygen and nutrients, and lack of supply of these triggers tumor cell death.[15] Overall, this competition for raw materials results in development of highly disordered and fenestrated (porated) blood vessels in tumor tissues separated by vascular basal membrane. These fenestrations are typically of 200- to 2000-nm diameter, depending on the tumor type.[16,17] Fenestrated blood vessels favor extravasation (leakage) of both small-molecule and macromolecular therapeutics, including drug-carrier conjugates and drug inclusion complexes, from blood to the tumor interstitial fluid. Small molecules can readily diffuse back into blood circulation via the fenestrations, but macromolecules (>4 nm or 30 kDa) are retained in the interstitial fluid due to their larger hydrodynamic radii and the defective intratumor lymphatic drainage.[18–21] This passive targeting leads to the preferential accumulation of macromolecular therapeutics around tumors, through the *enhanced permeation and retention (EPR)* effect.[22]

Uncontrolled tumor tissue expansion and angiogenesis promote disorganization of the tumor interstitial space, which is also congested with collagen fibers, glycosaminoglycans, proteins, and cellular debris,[23] as well as fenestrations in tumor neovasculature.[24] Overall, these effects produce relatively high pressure in the tumor interstitial space (tumor back pressure), particularly at its core. Tumor back pressure strongly distorts macromolecule diffusion patterns in tumor tissue.[25,26] These effects synergize with residual lymphatic activity and de novo lymph-angiogenesis in the peripheral tumor tissues[27] to promote drug clearance and disseminate metastases.[28]

B. MDR and Efflux from Cells

Ineffective chemotherapy is often due to drug resistance. Factors that contribute to multidrug resistance (MDR) include changes in the tumor geometry and extracellular matrix,[29] impaired delivery of cytotoxic agents,[30] genetic and epigenetic alterations leading to overexpression of the cell membrane transporter P-glycoprotein (P-gp), and ATP-dependent transporter expression, that is, "the drug efflux pump."[31–33] MDR inhibitors such as verapamil, tariquidar, OC-1440935, laniquidar, and elacridar have been used in the clinic to block the P-gp function to prevent efflux function of cells in cancer chemotherapy.[34–37] Active targeting can also counteract the MDR effect compared with targeted therapy.[38–40]

C. Rate of Infusion/Dosing Rates

It was known that receptors involved in receptor-mediated internalization of drugs tend to be recycled back to cell surface (Figure 2). Several factors may regulate the receptor internalization and trafficking, thus impacting the efficacy of receptor-mediated drug delivery for cancer therapy. These factors include the following: (i) the rate of ligand-receptor binding before being cleared by metabolism, (ii) level of receptor occupancy or saturation, (iii) rate of receptor recycling, and (iv) rate of drug release from linker upon internalization.[41,42] Cell surface receptor internalization and recycling parameters vary among cell and cancer types. In the absence of information about what these parameters are, continuous administration of drug conjugates might be used, but it can result in downregulation of the receptor, elevated toxicities, and reduced therapeutic efficacies.

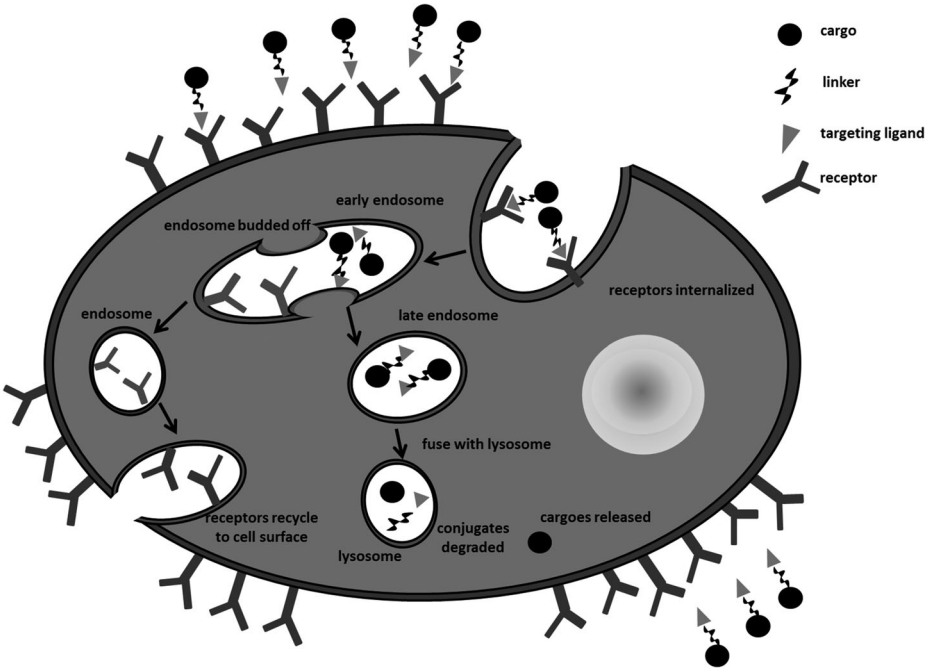

Figure 2. Receptor-mediated internalization. Generally, receptor targeted ligands bind to the receptors and are internalized together. An early endosome is formed, followed by budding off separation to form late endosomes with receptors and targeted ligands in separate units. The vesicle with receptors will return to the plasma membrane (recycling). The late endosome with targeted ligands will fuse with lysosome for subsequent degradation.

3. MONOCLONAL ANTIBODIES VERSUS SMALL-MOLECULAR FRAGMENTS FOR ACTIVE TARGETING

mAbs are widely used for active targeting, but they have serious limitations. Paramount among these is that mAbs do not easily penetrate into solid tumors.[17,21,43] Most mAbs do not penetrate into tumors because they are too big to easily leave blood vessels and efficiently diffuse into tissue. mAbs that *do* diffuse into tissue tend to be trapped by antigens located on the perivascular tumor cells, preventing permeation into the tumor mass,[44] that is, there is an "antigen barrier,"[45–47] even around micrometastases.[45] Moreover, slow clearance of mAbs from the body results in high normal tissue exposure[48–50]; hence, most mAbs tend to accumulate in the excretory organs (intact mAbs in the liver, fragments in the kidneys) and do *not* reach their targets.[51,52] mAbs also can be immunogenic, even when they are humanized[53]; this can cause hypersensitivity, neutralizing effects, and changeable pharmacokinetic properties.[52] These limitations should be considered alongside problems with nonspecific conjugation chemistry leading to reduced product homogeneity,[54] cost, and stability/shelf life issues. Despite these factors, interest in mAb targeting has surged because it is comparatively easy to raise antibodies to cell surface receptors.[55]

Small-molecule targeting entities are not constrained by the factors outlined above for mAbs. For instance, fluorescence studies have shown that folate–rhodamine conjugates rapidly exit blood vessels and can saturate folate receptors (FRs) on tumors within 5 min of intravenous injection.[56] The antigen barrier still perceptibly impacts folate–small molecule conjugates, but it has a negligible effect at saturating doses.[56] This implies small-molecule conjugates can be

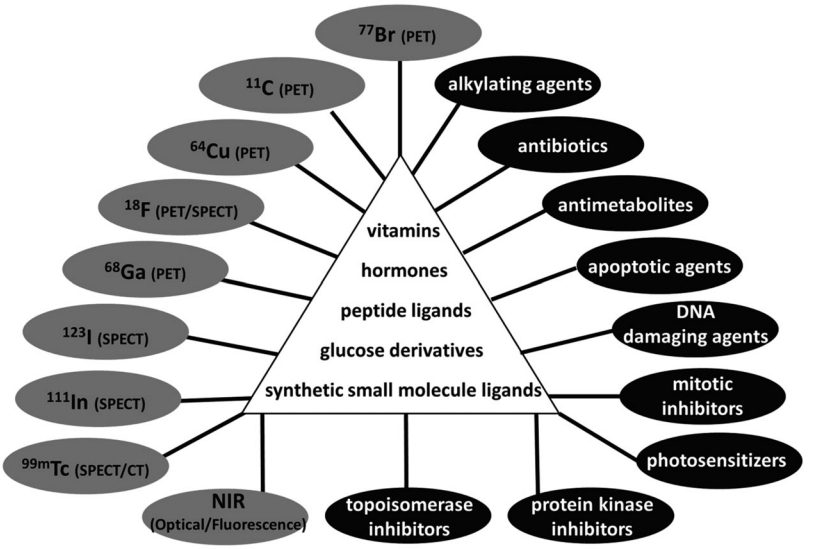

Figure 3. Common classes of ligands and cargoes used for active targeting in cancer. The common targeting agents used are vitamins (biotin, folate), hormones (estradiol, DHT, progestin), peptide ligands, glucose derivatives, and synthetic small-molecule ligands. These targeting agents are known to have high binding affinity to their respective receptors. The common cargoes used for anticancer therapy are alkylating agents (chlorambucil, isosfamide), antibiotic (mitomycin-C, geldanamycin), antimetabolites (5-fluorouracil), apoptotic agents (Bim, Smac), DNA intercalating/damaging agents (histone deacetylase, cisplatin), mitotic inhibitors (paclitaxel, maytansinoids, desacetylvinblastine monohydrazine, tubulysin b hydrazide), photosensitizers (Boron-dipyrromethene, pheophorbide-a), protein kinase inhibitor (mitogen activated protein kinase kinase inhibitor), and topoisomerase inhibitor (indenoisoquinolines, camptothecin). For imaging of cancer using PET/SPECT/CT/optical or fluorescence imaging system, the common agents used are bromine-77, carbon-11, copper-64, fluorine-18, gallium-68, indium-111, iodine-123, technetium 99m, and near-infrared dye.

ideal for rapid accumulation in solid tumors, and for brisk clearance afterward. Overall, small molecules tend to quickly reach their target in vivo, and be nonimmunogenic; they are amenable to chemical synthesis, have superior stability/shelf lives, and tend to be cheaper than mAbs.

One of the core messages of this review is that active targeting with mAbs is far more common than with small molecules that have relatively few known examples. Further, many of the small molecules commonly used for active targeting, as discussed in this review, are limited because not all tumor types overexpress the corresponding receptors at usable cell surface copy-numbers, and some of these ligands have suboptimal properties for targeting entities.[57] Figure 3 summarized the common types of small molecules and their cargoes (radiolabelled imaging agent or cytotoxic agent) used for active targeting in cancer.

4. EXAMPLES OF TARGETING MOLECULES AND THEIR SMALL-MOLECULE CONJUGATES

A. Folic Acid Receptors

All living cells require vitamins for their survival, but cancer cells need them in greater amounts to sustain rapid growth,[38] so vitamin uptake receptors tend to be overexpressed on cancer cells. Among vitamin receptors, the FR is the one that has been most extensively studied as a biomarker for the imaging and identification of tumor cells as well as tumor-targeted drug delivery.

Folic acid (folate) is responsible for DNA (purines and thymine) synthesis, metabolic reactions, methylation, and repair.[58] Folate and its derivatives are taken up by cells via three different pathways. Normal cells take up folate via reduced folate carrier (RFC) at neutral pH with low affinity,[59] and in acidic environment such as the duodenum and intestine via *the proton-coupled folate transporter* (PCFT)[60]; both routes do not accommodate folate conjugates.[61] Cancer and embryonic cells instead preferentially use *the FR* that has high affinity for folic acid ($K_d = 1$–10 nM) to absorb folate via receptor-mediated endocytosis.[59]

FRs are glycosyl-phosphatidylinositol (GPI) anchored to cell surfaces. There are three functional FR gene isoforms: αFR, h-βFR, and h-γFR or FOLR1, FOLR2, and FOLR3, respectively.[62] αFR is displayed on the apical surface of polarized epithelial cells such as kidney and the choroid plexus for folate reabsorption and transcytosis via the kidney to central nervous system (CNS). βFR expression is restricted to the placenta during embryonic development, spleen, and thymus. Unlike the other two, γFR contains an imperfect GPI anchor sequence and is expressed in low levels on the cell surface of haematopoietic tissues, with the majority released as secreted proteins.[63,64] Among the three receptor isoforms, αFR is the most widely expressed. In many cases, it is seen at negligible levels in human normal tissues (<2.5 pmol FR/mg protein) but highly expressed on malignant tissues (>6–40 pmol FR/mg protein depending on cancer type).[65] Tumors that express high FR levels are ovarian, uterus, endometrial, cervical, lung, pancreas,[66] breast,[67] colorectal,[68] brain,[69] bladder,[70] and testicular.[71]

A significant fraction of all the research on active targeting concerns folate-conjugated pharmaceuticals targeting FR-positive cancers. Conjugation of agents to the γ-carboxylate of folate does not affect the receptor-binding affinities much[72] because that domain does not interact with the binding pocket of the FR during binding, as supported by the crystal structure of folate bound to the αFR.[73]

Receptor amino acids involved in folate–FR binding are conserved between the α- and β-FR isoforms, indicating that binding for αFR is similar to βFR. During binding, the pterin folate fragment becomes buried in a deep FR pocket, forming extensive interactions. Derivatives of folic acid that lack the exocyclic oxygen of the pterin ring cannot form the same interactions, and this accounts for why methotrexate and aminopterin have reduced affinity for αFR, relative to the reduced folate carrier. When folate binds FR, the two carboxylates of the glutamic acid region protrude from the positively charged entrance to the binding cavity. This mode of binding explains why the Glu carboxylic acids can be used for conjugation, and why functionalization of the γ-carboxylate has least impact on affinity.

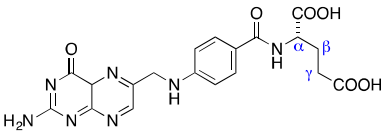

1

folic acid

Folic acid (**1**, also known as pteroylglutamate, MW 441) is water soluble and stable to diverse solvents and heat. It has functionalities that allow it to be conjugated to various cargoes for imaging or therapeutic purposes (though the chemistry is somewhat impeded because folic acid is insoluble in most organic solvents apart from DMSO). In general, folic acid tends to be nonimmunogenic, tissue permeable, and rapidly cleared from folic acid receptor negative tissues. Low receptor density restricts applications of folate conjugates to imaging agents for which the sensitivity of detection is such that high concentrations are not required, or to very toxic therapeutic agents. However, this requirement is less restrictive than those on untargeted drugs and opportunities arise to use cargoes that may be so toxic that they cannot be used without targeting. Folic acid also can be used to target cells that would otherwise be resistant

to untargeted drug cargoes.[74] Nevertheless, there are other limitations; for instance, the FR does not contain pores or channels, so the conjugates must themselves be cell permeable for the conjugates to be internalized into the cells. Conjugating folate directly to macromolecules, genes, or siRNA for nucleotide-based methods does not overcome the intrinsic issues surrounding the cell permeability of these entities, or endosomal release when these molecules are successfully imported into cells.[75] It is often necessary to tether drugs to folic acid via hydrophilic linkers since many potential cargoes are lipophilic. Impressive new applications of folate conjugates in targeting cancer emerged in the first decade of this century, primarily by Philip Low and co-workers at Purdue and Endocyte. Much of that work has been summarized in a series of excellent reviews[61,76–78] that have appeared as recently as 2015.[79] Consequently, what follow here are a summary of the highlights from that work and an update of recent developments.

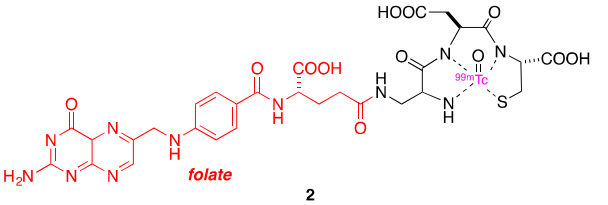

2

EC20

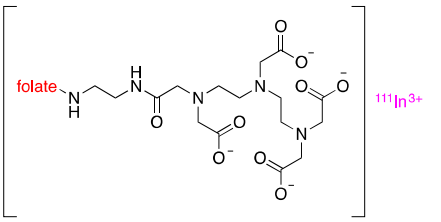

3

^{111}In-DTPA-folate

^{99m}Tc-EC20 or etarfolatide **(2)** and ^{111}In-DTPA-folate (DTPA is diethylenetriaminepentaacetic acid) **(3)**[80] are among the earliest FR-targeted imaging agents to reach the clinic. Conjugate **2** has high FR-binding affinity of K_d 3 nM,[81] whereas **3** has a 1 nM K_d and reached 50% saturation in 3 min[82] on FR$^+$ KB cells. Comparison of **2** and **3** was conducted in FR$^+$ syngeneic M109 lung tumor model.[81] Nearly identical biodistribution profiles were observed in all organs with the highest uptake in kidneys (138 and 191% injected dose [ID]/g tissue, respectively), followed by tumor (17 and 19% ID/g tissue, respectively). Clearance of **2** and **3** was rapid in blood, showing less than 1% ID/g at 4 hr post administration. These data suggest the efficacy and rapid clearance of **2** and **3** are independent of the half-lives of the radioisotopes (6 and 67 h, respectively).[81] Phase I clinical studies of **2** revealed that 68% of patients showed uptake of radiotracer **2** in solid tumors by planar scintigraphy or single-photon emission computed tomography (SPECT), whereas 67% of patients were positive for αFR in immunohistochemistry (IHC).[83] Only 72% of the patients with positive IHC staining for FR showed positive imaging result using **2**. The authors speculated that the poor correlation was due to the suboptimum time of tissue sampling as well as variations in the status and heterogeneity of FR in primary and metastasis tumors. Currently, **2** is in clinical studies to monitor the progress of FR-targeted therapeutic agents EC145 and EC1456 (see below; NCT01577654, NCT01999738).

Phase I/II clinical studies of **3** in ovarian cancer showed 100% success ($n = 7$) in the detection of malignancy for newly detected ovarian masses. All the malignant lesions had

increased radiotracer uptake and fast clearance in nontargeted organs. However, the detection of recurrent ovarian or endometrial tumors ($n = 7$) was difficult using **3** even though it gave good correlations with the anatomical imaging results.[84] Reasons for this are the small size of recurrent, compared with newly diagnosed, tumors and difficulties predicting the exact location of recurrent tumors. Agent **3** failed commercialization due to the high cost and long radiochemical half-life (67 hr) of 111-Indium.

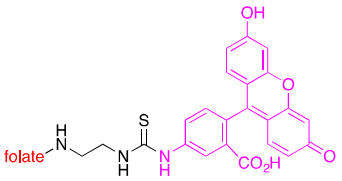

4

EC17

Folate-fluorescein, EC17 **(4)**, was designed to induce a hostile immune reaction toward FR-expressing tumors. A series of vaccinations with hapten fluorescein (EC90 vaccine) administrated with an adjuvant called GPI-0100 caused the induction of a high titer of antifluorescein mAbs. Treatment with EC17 labeled the tumors that expressed the FR with a bound immunogenic hapten, making them conspicuous to the host's immune system, and this led to elimination of the tumors while leaving healthy cells unaffected.[85–87] Phase I clinical evaluation of EC17 regimes in renal-cell carcinoma patients showed 4% of partial remission, 54% stable disease, and 43% progressive disease after the first cycle of therapy. Nevertheless, hypersensitivity or allergy with an increased in mAb titer was reported.[88] Recently, a similar phase I clinical application of the immunotherapeutic agent with cytokines interleukin (IL) 2 and interferon (IFN) α to stimulate the enhancement of antibody-dependent and cell-mediated killing against mAb opsonized tumor cells was conducted. Twenty-four kidney cancer patients featured in this work. This regime proved safe and had only mild-to-moderate clinical toxicities (less than 50% of the patients suffered from hypersensitivity). Moderate antitumor responses were observed (29% of patients had stable disease for 123–340 days and 4% had partial remission for 71 days).[89]

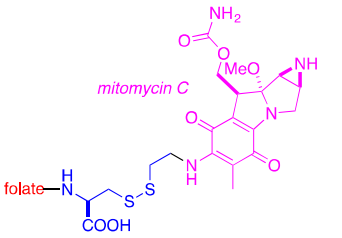

5

EC72

Another folate conjugated with cytotoxic cargo for cancer therapy was EC72 **(5)**: folic acid-γ-cysteine linked to 7-*N*-modified mitomycin-C (MMC) via disulfide bond. EC72 had a high affinity (relative binding affinity [RBA] of 0.59 relative to folic acid) to FR^+ KB cells and induced dose-dependent cytotoxic activity on FR^+ tumor cells with no activity on FR^- cells both in vitro and in vivo.[90] However, it was not a very potent anticancer drug compared with the therapeutic agent alone, as the reduction of tumor was moderate to negligible for huge-sized tumor (750 mm^3).[91]

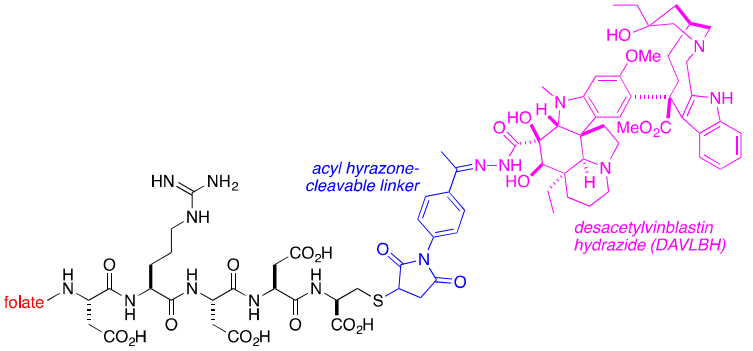

6

EC140

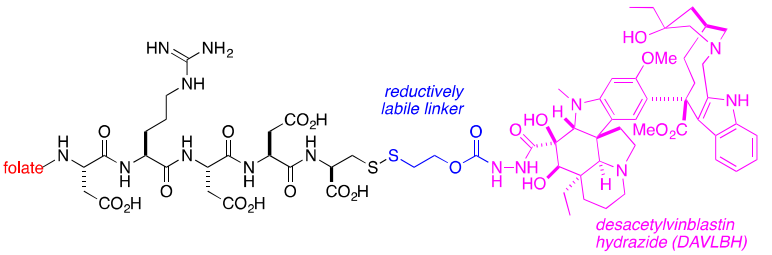

7

EC145

An important feature of delivery systems is release of drug in endosomes from the conjugate upon cellular internalization. Short intrinsic cleavage half-lives, especially when enforced by pH sensitivity, can improve the rate and efficiency of cargo release in endosomes.[92,93] For instance, endosome cleavable acylhydrazones and reducible disulfides were used in EC140[94] **(6)** and EC145[93,95] **(7)**, respectively. The binding affinities for the resultant conjugates were 0.35 (EC140) and 0.47 (EC145) relative to folic acid. Reduction-mediated release of the cargo from the disulfide bond from EC145 was highly efficient in endosomes: cleavage half-life 1 hr and complete cleavage within 6 hr.[93,95] Conversely, EC140 has a cleavage half-life of 5.5 hr in an endosome environment (pH 5.5).[94]

In animal studies, the maximum tolerated disease (MTD) of both EC140 and EC145 was 10 μmol/kg. When dosed three times per week for 3 weeks in mice xenografted with human nasopharyngeal KB tumors, the efficacy of EC145 was 100% full remission at half MTD, compared with EC140, which showed only 20% full remission.[96] One hundred percent full remission was also observed with a much lower dose of EC145 (1.2 μmol/kg) in more-frequent dosing regimens (i.e., daily administration for two consecutive weeks or daily administration at week 1 and 3) with no significant adverse effects.[97] Taken together, the authors claimed better efficacy of EC145 over EC140 due to the relative efficiency of linker cleavage in each construct. The acylhydrazone in EC140 was not expected to cleave efficiently inside cells based on its long cleavage half-life at pH 5.5.[97]

EC140 has not been investigated in the clinic, but phase I clinical studies of EC145 in patients with solid refractory tumors (mainly colorectal, head and neck, and ovarian) established MTD with no toxicities. Antitumor responses were effective against head and neck cancer, with 100% ($n = 3$) showing stable disease for 95–211 days, whereas ovarian cancer ($n = 2$) had 50% of partial response and 50% stable disease for periods of more than 100 days.[98] A phase

II study was then initiated in ovarian and endometrial cancer patients ($n = 43$). EC145 was effective in reducing tumor sizes and increasing survival of FR^+ cancer patients, where 57% showed Disease Control Rate (DCR, defined as total percentage of patients achieving complete response, partial response, and stable disease) in FR100% (all target lesions were FR^+) patients (90% confidence interval, 90% CI 29.1–55.5%), 36% DCR in FR10–90% (at least one but not all target lesions were FR^+) patients (90% CI 19.6–56.1%), and 33% DCR in FR0% (all target lesions were FR^-) patients (90% CI 1.7–86.5%). Median overall survival was 14.6 months for FR100% patients, 5 and 11.6 months higher than FR10–90% (hazard ratio = 0.574, $p = 0.135$) and FR0% patients (hazard ratio = 0.219, $p = 0.020$), respectively.[99] Adverse effects of EC145 were constipation and fatigue due to the hepatic clearance and metabolism of EC145 that caused the release of active vinca alkaloid agent to gastrointestinal organs.

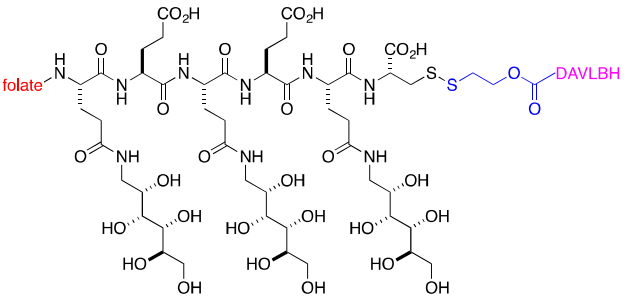

8

EC0489

Modification of EC145 by a carbohydrate to give EC0489 **(8)** was conducted to reduce hepatic clearance and metabolism. Compound **8** contains novel carbohydrate segments (1-amino-1-deoxy-glucitolyl-γ-glutamate) spaced in between the folate and vinca alkaloid moieties.[100] In biodistribution studies, EC0489 showed >4-fold reductions in elimination half-life in rat and dog compared with EC145. In addition, EC0489 had more tolerable toxicity profile with no mortality whereas with EC145 two animals died at an equimolar dosage. Antitumor efficacies of **8** and EC145 were identical.[101] Phase I clinical trial of **8** for refractory and metastatic solid tumors began in 2009; in December 2010, the study reported EC0489 was safely administered at weeks 1 and 3 of a 4-week cycle at dosages of equivalent to or less than 2.5 mg/m^2, with no significant or severe constipation and gastrointestinal toxicities.[101,102] This study was completed in 2012, with no further update reported.

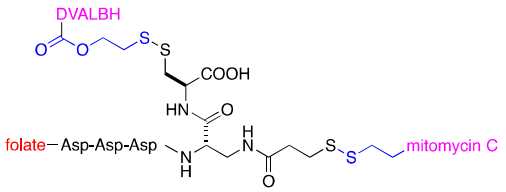

9

EC0225

Synergistic multidrug EC0225 **(9)** uses folate to deliver mitomycin C and desacetylvinblastine monohydrazide (DAVLBH).[103] Outstanding therapeutic efficacy was observed at three doses per week for two consecutive weeks. Specifically, **9** was able to eradicate tumors regardless of initial tumor sizes, and it showed increased antitumor response compared with folate-mitomycin C (EC72), folate-vinca alkaloid (EC145), or a combination of both (highly FR-expressing xenograft KB tumor).[104] EC0225 was brought to phase I clinical trial for

treatment of refractory and metastatic solid tumors, including colorectal, breast, and prostate in 2007 (NCT00441870). In December 2009, reports indicated that an intravenous bolus of EC0225 given at three times per week for 2 weeks within 28-day cycle has MTD of 2.3 mg/m^2, with anemia and constipation as the common adverse effects. Long-term disease stabilization was reported in colorectal (4.6 months), breast (4 months), prostate (10 months), leiomyosarcoma (4 months), and mesothelioma (4 months) cancers.[105] No further update on the clinical status of EC0225 is found to date.

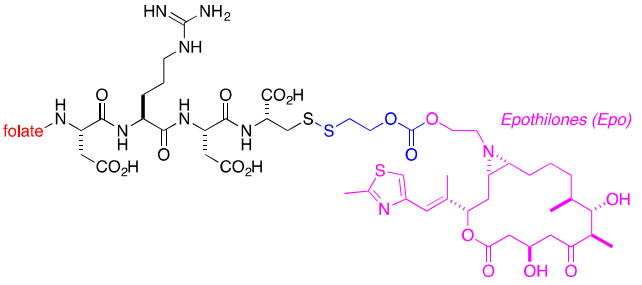

10

Epofolate

Folate conjugates containing epothilones and tubulysin, which act by disrupting and depolymerizing microtubules, have been studied. Conjugation of epothilones to folate via a disulfide bond and a bifunctional Asp–Arg peptide spacer to produce BMS-753493 (epofolate, **10**) was carried out by Endocyte and Bristol Myers Squibb (BMS).[106] Epofolate (K_d = 10 nM) was brought to phase I clinical trial for patients with advanced cancers and to phase IIa to determine its efficacy in shrinking or slowing the growth of cancer in patients with advanced ovarian, renal, or breast cancers (NCT00550017). Epofolate was tolerable with MTD of 26 mg/cycle (study 1; days 1, 4, 8, 11 with starting dose of 5 mg; 21-day cycle) and 15 mg/cycle (study 2; days 1–4 with starting dose of 2.5 mg; 21-day cycle) and was less toxic than epothilones alone. However, the antitumor responses were poor: 19% have disease stabilization with a median duration of 85 days and 50% progressive disease for study 1. For study 2, stable disease was 23% with a median duration of 88 days and 51% of progressive disease. In 2010, epofolate was discontinued from clinical studies due to the poor response.[107]

Tubulysin B hydrazide (TubBH, EC1456) was brought to phases 1 and 2 clinical studies (NCT01999738) due to its 100% cure rate in a high-FR$^+$ xenograft MDA-MB-231 breast cancer model and syngeneic M109 lung carcinoma.[108] However, no further update on the clinical status of EC1456 is found to date.

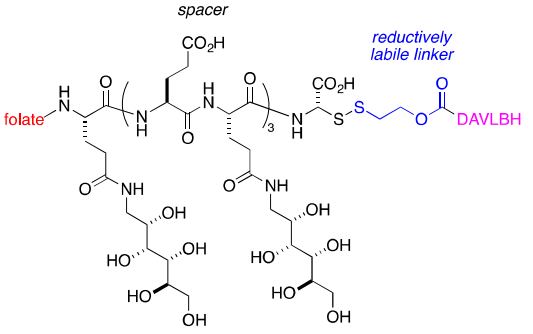

11

EC0905

Many novel potent folate conjugates have reached preclinical studies. One example is EC0905 **(11)**, which is similar to EC0489 (**8** discussed above) except for an additional unit of 1-amino-1-deoxy-glucitolyl-γ-glutamate in the spacer.[109] EC0905 showed high affinity and high cytotoxicity ($IC_{50} = 2$ nM) to FR^+ KB cells. Antitumor responses to EC0905 were studied in canine invasive urothelial carcinoma (iUC); 56% partial remission and 44% of disease stabilization, with a median overall survival of 115 days, were reported. Immunohistochemistry showed a higher percentage of human iUCs express FRs, with 78% of samples having immunoreactivity in the tumor cells,[70] suggesting that the translation of EC0905 to treating human iUC is possible. However, no further study of EC0905 on clinical was found to date.

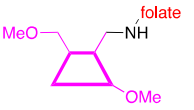

12

folate-methyl-β-cyclodextrin

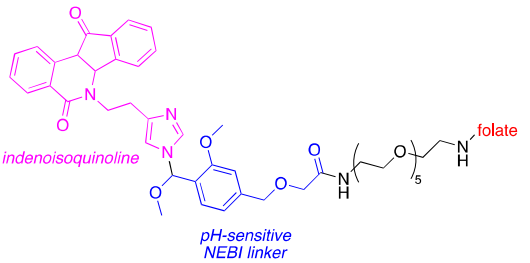

13

folate-indenoisoquinoline

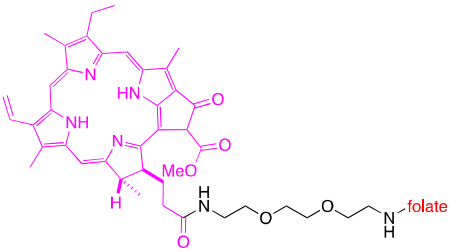

14

folate conjugate Pheophorbide-a

Methyl-β-cyclodextrin, a lipid-raft-disrupting agent was linked to folate to produce FA-M-β-CyD (**12**).[110] Methyl-β-cyclodextrin can extract cholesterol from lipid rafts that are highly abundant on cancer cells. Tumor suppression occurred for all mice treated with FA-M-β-CyD. They survived for up to 140 days whereas those treated with free doxorubicin (Dox) and M-β-CyD respectively all died within 70 days.[111] Other potent folate conjugates that are pending preclinical evaluation include folate-indenoisoquinoline **(13)** where indenoisoquinoline is a topoisomerase I inhibitor [92] and photosensitizer pheophorbide-a conjugated to folate **(14)**.[112] Both can target FR^+ tumor cells with minimal perturbation of normal cells.

B. Cholecystokin Receptor

Cholecystokin receptors (CCKRs) are membrane G protein coupled receptors. These can be categorized as CCK1R and CCK2R, where CCK1R was first characterized in pancreas of rat,[113] and CCK2R was found in mammalian brain.[114] In humans, the CCK1R gene is located at chromosome 4p15.1–p15.2 while CCK2R is located at 11p15.4.[115]

CCKR have different organ distributions and binding affinities toward their natural ligands cholecystokinin (regulation of appetite and energy intake) and gastrin (an important gastrointestinal hormone and neurotransmitter peptide in brain).[115] Studies have shown that CCK1R is mostly located in gall bladder and CNS, especially in the brain domain that regulates food intake.[116] CCK1R has about 500–1000× higher affinity toward sulfated cholecystokinin (CCK) than the unsulfated form.[117] Conversely, CCK2R binds to gastrin (hence also known as gastrin receptor) can also bind CCK with the same affinity regardless of their sulfation status.[117] CCK2R is distributed in the cerebral cortex and hypothalamus of brain,[118] and stomach mucosa for regulation of the physiological and pathological proliferation of mucosal cells.[119] Apart from normal expression in CNS and gastrointestinal tract, CCK2R especially and its splice variant are overexpressed in cancers of the pancreas,[120,121] medullary thyroid,[122] lung,[123] breast and ovarian,[124] gastrointestinal tract,[125,126] and colon. For each of these cases, there is no detection in their corresponding normal tissues.[127]

A few CCK2R-specific radiolabeled-imaging agents feature a CCK2R antagonist as a delivering agent. Use of synthetic molecules (nonpeptide) targeting ligands has several advantages over peptide ligands for CCKR. There are antagonists that bind in a similar manner to the natural ligand[128] and can access a greater number of binding sites because they dock to the inactive state of receptor whereas the natural ligand only binds to the active state.[129] Second, the natural peptide ligand tends to be taken up by peptide scavenging receptor, especially in liver,[130] resulting in high level of retention, which might give false-positive data for imaging metastases in malignant disease.

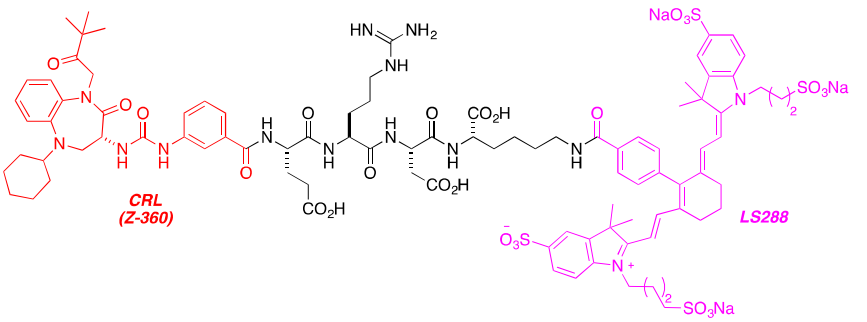

15

CRL-LS288

One imaging agent that uses an antagonist as a delivery ligand is CRL-LS288 **(15)**, composed of Z-360, a benzodiazepine-derived antagonist as targeting ligand (K_d = 0.47 nM, 672-fold lower affinity to CCK1R),[131] a highly charged hydrophilic tetrapeptide spacer, and a sulfonated NIR dye, LS-288. Conjugate **15** is the first CCK2R-targeted small-molecule conjugate.[132] It binds to CCK2R- and CCK2i4svR-transfected (splice variant of CCK2R) HEK293 cells with high affinity (K_d = 8 and 7 nM, respectively). In vivo biodistribution studies show high binding specificity of **15** in both primary and metastasized tumors. No uptake was observed in receptor-negative tumor, and fluorescence intensity decreased when a 100-fold excess of a nonfluorescent targeting ligand was added. A highly polar conjugate was designed in this case to limit nonspecific binding to CCK2R-expressing brain and gastrointestinal tract

tissue. In the event, kidney was the only normal organ that was positively stained other than tumor tissues. Significantly, the uptake in kidney is not receptor mediated and was reversible upon administration of excess natural ligand.[132]

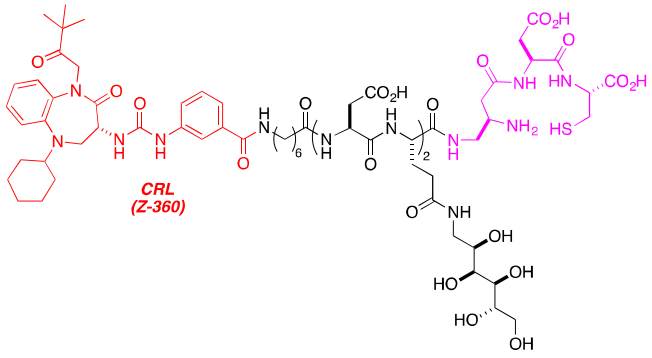

16

CRL-3

The effect of spacer chemistry on CCK2R targeting was evaluated for four conjugates (CRL1-4) with peptidosaccharide spacers of different lengths.[133] ^{99m}Tc-radiolabeled CRL-1 (tripeptide spacer) and CRL-4 (no spacer) showed nonspecific binding with indeterminate K_d values, suggesting the need for a more hydrophilic spacer to offset the hydrophobicity of the core ligand Z-360. A hydrophilic spacer is included in CRL-3 (peptidosaccharides with a octanoyl moiety, **16)**; this has K_d values of 30 and 4 nM on HEK293-transfected CCK2R and CCK2i4svR, respectively. Conjugate **16** was administered into CCK2R$^+$ xenograft embryonic kidney tumor bearing mice and examined by γ-scintigraphy and SPECT/CT. Uptake of **16** was negligible in normal tissues (0.051–2.5% ID/g), but not in kidney (7.6–8.4% ID/g) at 2 hr post administration. In tumor, the accumulation was 8.1% ID/g at 2 hr and remained relatively high compared with the other organs up to 24 hr. The retention in the kidney was independent of CCK2R expression, as the uptake of **16** was not affected by excess CRL-3. The data suggest that ^{99m}Tc-CRL-3 is a useful radioimaging agent for detecting, sizing, and monitoring CCK2R-expressing tumor.

Two new CCK2R-seeking therapeutic agents feature a targeting warhead and a hydrophilic peptide linker, just as in **16**, but they carry different antimicrotubule cargos: (i) desacetyl vinblastine hydrazide (DAVBH) and (ii) TubBH. Preclinical data for the DAVBH conjugate was encouraging, but more significant antitumor activity and prolonged survival in CCK2R-expressing kidney cancer xenograft were observed for TubBH conjugate. For the latter agent, no tumor lesion was detected in all treated mice compared with nontargeted TubBH, which has comparable tumor growth with control groups. Receptor selectivity was confirmed when non-CCK2R-expressing xenografts showed similar antitumor activities to control.[134]

C. Prostate-Specific Membrane Antigen (PSMA)

PSMA is a type II membrane protein with a 19-amino-acid cytoplasmic amino-terminal region, a 24-amino-acid transmembrane domain, and a 707-amino-acid extracellular portion. The PSMA gene is located on the short (p) arm of chromosome 11 at position 11.2.[135,136] Expression of PSMA was first found in prostatic secretory epithelium cells and prostate cancer (PCa),[137] correlating with higher grade and metastatic PCa.[138] However, PSMA is also present (at low levels) in some normal cells such as those at small-intestine brush-border membrane, proximal renal tubules, and salivary glands.[139,140]

PSMA is a surface glycoprotein[141,142] that behaves like a cell surface receptor under scanning confocal microscopy. It has a high rate of internalization after binding mAbs or other ligands, but it is then transported to endosomal compartment and recycled back to plasma membrane surface through recycling endosomal compartment. PSMA also has glutamate carboxypeptidase and folate hydrolase activities due to its role in facilitating the generation and uptake of nutrients as substrates, especially glutamate and folate.[143–145]

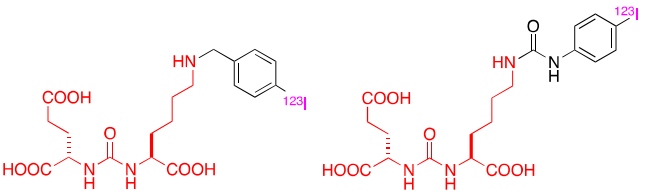

Two small-molecule inhibitors of glutamate carboxypeptidase are based on glutamate-urea-lysine, MIP-1072 ($K_i = 4.6 \pm 1.6$ nM), and MIP-1095 ($K_i = 0.24 \pm 0.14$ nM). These inhibitors were modified with an iodo-aromatic substituent at the lysine nitrogen to produce ^{123}I-MIP-1072 **(17)** and ^{123}I-MIP-1095 **(18)**. Conjugates **17** and **18** exhibited high affinity and specificity ($K_d = 3.8 \pm 1.3$ and 0.81 ± 0.39 nM, respectively) for PSMA-expressing cancer cells (LNCaP) in vitro and in vivo[146,147] with no or minimal effects on non-PSMA-expressing cancer (PC3) and normal cells. Conjugate **17** has been used with paclitaxel (PTX) in PCa preclinical studies[148] to verify the suitability of this agent in monitoring tumor progression post chemotherapy. Tumor uptake of radiolabeled agent was proportional to the tumor mass and this demonstrated the potential of this compound to track tumor mass changes in response to therapy. Following this, **17**, trade named as **TROFEX**, underwent phase I clinical trials for imaging metastatic tumors of PCa patients undergoing prostatectomy (NCT00712829) and **18** was included in this study for comparison. Both **17** and **18** showed rapid uptake and localization to lesions of bone and soft tissues in metastatic PCa patients at 1–4 hr post administration. They had different pharmacokinetics profiles, with **17** having fivefold faster clearance from circulation and nontargeted tissues compared with **18.**[149] Both these molecules are promising for diagnosis and imaging PCa, but there are still challenges to be overcome regarding the nonspecific uptake in lymph nodes, salivary glands, liver, and kidney in PCa patients.[150]

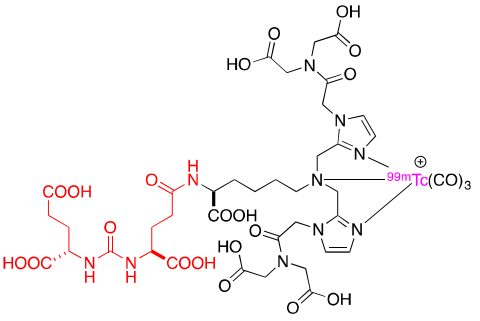

19

^{99m}Tc-MIP-1404

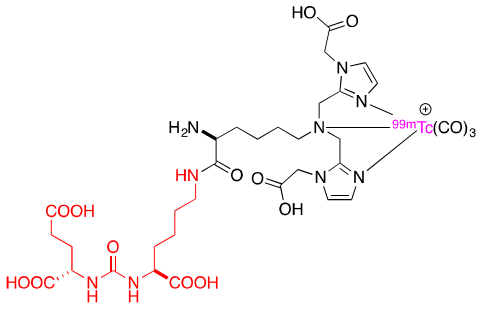

20

^{99m}Tc-MIP-1405

More hydrophilic small-molecule ligands, with better pharmacokinetic profiles than **17** and **18**, were also designed. The PSMA inhibitors from the MIP-1072 and MIP-1095 glutamate-urea-glutamate/lysine analogs were functionalized at the polar lysine imidazole derivatives to include alcohols, ether, and acids, which were then labeled with radionuclide technetium-99m (^{99m}Tc), to yield four agents: ^{99m}Tc-MIP-1427 ($K_d = 0.64 \pm 0.46$ nM), ^{99m}Tc-MIP-1405 ($K_d = 4.35 \pm 0.35$ nM), ^{99m}Tc-MIP-1404 ($K_d = 1.07 \pm 0.89$ nM), and ^{99m}Tc-MIP-1428 ($K_d = 1.75 \pm 0.32$ nM).[151] In animal studies, these four compounds showed low nontargeted cells uptake by hepatobiliary and normal tissues, and rapid renal clearance. ^{99m}Tc-MIP-1404 **(19)** had the best localization in PSMA$^+$ LNCaP xenograft tumors over 4 hr.[151,152] These four drugs were brought to phase I clinical trials for SPECT imaging in patients with metastatic disease, in comparison with **17** and **18**, and the mAb ^{111}In capromab pendetide (Prostascint). Both **19** and ^{99m}Tc-MIP-1405 **(20)** gave promising results with rapid detection of metastatic PCa in soft tissues and bone with high specificity. The diagnosis accuracy and sensitivity were both 83% for **19** and 84% for **20**, that is, better than **17** and Prostascint (diagnosis accuracy and sensitivity of 67% for **17** and 63% for Prostascint).[153] Conjugate **19** is now in phase II clinical trials for high-risk PCa patients who have been scheduled for radical prostatectomy and extended pelvic lymph node dissection (NCT01667536).

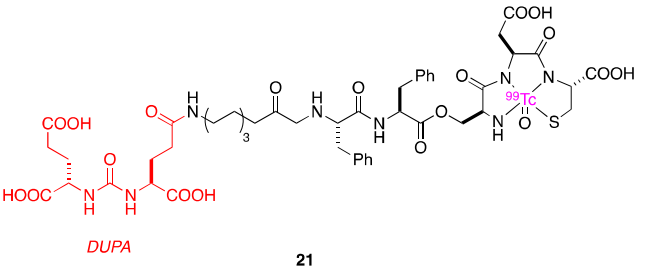

21

EC0652

The high-affinity PSMA-targeting ligand 2-[3-(1,3-dicarboxy propyl)-ureido] pentanedioic acid (DUPA) conjugated to technetium 99m (^{99m}Tc) with peptide spacer NH-$(CH_2)_7$-CO-Phe-Phe gives a novel radionucleotide EC0652 **(21).**[154] In phase 0 trials, high-affinity localization of EC0652 in all obvious cancerous areas in seven patients was confirmed by CT and bone scan and there were no reported toxicities.[155] Conjugate **21** is now in phase I/II trials with larger patient populations.

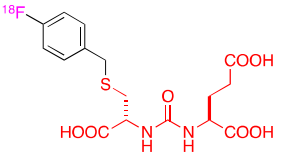

22

^{18}F-DCFBC

Imaging agent ^{18}F-DCFBC **(22)**, sponsored by Sidney Kimmel Comprehensive Cancer Center to undergo phase I trials, was found to be concordant with the conventional imaging as well as applicable for the use in early bone metastases that are not detectable by conventional imaging.[156]

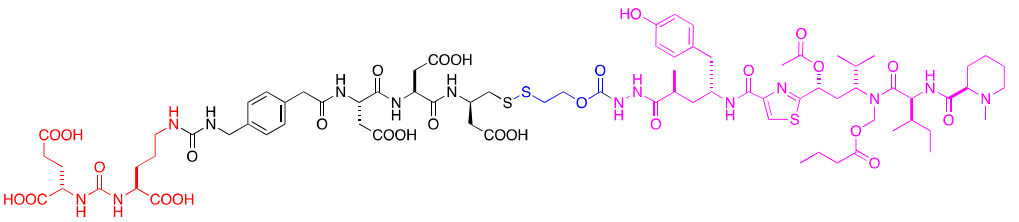

23

EC1169

Antineoplastic agent TubBH conjugated with a PSMA inhibitor EC1169 **(23)** inhibited growth of PSMA-positive cells with no activity against PSMA negative cells ex vivo. Treatment of EC1169 in a xenograft nude mice model bearing human LNCaP led to tumor remission in five of seven animals and the remaining two were "cured," that is, no tumor regrowth up to 90 days. EC1169 did not have any effects on a PSMA negative xenograft model, neither did the nontargeted TubBH conjugated have effects on the PSMA-positive tumor model.[157] This targeted therapeutic agent is currently undergoing phase I clinical trials for patients with metastatic PCa under sponsorship by Endocyte (NCT02202447).

D. Sigma-2 Receptor

Receptors sigma-1 and sigma-2 (25.3 and 21.5 kDa, respectively)[158] are found in the CNS and peripheral tissues such as liver, kidney, and gastrointestinal tract.[159,160] Sigma-1 modulates ion channels and mobilizes intracellular ions, such as calcium and potassium ions, especially in glutamatergic neurotransmission.[161,162] It has been widely studied in learning and memory processes, depression and anxiety, schizophrenia, and analgesia.[162]

Unlike sigma-1, sigma-2 regulates cell differentiation, morphology, survival, and growth[163,164] and is eight to ten times overexpressed in rapidly proliferating cells (stem and cancer) compared with quiescent mouse mammary adenocarcinoma lines.[165,166] The sigma-2 receptor therefore is a biomarker for proliferating status and a focus for targeted cancer therapy of solid tumors.[167] It is abundant in human and murine pancreatic and ovarian cancer cell lines, and is expressed minimally in brain, liver, pancreas, spleen, lung, and kidney. Sigma-2 in the ligand bound form is internalized via endocytosis before localizing in lysosomes, the endoplasmic reticulum, and mitochondria. It participates in both caspase-dependent and caspase-independent pathways of cell death.[168]

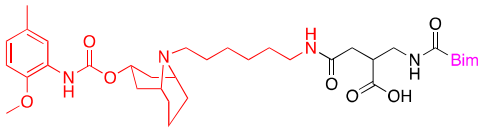

24

Conjugate **24** containing synthetic ligand SV119 did not interfere with the proapoptotic *Bim* activity in inducing apoptosis ($IC_{50} = 71$ nM), and the caspase-3 activity was augmented by 1.6-fold in vitro compared with SV119 alone ($IC_{50} = 460$ nM). Preclinical studies of **24** on a syngenic murine pancreatic tumor model and a xenograft human pancreatic tumor model showed it significantly reduced tumor growth and increased animal survival. This targeting agent preferentially localized in the pancreas relative to other organs. A mild increase in caspase activity was detected in normal pancreas, but there was no toxicity and caspase activity diminished quickly once treatment was ceased.

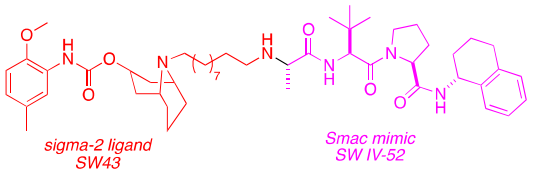

25

SW-IV-134 or **SW III-123**

SW IV-134 **(25)** is a chimera of SW43 and a Smac mimetic SW IV-52.[170] Smac induces apoptosis by deactivating the Inhibitor of Apoptosis (IOP) protein in cells. Chimeric **25** has a lower binding affinity to sigma-2 receptor ($K_i = 22.6 \pm 1.8$ nM) than SW43 ($K_i = 7.1 \pm 1.3$ nM), but five- to sevenfold lower IC_{50} in six pancreatic cancer cell lines compared with its components SW43 and SW IV-52. Furthermore, xenografts in murine models demonstrated that **25** treated mice have delayed tumor growth and increased survival compared to SW43 and SW IV-52 controls.[171]

A different group used **25**, but with a different name SW III-123 and for treating ovarian cancer ($K_i = 189.90$ nM).[172] In that model, **25** is a potent active targeting cytotoxic agent, inducing TNF-α-dependent cell death through rapid degradation of the apoptosis inhibitor

proteins cIAP1 and cIAP2. In a xenograft model of ovarian cancer, the median survival for mice treated with **25** was 86.5, 10, and 12 days more than mice treated with SW43 and vehicle solvent, respectively.[173]

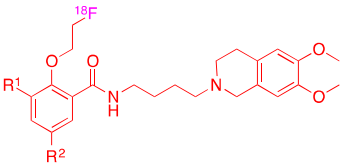

26, [^{18}F]3c: R^1 = H, R^2 = CH_3

27, [^{18}F]3f: R^1 = OCH_3, R^2 = I

Radiotracer agents that selectively target the sigma-2 rather than sigma-1 receptor have been developed to detect and stage solid tumors, as well as to monitor therapeutic efficiency. The first two radiolabeled small-molecule ligands in this series were benzamide analogues [^{18}F]3c **(26)** and [^{18}F]3f **(27)**. These gave high tumor-to-normal tissues ratios, rapid blood clearance, and minimal defluorination in a mouse mammary tumor model.[174] Conjugate **26**, also referred to as ^{18}F-ISO1 ($K_d = 4.66 \pm 0.87$ nM)[175] was assessed in 30 patients with breast ($n = 13$), head and neck ($n = 10$), and lymphoma ($n = 7$) cancers.[176] There was a significant positive correlation between Ki-67 staining (a cellular proliferation marker) with **26** uptake, as assessed by tumor-to-muscle ratio and tumor maximum standardized uptake value, suggesting that this imaging agent may be an alternative to diagnosis via specimen biopsy. Moreover, **26** almost completely cleared from blood in 5 min, had high tumor uptake within minutes post injection, and a tumor uptake level that remained at peak throughout 60 min of imaging.[176] These data suggest that **26** is safe for imaging proliferation and growth of cancer cells. Indeed, **26** is currently used for PET/CT imaging of sigma-2 receptor expression in primary breast cancers (University of Pennsylvania; NCT02284919).

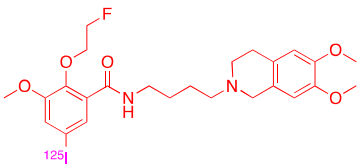

28

[^{125}I]ISO-1 or [^{125}I]3f

The long half-life of iodine-125 (59 days) is ideal for animal biodistrubution studies compared with fluorine-18 ($t_{1/2}$ 110 min). Both [^{18}F]3f **(27)** and [^{125}I]3f **(28)** have high tumor-to-normal tissues ratios and rapid clearance from blood, muscle, fat, and lung (5–120 minutes),[177] suggesting that the high affinities of **27** ($K_i = 0.26$ nM) and **28** ($K_d = 2.8$ nM) were not affected by the radioisotope attached. However, **28** is unlikely to be useful in imaging human tumor because of it low gamma energy from iodine-125.

E. Tropomyosin Receptor Kinase (Trk)

Tropomyosin receptor kinase (Trk) includes three common receptor tyrosine kinases, TrkA-C. Each neurotrophin ligand has different Trk-binding specificities; TrkA predominantly binds to neurotrophin growth factor (NGF), TrkB to brain-derived neurotrophic factor (BDNF) and neurotrophin-4 (NT-4), TrkC has greatest affinity for neurotrophin-3 (NT-3). p75NTR is a cell surface receptor that binds all the neurotrophins.[178] Extracellular domains of Trk receptors include a combination of two cysteine clusters, a tandem array of leucine-rich

motifs, and two immunoglobulin-like domain in the membrane proximal region.[179] Specificity and affinity to neurotrophin ligands are dictated by the second immunoglobulin-like domain (residues 266–381) of the receptor,[180] whereas the leucine-rich motif serves as a binding site for neurotrophins.[181]

Trk receptors were first identified as a colon-derived oncogene, and subsequently in the normal cellular counterpart of adult neurons with functions that include regulation of neuronal cell survival, proliferation, differentiation, axon and dendrite growth, as well as regulation of synaptic strength and plasticity.[182] Trk receptors are expressed in neurons, but overexpressed in various cancers including neuroblastoma,[183,184] glioblastoma,[185,186] thyroid cancer,[187] melanoma,[188] and breast cancer.[189,190] Consequently, Trk receptors are potential molecular targets for new chemotherapeutics, and useful biomarkers for prognosis of tumor progression and invasion.[191]

Studies of Trk internalization in lysosomes upon neurotrophin binding[192] have led to small-molecule ligands that target this receptor for drug delivery. A series of small-molecule agonistic ligands have been discovered to bind to the ectodomain of TrkC receptor and transduce signals similar to the natural ligand NT-3 for regulating neuritogenesis.[193] Subsequently, the same group conjugated a synthetic bivalent peptidomimetic (IY-IY) composed of fragments containing isoleucine (I) and tyrosine (Y) side chains, to cytotoxic cargoes. Conjugates to a rosamine and to 6-mercaptopurine were delivered into lysosomes, just as NT-3 is, and showed increased cytotoxicity in cells transfected with TrkC compared to wild-type cells. Competitive binding assays between the conjugated agents with NT-3 or a synthetic control ligand demonstrated that these compounds mediated dose-dependent cytotoxicities via TrkC binding.[194]

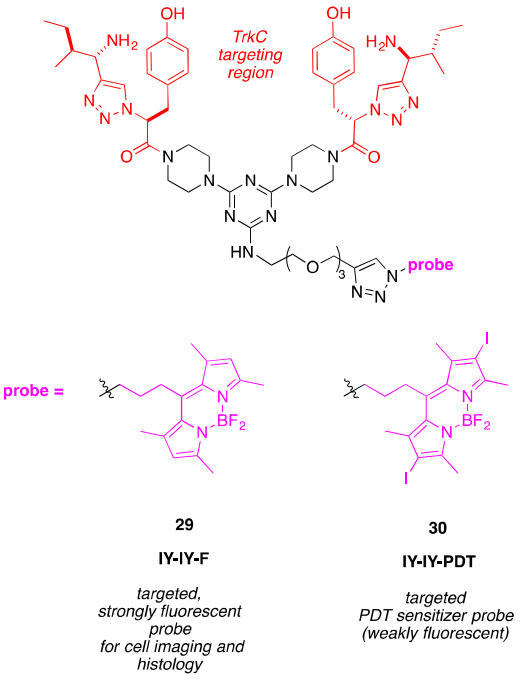

Solubility and toxicity issues restricted further development of the 6-mercaptopurine and rosamine conjugates, so the same targeting group was conjugated with boron dipyrromethene (BODIPY) to give IY-IY-F **(29)** for fluorescence imaging studies, and to an iodinated BODIPY, resulting in IY-IY-PDT **(30)** for targeted photodynamic therapy (PDT). Conjugate

30 induced significant photocytotoxicity in TrkC-transfected NIH-3T3 and TrkC-expressing SY5Y neuroblastoma cells in a dose-dependent manner upon irradiation as compared to TrkC-negative cells (NIH-3T3). A non-TrkC-targeted scrambled control (YI-YI) induced less photocytotoxicity.[195] In another study featuring both human and murine breast cancer cell lines, **30** was shown to have a significantly lower IC_{50} in TrkC overexpressing murine 4T1 ($IC_{50} = 0.325\ \mu M$) and human HS578t cell lines ($IC_{50} = 0.285\ \mu M$) compared to non-TrkC-expressing murine 67NR and human MCF-10A. Biodistribution of **30** in a syngeneic murine model showed that it accumulated maximally in 4T1 tumors at 1 hr post intravenous administration and maintained a high level up to 6 hr. YI-YI-PDT had a similar accumulation pattern but at twofold less tumor-uptake. Outstanding antitumor activity was observed in **30** in a 4T1 breast cancer model: 71% of the 4T1 tumor-bearing mice healed from cancer up to 90 days with no evidence of metastasis in major organs as verified by histopathological analyses. Surprisingly, tumor remission was also not observed in mice bearing 67NR ($TrkC^-$) tumors, or for YI-YI-PDT treated 4T1 tumor-bearing mice.[196] Relatively high toxicity was observed for **30** (MTD 20 mg/kg) and this could be because many types of neuronal cells also expressed TrkC receptors

F. Carbonic Anhydrase IX

Carbonic anhydrase (CA) is a transmembrane zinc metalloenzyme found in cervical cancer HeLa cells.[197] It regulates physiological pH homeostasis by reversibly converting carbon dioxide to bicarbonate.[198] In humans, CA exists in 16 different isoforms having varying subcellular localizations, catalytic activities, and susceptibility to different inhibitors. These isozymes exist in diverse tissues such as gastrointestinal and reproductive tract, nervous system, kidney, lung, skin, and eyes.[199] Among the 16 isozymes, membrane-bound CA-IX and CA-XII have been shown to link to carcinogenesis.

CA-IX contains 459 amino acids, with an *N*-terminal signal peptide region, a long extracellular CA domain, a transmembrane region, and an intracellular *C*-terminus domain.[200] It exists as a dimeric protein and is the most active form of CA for CO_2 hydration.[201] CA-IX is not expressed in most normal tissues except for stomach and gallbladder epithelia,[202] but is highly expressed in aggressive glioblastoma,[203] colorectal,[204] and breast cancers.[205] CA-IX expression has been studied as a prognosis biomarker for survival in patients.[206] CA-IX and CA-XII expression apparently do not overlap; the latter is only a marker for less-aggressive tumors.[207]

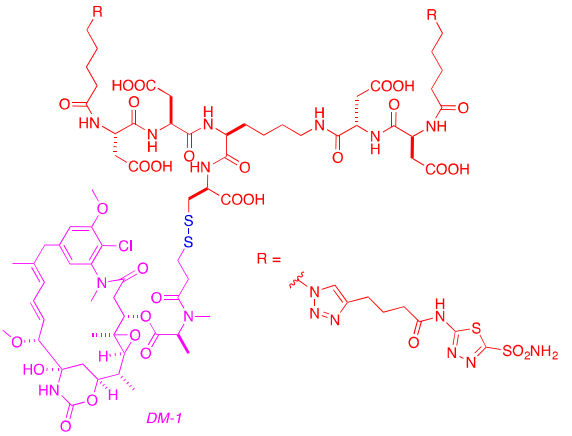

31

There are highly specific small-molecule delivery vehicles applicable in CA-IX due to its high and constitutive expression. Neri et al. has synthesized a few ligand-linker dye conjugates to study their CA-IX binding affinity and biodistribution: the FITC-conjugated (FITC is fluorescein isothiocyanate) CA inhibitor acetalozamide (AAZ) targeted CA-IX positive cells (K_d = 12.6 nM). The biodistribution in mouse model revealed that the dye accumulated in tumor at 1 hr post administration, and the accumulation value was 22-fold higher than nontargeted ligand,[208] further confirming the selectivity of this ligand conjugate. In determining the therapeutic efficacy, the AAZ was conjugated with the cytotoxic agent duocarmycin. The conjugate possessed high affinity for CA-IX receptor. Disappointingly, a human renal-cell carcinoma xenograft model indicated only moderate tumor growth inhibition compared with untargeted conjugates.[208] Conversely, another cytotoxic drug, maytansinoid or "DM-1," conjugated to the same ligand produced pronounced tumor shrinkage after seven consecutive days of treatment, though regrowth was observed at 20 days post therapy when no additional drugs were given. DM-1 conjugates were more effective than the clinical chemotherapy agents, sorafenib and sunitinib, in preclinical studies.[208] A bivalent AAZ-maytansinoid DM-1 **(31)** gave superior characteristics compared to the monovalent AAZ with respect to the following: (i) affinity with no apparent dissociation from CA-IX coated surface, (ii) approximately threefold higher tumor accumulation than the monovalent conjugate, (iii) longer persistence in tumor (fluorescence signal of 40% compared with 14% for the monovalent 24 hr post administration) and, (iv) ablation of approximately 75% of the tumor compared to initial, with 33% of mice disease free up to 90 days in human renal carcinoma SKRC52 xenograft model.[209]

G. Glucose Transport System

Glucose is obtained through the small intestine before being transported into circulation and target cells. It is an essential energy source for eukaryotic organisms, as it generates adenosine-5 triphosphate (ATP).[210] Uptake of glucose across plasma membrane depends on glucose transporter carrier proteins. Transporters for uptake of glucose into cells have been identified, namely sodium-dependent glucose cotransporters (SGLT family) and facilitative sodium-independent transporters (GLUT family).[211] SGLT family of transporters (SGLTs 1–6) transports glucose via active transport, which is mainly found in small intestines and renal proximal tubules,[211] while the GLUT transporter family (GLUTs 1–14) are expressed in specific cells and tissues and they vary in binding affinities and substrate selectivities.[212] Among the 14 transporters in the GLUT family, only GLUT 1 and GLUT 3 have high affinity for glucose. They are closely linked to cell growth and development, especially in malignant cancer but not in normal epithelial and benign epithelial tumors.[213] Studies have proposed that cancer cells highly rely on glucose and glycolysis for survival (Warburg effect)[214] and express GLUT, especially GLUT 1 abundantly to increase glucose uptake and energy usage.[215] This explains how GLUT 1 expression is correlated with the aggressive behavior of cancer.

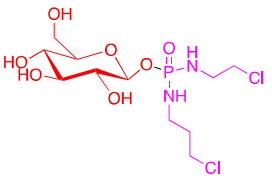

32

glufosfamide

A glucose transporter targeting agent glufosfamide (D-19575, **32**) was synthesized by linking β-*D*-glucose as a ligand covalently to an alkylating agent isophosphoramide mustard

in 1990s through a collaboration between Baxter Oncology (Asta Medica) and the Cancer Research Centre (DKFZ) in Heidelberg, Germany.[216] Compound **32** is cytotoxic in glucose transporter overexpressing cancer cells and its potency is correlated with the amount of enzyme β-glucosidase in cytosol and lysosome, which were required to hydrolyze **32** to release its cytotoxic agent.[217] Cytotoxic action of **32** involves inhibition of DNA and protein synthesis, followed by reduction in the level of anti-apoptotic Bcl-2 protein and activation of caspase-3, caspase-8, and caspase-9.[217–219]

Clinical evaluation of the toxicity of **32** showed increased serum creatinine and renal acidosis,[220,221] probably caused by acute tubular necrosis. Other reported toxicities include neutropenia, leukopenia, and thrombocytopenia when administrated intravenously at dosage of more than 5000 mg/m^2 regardless of infusion schedules.[220–223] Phase I studies of **32** on refractory solid tumors indicated clear antitumor activity. Treatment with 800–6000 mg/m^2 of drug every 3 weeks yielded long-lasting complete response for an advanced pancreatic adenocarcinoma, as well as minor tumor shrinkage for two refractory colon carcinomas and one heavily pretreated breast cancer.[220]

The efficacy of conjugate **32** in phase II metastatic pancreatic cancer and non-small-cell lung cancer was reported moderate when administrated at dosage of 5000 mg/m^2 every 3 weeks, with median overall survival of 5.3 months for PCa,[224] and 5.8 months for lung cancer.[221] Moreover, insignificant antitumor activity was observed for patients with glioblastoma multiforme and treatment was thus discontinued.[223] The lack of activity for glioblastoma could be due to failure to cross the blood–brain barrier as no neurological toxicity was reported. Hence, it was suggested that the efficacy of **32** is cancer-type-dependent regardless of GLUT expression. Ex vivo studies of **32** in head and neck squamous cell from carcinoma patients (HNSCC) were also conducted, where biopsy specimens from cancer patients with primary and metastasis tumors were isolated for colony formation assay in response to **32**. *Cis*-dichlorodiammine platinum (*cis*-DDP), the current chemotherapeutic regime for HNSCC, was used as a reference. While almost all primary tumor specimens were clinically resistant to *cis*-DDP, 31.3 % of them were found to be sensitive to **32**. However, neither cisplatin nor **32** was effective in reducing colony formation of metastatic tumor cells. Thus, it was proposed that **32** was equally, if not more effective than cisplatin to treat HNSCC.[225] As **32** could overcome the drug resistance and increase the sensitivity of cancer cells to chemotherapeutic drugs, it may be used in combination with chemotherapeutic regime.

Synergistic efficacies of **32** with gemcitabine have been studied in phase I combination regimes in pancreatic adenocarcinoma; 53 % of patients were stabilized, 70% of them stable for 4 months, and 30% stable for 6 months,[222] proving the effectiveness of this combination regime. In contrast, **32** in phase III metastatic pancreatic cancer patients after receiving gemcitabine as primary treatment did not show significant improvement in median overall survival (105 days) compared with gemcitabine alone (84 days, $p = 0.19$). This phase III study has also revealed that **32** has low therapeutic activity, the best response for this study was stable disease, which is 31% in dual drug treatment and 19% in gemcitabine alone ($p = 0.016$).[226] The variance in therapeutic efficacy between phase I and phase III might be due to difference in cancer staging between patient populations. Another ongoing phase III trial, sponsored by Eleison Pharmaceuticals, involved comparing **32** and 5-fluorouracil in metastatic pancreatic cancer that had progressed or failed first-line therapy with gemcitabine (NCT01954992).

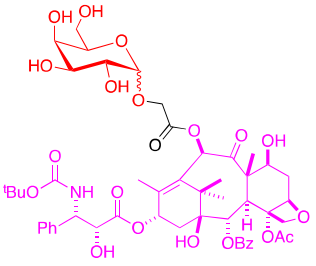

33

galactose-docetaxel (10-α-GAG-DT)

Inspired by these studies on **32**, the sugar moieties glucose, galactose, and glucuronic acid were conjugated with taxoids.[227–229] The conjugated compounds were more soluble and stable than the taxoids, and reduced the toxicity of PTX on both normal and low GLUT expressing cancer cells in vitro.[227,228] Preclinical assessment of galactose conjugated docetaxel (10-α-GAG-DT, **33**) showed that it was fast degraded (within 1 hr) to release the free drug and possessed superior antitumor activity compared with PTX alone but equipotent with docetaxel in a syngeneic model murine leukemia cells.[228]

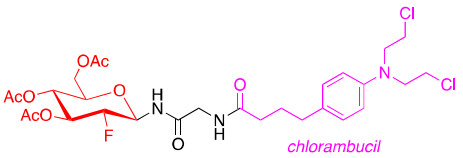

34

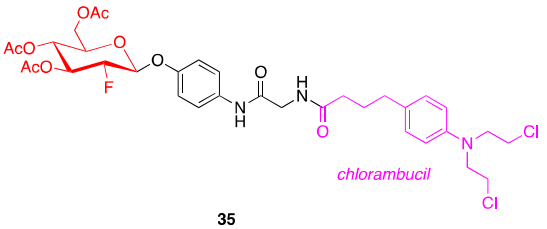

35

FDG-chlorambucil

19-Fluorodeoxyglucose (FDG) conjugated to chlorambucil (CLB) derivatives through different spacer groups has been studied.[230] Screening of various cancer cell lines with the conjugates demonstrated significant improvement in cytotoxicity of glycoconjugate CLB compared with the free drug. In brief, glycoconjugates that possess two amide bonds in the spacer linker showed high cytotoxicity (**34**), and cytotoxicity was not further improved by the length of alkyl chain in the spacer. The presence of an aminophenol between FDG and the amidic bond spacer also improved cytotoxicity **(35)**.[230] Preclinical evaluation of **34** and **35** on a syngeneic murine model of melanoma and colon cancer[231] proved that both were better tolerated than CLB alone, with MTD of 0.14 mmol/kg for both compounds compared with 0.05 mmol/kg for CLB. Drug efficacy studies in melanoma at the MTD showed **34** induced 80% inhibition in tumor growth at day 21 post tumor inoculation, whereas compound **35** induced 90% inhibition (day 23). Both showed significant inhibition compared with CLB-treated mice with 57% inhibition at day 26. In the colon cancer model, **34** and **35** had 75 and 88% inhibition at day 26 when given at 0.75 MTD, compared with 66% at day 23 for CLB at MTD.

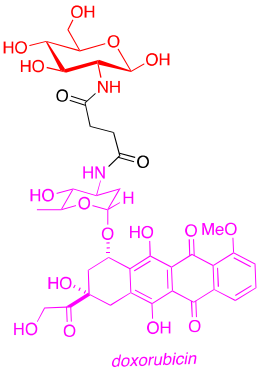

36

2DG-SUC-ADM

A conjugate of 2-amino-2-deoxy-*D*-glucose via succinic acid to adriamycin (ADM, 2DG–SUC–ADM, **36**) showed uptake in high GLUT-1 cells, delivery into the cytoplasmic region in 5 min, and penetration into the nucleus 10 min post treatment. GLUT-1-mediated uptake of **36** was proposed as the addition of 2DG ligand or GLUT-1 inhibitor reduced the mean fluorescence intensity of ADM in cells. Interestingly, not only did **36** reduce the viability of GLUT-1-overexpressing cancer cells in a dose-dependent manner, it was also effective against ADM drug-resistant MCF-7 cells (MCF-7/ADR) and had negligible cytotoxicity in normal cells. In preclinical biodistribution studies, **36** accumulated in high levels in tumor 2 hs post injection and continued to give detectable high levels in tumors 48 hr post administration, whereas the dye in other organs was cleared by 24 hr. Antitumor efficacy studies in syngeneic S180 sarcoma model and xenograft SKOV3 ovarian model revealed that **36** has 64 and 69% tumor inhibition, respectively, with negligible side effects, as compared to the parent drug, which has 50 and 47% inhibition of tumor volume in S180 and SKOV3, respectively.[232]

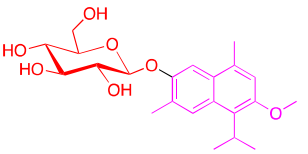

37

β-glc-O-cadalene

Glycosylation of cadalene, a natural product reported to have antitumor effects, produced *β*-Glc-*O*-cadalene **(37)**, which had improved physicochemical properties, notably water solubility. Pharmacokinetic properties were not determined for this conjugate, but an antitumor efficacy study in xenograft of lung carcinoma model via oral administration showed a 50% reduction in tumor size.[233]

A 63-member library of neoglycoside conjugates to CLB and 32 similar neoglycoside conjugates of the alkaloid cyclopamine were prepared to study the effects of the sugar moiety and linker on biological activity. The studies indicated that nonmetabolic sugar conjugates such as *D-threose* inhibited growth of solid tumor cell lines with lower IC_{50} compared with parent drugs and metabolic sugar conjugates, *D-glucose*.[234,235]

In contrast to conjugates that showed successful targeted delivery, there are some glucoconjugate drugs that negatively regulate tumor growth. Conjugation of 8-hydroxyquinolines and clioquinol to glucose resulted in glucoconjugates with weaker antiproliferative activity

compared with the parent drugs.[236] This was due to the incomplete hydrolysis of the conjugates by enzymes to release their cytotoxic agents in cancer cells.

H. Estrogen Receptor

Estrogen, the primary female sex hormone, is essential for the growth and maintenance of female reproductive tissues. It is mainly biosynthesized in the ovaries, and three major endogenous estrogens are produced in varying amounts throughout the female reproductive cycle: estrone (E1), estradiol (E2), and estriol (E3). Estrogen receptor (ER) binds the endogenous estrogens inside cells and translocates them to the nucleus. It is a transcription factor of the nuclear receptor family. There are two isoforms of ER: αER, predominantly expressed in breast, ovary, and endometrium and βER, found mostly in kidney, CNS, prostate, cardiovascular, and bone tissues.[237] αER and βER have similar ligand-binding domains but different affinities toward their ligands.[238] Moreover, both αER and βER demonstrate opposing transcriptional activities. Therefore, different ER combinations may respond differently to various ligands, which may translate into tissue selective agonistic or antagonistic effects.[239]

Estrogen is associated with carcinogenesis, as the ER can drive cellular proliferation and increase in mutation rate.[240,241] αER is over-expressed in more than 70% of all diagnosed breast cancer.[242,243] For this reason, it has been exploited as a therapeutic target, a predictive marker, and a prognostic factor for the breast malignancies.

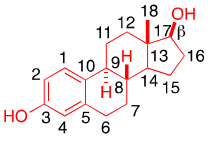

38

17β-estradiol

17α-estradiol

17β-estradiol

E2 (17β-estradiol) and their derivatives are attractive ligands for receptor-based drug delivery as they are highly distributed in ER-expressing cancer cells,[244,245] and provide a basis for development of estrogen-targeted conjugate. Early work in this area features coupling of E2 or derivatives to chemotherapeutic drugs such as alkylating agent, antimetabolite, antimitotic agents, antibiotics, or photosensitizers. Details related to these E2–drug conjugates have been reviewed.[246] Most of this work featured attachment to E2 at the 3, 6, 7, 11, 16, and 17 carbons of **38**. It emerged that the $C^3$and C^{17} hydroxyls are important for ER binding,[247] suggesting that conjugates avoiding these positions would result in better binding affinity.[248–250] In one study, linking drug molecules to the E2 6α, 7α, 16α, and 17α positions compromised binding affinities to ER, and lowered cytotoxicities relative to free drugs. Presumably this was due to steric hindrance in the binding pockets.[248,249,251–253] Conversely, drugs conjugated to position 11β improved RBA and were threefold more cytotoxic in ER^+ compared to ER^- cells, relative to conjugation at the 11α position.[254] Conjugation at 3β^- and 17β^- resulted in significant cytotoxicities but lower binding affinities,[255] suggesting that binding and cytotoxicity are not perfectly correlated. Overall, early findings showed that β-conjugates gave better binding affinity

to ER and none of the α-conjugates were suitable. Consequently, subsequent research has focused on β-connectivity.

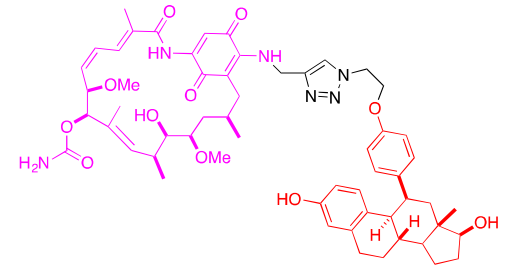

39

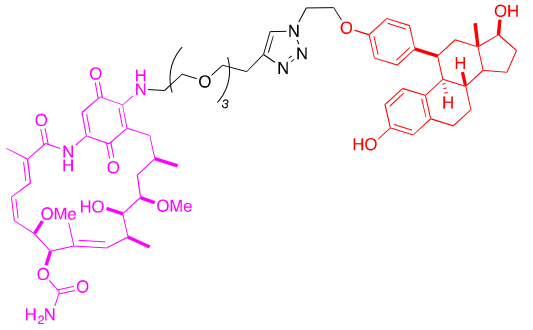

40

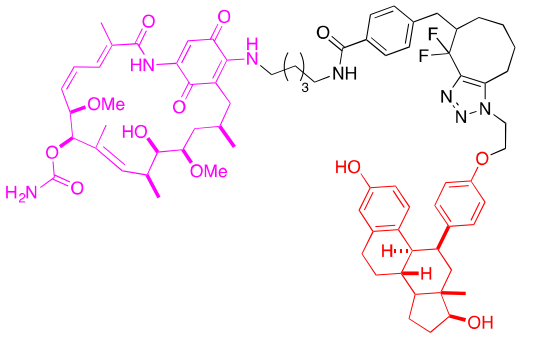

41

Hanson's group proposed E2 is an agonist when 11β position is not conjugated and becomes an antagonist when the same position is substituted with an aromatic ring. Subsequently, many studies focused on 11β E2 antiestrogen (AE), with appropriate substitutions at 11β position to facilitate binding to the ER pocket.[256] Three new E2-geldanamycin (GDA, Hsp90 inhibitor) conjugates were prepared to study the effect of linker length on binding affinity: **39**, **40**, and **41**. These 11β-E2-GDA hydrids have higher binding affinity for ER but were less cytotoxic to ER^+ cells compared to ER^- cells than the free drug GDA. Longer spacer lengths such as that in **40** tended to increase the binding efficacies (RBA of 39% relative to AE RU39411).[257]

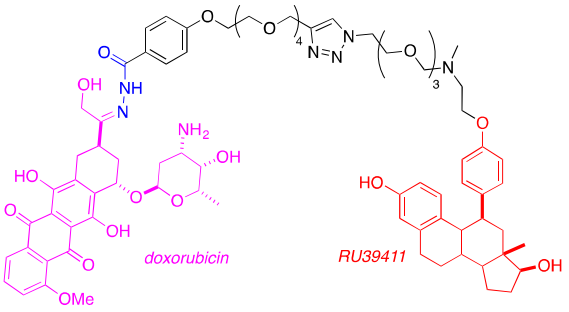

42

11β-AE-Dox

Tetraethylene glycol was used to attach RU39411, an AE antagonist to benzoyl hydrazone Dox giving 11β-AE-Dox **(42)**. The azido-AE and alkynated-Dox functions were not significantly perturbed by the linker. Moreover, **42** was more selective than free-Dox and linker-Dox in ER overexpressing MCF-7 cells, with approximately 70-fold lower IC_{50} values. Conversely in non-ER-expressing cells, **42**, free-Dox and linker-Dox had comparable IC_{50} values. Fluorescence microscopy showed that uptake of conjugates was mediated by membrane ER and enhanced cytoplasmic accumulation of Dox occurred via cleavage of pH-sensitive hydrazone linker.[258] An in vitro evaluation of **42** showed that it was potent for ER targeting while no in vivo evaluation has been reported so far.

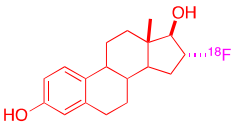

43

^{18}F-FES

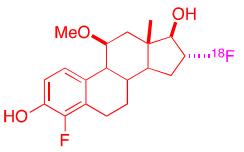

44

4FMFES

E2 conjugates that have imaging probes include 16α-[^{18}F]fluoroestradiol (^{18}F-FES, **43**).[259] Preclinical evaluation in a murine model showed high accumulation of **43** in ER$^+$ uterus and ovarian tissues.[260,261] Clinical development and efficacies of **43** and related agents have been reviewed.[262] Briefly, uptake of **43** is receptor mediated and it is effective in detecting local and metastatic breast cancer. Improved biodistribution was obtained when fluorine was substituted at C^4 of E2 with an 11β-methoxy group to produce 4-fluoro-11β-methoxy-16α-[^{18}F]-fluoroestradiol (4FMFES, **44**).[261] Phase II trials of **44** showed good efficacy in detecting ER$^+$ breast cancer with high tumor to background ratio relative to **43**.[263] However, no further update on the clinical status of **44** is found to date.

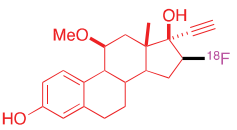

45

β^{18}F-FMOX

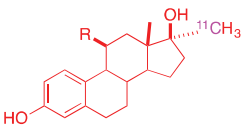

46, **17α-[^{11}C]methylestradiol**; R = H
47, **11α-ethyl-17β-[^{11}C]methylestradiol;** R = Et

Other modifications of **43** included substitution at 11- and 17-positions on 16α/16β-[^{18}F]fluoroestradiol, as 11- and 17-substitutions were known to increase uptake selectivity.[264,265] Among the hydrids synthesized, 17α-ethynyl-11β-methoxy-16β-^{18}F-fluoroestradiol (β–^{18}F-FMOX, **45**) gave the best binding affinity and fourfold higher uterus uptake than **43** in rats.[266]

However, subsequent clinical data were inconsistent with the animal imaging data. Conjugate **45** had poor localization in human breast tumor lesion compared to **43**, hence the study was discontinued.[267] In spite of many rounds of modification, **43** is the only agent in this series that remains in active clinical trials. Currently, it is being studied as a molecular imaging agent for desmoid tumor and metastasis breast cancer (NCT02374931, NCT01957332).

E2 has also been conjugated with the short-lived ($t_{1/2}$ = 20.4 min) positron-emitting radionucleotide ^{11}C to generate 17α-[^{11}C]methylestradiol **(46)** and 11β-ethyl-17α-[^{11}C]methylestradiol **(47)**.[268] Both derivatives were safe and effective in rats, with selective accumulation in uterus and ovary at 20–40 min post injection.

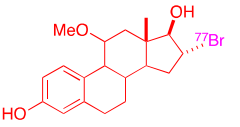

48

16α-[^{77}Br]-bromo-11β-methoxyestradiol

Several other ER$^+$ targeted ligands have undergone clinical studies for imaging. One of these is an 18-fluorine conjugate of Snon-steroidal tamoxifen (^{18}F-fluorotamoxifen, FTX), which shows good correlation between FTX uptake and response to tamoxifen therapy in primary and metastasis breast cancer.[269] Another ligand, 16α-[^{77}Br]bromoestradiol could image ER$^+$ cancer and showed fast clearance,[270] but there has not been an update on the clinical status of these two imaging agents for the past 10–20 years. In the meantime, 16α-[^{77}Br]-bromo-11β-methoxyestradiol **(48)** has given successful results in the preclinical setting.[271]

I. Progesterone Receptor

Progesterone (**49**) is a steroid hormone important for female reproductive function, for example, in preparing the uterus for pregnancy. Progesterone is physiologically active when bound to the nuclear progesterone receptor (PgR). PgR is a type-I nuclear receptor, like estrogen, androgen, glucocorticoid, and mineralocorticoid receptors. It exists as isoforms PgR-A and PgR-B with an additional stretch of 164 amino acids at the *N*-terminus for protein PgR-B.[272] PgR was found in uterus, ovary, and brain,[273] with little expression on normal breast epithelia for both isoforms.[274] However, similar to αER expression, PgR expression is much higher in pre-neoplastic breast lesions and the expression of the isoforms varies during tumorigenesis. There is a better prognosis for patients expressing both αER and PgR as they have the highest chance of responding to endocrine therapy.[275] Conversely, primary breast tumors that are PgR negative (PgR$^-$) have higher possibility of becoming malignant, suggesting that reduced PgR expression is associated with cancer aggressiveness and poor prognosis.[275]

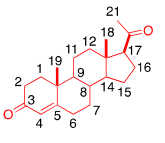

49

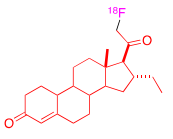

50

^{18}F-FENP

21-[^{18}F]-Fluoro-16α-ethyl-19-norprogesterone ([^{18}F]-FENP, **50**) showed higher binding affinities to PgR than progesterone (60×) and ORG2058 (4×), an analog of synthetic progestin 21-hydroxy-16α-ethyl-19-norprogesterone. In clinical breast cancer imaging, only 50% of PgR$^+$ patients stained positive and uptake was not PgR dependent. Moreover, it had a low target-to-background ratio and high uptake in the spine, blood, liver, and some other normal tissues,[276] suggesting that it was metabolically unstable (high accumulation in bone) and had excessive lipophilicity (high accumulation in liver and fat). To solve these issues, modification of **50** was conducted, where progestin was incorporated with furanyl 16α,17α-acetals or -ketals, yielding two different compounds called ^{18}F-FFNP **(51)** and 16α,17α-ketal-progestin **(52)**.[277]

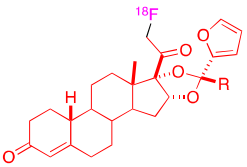

51, furanyl 16α, 17α-acetal-progestin (^{18}F-FFNP); R = H

52, furanyl 16α, 17α-ketal-progestin; R = Me

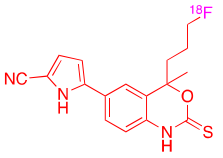

53

^{18}F-FPTP

Compared to **50**, fat and bone uptake were significantly reduced in **51** and **52**, while maintaining high PgR uptake in the uterus and ovary (190 and 173%, relative to R5020). The metabolic stability of both **51** and **52** was due to the presence of the bulky furan-substituted dioxolane ring at the 16α, 17α-position **(49)**. This steric ring can slow down the defluorination at C^{21} as well as reduce the in vivo metabolism of the conjugates by 20-hydroxy-steroid dehydrogenase, a progesterone metabolizing enzyme.[277] Compound **51** was subjected to clinical studies to evaluate its safety, dosimetry, and feasibility of imaging PgR$^+$ breast cancer by PET. Clinical studies on 22 breast cancer patients (16 PgR$^+$, 6 PgR$^-$) revealed that the difference in tumor lesion uptake (tumor maximal standardized uptake) was insignificant between PgR$^+$ and PgR$^-$ subjects (mean 2.5 vs. 2.0, respectively) but significant in terms of tumor-to-normal breast ratio (2.6 vs. 1.5, respectively) in PgR$^+$ breast cancer.[278] This suggests that compound **51** is more suitable to be used to determine the degree of PgR status of individual breast cancer lesions instead of in general diagnosis and staging. Conversely, there is no clinical trial reported for compound **52**.

Derivatives of nonsteroidal PgR agonist tanaproget containing fluoroethyl or fluoropropyl substituents have higher affinities toward PgR than PgR-ligand, R5020, and tanaproget itself.[279] ^{18}F-Fluoropropyl tanaproget (^{18}F-FPTP, **53**) has RBA of 189 in relation to R5020.[280] Biodistribution in estrogen-primed rats showed low uptake of **53** in both uterus and ovary at both 1 and 3 hr, but high uterus-to-blood and muscle ratios at 1–3 hr. Biodistribution of **53** compared favorably to **50** and **51**, suggesting that it has excellent potential for PET imaging PgR$^+$ breast tumors.

Another PgR targeted imaging agent that requires modification to achieve desired receptor specificity is 99mTc(CO)3-11β-progesterone. It has 30% PgR-binding affinity and high uterus-to-muscle ratio at 1 and 3 hr (2.8 and 2.2, respectively) post injection, and slow washout from uterus at 24 hr (uterus/muscle ratio of 2.8). It is likely to be metabolically unstable as there was high uptake observed in liver, which is the main site of steroid metabolism.[281]

J. Androgen Receptor

Endogenous androgens such as 5α-dihydrotestosterone (DHT) and testosterone, bind the androgen receptor (AR). AR is a 110-kDa ligand-dependent transcription factor that shares

sequence homology with progesterone, estrogen, and glucocorticoid receptors.[272] Upon binding to androgen, AR regulates development and differentiation of male reproductive organs such as the prostate.[272,282] Endogenous androgens such as DHT and testosterone (i.e., 19-carbon derivatives of cholesterol) are mainly synthesized by testis and adrenal gland.[283] Unsurprisingly, based on the name, these androgenic hormones exist in both sexes, and testosterone can be metabolized by the activity of aromatase and 5α-reductase into estrogenic hormones, or DHT.[284] Circulating testosterone may regulate the proliferation of breast epithelial cells depending on the existence of enzymes within the breast tissues.

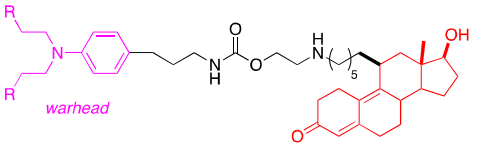

54, **11β-dichloro**; R = Cl

55, **11β-dimethoxy**; R = OCH_3

AR-ligand-drug conjugates have been developed with anti-androgens such as enzalutamide. A steroid ligand–drug conjugate 11β-dichloro **(54)** was prepared from linking the alkylating agent *N,N*-bis-(2-chloroethyl)-aniline to the high-affinity AR ligand 11β-substituted estradien-3-one. The 11β-dimethoxy conjugate **(55)** was prepared as an unreactive analog.[285] In human PCa cells, **54** had AR binding affinity equivalent to approximately 20% of the natural ligand and had low affinity (4%) on PgR. It induced rapid morphological changes 6 hr post treatment and was associated with activation of an apoptosis endonuclease and cleavage of the poly-ADP ribose polymerase (apoptotic marker). Conversely, these observations were not observed in control groups. Preclinical studies further supported the efficacy of **54**, in which intraperitoneal administration on a 5-day cycle with daily dose of 30 mg/kg for seven consecutive weeks induced tolerable toxicity but high antitumor efficacy, and suppressed 90% of the tumor volume at the end of study.

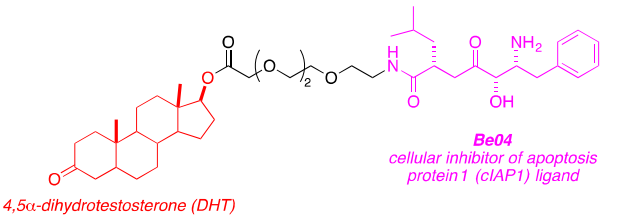

56

SNIPER-13

A few androgenic ligand-drug conjugates for breast cancer treatment reached early stage ex vivo studies. One of these is Specific and Nongenetic IAPs-dependent Protein Erasers (SNIPER), which consists of DHT targeting ligand, and a linker connected to different inhibitors of apoptosis protein such as methyl bestatin and Be04. SNIPER-13 **(56)** (Be04 inhibitor cargo), reduced AR protein expression in human MCF-7 cells compared to inhibitor alone without a targeting ligand.[286]

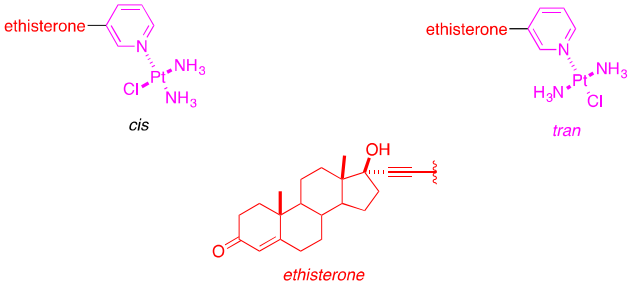

57

Another AR-targeted strategy for breast cancer involves ethisterone-cisplatin conjugates **(57)**. Here, the 17α position of ethisterone was coupled to pyridines, quinolines and isoquinolines through an ethynyl group and then attached to *cis*or *trans*- fragment of nonconventional platinum (II) complexes ($Pt(NH_3)_2Cl$) via the heterocycle to yield eight cytotoxic steroidal-drugs.[287] The *cis*-conjugates had two- to threefold higher cytotoxicities than *trans* conjugates and cisplatin alone in the AR^+ breast cell line, but not in AR^- cells. Subsequent reports demonstrated that the steroid conjugates caused more significant unwinding and bending of the DNA helix than non-steroidal control complexes and cisplatin.[288]

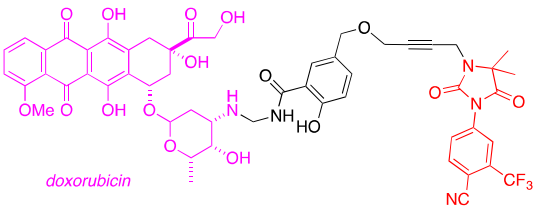

58

cyanonilutamide-doxorubicin-formaldehyde

Following the clinical success of anti-androgen therapy in PCa, a few small-molecule AR antagonist conjugates have been developed. Anti-androgen cyanonilutamide was conjugated with Dox-formaldehyde **(58)** via a cleavable *N*-salicylamide derivative for intracellular tracking studies. The conjugate **58** was translocated into cytosol and released Dox into nucleus with a half-life of 57 min in AR^+ PCa cells.[289] However, no further studies have been reported for this conjugate.

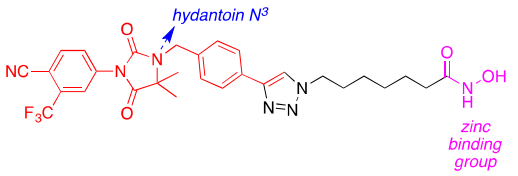

59

nonsteroidal heterobifunctional conjugated with histone deacetylase inhibitor

Recently, a series of nonsteroidal heterobifunctional anti-androgen nilutamide conjugates with histone deacetylase (HDAC) inhibitors (zinc binding group) was developed. These 12 synthesized conjugates had a 1,2,3-triazole moiety connecting the targeting group via either an aryl or alkyl cap at the hydantoin N^3 and the zinc chelating hydroxamate group through alkyl linkers of variable length. Conjugates with an aryl cap gave greater HDAC inhibition than those with an alkyl cap, and this was also the case when other antiandrogens such as cyanonilutamide, bicalutamide, and enzalutamide were used. In addition, conjugates with

longer linkers (chain length $n = 3$–8) had high binding affinity to AR ($K_i = 0.44$–4.48 μM), suggesting that attachment of HDAC inhibitors to antiandrogen did not abolish the interaction with AR. Selective cytotoxicity in an AR^+ PCa cell line was observed for 10 out of 12 conjugates, with more than twofold lower IC_{50} values compared to AR^- DU145 PCa cells.[290] The most promising compound (aryl nilutamide with linker length $n = 6$, **59**) has 80- and 40-fold lower IC_{50} in AR^+ cells compared to bicalutamide and enzalutamide, respectively. These conjugates warrant further studies in preclinical animal models.

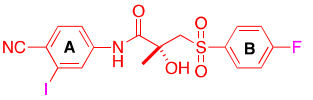

60

S-26

An AR ligand conjugate based on nonsteroidal antiandrogen bicalutamide by substituting trifluoromethyl in A-ring with iodine is **60**.[291] The presence of A-ring iodine was important for increasing the binding affinity of **60**.[292] Indeed the resultant conjugate exhibited as good affinity as testosterone to AR ($K_i = 3.3$ nM) in rat prostate cytosol.[293] Eight iodinated and noniodinated bicalutamide derivatives have been studied to compare the effects of different halogen substitutions (F, Cl, Br, $NHC(O)CH_3$) on the B-ring.[291] S-26 **(60)** with the A-ring substituted with iodine and the B-ring substituted with fluorine, exhibited the highest affinity ($K_i = 4.4$ nM) to AR compared to DHT and testosterone ($K_i = 45$ and 33 nM, respectively) in AR-transfected monkey kidney fibroblast COS-7 cells. In addition, **60** specifically bound to AR and induced AR-mediated transcriptional activity but not to other homologous steroid hormone receptors, showcasing the specificity and selectivity of a radiolabeled analogue (at F or I) of this conjugate as an effective imaging agent.

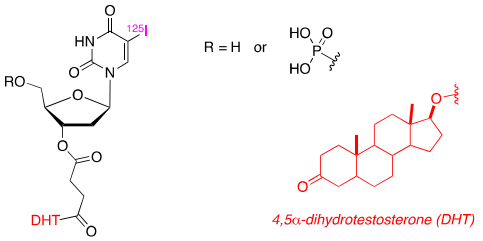

61

RISAD-P

A novel AR agent for SPECT/PET imaging, iodine-125 labeled RISAD-P **(61)** in preclinical studies revealed tumor uptake of 10% at 1 hr post administration, and accumulation proportional to tumor size and time, with no noticeable toxicity. Moreover, when used in radiation therapy, 5 Mbq of **61** was able to delay tumor growth.[294]

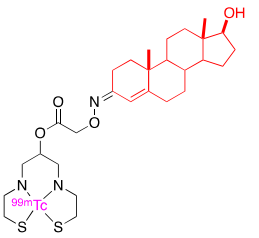

62

^{99m}Tc-DAHPES-testosterone

Another bifunctional chelating imaging agent, ^{99m}Tc-radiolabeled 5-hydroxy-3,7-diazanonan-1,9-dithiol (DAHPES) conjugated with testosterone **(62)** showed specific affinity toward an AR^+ breast cancer cell-line with negligible effect on AR^- lines. The specificity on AR suggests that it is useful as an imaging agent.[295]

K. Biotin Receptor

Other than the FR (see Section 4-A), biotin is a promising vitamin-based agent for targeted delivery of drugs or diagnostic.[296] Biotin is required for cell growth,[297,298] and the biotin demand in tumors is higher than in normal tissues. The main transporter for biotin, sodium-dependent multivitamin transporter (SMVT), is overexpressed in several aggressive cancer cell lines including leukemia (L1210FR), ovarian (OV 2008, ID8), colon (Colo-26), mastocytoma (P815), lung (M109), renal (RENCA, RD0995), and breast (4T1, JC, MMT06056) cancer cell lines.[38,299] Overexpression of SMVT was found superior in these cells compared to that of FR.

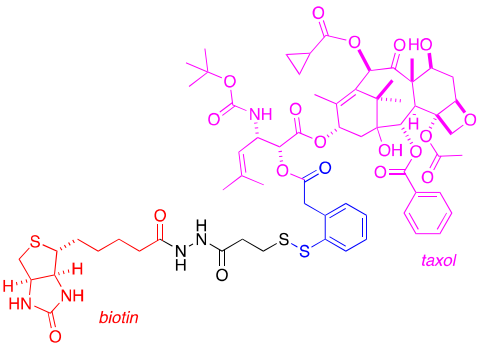

63

biotin-taxoid SBT-1214

Biotin conjugate SBT-1214 **(63)** features a new-generation taxoid, and an intracellularly labile disulfide linkage.[300] The conjugate was highly cytotoxic against biotin receptor (BR) positive murine leukemia cells (IC_{50} = 8.8 nM; *cf* for BR- murine leukemia cells the IC_{50} was 522 nM). With this and other experiments performed using several related fluorescent analogs, the authors were able to confirm the following: (i) the biotin-drug conjugate was preferentially internalized into cancer cells, (ii) the toxicity against normal cells was significantly reduced and, (iii) the disulfide spacer facilitated systemic stability.

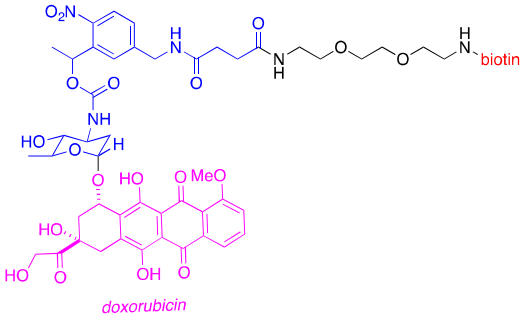

64

biotin-doxorubicin

Biotin-Dox conjugate **(64)** was designed to limit the adverse side effects of Dox. In this, the amine group of Dox was connected with a photocleavable biotinylated spacer.[301] Fluorescence microscopy on PTK2 epithelial cells proved the **64** was internalized ten times more than Dox. Unlike free Dox, which concentrated in nucleus, **64** remained outside the nucleus until photocleaved (UV 350 nm) to release Dox, which then accumulated inside the nucleus. Moreover, cytotoxicity of both Dox and its conjugates on the human lung cancer cell line showed a 200-fold lower cytotoxicity for the conjugate compared to that of free Dox. As expected, the cytotoxicities of both drugs become comparable after UV exposure. An in vivo application of this strategy is likely to be limited by the problems associated with permeation of light into tissues, especially at short wavelengths.

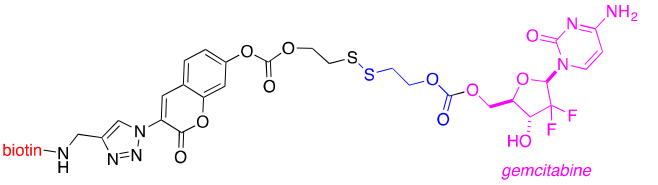

65

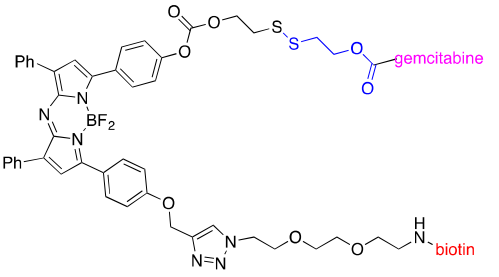

66

Some experimental theranostic targeted prodrugs **(65** and **66)** of gemcitabine also feature a disulfide cleavable linker. The prodrugs are fluorescent by virtue of the coumarin **(65)** or BODIPY **(66)** fluorophores. Upon addition of free thiols, disulfide bond cleavage occurs as well as release of active drug and concomitant increase of fluorescence intensity. Studies of these showed higher accumulation and cytotoxicity in biotin-sensitive cells.[302,303] Such theranostic agents are able to provide not only specific cellular drug release, but also real-time monitoring of the drug release in tissue.

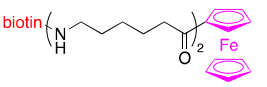

67

biotin-ferrocene

Ferrocene–biotin bioconjugates **(67)**[304] were most toxic to cells that expressed high levels of BR. Compounds with longer spacers attached to biotin were less cytotoxic.

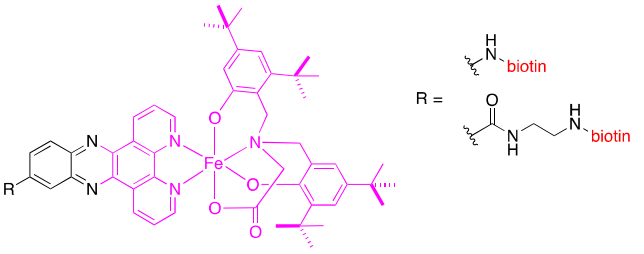

68

biotin-dipyridophenazine (dppz) iron (III) complex

Photocytotoxocities of iron (III) complexes of a tetradentate phenolate-based ligand and biotin-conjugated dipyridophenazine (dppz) bases **(68)** also seem to correlate with SMVT expression levels.[305]

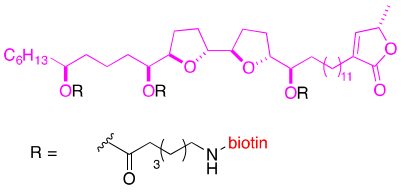

69

biotinylated-squamocin

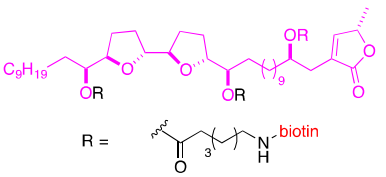

70

biotinylated-bullatacin

Cytotoxicities of biotinylated derivatives of squamocin **(69)** and bullatacin **(70)** are similar to the parent squamocin and bullatacin against a BR^- cell line.[306] However, the biotin conjugates showed significantly higher cytotoxicity than their parental drugs against BR^+ 4T1 (breast) and P815 (mastocytoma) cell lines, probably as a result of active targeting by biotin. These cytotoxicities were affected by the number of biotinyl residues included in the conjugates, the point of attachment of the biotinyl residue, and the spacer between the cytotoxic agent and biotin.

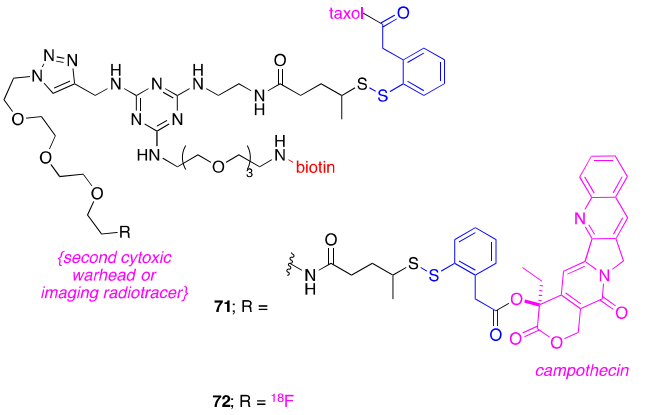

Dual-warhead conjugate DW-1 **(71)** consists of taxoid **(63)** and camptothecin, with biotin as the tumor-targeting moiety. Other features of the molecule include a 1,3,5-triazine splitter module, self-immolative disulfide linkers, and a tetraethylene glycol diamine spacer to increase the water solubility.[307] Compound **71** was evaluated against BR^+ and normal cell lines in the absence and presence of glutathione. With glutathione, **71** exhibited IC_{50} values of 3.22–9.80 nM against all BR^+ cancer cell lines, and 705 nM against the normal cells. Moreover, a cooperative effect was observed for the taxoid-camptothecin combination when two drugs were delivered to the cancer cells simultaneously in the form of dual-warhead conjugates and cleaved by exogenously added glutathione.

Similar tumor-targeting theranostic conjugates, bearing either a fluorine-labeled prosthetic as a potential ^{18}F-PET radiotracer ($R = {}^{18}F$, **72**) or a fluorescence probe-FITC in place of a second cytotoxic warhead, have also been prepared.[308] Efficient internalization and high selectivity for BR^+ cancer cells was confirmed. The **72** consistently showed higher potency towards BR^+ rather than BR^- cells independent of the addition of exogenous glutathione, with up to two orders of magnitude difference in IC_{50} values in line with the tumor-targeting feature of this drug delivery system. In terms of imaging, the multi-functionalized 1,3,5-triazine-based template is versatile and applicable to modalities such as PET, SPECT, or MRI by changing to a suitable probe or contrast agent.

L. Aminopeptidase N (CD13) Receptor

Angiogenic tumor vessels are important for tumor growth and metastasis. Metalloexopeptidase CD13 or aminopeptidase N (APN) is overexpressed on the endothelial cells of angiogenic tumor vessels.[309] Depending on which isoform, CD13 is a zinc-dependent, trans-membrane exoproteinase with sizes of 150–240 kDa. CD13 functions in protein degradation, cytokine regulation, antigen presentation, cell proliferation, cell migration, and plays a critical role in angiogenesis in cancer. High expression of CD13 occurs in some human solid tumors, including melanoma, prostate, lung and ovarian cancer.[310] CD13 is also expressed by many normal tissues, including epithelial cells from small intestine, renal proximal tubules, prostate, and bile duct canaliculi, keratinocytes, mast cells, myeloid cells, and antigen-presenting cells. Immunological studies with various anti-CD13 antibodies revealed different immunoreactive forms of CD13 in tumors in comparison with other tissues,[311] which is a feature that is critical when targeting this receptor for drug delivery or imaging.

Asparaginyl-glycinyl-arginine (NGR) peptide sequences were identified via phage display as a specific ligand of CD13.[309,312,313] NGR peptides have a threefold higher specificity for the detection of neoangiogenic vessels than RGD (argininyl-glycinyl-aspartic acid) peptides that

are widely used for the detection of $\alpha v\beta 3$ and $\alpha v\beta 5$ integrin expression (see Section 4-M). In addition, it has been shown that NGR can bind with new vasculature via APN (CD13) as well as integrin $\alpha v\beta 3$ receptors, although the binding mechanisms are different.[309]

NGR of pentapeptides appear to be the minimum binding motif, with the NGR sequence flanked by one amino acid at each end.[314] Cyclized forms featuring disulfide, amide, and triazole linkages NGR (generally, cNGR) can display stronger affinity and higher specificity toward the APN/CD13 receptors.[315] Immunohistochemical and biodistribution studies showed that the disulfide linked *cyclo*-{CNGRC}-bound CD13-positive tumor blood vessels (CNGRC is Cys-Asn-Gly-Arg-Cys) but not other CD13-rich normal tissue, presumably because there are different CD13 isoforms in cancer versus normal tissues.[311] Further, molecular dynamics simulations predicted that the most populated structures of CNGRC and GNGRG peptides are superimposable onto the highly conserved CTGNGRGEWKC loop of fibronectin type-I repeat. These observations perhaps account for the low immunogenicity of NGR peptides even when they are conjugated with highly immunogenic carriers, that is, they might mimic a self-antigen.[316]

In recent years, studies have shown that the NGR motif can rapidly convert to isoaspartate-glycine-arginine (isoDGR) by asparagine deamidation. This deamination can generate ligands for $\alpha v\beta 3$ integrin receptors that are capable of affecting endothelial cell functions and tumor growth.[309] Biochemical, NMR structure analysis, and alpha docking studies showed that isoDGR, but not NGR and DGR, can fit into the RGD-binding pocket of $\alpha v\beta 3$ receptor. However, it is unclear whether cyclic CNGRC peptide based constructs reported so far bind to CD13 or integrin receptor under tested in vivo conditions.

Several studies have reported conjugation of an NGR motif with chemotherapeutic drugs. A conjugated of an NGR peptide *cyclo*-{CNGRC} with Dox[314] showed reduced toxicity and improved efficacy against human cancer xenografts in nude mice, compared with free Dox. Marked reduction in metastasis development and prolongation of long-term survival were also observed.

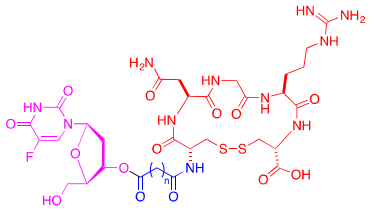

73, **CNF1**; n = 2 (fast hydrolyzed)

74, **CNF2**; n = 3 (slow hydrolyzed)

5-FdUrd-CNGRC conjugates

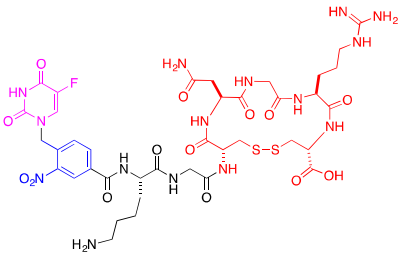

75

5-FU-CNGRC conjugates

Cyclo-{CNGRC} has been conjugated to 5-fluoro-2'-deoxyuridine (5-FdUrd) (**73, 74**) and to 5-fluorouracil **(75)** via succinate **(73)** and glutarate **(74)**-based esters, or a photolabile 2-nitrobenzyl chromophore cleavable upon UV-irradiation at *k*ex = 365 nm.[317,318] The 5-FdUrd conjugates were of lower cytotoxicity compared to free 5-FdUrd, showing more selective cytotoxicity toward CD13 positive cells (HT-1080) than toward APN/CD13 negative cells (HT-29, MDA-MB-231). The bioactivity of the **75** was not reported.

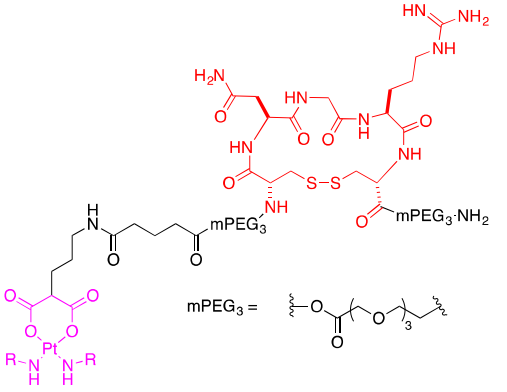

76, **cyclic mPEG-CNGRC-Pt**; R = H

77, **cyclic mPEG-CNGRC-Pten**; R = CH_2CH_2;

NGR-carboplatin

Two Pt-peptide conjugates, cyclic mPEG-CNGRC-Pt **(76)** and cyclic mPEG-CNGRC-Pten **(77)** bearing the NGR targeting sequence, a malonoyl linker, and oligoethylene glycol groups, have been prepared.[319] The pegylated peptide is nontoxic, water soluble, and has insignificant peptide immunogenicity. The targeted Pt-peptide conjugates are more cytotoxic to PC-3 (CD13+) cells than untargeted carboplatin. Platinum uptake on PC-3 cells was 12-fold more for **76** and threefold more for **77** compared to that of the untargeted carboplatin, indicating selective binding of the CD13 receptors and delivery of the conjugates to CD13 positive cells.

There are several NGR peptide-derivatives for tumor imaging. An NGR peptide YGG-*cyclo*-{CNGRC} was directly labeled with the ^{99m}Tc SPECT label (full structure was evaluated in nude mice bearing a $CD13^+$ liver tumor).[320] Rapid, significant tumor uptake and slow tumor washout was observed for this conjugate. The xenografted tumor became visible at 1 hr and the highest tumor-to-muscle ratio was observed at 8 hr.

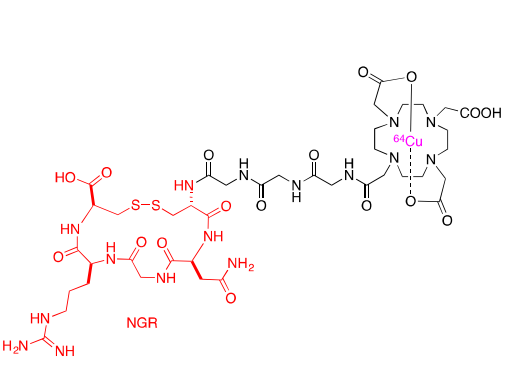

78

^{64}Cu-DOTA-NGR1

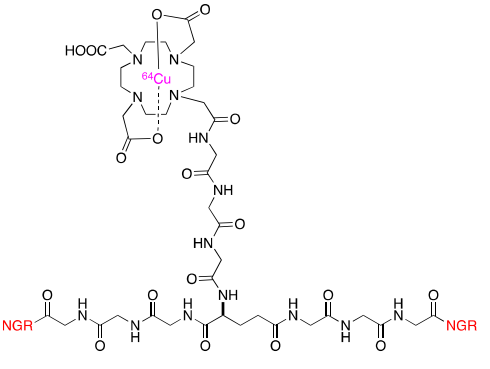

79

^{64}Cu-DOTA-NGR2

Radiolabeled NGR derivatives have also been made for PET imaging via ^{64}Cu or ^{68}Ga.[321] Monovalent ^{64}Cu-DOTA–NGR1 **(78)** and bivalent ^{64}Cu-DOTA–NGR2 **(79)** both bound CD13^{+} HT-1080 cells in the low nanomolar range. The binding affinity was 1.27 nM in **79,** which was about twofold higher than the **78**. For small animal microPET studies, **79** showed higher tumor uptake and slower tumor washout in CD13-positive HT-1080 tumor xenografts as compared to **78**. Both **78** and **79** had higher tumor uptake and better tumor-to-normal organ contrast in CD13-positive HT-1080 tumor xenografts compared with CD13-negative HT-29 tumor xenografts. The high uptake was reduced by coinjecting a blocking dose of cyclic NGR peptide [c(CNGRC)]. Compound **79** showed higher tumor uptake and better tumor retention than **78**, presumably due to the bivalency effect and increase in apparent molecular size.

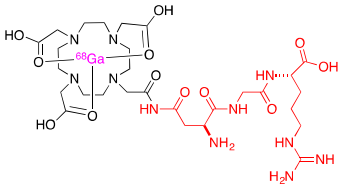

80

^{68}Ga-DOTA-NGR

^{68}Ga-DOTA-NGR **(80)** was studied as a PET probe for noninvasive detection of CD13-positive tumors and their neovasculature.[322] Cellular uptake was measured in A549 (CD13^{+}) and MDA-MB-231 (CD13^{-}) cells, while biodistribution and PET imaging were performed in A549 and MDA-MB-231 xenografts. CD13 expression in tumors and new vasculatures were analyzed by immunohistochemistry. Conjugate **80** was taken up by A549 cells (blocked by unlabeled DOTA-NGR) but not by MDA-MB231 cells. An in vivo biodistribution study showed that **80** was mainly excreted from the kidney and was rapidly cleared from blood and other organs. MicroPET imaging showed that high focal accumulation had occurred at the tumor site 1 hr post injection in A549 tumor xenografts. A significant reduction of tumor uptake was observed following coinjection with a blocking dose of DOTA-NGR, whereas only mild uptake was found in MDA-MB-231 tumor xenografts. Maximum tumor-to-normal tissue signal value was observed at 1.5 hr post injection.

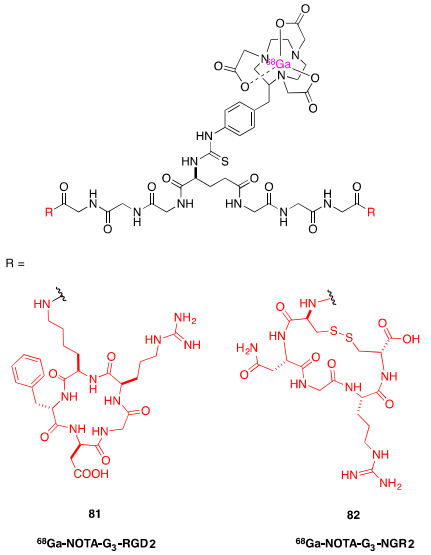

81 **82**

^{68}Ga-NOTA-G$_3$-RGD2 **^{68}Ga-NOTA-G$_3$-NGR2**

Two PET probes, ^{68}Ga-NOTA- G_3-RGD2 (NOTA is 1,4,7-triazacyclononane-N,N0,N00-triacetic acid) **(81)** and ^{68}Ga-NOTA-G_3-NGR2 **(82)**, have been made for noninvasive monitoring of CD13 positive fibrosarcoma.[323] Both were hydrophilic, stable in vitro and in vivo, and were excreted predominantly and rapidly through the kidneys. For both probes, the tumor uptake by fibrosarcoma xenografts and accumulation in vital organs were determined. However, no significant difference in tumor uptake and *in vivo* biodistribution was observed for the two probes.

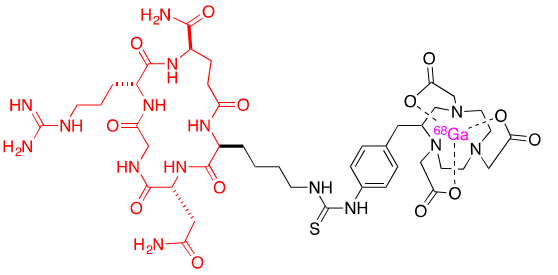

83

^{68}Ga-labeled NOTA-c(NGR)

CD13 specificity of ^{68}Ga-labeled NOTA-c(NGR) **(83)** in orthotopic and heterotopic transplanted mesoblastic nephroma (NeDe) bearing Fischer-344 rats using miniPET was studied.[310] Scans were performed for both **83** and $\alpha v\beta 3$ integrin selective ^{68}Ga-NODAGA-[c(RGD)]$_2$. Nonradiolabeled tracers selective for $\alpha v\beta 3$ integrin were also prepared and investigated as control. Both NeDe tumors and metastases were confirmed to express CD13 receptors by Western blot. Biodistribution studies in normal rats showed that uptake of the **83** was significantly lower in abdominal organs in comparison with ^{68}Ga-NODAGA-[c(RGD)]$_2$. In NeDe tumor bearing rats, higher **83** accumulation was found in the tumors than that of the ^{68}Ga-NODAGA-[c(RGD)]$_2$. In an orthotopic model, specific uptake of **83** was detected in metastatic tumors.

An inhibitor of CD13, probestin, is unique insofar as it has been radiolabeled for tumor specific imaging in a system that did not feature NGR peptides. However, the chelator ligand designed to complex with radiolabels Re(V) or ^{99m}Tc(V)[324] is peptidic: tripeptide *N,N*-dimethylglycyl-L-lysinyl-L-cysteinylamide (N_3S).[324] The conjugates showed high inhibition of CD13 enzyme activity, and strong tumor uptake relative to normal tissues that was blockable with a nonradioactive conjugate. This work has demonstrated the feasibility of using high affinity inhibitor conjugates for in vivo targeting of CD13 positive tumors.

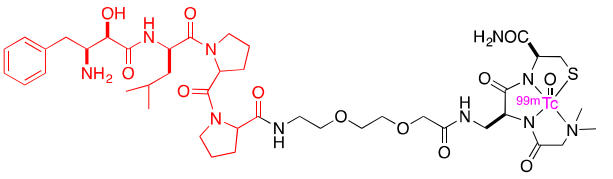

84

^{99m}TcO-N_3S-PEG$_2$-Probestin

CD13 is a zinc-dependent exopeptidase that catalyzes the removal of *N*-terminal amino acids from peptides and can be inhibited by antibodies and bestatin drug. ReO-N_3S-probestin conjugates demonstrated higher inhibition of CD13 enzyme activity than bestatin. An in vivo biodistribution study of ^{99m}TcO-N_3S-PEG$_2$-Probestin **(84)** in mice xenografted with fibrosarcoma tumors showed visible tumor uptake at 1 hr post injection. When CD13 was competitively blocked with a coinjection of excess nonradioactive ReO-N_3S-PEG$_2$-Probestin conjugate,

tumors were no longer visible, demonstrating the specificity of CD13 inhibitor conjugates for in vivo targeting of CD13-positive tumors.

M. Integrin Receptor

Integrins are heterodimeric transmembrane glycoproteins on cell surface. Among the integrins, $\alpha V\beta 3$ and $\alpha V\beta 5$ are frequently overexpressed in tumor endothelial cells as well as on lung, breast, melanoma, prostate, ovarian carcinoma, and brain tumors.[325] They mediate cell adhesion to the extracellular matrix and have a fundamental role in increasing migration, invasion, proliferation and survival of tumors. In addition, integrins have been linked to tumor angiogenesis, which is an essential process for tumor growth and metastasis. These cell adhesion molecules $\alpha V\beta 3$ and $\alpha V\beta 5$ are not readily detectable in quiescent vessels. The consensus tripeptide motif RGD (Arg-Gly-Asp) has high affinity for $\alpha V\beta 3$ and $\alpha V\beta 5$ integrins. The restricted expression profile of integrins offers the possibility of using carriers based on RGD-containing peptides or peptidomimetics to deliver chemotherapeutic drugs or radionuclides into cancer cells or for tumor imaging purposes.

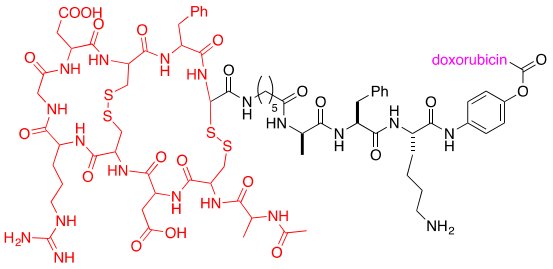

85

Dox-RGD-4C

Using an in vivo phage display technology, Arap and co-workers discovered cyclic RGD-4C peptides bind to integrins $\alpha V\beta 3$ and $\alpha V\beta 5$[314] and developed a Dox conjugate **(85)** bearing a bivalent RGD-4C peptide (ACDCRGDCFCG). Conjugate **85** showed improved activity and toxicity profile over Dox in a mouse breast cancer model having integrin $\alpha V\beta 3$ expression in the tumor vessels as well as on the tumor cell themselves. Interestingly, superior efficacy of the **85** was confirmed in another model (hepatoma) in which the tumor cells did not express integrin $\alpha V\beta 3$ suggesting that a direct endothelial effect was responsible.[326] Using the same RGD-4C ligand, a second tumor-specific peptide sequence (D-Ala-Phe-Lys) was added to generate a dual-targeted Dox prodrug. D-Ala-Phe-Lys is selectively recognized by the tumor associated protease plasmin involved in tumor invasion and metastasis.[327] The resultant conjugate was able to bind integrin receptors and showed cytotoxicity for endothelial cells and fibrosarcoma cells in a plasmin-dependent manner. No in vivo data were reported.

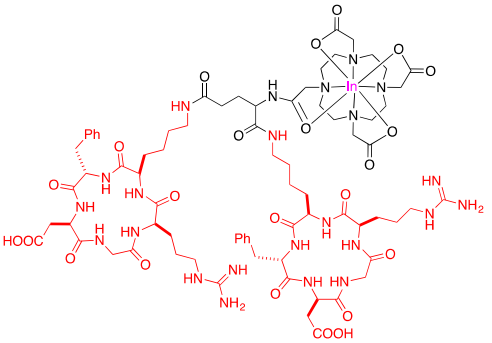

86

^{111}In-[c(RGDfK)]$_2$

A radiolabeled dimeric RGD peptides E-[c(RGDfK)]$_2$ **(86)** showed improved tumor targeting properties over the monomeric form in both in vitro and in vivo mouse models.[328] In vitro, the IC_{50} showed a tenfold higher affinity of the dimer for the $\alpha V\beta 3$ integrin as compared to the monomer (0.1 vs. 1.0 nM). In biodistribution studies, **86** demonstrated integrin $\alpha V\beta 3$ receptor binding specificity despite significant uptake in nontarget organs such as liver and spleen. Tumor uptake peaked at 1–2 hr post injection. An MTD dose of ^{90}Y-labeled conjugate in mice with small subcutaneous tumors caused significant growth delay as compared with mice treated with ^{90}Y-labeled scrambled peptide or untreated mice.[329] Potentially, these peptides can be used for peptide receptor radionuclide imaging as well as therapy.

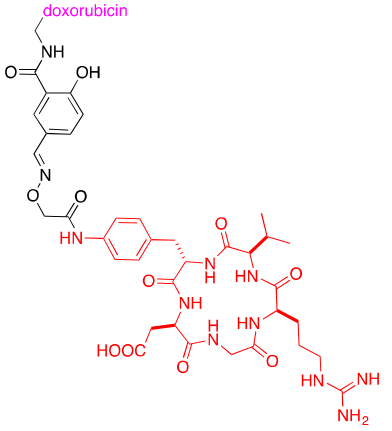

87

cyclic-(N-Me-VRGDf-NH)-doxsaliform

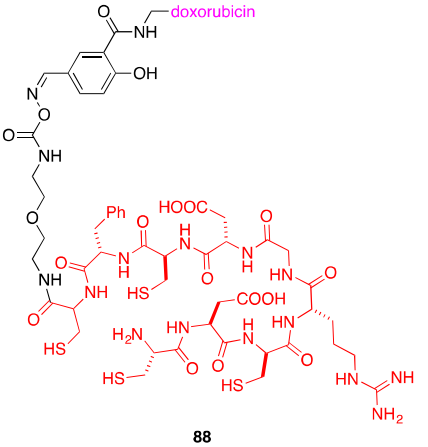

88

acyclic-RGD-4C-doxsaliform

Doxsaliform, a Dox prodrug was conjugated to two different $\alpha V\beta 3$-targeting peptides, CDCRGDCFC (RGD-4C) and cyclic-(N-Me-VRGDf) (Cilengitide) to form cyclic-(*N*-Me-VRGDf-NH)-doxsaliform **(87)** and acyclic-RGD-4C-doxsaliform **(88)**. Cilengitide has completed phase III clinical trials (data unpublished) as an angiogenesis inhibitor for patients with glioblastoma multiforme (NCT00689221). Acyclic agent **88** exhibited good binding affinity for $\alpha V\beta 3$ but less tightly relative to the peptide alone (10 versus 1 nmol/L). The cyclic **87** maintained high affinity for $\alpha V\beta 3$ (5 nmol/L). Both **87** and **88** were more cytotoxic than clinical

Dox and comparable in cytotoxicity to doxsaliform when tested in mouse breast cancer cells. The authors suggested that the complete drug construct did not penetrate through the plasma membrane, but the active metabolite did on release from the targeting group.

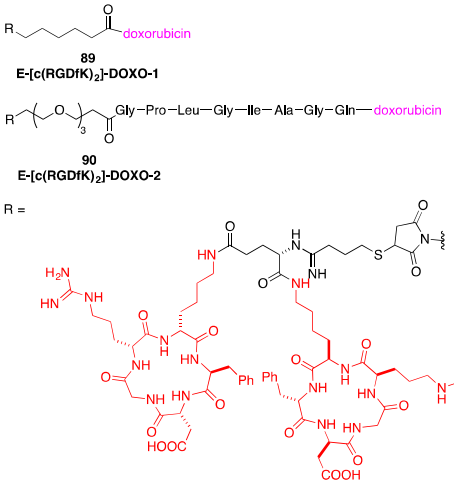

Water-soluble Dox conjugates with E-[c(RGDfK)2] were generated by binding to maleimide Dox via two different linkers to generate E-[c(RGDfK)$_2$]-DOXO-1 **(89)** and E-[c(RGDfK)$_2$]-DOXO-2 **(90)**.[330] In **89**, Dox was bound to the peptide through a stable amide bond. In **90**, a matrix metalloproteinase (MMP) 2/MMP-9 cleavable octapeptide was introduced between Dox and the peptide to target the tumor vasculature. Proliferation of endothelial cells in the presence of **90** was reduced six- to tenfold higher compared to that of **89**. In addition, inhibition of HUVEC sprouting during a 24-hr exposure was approximately threefold stronger for **90** than for Dox alone. Disappointingly, in vivo studies in a xenograft model demonstrated no or only moderate antitumor efficacy for either conjugate compared to Dox. The authors suggested that the lack of activity could have been due to the inefficient drug cleavage by MMP-2 or the low potency of Dox drug and rapid drug clearance in vivo.

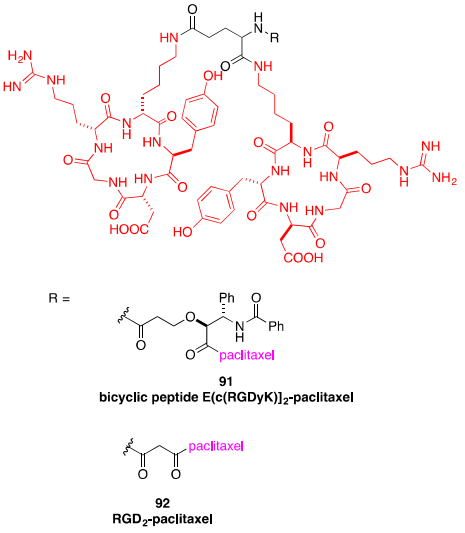

Another cytotoxic agent that has been conjugated to synthetic integrin ligands, specifically E[c(RGDyK)]$_2$, is PTX to give **91**.[331] Similar to free PTX, the **91** inhibited cell proliferation through an arrest of G(2)/M-phase of the cell cycle and induced apoptosis. Although the **91** showed slightly decreased integrin binding affinity than the unconjugated peptide, it had integrin specific accumulation in vivo. ^{125}I-labeled **91** showed highest tumor uptake at 2 hr post injection and best tumor-to-background contrast after 4 hr post injection. Another report involving PTX conjugation was a dimeric RGD peptide-PTX conjugates (RGD$_2$-PTX **92**).[332] Radiolabeled ^{3}H-**92** had higher initial tumor exposure dose and prolonged tumor retention than ^{3}H-PTX in mouse breast cancer. Metronomic low-dose treatment of breast cancer using **92** is significantly more effective than PTX+RGD$_2$ combination and solvent control. Although in vivo of 3′-deoxy-3′[^{18}F]-fluorothymidine (^{18}F-FLT) PET imaging and ex vivo Ki67 staining indicated little effect of the PTX-based drug on cell proliferation, ^{18}F-fludeoxyglucose (^{18}F-FDG) PET imaging showed significantly reduced tumor metabolism in the **92**-treated mice versus those treated with PTX+RGD$_2$ and solvent control. Moreover, the microvessel density was significantly reduced after **92** conjugate treatment. These results demonstrate that integrin-targeted delivery of PTX allows preferential cytotoxicity to integrin-expressing tumor cells and tumor vasculature.

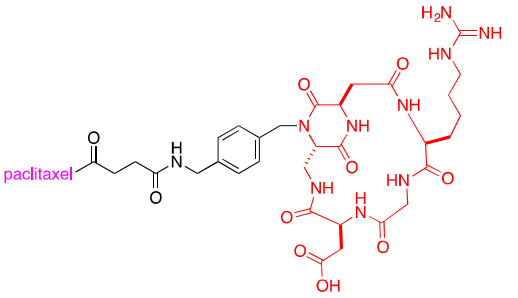

93

***cyclo*[DKP-*f3*-RGD]-PTX**

Another series of RGD-PTX conjugates bound the purified $\alpha V\beta 3$ integrin receptor at low nanomolar concentration and showed similar in vitro cytotoxic activity to PTX even against the cisplatin-resistant IGROV-1/Pt1 cells expressing high levels of integrin $\alpha V\beta 3$.[333] One of the conjugates, cyclo[DKP-f3-RGD]-PTX **(93)** had good stability in both human and murine plasma, and superior tumor-targeting in mice with the IGROV-1/Pt1 human ovarian carcinoma.

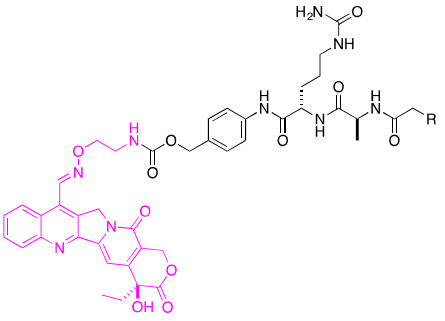

NMT (ST1968, Namitecan)

94; R =

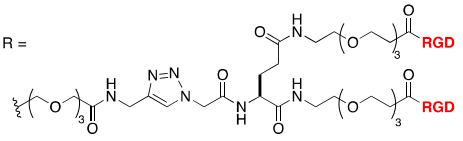

95; R =

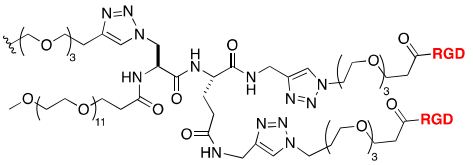

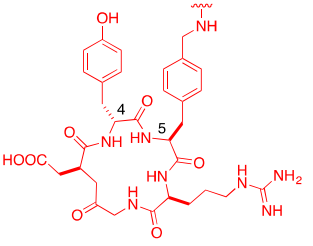

RGD

Eight RGD conjugates of a camptothecin derivative[334] were investigated for different linkage conformations, lengths and chemistries including heterofunctional glycol fragments and a lysosomally cleavable peptide, and their effects on solubility, receptor affinity, systemic stability, and cytotoxicity. Among the conjugates prepared, only drugs which consist of dimeric RGD ligands **(94, 95)** connected to the camptothecin derivative through multiple glycol chains in a branched conformation showed high receptor affinity and tumor cell adhesion, had acceptable stability in murine blood and high cytotoxic activity (IC_{50} = 8 nM).

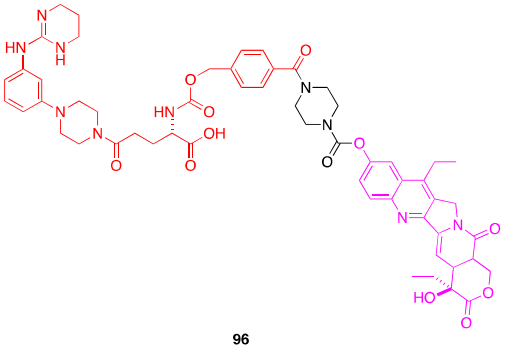

96

ST7456CL1

Four camptothecin analogs with an RGD peptide mimetic were prepared to improve their therapeutic index.[335] The conjugate with SN-38 (10-hydroxy-7-ethylcamptothecin) ST7456CL1 **(96)** bound strongly to integrin receptors (IC_{50} = 1.3 nM for $\alpha V\beta 3$, 1.0 nM for $\alpha V\beta 5$), inhibited adhesion of vitronectin on tumor cells and showed better antiproliferative activity on high integrin-expresser cells than cells with low integrin levels. In vivo, **96** was more stable than irinotecan in rat plasma. It also increased the life span of mice with PC3 prostate tumors

and reduced the area of metastases compared with vehicle-treated group. This conjugate also showed similar tumor growth inhibition (39%) pattern in a renal carcinoma mouse model overexpressing $\alpha V\beta 3$ and $\alpha V\beta 5$, comparable to those observed with irinotecan.

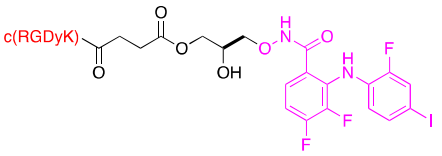

97

RGD-MEK1

Two series of RGD conjugates containing an MEK1/2 kinase inhibitor **(97)** were rare insofar as they carry a drug cargo that is an enzyme inhibitor.[336] The first series, alkoxylamine analog RGD-MEKI conjugates showed moderate antiproliferation activity in melanoma cells harboring $BRAF^{v600E}$ (v-raf murine sarcoma viral oncogene homolog B1) mutation (the valine 600 to glutamate mutation of BRAF kinase). This mutation causes increased kinase activity and these cells are known to be exquisitely sensitive to MEK inhibitor treatment. PEGylation increased the IC_{50} value of an analogue by threefold in the $BRAF^{v600E}$ melanoma cells. A multi-cRGD peptide analog improved the receptor specific antiproliferation activity in integrin-overexpressing cells. In the second series, a succinic anhydride group was added between RGD and the MEK inhibitor. It had better antitumor properties compared to the first series by both inhibition of kinase activity and DNA replication, resulting in higher proliferation inhibition of integrin-overexpressing cells than the parent drug in a dose-dependent manner.

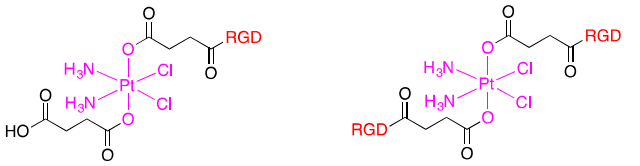

98 **99**

mono-and difunctionalized platinum (IV) complexes

An RGD peptide motif was conjugated to a series of mono- **(98)** and difunctionalized **(99)** platinum (IV) complexes to target tumor endothelial cells selectively over healthy cells.[337] From concentration–response curves against different endothelial and human cancer cells expressing $\alpha v\beta 3$ and $\alpha v\beta 5$, conjugates **98** and **99** were equally potent inhibitors of cellular proliferation and more so when compared to platinum(IV) compounds with NGR or nonspecific peptide moieties. Integrin $\alpha v\beta 3$ mediated the antiproliferative effect, as demonstrated by a decreased inhibitory response when endothelial cells were either (1) incubated with an excess of $\alpha v\beta 3$/$\alpha v\beta 5$-specific RGD pentapeptides or (2) transfected with RNAi for $\beta 3$, but not $\beta 1$, integrins.

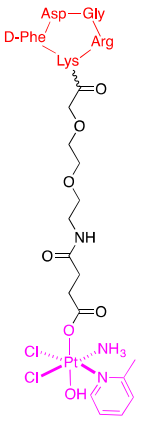

100

Pt-RAFT-c(RGDfK)

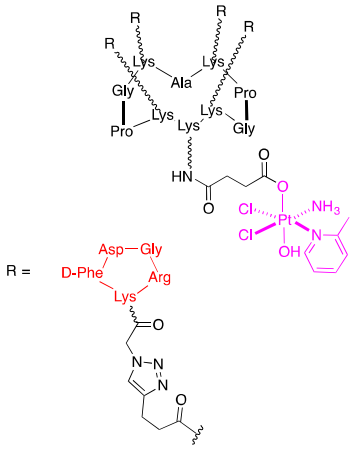

101

Pt-RAFT-{c(RGDfK)}$_4$

Another example of RDG-Pt(IV) derivatives involved conjugates with monomeric **(100)** and tetrameric **(101)** RGD-containing peptides.[338] The antitumor activity of Pt(IV) drug in high integrin expressing melanoma cells was increased by 2.6-fold when it was conjugated to monomeric and by 20-fold when conjugated to tetrameric. In contrast, the cytotoxicity of the conjugates was less in control cells lacking $\alpha V\beta 3$ and $\alpha V\beta 5$ integrin expression. Cellular uptake studies confirmed a good correlation between the levels of expression of integrins, intracellular platinum accumulation and antitumor activity. Indeed, accumulation and cytotoxicity were much higher in integrin positive cells than in integrin negative cells, being particularly higher in the case of the **101**, alluding to the importance of having multivalency. In addition, the authors also observed that exposure of the cells to the unconjugated peptides alone induced morphological changes followed by cell detachment from the plate surface—a cell death phenomenon known as anoikis that is reportedly associated with RDG-containing peptides.[339]

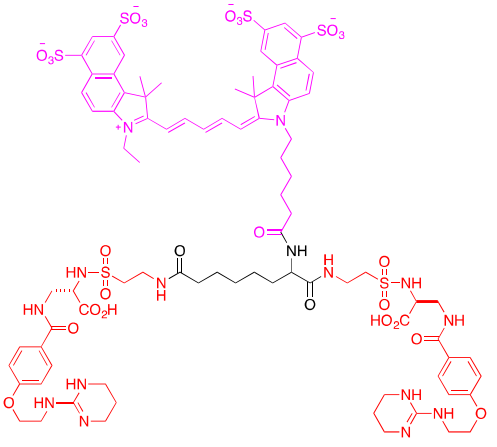

102

bivalent IA Cy5.5

A bivalent imaging compound bivalent-IA-Cy5.5 **(102)** consisting of a rare non-peptidic targeting ligand for integrin $\alpha V\beta 3$ receptor was prepared on the basis of an in silico rational design approach.[340] Compound **102,** which has a near-infrared fluorescent imaging probe, demonstrated strong binding affinity to integrin receptor ($IC_{50} = 0.13 \pm 0.02$ nM), integrin-mediated endocytosis in cells that was effectively blocked by a similar nonfluorescent bivalent compound and tumor accumulation in integrin positive mouse xenograft. The bivalent ligand without the imaging probe binds 50-fold more tightly than the equivalent monovalent ligand.

5. CANCER TYPES AND THEIR SMALL-MOLECULES CONJUGATES

We have tabulated some small-molecule conjugates that have been studied in preclinical animal models and clinical settings according to the target tumor organ. Newly developed small-molecule conjugates that are currently being studied in ex vivo stages are excluded (but are described in Section 4). Table I focuses on cancer therapeutics whereas Table II is for cancer imaging.

6. OTHER IMPACTS OF ACTIVE TARGETING

Active targeting tends to be imperfect because most of the delivering agents used are natural ligands. Moreover, most of the receptors discussed here are expressed on normal healthy cells, albeit at lower levels than in cancer cells. For example, kidney cells express the FR and receptor mediated uptake of folate-cargoes conjugates in renal cells has been reported to induce renal toxicities or high level of nontarget retention of imaging agents.[83]

Immunomodulation is another impact of small-molecule ligand conjugates. Some small-molecules ligands used in targeting are inhibitors and antagonists of transcription factors involved in cytokines production.[341] In a specific example, FRs are expressed in activated monocytes and lymphocytes.[342,343] Binding of folate substrates to FR can promote survival of these immune cells while blocking of FR can lead to cell death. Regulatory T cells are immunosuppressive and high expressors of FR. FR-targeted therapies have potential in antitumor immunity as well as therapies for autoimmune and inflammatory diseases.[344] E2 is another small-molecule ligand with immunomodulation capability. Indeed it has been used to suppress inflammatory cytokines such as TNF-α and IFN-γ in the treatment of autoimmune disease[345] while promoting antiinflammatory IL-10 cytokine secretion and enhancing regulatory T cells function via upregulation of programmed death-1 and FoxP3 expressions.[346] Therefore, when using receptor targeted ligands as delivery agents for anticancer drugs, modulation of the immune system can be counterproductive. In cases where the ligand is eliciting an antitumor immune response, combination immunotherapy can increase the antitumor immune responses of the conjugate.[89,347] Figure 4 shows some possible impacts induced by active targeting agent on nontargeted cells.

7. CONCLUSIONS

Some generalities apply to every receptor used for targeting. Successful delivery requires favorable expression levels of the relevant cell surface receptors. Rates of recycling or regeneration of these receptors are also important. Active delivery of toxic drugs can be used to target cells that would otherwise be resistant to the untargeted drug cargo. Conversely, some compounds that might be too toxic to use "as is" can be usable in active targeting because this increases their

Table I. Small-Molecule Conjugates for Cancer Therapeutics in Preclinical Animal Model and Clinical

Cancer type	Small-molecule conjugates (structure numbering)	Target	Study stages	Status	Graft/ tumor	Remarks	References
Breast	Folate-tubulysin B hydrazide (EC1456)	FR	In vivo	Preclinical	Xenograft MDA-MD-231	100% cure in large size tumor (750 mm^3) and syngeneic M109 murine lung carcinoma	106
			Clinical phase I/II	Ongoing	Advanced solid tumor	Active, recruiting participants	NCT01999738
	CNGRC-doxorubicin	CD13	In vivo	Preclinical	Xenograft MDA-MD-435	Tumors were 0.2–0.25 of the size of control tumors, reduced metastasis, prolonged survival, less toxic	337
	RDG-4C-doxorubicin (**85**)	Integrin	In vivo	Preclinical	Xenograft MDA-MD-435	Compared to Dox-treated control, all mice outlived by >6 months, had smaller tumors, less lymph spreading and lung metastasis, had widespread tumor cell death, less toxic to liver and heart	337
	RGD-paclitaxel (**91**)	Integrin	In vivo	Preclinical	Xenograft MDA-MD-435	Showed integrin-specific accumulation, highest tumor uptake at 2 hr post injection, best tumor/background ratio after 4 hr post injection, no efficacy data	352
	RGD2-paclitaxel **(92)**	Integrin	In vivo	Preclinical	Xenograft MDA-MD-435	Higher initial tumor dose and prolonged tumor retention than PTX, more effective and more apoptosis than PTX + RGD2, little effect on cell proliferation, reduced tumor metabolism and microvessel density	353
	IY-IY-Boron dipyrromethene (**30**)	TrkC	In vivo	Preclinical	Syngeneic 4T1	High accumulation in tumor at 1–6 hr, 71% full remission up to 90 days with no metastasis	195
Kidney	Monovalent AAZ-DM1	CAIX	In vivo	Preclinical	Xenograft SKRC52	Promote tumor shrinkage and delay tumor growth, 22× higher accumulation in tumor vs. scrambled control	209

Continued

Table I. Continued

Cancer type	Small-molecule conjugates (structure numbering)	Target	Study stages	Status	Graft/ tumor	Remarks	References
	Divalent AAZ-DM1 (**31**)	CAIX	In vivo	Preclinical	Xenograft SKRC52	75% tumor reduction vs. initial size, 33% full remission up to 90 days	210
	EC17 (**4**) + EC90 vaccine + GPI 0100 adjuvant	FR	Clinical phase I	Completed	—	Moderate antitumor activity, 4% PR, 54% SD, 43% PD after first cycle. 53.6% SD after three cycles.	84
	EC17 (**4**) + EC90 + GPI0100 + IL-2 + IFN-α	FR	Clinical phase I	Terminated	—	Moderate antitumor activity, 29% SD (123–340 days), 4% PR (71 days)	85 NCT00485563
	ST7456CL1 (**96**)	Integrin	In vivo	Preclinical	Xenograft A498 carcinoma	Inhibit tumor growth by 39%	356
	CRL-L1-tubulysin B hydrazide	CCK2R	In vivo	Preclinical	Xenograft HEK293	Eliminate all tumor lesions and prolong survival in $CCK2R^+$ tumor	132
Pancreatic	SV119-Bim (**24**)	Sigma-2	In vivo	Preclinical	Syngeneic Panc02	Significantly reduced tumor growth treated for 12 days (2 days once) and approximately 50% of mice survive without clinical toxicities	167
					Xenograft CEPAC	Tumor regression within 7-day continuous treatment and regrowth when treatment discountinued	167
	SWIV-134 (**25**)	Sigma 2	In vivo	Preclinical	Syngeneic KCM, xenograft AsPC-1	Delayed tumor growth and increase survival. Improved survival in AsPC-1 (88 days in SWIV-134 vs. 52 days in control) with one tumor free and survive up to 11 months	169
	Glufosfamide (**32**)	GLUT	Clinical phase I/II	Completed	—	5.8% PR, 32.4% SD (median OS 5.3 months, PFS 1.6 months)	169, 225, 229 NCT00005053
	Glufosfamide + gemcitabine as first-line therapy	GLUT	Clinical phase III	Completed	—	31% SD in glufosfamide + gemcitabine, 19% SD in gemcitabine alone	232 NCT00099294
	Glufosfamide + gemcitabine	GLUT	Clinical phase I/II	Completed	—	52.6% SD (70% SD for 4 months, 30% SD for 6 months)	227 NCT00102752

Continued

Table I. Continued

Cancer type	Small-molecule conjugates (structure numbering)	Target	Study stages	Status	Graft/ tumor	Remarks	References
Non-small-cell lung cancer	Glufosfamide (**32**)	GLUT	Clinical phase II	Completed	—	2.7% PR, 49% SD (median OS 5.8 months)	226 NCT00005055
	EC145 (**7**) ± docetaxel	FR	Clinical phase II	Ongoing	—	Active but yet recruiting participants	NCT01577654
Ovarian	SW-III-123 (**25**)	Sigma 2	In vivo	Preclinical	Xenograft SKOV3	Median OS 86.5 days, 10 days higher than control and ligand alone	171
	Glufosfamide + platinum-based chemotherapy	GLUT	Clinical phase II	Terminated	—	Renal function limits the enrolment. No confirmed tumor responses reported	Threshold Pharmaceuticals NCT00442598
	D-glucose- succinic acid-adriamycin (**36**) (2DG-SUC-ADM)[a]	GLUT-1	In vivo	Preclinical	Xenograft SKOV3	High accumulation in tumor post 2 hr administration, detectable up to 48 hr in tumor, 68.8% tumor growth inhibited vs. free drug 47.1%	239
	EC145 (**7**)	FR	Clinical phase II	Completed	—	42% DCR (Median OS: 14.6 months for 100% FR, 9.6 months for 10–90% FR, 3 months for 0% FR expression).	95 NCT00507741
	Epofolate (**10**) BMS-753493[b]	FR	Clinical phase I/IIa	Discontinued	Solid tumors	Majority was ovarian cancer (n = 16) studied with other solid tumors, best overall response is 19–23% SD, 50% PD	105 NCT00550017
	E-[c(RGDfk)2]-DOXO-1 (**89**) E-[c(RGDfk)2]-DOXO-2 (**90**)	Integrin	In vivo	Preclinical	Xenograft NIH: OVCAR-3	No or only moderate antitumor efficacy compared to doxorubicin	351
	Cyclo[DKP-f3-RGD]-paclitaxel (**93**)	Integrin	In vivo	Preclinical	Xenograft IGROV-1/Pt1	Dose-related antitumor effect observed, better tumor volume inhibition than paclitaxel, no deaths or significant weight losses	354

Continued

Table I. Continued

Cancer type	Small-molecule conjugates (structure numbering)	Target	Study stages	Status	Graft/ tumor	Remarks	References
Melanoma	Fluorodeoxyglucose-chlorambucil(FDG-chlorambucil) (**34**, **35**)	GLUT	In vivo	Preclinical	Syngeneic B16F0	80–90% inhibition in tumor sizes at 20 days post tumor inoculation, 57% inhibition in free drug	238
Glioblastoma	Glufosfamide (**32**)	GLUT	Clinical phase II	Completed-discontinued	—	No significant antitumor activity	228 NCT00014300
Head and neck	Glufosfamide (**32**)	GLUT	Clinical ex vivo	Biopsy sample for colony formation assay	—	31% of primary tumor specimen that resist to cisplatin was sensitive to glufosfamide.	230
	EC145 (**7**)	FR	Clinical phase I	Completed	—	100% SD (95–211 days)	94 NCT00308269
Nasopharyngeal	EC0489 (**8**) (completed phase i clinical trial, unpublished)	FR	In vivo	Preclinical	Xenograft KB cell	100% cure at dosage of more than 2 μmol/kg, higher tolerability and clearance via urine	97 NCT00852189
Colorectal	Fluorodeoxyglucose-chlorambucil(FDG-chlorambucil, **34, 35**)	GLUT	In vivo	Preclinical	Syngeneic CT-26	75–90% inhibition at 26 days post tumor inoculation, 66% inhibition in free drug	238
	Glufosfamide (**32**)[c]	GLUT	Clinical phase I	Completed	—	Minor tumor shrinkage, 57% SD	362
	Folate-methyl-β-cyclodextrin (FA-M-β-CyD) (**12**)	FR	In vivo	Preclinical	Syngeneic CT-26	100% regression in tumor and survive up to 140 days at 5 mg/kg.	108
Prostate	EC 1169 (PSMA inhibitor-tubulysin b hydrazide) (**23**)	PSMA	In vivo	Preclinical	Xenograft LNCaP	71% tumor regression, 29% cure with disease free more than 90 days	155
			Clinical phase I	Ongoing	—	Recruiting participants	NCT02202447
	EC0225 (**9**)[d]	FR	Clinical phase I	Completed	—	MTD 2.3 mg/m^2; SD for 10 months	102 NCT00441870
	11β-dichloro (**54**)	AR	In vivo	Preclinical	Xenograft LNCaP	90% inhibition of tumor volume at 30 mg/kg (5 days daily for seven consecutive weeks)	306

Continued

Table I. Continued

Cancer type	Small-molecule conjugates (structure numbering)	Target	Study stages	Status	Graft/ tumor	Remarks	References
	ST7456CL1 (**96**)	Integrin	In vivo	Preclinical	Xenograft PC3	Increased the life span by 34% and reduced metastases by 64% compared with vehicle control	356
Urinary bladder	EC0905 (**11**)	FR	In vivo	Preclinical	Canine invasive urothelial carcinoma	56% PR, 44% SD. Median OS is 115 days.	65
Liver	RGD-4C-doxorubicin (**85**)	Integrin	In vivo	Preclinical	Allograft MH134	Suppressed tumor growth more than free dox, prominent tumor cell death, complete tumor cell necrosis in 40% of cases	347

[a]Conducted syngeneic S180 sarcoma model with 64% inhibition in tumor sizes compared to adriamycin with 50% inhibition.

[b]Other solid tumors are colorectal ($n = 12$), lung ($n = 7$), breast ($n = 6$), endometrium ($n = 2$), prostate ($n = 3$), pancreas ($n = 2$), kidney ($n = 2$), one each for the uterine, anal, urothelial, head and neck, hepatocellular, melanoma, uterine leiomyosarcoma, gastric cancer, gastrointestinal stromal tumor, chondrosarcoma, testicular cancer, mesothelioma, thymoma, sinus cancer, and small bowel cancer.

[c]Conducted for one patient for NSCLC (SD), thymic cancer (SD), gallbladder cancer (PR > 5 months with fluorouracil, cisplatin, gemcitabine), gastric cancer (SD), and uterine corpus-endometrial cancer.

[d]Conducted on colorectal (SD, 4.6 months), breast (SD, 4 months), leiomyosarcoma (SD, 4 months), and mesothelioma (SD, 4 months).

TrkC, tropomyosin receptor kinase-C; ER, estrogen receptor; GLUT, glucose transport system; FR, folate receptor; AR, androgen receptor; CaIX, carbonic anhydrase-9; PSMA, prostate specific membrane antigen; PR, partial remission; SD, stable disease; OS, overall survival; PFS, progression free survival; PD, progressive disease; DCR, complete remission + partial remission + stable disease.

Table II. Small-Molecule Conjugates for Cancer Imaging in the Clinic and in Preclinical Animal Models

Cancer type	Small-molecule conjugates (structure numbering)	Target	Study stages	Status Status	Graft/ tumors	Remarks	References
Prostate	^{123}I-MIP-1072 (**17**) and ^{123}I-MIP-1095 (**18**)	PSMA	Clinical phase I	Completed	Recurrent metastatic	Localized in tumor lesion post 1–4 hr administration, ^{123}I-MIP-1072 has fivefold rapid clearance compared to ^{123}I-MIP-1095	148 NCT00712829
	$^{99\,m}$Tc-MIP-1404 (**19**) and ^{99m}Tc-MIP-1405 (**20**)	PSMA	Clinical phase I/II	Phase I-completed	Metastatic	20% increase in accuracy and sensitivity compared to ^{123}I-MIP-1072 and ^{123}I-MIP-1095	152 NCT01261754
				Phase II-ongoing		Ongoing, not recruiting participants	NCT01667536
	EC0652 (^{99m}Tc-DUPA) (**21**)	PSMA	Clinical phase 0	Ongoing	Advanced, metastatic	No reported toxicity and 7/9 showed high affinity localization in cancer lesion	153
	^{18}F-DCFBC (**22**)	PSMA	Clinical phase I/II	Ongoing	Primary and metastatic	66% ^{18}F-DCFBC pet patient was concordant with conventional imaging, and able to detect early bone metastasis	154, NCT01815515, NCT01417182, NCT01496157
	^{125}I-RISAD-P (**61**)	AR	In vivo	Preclinical	TRAMP for prostate cancer	High uptake in tumor and proportional to time and sizes; studied for radiotherapy and showed delayed tumor growth by sizes	314
Breast	^{18}F-ISO1 (**26**)[a]	Sigma-2	Clinical phase I	Ongoing	Primary cancer	Tumor cell proliferation status significant correlated with control proliferation marker (KI-67). MTD of 550 mbq	NCT02284919
	^{18}F-3f (**27**) and ^{123}I-3f (**28**)	Sigma-2	In vivo	Preclinical	Syngeneic clone 66 breast tumor	High tumor to normal tissue ratios, rapid clearance from nontargeted organs (5–120 min)	174
	^{18}F-fluoroestradiol (^{18}F-FES) (**43**)	ER	Clinical phase I/II	Ongoing	Metastatic breast and desmoid tumor	Recruiting patients	NCT02374931 NCT01957332
	4FMFES (**44**)	ER	Clinical phase II	Ongoing	Primary and metastatic	Threefold higher tumor to background ratio compared to ^{18}F-FES	275

Continued

Table II. Continued

Cancer type	Small-molecule conjugates (structure numbering)	Target	Study stages	Status Status	Graft/ tumors	Remarks	References
	β-^{18}F-FMOX (**45**)	ER	Clinical phase I	Discontinued	Primary	Low affinity and poor localization	279
	^{18}F-FENP (**50**)	PgR	Clinical phase I	Discontinued	Primary	50% uptake in breast and was not receptor-mediated	290
	^{18}F-FFNP (**51**)	PgR	Clinical phase I	Completed	Carcinoma	Significant tumor to normal breast, muscle and blood ratio, insignificant in PgR^+ and PgR^- uptake	NCT00968409 294
	IYIY-BODIPY (**29**)	TrkC	In vitro staining	Preclinical	Human tissue microarray BRC962	All 36 malignant breast tissue uptake, but not in normal breast tissue	195
Ovarian	^{111}In-DTPA-folate (**3**)	FR	Clinical phase I/II	Completed	Primary, recurrent	100% sensitivity and concordant with conventional imaging for primary ovarian cancer; less effective in recurrent endometrium cancer	77
	^{99m}Tc-EC20 (**2**)	FR	Clinical phase II	Completed	Recurrent	87% sensitive in FR(10–90%) expression.	363 NCT01689714
			Phase III	Suspended	Platinum-resistant ovarian	Suspended participant recruitment	NCT01170650
	^{18}F-FPTP (**53**)	PgR		Preclinical	Uterus and ovary imaging	High uterus and ovarian uptake at 1 and 3 hr post injection	296
	^{111}In-DOTA-E-[c(RDGfK)]$_2$ (**86**)	Integrin	In vivo	Preclinical	Xenograft NIH:OVCAR-3	Tumor uptake peaked at 6–7.5% dose/g at 1–2 hr post injection, rapid renal excretion, considerable uptake in liver and spleen, receptor binding demonstrated, tumor growth delay observed	350
Kidney	^{99m}Tc-EC20 (**2**)[b]	FR	Clinical phase I	Completed	Primary, metastasis	74% ($n = 119$) uptake in renal cancer (68% uptake in all solid tumors); less effective in detecting metastatic lesion.	80

Continued

Table II. Continued

Cancer type	Small-molecule conjugates (structure numbering)	Target	Study stages	Status Status	Graft/ tumors	Remarks	References
	CRL-LS288 (**15**)	CCK2R	In vivo	Preclinical	Xenograft CCK2R transfected HEK293 cells	High binding specificity in primary and metastasis CCK2R expressing cancer, uptake in kidney is nonmediated receptor, no other nonmalignant organ uptake	130
	^{68}Ga-NOTAc-(NGR) (**83**)	CD13	In vivo	Preclinical	Xenograft NeDe mesoblastic nephroma	^{68}Ga-NOTA-c(NGR) has lower abdominal uptake than ^{68}Ga-NODAGA-[c(RGD)]$_2$, both excreted from kidneys, NGR conjugate has higher tumor uptake than RGD	331
Non-small-cell lung cancer	^{99m}Tc-EC20 (**2**)	FR	Clinical phase II	Ongoing	Adenocarcinoma, squamous.	Monitoring efficacy of EC145 ± docetaxel via imaging. Ongoing, not recruiting	NCT01577654
			Phase III	Unknown	Primary, metastatic	Unknown status, information not updated	NCT01394679
	^{68}Ga-DOTA-NGR (**80**)	CD13	In vivo	Preclinical	Xenograft A549 lung adenocarcinoma	Tumor uptake was blocked by unlabelled DOTA-NGR, excreted from kidney and rapidly cleared from blood and normal organs, tumor visible at 1 hr post injection with highest tumor/lung ratio at 1.5 hr	343
Liver	^{99m}Tc-NGR	CD13	In vivo	Preclinical	Xenograft HepG2 hepatoma	Rapid, significant tumor uptake and slow tumor washout, tumors visible at 1 hr post injection with highest T/NT at 8 hr	341

Continued

Table II. Continued

Cancer type	Small-molecule conjugates (structure numbering)	Target	Study stages	Status Status	Graft/ tumors	Remarks	References
Fibrosarcoma	^{64}Cu-DOTA-NGR1 (**78**),^{64}Cu-DOTA-NGR2 (**79**)	CD13	In vivo	Preclinical	Xenograft HT-1080	^{64}Cu-DOTA-NGR2 has higher tumor uptake and slower tumor washout than ^{64}Cu-DOTA-NGR1, both conjugates show less tumor uptake if first blocked with cyclic CNGRC	342
	^{68}Ga-NOTA-G_3-NGR2 (**82**)	CD13	In vivo	Preclinical	Xenograft HT-1080	Excreted mainly and rapidly through kidneys, higher tumor uptake and lower accumulation in vital organs, tumor uptake blocked by unlabelled conjugates	344
	^{99m}TcO-N_3S-PEG_2-Probestin (**84**)	CD13	In vivo	Preclinical	Xenograft HT-1080	Visible tumor uptake at 1 hr post injection, which was blocked by nonradioactive ReO-N3S-PEG2-Probestin	345
Brain	Bivalent-IA-Cy5.5 (**102**)	Integrin	In vivo	Preclinical	Xenograft U87	Highest tumor-to-normal tissue contrast 24–48 hr post injection	361

[a] Includes head and neck cancer ($n = 10$) and lymphoma ($n = 7$).

[b] Conducted on benign ovarian tumors ($n = 8$), ovarian carcinomas ($n = 7$), breast carcinomas ($n = 6$), and pituitary adenomas ($n = 6$). One patient each for small cell lung carcinoma, lung carcinoma (type unspecified), colon, endometrial, thyroid carcinomas, non-Hodgkin's lymphoma, sarcoma, and glioma.

^{18}F-DCFBC, *N*-[*N*-[(*S*)-1,3-dicarboxypropyl]carbamoyl]-4-[^{18}F]fluorobenzyl-L-cysteine; ^{18}F-3f, *N*-(4-(6,7-dimethoxy-3,4-dihydroisoquinolin-2(1*H*)-yl)butyl)-2-(2-[^{18}F]-fluoroethoxy)-5-iodo-3-methoxybenzamide; 4FMFES, 4-fluoro-11β-methoxy-16α-[^{18}F]-fluoroestradiol; β-^{18}F-FMOX, 17α-ethynyl-11β-methoxy-16β-^{18}F-fluoroestradiol; ^{18}F-FENP, 21-[^{18}F]-fluoro-16α-ethyl-19-norprogesterone; ^{18}F-FFNP, 21-Fluoro-16α,l7α -[(R)-(1′-α-furylmethylidene)dioxy]-19-norpregn-4-ene-3,2-O-dione, ^{18}F-FPTP, F-fluoropropyl tanaproget.

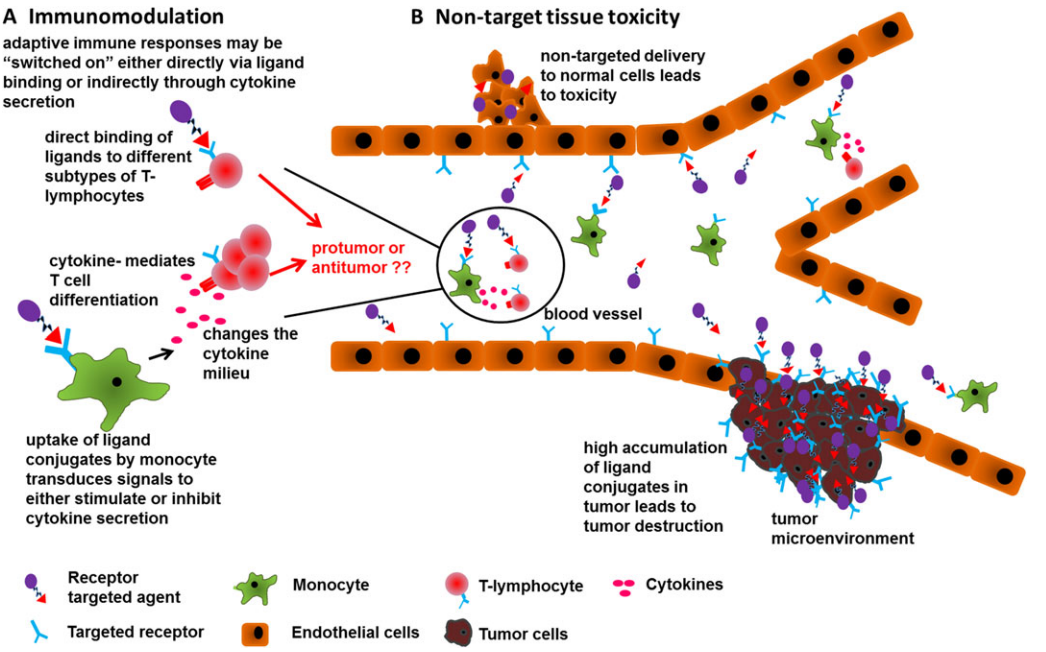

Figure 4. Other impacts of active targeting. (A) Immunomodulation is one of the possible effects of active targeting. Targeted ligands generally possess similar abilities as the natural ligands and can transduce signals upon binding to receptors that are expressed on normal cells, for example, immune cells. The ligands are known to be able to modulate immune responses in two different ways: (i) direct binding on monocytes to promote or inhibit the release of cytokines, which can then alter the cytokine milieu systemically, thereby affecting the adaptive immune cell (T-lymphocytes) differentiation and (ii) binding of ligand conjugates to different subtypes of T-lymphocytes to regulate their survival and functions. In both ways, the overall effect may be either protumor or antitumor depending on the ligand and receptor involved. In addition, the therapeutic cargo carried by the ligand conjugate may also modulate the immune response, for examle, cyclophosphamide (an anticancer drug with immune modulation properties such as reduces T-suppressor cells). (B) Nontarget tissue toxicity is another possible effect of active targeting. Some receptors that are overexpressed in cancer cells are also highly expressed in the normal cells in healthy organs. Therefore, while killing cancer cells with overexpressed targeted molecules, mild or acute toxicity to nontargeted tissues might also happen in active targeted therapy.

therapeutic indices allowing the targeted conjugates to be administered at lower doses. One of the best examples involves taxoids, which also have limited bioavailability due to hydrophobicity. Actively targeted drug delivery platforms featuring taxoids have reduced overall systemic toxicity. Taxoid conjugates may hence be better tolerated in patients and high therapeutic doses may be used for advanced disease states.[227,348]

At the current time, mAbs are having a far greater impact on active targeting than small molecules,[349] and research continues to overcome some of their limitations.[13] For instance, there is a community of researchers who focus on mAb modifications to promote permeation into cells and tissue (e.g., transbodies).[350] Similarly, another strategy may be small polymeric micelles whose the diameter is such that they can avoid being trapped in superficial regions of solid tumors (but then it is hard to load cargoes and targeting entities and retain small size, and there may be persistent issues with off-target uptake in organs such as the liver, spleen, and heart). Much of the research on active targeting via mAbs, nanoparticles, liposomes is superb, and in the case of mAbs has potential or proven clinical value. However, we think the following three assertions are fair: (i) the unexplored potential for small-molecule targeting agents is probably more than for mAb systems because relatively few synthetic ligands have been prepared for this (as opposed to natural ones like folate and biotin), (ii) strategies involving nanoparticles,

polymers, large dendrimers, tend to be restricted by the same delivery-related issues that limit use of mAbs, and (iii) in any event, targeting of nanoparticles, polymers, large dendrimers using small-molecule agents gives smaller constructs than comparable systems targeted with mAbs. Smaller constructs tend to be more easily prepared with acceptable batch-to-batch variations, less vulnerable to degradation in vivo, and more permeable to tumor penetration.

Only 13 receptor types are featured in this review (those for: folate, cholecystokin, PSMA, sigma-2 ligands, neurotrophins, carbonic anhydrase ligands, glucose, estrogen, progesterone, androgen, biotin, amino peptidase N, and integrin). Most of these are receptors for naturally occurring vitamins or steroids, and most of the others were initially studied as therapeutic targets. With respect to the ligands that have been used for active targeting, most are closely related to the endogenous ligands (e.g,. folate and estrogen). There are a few examples of compounds that emerged from medicinal chemistry efforts being used (e.g., sigma-2 and Trk receptor ligands). There are also examples of derivatives of endogenous ligands significantly modified by medicinal chemistry (e.g., peptidomimetics of RGD for integrin sequences).

The outline of receptors and ligands for active targeting presented above leads to a conclusion that applies to both small molecules and mAbs. Most of the receptors used so far are ones that have been widely studied for a long time. They have been studied intensely because they interact with endogenous ligands to give responses that trigger in vivo responses that were recognized to be physiologically important (e.g., folic acid, estrogen, integrins). That area of research was well advanced before anyone considered using those receptors for active targeting. In a sense, research in active targeting is "piggy-backing" on what others have discovered about those common receptors that happen to be overexpressed in particular tumor types. It is highly likely that there are many other cell surface receptors that are overexpressed in different tumor types that have not been widely studied and are "flying under the radar" with respect to active targeting.

Based on the observations in this review, we predict the field of active targeting will develop in several ways. First, interest in small molecules for active targeting will increase as more receptors are validated as suitable targets in mAb-based strategies, and as researchers look for smaller, more tumor-permeable constructs that will perform the same function. Second, more synthetic molecules that bind cell surface receptors will be used for active targeting, and the number of these may quickly surpass the number of natural ligands that are used. This assertion is based on the fact that medicinal chemistry consistently uncovers new structures that bind cell surface receptors, whereas the number of useful small molecules endogenous ligands (eg. folate and estrogen) is finite and not particularly large. Finally, to date there has been very little use of genetic and proteomic methods specifically directed to identification of receptors that have ideal characteristics for active targeting (high levels of expression overall, high ratios of expression in cancer relative to normal cells, and frequent recycling to the cell surface). Good progress has been made in this area, but the best is probably still to come.

8. ABBREVIATIONS

ADM = adriamycin
AE = antiestrogen
APN = aminopeptidase N
AR = androgen receptor
BR = biotin receptor
BRAF = v-raf murine sarcoma viral oncogene homolog B1
BODIPY = boron dipyrromethene
CCKR = cholecystokin receptor

CI = confidence interval
CLB = chlorambucil
CNGRC = Cys-Asn-Gly-Arg-Cys
CNS = central nervous system
DAHPES = 5-hydroxy-3,7-diazanonan-1,9-dithiol
DCR = complete response, partial response, stable disease
DHT = dihydrotestosterone
DOTA = 1,4,7,10-tetraazacyclododecane-N,N′,N″,N‴-tetraacetic acid
Dox = doxorubicin
DTPA = diethylenetriaminepentaacetic acid
E2 = estradiol
EPR = enhanced permeation retention
ER = estrogen receptor
FITC = fluorescein isothiocyanate
FR = folate receptor
GDA = geldanamycin
GLUT = glucose transport system
IFN = interferon
IHC = immunohistochemistry
IL = interleukin
mAb = monoclonal antibody
MDR = multidrug resistance
MEK = mitogen activated protein kinase kinase
MMP = matrix metalloproteinase
MR = magnetic resonance
MTD = maximum tolerated dose
NGR = asparaginyl-glycinyl-argininyl
NOTA = 1,4,7-triazacyclononane-N,N0,N00-triacetic acid
PCa = prostate cancer
PCFT = proton-coupled folate transporter
PET = positron emission tomography
PgR = progesterone receptor
PSMA = prostate-specific membrane antigen
PTX = paclitaxel
RBA = relative binding affinity
RFC = reduced folate carrier
RGD = argininyl-glycinyl-aspartic acid
SMVT = sodium-dependent multivitamin transporter
SPECT = single photon emission computed tomography
Trk = tropomyosin receptor kinase

ACKNOWLEDGMENTS

This project was supported by High Impact Research (HIR, UM.C/625/1/HIR/MOHE/MED/17 and UM.C/625/1/HIR/MOHE/MED/33) from the Ministry of Higher Education, Malaysia. Financial support to K.B. was provided by the Robert A. Welch Foundation (A-1121), a DoD BCRP Breakthrough Award (BC141561), and CONACYT (M1401981).

REFERENCES

1. Torchilin VP. Passive and active drug targeting: Drug delivery to tumors as an example. In: Monika Schäfer-Korting, Ed. Handbook of Experimental Pharmacology, Vol. 197. Springer Berlin Heidelberg: Berlin; 2010. p 3–53.
2. Aggarwal S. Targeted cancer therapies. Nat Rev Drug Discov 2010;9(6):427–428.
3. Huang M, Shen A, Ding J, Geng M. Molecularly targeted cancer therapy: Some lessons from the past decade. Trends Pharmacol Sci 2014;35(1):41–50.
4. Widakowich C, de Castro G, Jr., de Azambuja E, Dinh P, Awada A. Review: Side effects of approved molecular targeted therapies in solid cancers. Oncologist 2007;12(12):1443–1455.
5. Tannock IF, Lee CM, Tunggal JK, Cowan DS, Egorin MJ. Limited penetration of anticancer drugs through tumor tissue: A potential cause of resistance of solid tumors to chemotherapy. Clin Cancer Res 2002;8(3):878–884.
6. Brown R, Links M. Clinical relevance of the molecular mechanisms of resistance to anti-cancer drugs. Exp Rev Mol Med 1999;1(15):1–21.
7. Byrne JD, Betancourt T, Brannon-Peppas L. Active targeting schemes for nanoparticle systems in cancer therapeutics. Adv Drug Deliv Rev 2008;60(15):1615–1626.
8. Alexis F, Pridgen E, Molnar LK, Farokhzad OC. Factors affecting the clearance and biodistribution of polymeric nanoparticles. Mol Pharm 2008;5(4):505–515.
9. Cheng Z, Al Zaki A, Hui JZ, Muzykantov VR, Tsourkas A. Multifunctional nanoparticles: Cost versus benefit of adding targeting and imaging capabilities. Science 2012;338(6109):903–910.
10. des Rieux A, Pourcelle V, Cani PD, Marchand-Brynaert J, Preat V. Targeted nanoparticles with novel non-peptidic ligands for oral delivery. Adv Drug Deliv Rev 2013;65(6):833–844.
11. Koshkaryev A, Sawant R, Deshpande M, Torchilin V. Immunoconjugates and long circulating systems: Origins, current state of the art and future directions. Adv Drug Deliv Rev 2013;65(1):24–35.
12. Muller PY, Milton MN. The determination and interpretation of the therapeutic index in drug development. Nat Rev Drug Discov 2012;11(10):751–761.
13. Casi G, Neri D. Antibody-drug conjugates and small molecule-drug conjugates: Opportunities and challenges for the development of selective anticancer cytotoxic agents. J Med Chem 2015;58(22):8751–8761.
14. Vlashi E, Kelderhouse LE, Sturgis JE, Low PS. Effect of folate-targeted nanoparticle size on their rates of penetration into solid tumors. ACS Nano 2013;7(10):8573–8582.
15. Bates DO, Hillman NJ, Williams B, Neal CR, Pocock TM. Regulation of microvascular permeability by vascular endothelial growth factors. J Anat 2002;200(6):581–597.
16. Hobbs SK, Monsky WL, Yuan F, Roberts WG, Griffith L, Torchilin VP, Jain RK. Regulation of transport pathways in tumor vessels: Role of tumor type and microenvironment. Proc Natl Acad Sci USA 1998;95(8):4607–4612.
17. Jain RK, Stylianopoulos T. Delivering nanomedicine to solid tumors. Nat Rev Clin Oncol 2010;7(11):653–664.
18. Jain RK. Transport of molecules across tumor vasculature. Cancer Metastasis Rev 1987;6(4):559–593.
19. Noguchi Y, Wu J, Duncan R, Strohalm J, Ulbrich K, Akaike T, Maeda H. Early phase tumor accumulation of macromolecules: A great difference in clearance rate between tumor and normal tissues. Jpn J Cancer Res 1998;89(3):307–314.
20. Swartz MA. The physiology of the lymphatic system. Adv Drug Deliv Rev 2001;50(1–2):3–20.
21. Dreher MR, Liu W, Michelich CR, Dewhirst MW, Yuan F, Chilkoti A. Tumor vascular permeability, accumulation, and penetration of macromolecular drug carriers. J Natl Cancer Inst 2006;98(5):335–344.

22. Matsumura Y, Maeda H. A new concept for macromolecular therapeutics in cancer chemotherapy: Mechanism of tumoritropic accumulation of proteins and the antitumor agent smancs. Cancer Res 1986;46(12, Pt. 1):6387–6392.
23. Rabanel JM, Aoun V, Elkin I, Mokhtar M, Hildgen P. Drug-loaded nanocarriers: Passive targeting and crossing of biological barriers. Curr Med Chem 2012;19(19):3070–3102.
24. Carmeliet P, Jain RK. Principles and mechanisms of vessel normalization for cancer and other angiogenic diseases. Nat Rev Drug Discov 2011;10(6):417–427.
25. Boucher Y, Baxter LT, Jain RK. Interstitial pressure gradients in tissue-isolated and subcutaneous tumors: Implications for therapy. Cancer Res 1990;50(15):4478–4484.
26. Wu H-C, Chang D-K, Huang C-T. Targeted therapy for cancer. J Cancer Molecules 2006;2(2):57–66.
27. Padera TP, Stoll BR, Tooredman JB, Capen D, di Tomaso E, Jain RK. Pathology: Cancer cells compress intratumour vessels. Nature 2004;427(6976):695.
28. Stacker SA, Achen MG, Jussila L, Baldwin ME, Alitalo K. Metastasis: Lymphangiogenesis and cancer metastasis. Nat Rev Cancer 2002;2(8):573–583.
29. Green SK, Frankel A, Kerbel RS. Adhesion-dependent multicellular drug resistance. Anticancer Drug Des 1999;14(2):153–168.
30. Jain RK. Delivery of molecular and cellular medicine to solid tumors. Adv Drug Deliv Rev 2012;64(Suppl):353–365.
31. Ambudkar SV, Dey S, Hrycyna CA, Ramachandra M, Pastan I, Gottesman MM. Biochemical, cellular, and pharmacological aspects of the multidrug transporter. Annu Rev Pharmacol Toxicol 1999;39:361–398.
32. Gottesman MM, Fojo T, Bates SE. Multidrug resistance in cancer: Role of ATP-dependent transporters. Nat Rev Cancer 2002;2(1):48–58.
33. Thomas H, Coley HM. Overcoming multidrug resistance in cancer: An update on the clinical strategy of inhibiting p-glycoprotein. Cancer Control 2003;10(2):159–165.
34. Gong Y, Han W, Liu J, Chen F, Han J, Jin Y, Yong RO. Synergistic effects of verapamil and anti-mdr1 ribozyme on reversion of multidrug resistance in the P-glycoprotein-positive K562 cell line. Leukemia 2001;15(4):696–697.
35. Tsuruo T, Iida H, Tsukagoshi S, Sakurai Y. Overcoming of vincristine resistance in P388 leukemia in vivo and in vitro through enhanced cytotoxicity of vincristine and vinblastine by verapamil. Cancer Res 1981;41(5):1967–1972.
36. Abraham J, Edgerly M, Wilson R, Chen C, Rutt A, Bakke S, Robey R, Dwyer A, Goldspiel B, Balis F, Van Tellingen O, Bates SE, Fojo T. A phase I study of the P-glycoprotein antagonist tariquidar in combination with vinorelbine. Clinical Cancer Res 2009;15(10):3574–3582.
37. de Bruin M, Miyake K, Litman T, Robey R, Bates SE. Reversal of resistance by GF120918 in cell lines expressing the ABC half-transporter, MXR. Cancer Lett 1999;146(2):117–126.
38. Russell-Jones G, McTavish K, McEwan J, Rice J, Nowotnik D. Vitamin-mediated targeting as a potential mechanism to increase drug uptake by tumours. J Inorg Biochem 2004;98(10):1625–1633.
39. Yang W, Cheng Y, Xu T, Wang X, Wen LP. Targeting cancer cells with biotin-dendrimer conjugates. Eur J Med Chem 2009;44(2):862–868.
40. Zhang XG, Miao J, Dai YQ, Du YZ, Yuan H, Hu FQ. Reversal activity of nanostructured lipid carriers loading cytotoxic drug in multi-drug resistant cancer cells. Int J Pharm 2008;361(1–2):239–244.
41. Paulos CM, Reddy JA, Leamon CP, Turk MJ, Low PS. Ligand binding and kinetics of folate receptor recycling in vivo: Impact on receptor-mediated drug delivery. Mol Pharmacol 2004;66(6):1406–1414.
42. Bandara NA, Hansen MJ, Low PS. Effect of receptor occupancy on folate receptor internalization. Mol Pharm 2014;11(3):1007–1013.
43. Cabral H, Matsumoto Y, Mizuno K, Chen Q, Murakami M, Kimura M, Terada Y, Kano MR, Miyazono K, Uesaka M, Nishiyama N, Kataoka K. Accumulation of sub-100 nm polymeric micelles in poorly permeable tumors depends on size. Nat Nanotechnol 2011;6(12):815–823.

44. Dennis MS, Jin H, Dugger D, Yang R, McFarland L, Ogasawara A, Williams S, Cole MJ, Ross S, Schwall R. Imaging tumors with an albumin-binding Fab, a novel tumor-targeting agent. Cancer Res 2007;67(1):254–261.
45. Saga T, Neumann RD, Heya T, Sato J, Kinuya S, Le N, Paik CH, Weinstein JN. Targeting cancer micrometastases with monoclonal antibodies: A binding-site barrier. Proc Natl Acad Sci USA 1995;92(19):8999–9003.
46. Adams GP, Schier R, McCall AM, Simmons HH, Horak EM, Alpaugh RK, Marks JD, Weiner LM. High affinity restricts the localization and tumor penetration of single-chain Fv antibody molecules. Cancer Res 2001;61(12):4750–4755.
47. Rudnick SI, Lou J, Shaller CC, Tang Y, Klein-Szanto AJP, Weiner LM, Marks JD, Adams GP. Influence of affinity and antigen internalization on the uptake and penetration of anti-HER2 antibodies in solid tumors. Cancer Res 2011;71(6):2250–2259.
48. Baluk P, Morikawa S, Haskell A, Mancuso M, McDonald Donald M. Abnormalities of basement membrane on blood vessels and endothelial sprouts in tumors. Am J Pathol 2003;163(5):1801–1815.
49. di Tomaso E, Capen D, Haskell A, Hart J, Logie JJ, Jain RK, McDonald DM, Jones R, Munn LL. Mosaic tumor vessels: Cellular basis and ultrastructure of focal regions lacking endothelial cell markers. Cancer Res 2005;65(13):5740–5749.
50. O'Connor R. The pharmacology of cancer resistance. Anticancer Res 2007;27(3A):1267–1272.
51. Borsi L, Balza E, Bestagno M, Castellani P, Carnemolla B, Biro A, Leprini A, Sepulveda J, Burrone O, Neri D, Zardi L. Selective targeting of tumoral vasculature: comparison of different formats of an antibody (L19) to the ED-B domain of fibronectin. Int J Cancer 2002;102(1):75–85.
52. Carrasco-Triguero M, Yi J-H, Dere R, Qiu ZJ, Lei C, Li Y, Mahood C, Wang B, Leipold D, Poon KA, Kaur S. Immunogenicity assays for antibody-drug conjugates: case study with ado-trastuzumab emtansine. Bioanalysis 2013;5(9):1007–1023.
53. van Schouwenburg PA, Bartelds GM, Hart MH, Aarden L, Wolbink GJ, Wouters D. A novel method for the detection of antibodies to adalimumab in the presence of drug reveals "hidden" immunogenicity in rheumatoid arthritis patients. J Immunol Methods 2010;362(1–2):82–88.
54. Firer MA, Gellerman G. Targeted drug delivery for cancer therapy: The other side of antibodies. J Hematol Oncol 2012;5:70–86.
55. Li J, Chen F, Cona Marlein M, Feng Y, Himmelreich U, Oyen R, Verbruggen A, Ni Y. A review on various targeted anticancer therapies. Target Oncol 2012;7(1):69–85.
56. Vlashi E, Sturgis JE, Thomas M, Low PS. Real time, noninvasive imaging and quantitation of the accumulation of ligand-targeted drugs into receptor-expressing solid tumors. Mol Pharm 2009;6(6):1868–1875.
57. Krall N, Scheuermann J, Neri D. Small targeted cytotoxics: Current state and promises from DNA-encoded chemical libraries. Angew Chem Int Ed Engl 2013;52(5):1384–1402.
58. Bailey LB, Gregory JF, 3rd. Folate metabolism and requirements. J Nutr 1999;129(4):779–782.
59. Zhao R, Matherly LH, Goldman ID. Membrane transporters and folate homeostasis: Intestinal absorption and transport into systemic compartments and tissues. Exp Rev Mol Med 2009;11:e4.
60. Matherly LH, Goldman DI. Membrane transport of folates. Vitam Horm 2003;66:403–456.
61. Low PS, Kularatne SA. Folate-targeted therapeutic and imaging agents for cancer. Curr Opin Chem Biol 2009;13(3):256–262.
62. Shen F, Ross JF, Wang X, Ratnam M. Identification of a novel folate receptor, a truncated receptor, and receptor type beta in hematopoietic cells: cDNA cloning, expression, immunoreactivity, and tissue specificity. Biochemistry 1994;33(5):1209–1215.
63. Ross JF, Chaudhuri PK, Ratnam M. Differential regulation of folate receptor isoforms in normal and malignant tissues in vivo and in established cell lines. Physiologic and clinical implications. Cancer 1994;73(9):2432–2443.
64. Shen F, Wu M, Ross JF, Miller D, Ratnam M. Folate receptor type gamma is primarily a secretory protein due to lack of an efficient signal for glycosylphosphatidylinositol modification: Protein characterization and cell type specificity. Biochemistry 1995;34(16):5660–5665.

65. Parker N, Turk MJ, Westrick E, Lewis JD, Low PS, Leamon CP. Folate receptor expression in carcinomas and normal tissues determined by a quantitative radioligand binding assay. Anal Biochem 2005;338(2):284–293.
66. Wu M, Gunning W, Ratnam M. Expression of folate receptor type alpha in relation to cell type, malignancy, and differentiation in ovary, uterus, and cervix. Cancer Epidemiol Biomarkers Prev 1999;8(9):775–782.
67. O'Shannessy DJ, Somers EB, Maltzman J, Smale R, Fu YS. Folate receptor alpha (FRA) expression in breast cancer: Identification of a new molecular subtype and association with triple negative disease. SpringerPlus 2012;1:22–30.
68. Shia J, Klimstra DS, Nitzkorski JR, Low PS, Gonen M, Landmann R, Weiser MR, Franklin WA, Prendergast FG, Murphy L, Tang LH, Temple L, Guillem JG, Wong WD, Paty PB. Immunohistochemical expression of folate receptor alpha in colorectal carcinoma: Patterns and biological significance. Hum Pathol 2008;39(4):498–505.
69. Evans CO, Reddy P, Brat DJ, O'Neill EB, Craige B, Stevens VL, Oyesiku NM. Differential expression of folate receptor in pituitary adenomas. Cancer Res 2003;63(14):4218–4224.
70. Dhawan D, Ramos-Vara JA, Naughton JF, Cheng L, Low PS, Rothenbuhler R, Leamon CP, Parker N, Klein PJ, Vlahov IR, Reddy JA, Koch M, Murphy L, Fourez LM, Stewart JC, Knapp DW. Targeting folate receptors to treat invasive urinary bladder cancer. Cancer Res 2013;73(2):875–884.
71. Holm J, Hansen SI, Hoier-Madsen M, Christensen TB, Nichols CW. Characterization of a high-affinity folate receptor in normal and malignant human testicular tissue. Biosci Rep 1999;19(6):571–580.
72. Leamon CP, Low PS. Cytotoxicity of momordin-folate conjugates in cultured human cells. J Biol Chem 1992;267(35):24966–24971.
73. Chen C, Ke J, Zhou XE, Yi W, Brunzelle JS, Li J, Yong E-L, Xu HE, Melcher K. Structural basis for molecular recognition of folic acid by folate receptors. Nature 2013;500(7463):486–489.
74. Liu J, Kolar C, Lawson TA, Gmeiner WH. Targeted drug delivery to chemoresistant cells: Folic acid derivatization of FdUMP[10] enhances cytotoxicity toward 5-FU-resistant human colorectal tumor cells. J Org Chem 2001;66(17):5655–5663.
75. Lu Y, Low Philip S. Folate-mediated delivery of macromolecular anticancer therapeutic agents. Adv Drug Deliv Rev 2012;64:342–352.
76. Hilgenbrink AR, Low PS. Folate receptor-mediated drug targeting: From therapeutics to diagnostics. J Pharm Sci 2005;94(10):2135–2146.
77. Low PS, Henne WA, Doorneweerd DD. Discovery and development of folic-acid-based receptor targeting for imaging and therapy of cancer and inflammatory diseases. Acc Chem Res 2008;41:120–129.
78. Xia W, Low PS. Folate-targeted therapies for cancer. J Med Chem 2010;53(19):6811–6824.
79. Srinivasarao M, Galliford CV, Low PS. Principles in the design of ligand-targeted cancer therapeutics and imaging agents. Nat Rev Drug Discov 2015;14(3):203–219.
80. Reddy JA, Xu LC, Parker N, Vetzel M, Leamon CP. Preclinical evaluation of (99m)Tc-EC20 for imaging folate receptor-positive tumors. J Nucl Med 2004;45(5):857–866.
81. Leamon CP, Parker MA, Vlahov IR, Xu LC, Reddy JA, Vetzel M, Douglas N. Synthesis and biological evaluation of EC20: A new folate-derived, (99m)Tc-based radiopharmaceutical. Bioconjug Chem 2002;13(6):1200–1210.
82. Wang S, Luo J, Lantrip DA, Waters DJ, Mathias CJ, Green MA, Fuchs PL, Low PS. Design and synthesis of [111In]DTPA-folate for use as a tumor-targeted radiopharmaceutical. Bioconjug Chem 1997;8(5):673–679.
83. Fisher RE, Siegel BA, Edell SL, Oyesiku NM, Morgenstern DE, Messmann RA, Amato RJ. Exploratory study of 99mTc-EC20 imaging for identifying patients with folate receptor-positive solid tumors. J Nucl Med 2008;49(6):899–906.
84. Siegel BA, Dehdashti F, Mutch DG, Podoloff DA, Wendt R, Sutton GP, Burt RW, Ellis PR, Mathias CJ, Green MA, Gershenson DM. Evaluation of 111In-DTPA-folate as a receptor-

targeted diagnostic agent for ovarian cancer: Initial clinical results. J Nucl Med 2003;44(5):700–707.

85. Lu Y, Sega E, Leamon CP, Low PS. Folate receptor-targeted immunotherapy of cancer: Mechanism and therapeutic potential. Advanced Drug Deliv Rev 2004;56(8):1161–1176.
86. Lu Y, Low PS. Folate targeting of haptens to cancer cell surfaces mediates immunotherapy of syngeneic murine tumors. Cancer Immunol Immunother 2002;51(3):153–162.
87. Lu Y, Sega E, Low PS. Folate receptor-targeted immunotherapy: Induction of humoral and cellular immunity against hapten-decorated cancer cells. Int J Cancer 2005;116(5):710–719.
88. Amato RJ, Shetty A, Lu Y, Ellis R, Low PS. A phase I study of folate immune therapy (EC90 vaccine administered with GPI-0100 adjuvant followed by EC17) in patients with renal cell carcinoma. J Immunother 2013;36(4):268–275.
89. Amato RJ, Shetty A, Lu Y, Ellis PR, Mohlere V, Carnahan N, Low PS. A phase I/Ib study of folate immune (EC90 vaccine administered with GPI-0100 adjuvant followed by EC17) with interferon-alpha and interleukin-2 in patients with renal cell carcinoma. J Immunother 2014;37(4):237–244.
90. Leamon CP, Reddy JA, Vlahov IR, Vetzel M, Parker N, Nicoson JS, Xu LC, Westrick E. Synthesis and biological evaluation of EC72: a new folate-targeted chemotherapeutic. Bioconjug Chem 2005;16(4):803–811.
91. Reddy JA, Westrick E, Vlahov I, Howard SJ, Santhapuram HK, Leamon CP. Folate receptor specific anti-tumor activity of folate-mitomycin conjugates. Cancer Chemother Pharmacol 2006;58(2):229–236.
92. Cao Y, Yang J. Development of a folate receptor (FR)-targeted indenoisoquinoline using a pH-sensitive N-ethoxybenzylimidazole (NEBI) bifunctional cross-linker. Bioconjug Chem 2014;25(5):873–878.
93. Yang J, Chen H, Vlahov IR, Cheng JX, Low PS. Evaluation of disulfide reduction during receptor-mediated endocytosis by using FRET imaging. Proc Natl Acad Sci USA 2006;103(37):13872–13877.
94. Leamon CP, Reddy JA, Vlahov IR, Kleindl PJ, Vetzel M, Westrick E. Synthesis and biological evaluation of EC140: a novel folate-targeted vinca alkaloid conjugate. Bioconjug Chem 2006;17(5):1226–1232.
95. Vlahov IR, Santhapuram HK, Kleindl PJ, Howard SJ, Stanford KM, Leamon CP. Design and regioselective synthesis of a new generation of targeted chemotherapeutics. Part 1: EC145, a folic acid conjugate of desacetylvinblastine monohydrazide. Bioorg Med Chem Lett 2006;16(19):5093–5096.
96. Leamon CP, Reddy JA, Vlahov IR, Westrick E, Parker N, Nicoson JS, Vetzel M. Comparative preclinical activity of the folate-targeted Vinca alkaloid conjugates EC140 and EC145. Int J Cancer 2007;121(7):1585–1592.
97. Reddy JA, Dorton R, Westrick E, Dawson A, Smith T, Xu LC, Vetzel M, Kleindl P, Vlahov IR, Leamon CP. Preclinical evaluation of EC145, a folate-vinca alkaloid conjugate. Cancer Res 2007;67(9):4434–4442.
98. Lorusso PM, Edelman MJ, Bever SL, Forman KM, Pilat M, Quinn MF, Li J, Heath EI, Malburg LM, Klein PJ, Leamon CP, Messmann RA, Sausville EA. Phase I study of folate conjugate EC145 (Vintafolide) in patients with refractory solid tumors. J Clin Oncol 2012;30(32):4011–4016.
99. Morris RT, Joyrich RN, Naumann RW, Shah NP, Maurer AH, Strauss HW, Uszler JM, Symanowski JT, Ellis PR, Harb WA. Phase II study of treatment of advanced ovarian cancer with folate-receptor-targeted therapeutic (Vintafolide) and companion SPECT-based imaging agent (99mTc-etarfolatide). Ann Oncol 2014;25(4):852–858.
100. Vlahov IR, Santhapuram HK, You F, Wang Y, Kleindl PJ, Hahn SJ, Vaughn JF, Reno DS, Leamon CP. Carbohydrate-based synthetic approach to control toxicity profiles of folate-drug conjugates. J Org Chem 2010;75(11):3685–3691.
101. Leamon CP, Reddy JA, Klein PJ, Vlahov IR, Dorton R, Bloomfield A, Nelson M, Westrick E, Parker N, Bruna K, Vetzel M, Gehrke M, Nicoson JS, Messmann RA, LoRusso PM, Sausville EA.

Reducing undesirable hepatic clearance of a tumor-targeted vinca alkaloid via novel saccharopeptidic modifications. J Pharmacol Exp Ther 2011;336(2):336–343.

102. Harb WA, Conley BA, LoRusso P, Sausville EA, Heath EI, Chandana SR, Hamm M, Carter J, Perez WJ, Messmann RA. A phase I study of the folate-targeted conjugate EC0489 in patients with refractory or advanced metastatic cancer. J Clin Oncol 2010;28:15s.
103. Reddy JA, Santhapuram HK, Westrick E, Vetzel M, Dawson A, Dorton R, Smith T, Vlahov I, Leamon CP. Folate receptor targeted anti-tumor activity of EC-0225, a folate-targeted dual drug conjugate. Cancer Res 2006;66(8 Supplement):135.
104. Leamon CP, Reddy JA, Vlahov IR, Westrick E, Dawson A, Dorton R, Vetzel M, Santhapuram HK, Wang Y. Preclinical antitumor activity of a novel folate-targeted dual drug conjugate. Mol Pharm 2007;4(5):659–667.
105. Sharma S, Sausville EA, LoRusso P, Vogelzang NJ, Samlowski WE, Carter J, Forman K, Bever S, Messmann RA. A phase I study of EC0225 administered weeks 1 and 2 of a 4-week cycle. J Clin Oncol 2010;28:15s.
106. Vlahov IR VG, Kleindl PJ, Wang Y, Santhapuram HK, You F, Howard SJ, Kim SH, Lee FF, Leamon CP. Regioselective synthesis of folate receptor-targeted agents derived from epothilone analogs and folic acid. Bioorg Med Chem Lett 2010;20(15):4578–4581.
107. Peethambaram PP, Hartmann LC, Jonker DJ, de Jonge M, Plummer ER, Martin L, Konner J, Marshall J, Goss GD, Teslenko V, Clemens PL, Cohen LJ, Ahlers CM, Alland L. A phase I pharmacokinetic and safety analysis of epothilone folate (BMS-753493), a folate receptor targeted chemotherapeutic agent in humans with advanced solid tumors. Invest New Drugs 2015;33(2):321–331.
108. Reddy JA, Bloomfield A, Nelson M, Dorton R, Vetzel M, Leamon CP. Abstract 832: Pre-clinical development of EC1456: A potent folate targeted tubulysin SMDC. Cancer Res 2014;74(19 Supplement):832.
109. Vlahov IR, Santhapuram HKR, You F, Wang Y, Kleindl PJ, Hahn SJ, Vaughn JF, Reno DS, Leamon CP. Carbohydrate-based synthetic approach to control toxicity profiles of folate−drug conjugates. J Org Chem 2010;75(11):3685–3691.
110. Onodera R, Motoyama K, Arima H. Design and evaluation of folate-appended methyl-β-cyclodextrin as a new antitumor agent. J Incl Phenom Macrocycl Chem 2011;70(3–4):321–326.
111. Onodera R, Motoyama K, Okamatsu A, Higashi T, Arima H. Potential use of folate-appended methyl-beta-cyclodextrin as an anticancer agent. Sci Rep 2013;3:1104.
112. You H, Yoon HE, Jeong PH, Ko H, Yoon JH, Kim YC. Pheophorbide-a conjugates with cancer-targeting moieties for targeted photodynamic cancer therapy. Bioorg Med Chem 2015;23(7):1453–1462.
113. Jensen RT, Lemp GF, Gardner JD. Interaction of cholecystokinin with specific membrane receptors on pancreatic acinar cells. Proc Natl Acad Sci USA 1980;77(4):2079–2083.
114. Innis RB, Snyder SH. Distinct cholecystokinin receptors in brain and pancreas. Proc Natl Acad Sci USA 1980;77(11):6917–6921.
115. Little TJ, Horowitz M, Feinle-Bisset C. Role of cholecystokinin in appetite control and body weight regulation. Obesity Rev 2005;6(4):297–306.
116. Moran TH, Robinson PH, Goldrich MS, McHugh PR. Two brain cholecystokinin receptors: Implications for behavioral actions. Brain Res 1986;362(1):175–179.
117. Reeve JR, Jr., McVey DC, Bunnett NW, Solomon TE, Keire DA, Ho FJ, Davis MT, Lee TD, Shively JE, Vigna SR. Differences in receptor binding and stability to enzymatic digestion between CCK-8 and CCK-58. Pancreas 2002;25(3):e50–55.
118. Gaudreau P, Quirion R, St-Pierre S, Pert CB. Characterization and visualization of cholecystokinin receptors in rat brain using [3H]pentagastrin. Peptides 1983;4(5):755–762.
119. Nagata A, Ito M, Iwata N, Kuno J, Takano H, Minowa O, Chihara K, Matsui T, Noda T. G protein-coupled cholecystokinin-B/gastrin receptors are responsible for physiological cell growth of the stomach mucosa in vivo. Proc Natl Acad Sci USA 1996;93(21):11825–11830.

120. Savage K, Waller HA, Stubbs M, Khan K, Watson SA, Clarke PA, Grimes S, Michaeli D, Dhillon AP, Caplin ME. Targeting of cholecystokinin B/gastrin receptor in colonic, pancreatic and hepatocellular carcinoma cell lines. Int J Oncol 2006;29(6):1429–1435.
121. Weinberg DS, Ruggeri B, Barber MT, Biswas S, Miknyocki S, Waldman SA. Cholecystokinin A and B receptors are differentially expressed in normal pancreas and pancreatic adenocarcinoma. J Clin Invest 1997;100(3):597–603.
122. Reubi JC, Waser B. Unexpected high incidence of cholecystokinin-B/gastrin receptors in human medullary thyroid carcinomas. Int J Cancer 1996;67(5):644–647.
123. Sethi T, Herget T, Wu SV, Walsh JH, Rozengurt E. CCKA and CCKB receptors are expressed in small cell lung cancer lines and mediate Ca^{2+} mobilization and clonal growth. Cancer Res 1993;53(21):5208–5213.
124. Reubi JC, Schaer JC, Waser B. Cholecystokinin(CCK)-A and CCK-B/gastrin receptors in human tumors. Cancer Res 1997;57(7):1377–1386.
125. Hur K, Kwak MK, Lee HJ, Park DJ, Lee HK, Lee HS, Kim WH, Michaeli D, Yang HK. Expression of gastrin and its receptor in human gastric cancer tissues. J Cancer Res Clin Oncol 2006;132(2):85–91.
126. Zhou J, Chen M, Zhang Q, Hu J, Wang W. Human gastric tissues simultaneously express the classical and alternative splicing cholecystokinin-B/gastrin receptors. Receptors Channels 2004;10(5–6):185–188.
127. Korner M, Waser B, Reubi JC, Miller LJ. CCK(2) receptor splice variant with intron 4 retention in human gastrointestinal and lung tumours. J Cell Mol Med 2010;14(4):933–943.
128. Escrieut C, Gigoux V, Archer E, Verrier S, Maigret B, Behrendt R, Moroder L, Bignon E, Silvente-Poirot S, Pradayrol L, Fourmy D. The biologically crucial C terminus of cholecystokinin and the non-peptide agonist SR-146,131 share a common binding site in the human CCK1 receptor. Evidence for a crucial role of Met-121 in the activation process. J Biol Chem 2002;277(9):7546–7555.
129. Dufresne M, Seva C, Fourmy D. Cholecystokinin and gastrin receptors. Physiol Rev 2006;86(3):805–847.
130. Kossatz S, Behe M, Mansi R, Saur D, Czerney P, Kaiser WA, Hilger I. Multifactorial diagnostic NIR imaging of CCK2R expressing tumors. Biomaterials 2013;34(21):5172–5180.
131. Kawasaki D, Emori Y, Eta R, Iino Y, Hamano H, Yoshinaga K, Tanaka T, Takei M, Watson SA. Effect of Z-360, a novel orally active CCK-2/gastrin receptor antagonist on tumor growth in human pancreatic adenocarcinoma cell lines in vivo and mode of action determinations in vitro. Cancer Chemother Pharmacol 2008;61(5):883–892.
132. Wayua C, Low PS. Evaluation of a cholecystokinin 2 receptor-targeted near-infrared dye for fluorescence-guided surgery of cancer. Mol Pharm 2014;11(2):468–476.
133. Wayua C, Low PS. Evaluation of a nonpeptidic ligand for imaging of cholecystokinin 2 receptor-expressing cancers. J Nucl Med 2015;56(1):113–119.
134. Wayua C, Roy J, Putt KS, Low PS. Selective tumor targeting of desacetyl vinblastine hydrazide and tubulysin B via conjugation to a cholecystokinin 2 receptor (CCK2R) ligand. Mol Pharm 2015;12(7):2477–2483.
135. Leek J, Lench N, Maraj B, Bailey A, Carr IM, Andersen S, Cross J, Whelan P, MacLennan KA, Meredith DM, Markham AF. Prostate-specific membrane antigen: Evidence for the existence of a second related human gene. Br J Cancer 1995;72(3):583–588.
136. O'Keefe DS, Su SL, Bacich DJ, Horiguchi Y, Luo Y, Powell CT, Zandvliet D, Russell PJ, Molloy PL, Nowak NJ, Shows TB, Mullins C, Vonder Haar RA, Fair WR, Heston WD. Mapping, genomic organization and promoter analysis of the human prostate-specific membrane antigen gene. Biochim Biophys Acta 1998;1443(1–2):113–127.
137. Ross JS, Sheehan CE, Fisher HA, Kaufman RP, Jr., Kaur P, Gray K, Webb I, Gray GS, Mosher R, Kallakury BV. Correlation of primary tumor prostate-specific membrane antigen expression with disease recurrence in prostate cancer. Clin Cancer Res 2003;9(17):6357–6362.

138. Sweat SD, Pacelli A, Murphy GP, Bostwick DG. Prostate-specific membrane antigen expression is greatest in prostate adenocarcinoma and lymph node metastases. Urology 1998;52(4):637–640.

139. Troyer JK, Beckett ML, Wright GL, Jr. Detection and characterization of the prostate-specific membrane antigen (PSMA) in tissue extracts and body fluids. Int J Cancer 1995;62(5):552–558.

140. Wright GL, Jr., Haley C, Beckett ML, Schellhammer PF. Expression of prostate-specific membrane antigen in normal, benign, and malignant prostate tissues. Urol Oncol 1995;1(1):18–28.

141. Anilkumar G, Rajasekaran SA, Wang S, Hankinson O, Bander NH, Rajasekaran AK. Prostate-specific membrane antigen association with filamin A modulates its internalization and NAALADase activity. Cancer Res 2003;63(10):2645–2648.

142. Liu H, Rajasekaran AK, Moy P, Xia Y, Kim S, Navarro V, Rahmati R, Bander NH. Constitutive and antibody-induced internalization of prostate-specific membrane antigen. Cancer Res 1998;58(18):4055–4060.

143. Pinto JT, Suffoletto BP, Berzin TM, Qiao CH, Lin S, Tong WP, May F, Mukherjee B, Heston WD. Prostate-specific membrane antigen: a novel folate hydrolase in human prostatic carcinoma cells. Clin Cancer Res 1996;2(9):1445–1451.

144. Slusher BS, Vornov JJ, Thomas AG, Hurn PD, Harukuni I, Bhardwaj A, Traystman RJ, Robinson MB, Britton P, Lu XC, Tortella FC, Wozniak KM, Yudkoff M, Potter BM, Jackson PF. Selective inhibition of NAALADase, which converts NAAG to glutamate, reduces ischemic brain injury. Nat Med 1999;5(12):1396–1402.

145. Yao V, Berkman CE, Choi JK, O'Keefe DS, Bacich DJ. Expression of prostate-specific membrane antigen (PSMA), increases cell folate uptake and proliferation and suggests a novel role for PSMA in the uptake of the non-polyglutamated folate, folic acid. Prostate 2010;70(3):305–316.

146. Hillier SM, Maresca KP, Femia FJ, Marquis JC, Foss CA, Nguyen N, Zimmerman CN, Barrett JA, Eckelman WC, Pomper MG, Joyal JL, Babich JW. Preclinical evaluation of novel glutamate-urea-lysine analogues that target prostate-specific membrane antigen as molecular imaging pharmaceuticals for prostate cancer. Cancer Res 2009;69(17):6932–6940.

147. Maresca KP, Hillier SM, Femia FJ, Keith D, Barone C, Joyal JL, Zimmerman CN, Kozikowski AP, Barrett JA, Eckelman WC, Babich JW. A series of halogenated heterodimeric inhibitors of prostate specific membrane antigen (PSMA) as radiolabeled probes for targeting prostate cancer. J Med Chem 2009;52(2):347–357.

148. Hillier SM, Kern AM, Maresca KP, Marquis JC, Eckelman WC, Joyal JL, Babich JW. 123I-MIP-1072, a small-molecule inhibitor of prostate-specific membrane antigen, is effective at monitoring tumor response to taxane therapy. J Nucl Med 2011;52(7):1087–1093.

149. Barrett JA, Coleman RE, Goldsmith SJ, Vallabhajosula S, Petry NA, Cho S, Armor T, Stubbs JB, Maresca KP, Stabin MG, Joyal JL, Eckelman WC, Babich JW. First-in-man evaluation of 2 high-affinity PSMA-avid small molecules for imaging prostate cancer. J Nucl Med 2013;54(3):380–387.

150. Zechmann CM, Afshar-Oromieh A, Armor T, Stubbs JB, Mier W, Hadaschik B, Joyal J, Kopka K, Debus J, Babich JW, Haberkorn U. Radiation dosimetry and first therapy results with a (124)I/(131)I-labeled small molecule (MIP-1095) targeting PSMA for prostate cancer therapy. Eur J Nucl Med Mol Imaging 2014;41(7):1280–1292.

151. Maresca KP, Marquis JC, Hillier SM, Lu G, Femia FJ, Zimmerman CN, Eckelman WC, Joyal JL, Babich JW. Novel polar single amino acid chelates for technetium-99m tricarbonyl-based radiopharmaceuticals with enhanced renal clearance: Application to octreotide. Bioconjug Chem 2010;21(6):1032–1042.

152. Hillier SM, Maresca KP, Lu G, Merkin RD, Marquis JC, Zimmerman CN, Eckelman WC, Joyal JL, Babich JW. 99mTc-labeled small-molecule inhibitors of prostate-specific membrane antigen for molecular imaging of prostate cancer. J Nucl Med2013;54(8):1369–1376.

153. Babich J, Coleman RE, van Heertum R, Vallabhajosula S, Goldsmith S, Osborne J, Slawin K, Joyal J. Small molecule inhibitors of prostate specific membrane antigen (PSMA) for SPECT: Summary of phase I studies in patients with prostate cancer (PCa). J Nucl Med 2012;53(1_MeetingAbstracts):179.

154. Kularatne SA, Zhou Z, Yang J, Post CB, Low PS. Design, synthesis, and preclinical evaluation of prostate-specific membrane antigen targeted 99mTc-radioimaging agents. Mol Pharm 2009;6(3):790–800.
155. Gardner TA, Fletcher JW, Ko S-C, Low PS, Ratliff TL. Abstract LB-90: DUPA-99mTc localizes to prostate cancer in men with locally advanced and metastatic disease. Cancer Res 2013;73(8 Supplement):LB-90.
156. Cho SY, Gage KL, Mease RC, Senthamizhchelvan S, Holt DP, Jeffrey-Kwanisai A, Endres CJ, Dannals RF, Sgouros G, Lodge M, Eisenberger MA, Rodriguez R, Carducci MA, Rojas C, Slusher BS, Kozikowski AP, Pomper MG. Biodistribution, tumor detection, and radiation dosimetry of 18F-DCFBC, a low-molecular-weight inhibitor of prostate-specific membrane antigen, in patients with metastatic prostate cancer. J Nucl Med 2012;53(12):1883–1891.
157. Reddy JA, Bloomfield A, Dorton R, Nelson M, Vetzel M, Hahn S, Vlahov I, Leamon C. Abstract 2145: PSMA-specific anti-tumor activity of the targeted-tubulysin conjugate, EC1169. Cancer Res 2013;73(8 Supplement):2145.
158. Hellewell SB, Bruce A, Feinstein G, Orringer J, Williams W, Bowen WD. Rat liver and kidney contain high densities of sigma 1 and sigma 2 receptors: Characterization by ligand binding and photoaffinity labeling. Eur J Pharmacol 1994;268(1):9–18.
159. Huang YS, Lu HL, Zhang LJ, Wu Z. Sigma-2 receptor ligands and their perspectives in cancer diagnosis and therapy. Med Res Rev 2014;34(3):532–566.
160. Ogawa K, Shiba K, Akhter N, Yoshimoto M, Washiyama K, Kinuya S, Kawai K, Mori H. Evaluation of radioiodinated vesamicol analogs for sigma receptor imaging in tumor and radionuclide receptor therapy. Cancer Sci 2009;100(11):2188–2192.
161. Wilke RA, Mehta RP, Lupardus PJ, Chen Y, Ruoho AE, Jackson MB. Sigma receptor photolabeling and sigma receptor-mediated modulation of potassium channels in tumor cells. J Biol Chem 1999;274(26):18387–18392.
162. Cobos EJ, Entrena JM, Nieto FR, Cendan CM, Del Pozo E. Pharmacology and therapeutic potential of sigma(1) receptor ligands. Curr Neuropharmacol 2008;6(4):344–366.
163. Vilner BJ, Bowen WD. Sigma receptor-active neuroleptics are cytotoxic to C6 glioma cells in culture. Eur J Pharmacol 1993;244(2):199–201.
164. Vilner BJ, de Costa BR, Bowen WD. Cytotoxic effects of sigma ligands: Sigma receptor-mediated alterations in cellular morphology and viability. J Neurosci 1995;15(1 Pt 1):117–134.
165. Haller JL, Panyutin I, Chaudhry A, Zeng C, Mach RH, Frank JA. Sigma-2 receptor as potential indicator of stem cell differentiation. Mol Imaging Biol 2012;14(3):325–335.
166. Al-Nabulsi I, Mach RH, Wang LM, Wallen CA, Keng PC, Sten K, Childers SR, Wheeler KT. Effect of ploidy, recruitment, environmental factors, and tamoxifen treatment on the expression of sigma-2 receptors in proliferating and quiescent tumour cells. Br J Cancer 1999;81(6):925–933.
167. Wheeler KT, Wang LM, Wallen CA, Childers SR, Cline JM, Keng PC, Mach RH. Sigma-2 receptors as a biomarker of proliferation in solid tumours. Br J Cancer 2000;82(6):1223–1232.
168. Zeng C, Vangveravong S, Xu J, Chang KC, Hotchkiss RS, Wheeler KT, Shen D, Zhuang ZP, Kung HF, Mach RH. Subcellular localization of sigma-2 receptors in breast cancer cells using two-photon and confocal microscopy. Cancer Res 2007;67(14):6708–6716.
169. Spitzer D, Simon PO, Kashiwagi H, Xu J, Zeng C, Vangveravong S, Zhou D, Chang K, McDunn JE, Hornick JR, Goedegebuure P, Hotchkiss RS, Mach RH, Hawkins WG. Use of multifunctional sigma-2 receptor ligand conjugates to trigger cancer-selective cell death signaling. Cancer Res 2012;72(1):201–209.
170. Sun H, Nikolovska-Coleska Z, Yang CY, Qian D, Lu J, Qiu S, Bai L, Peng Y, Cai Q, Wang S. Design of small-molecule peptidic and nonpeptidic Smac mimetics. Acc Chem Res 2008;41(10):1264–1277.
171. Hashim YM, Spitzer D, Vangveravong S, Hornick MC, Garg G, Hornick JR, Goedegebuure P, Mach RH, Hawkins WG. Targeted pancreatic cancer therapy with the small molecule drug conjugate SW IV-134. Mol Oncol 2014;8(5):956–967.

172. Zeng C, Vangveravong S, McDunn JE, Hawkins WG, Mach RH. Sigma-2 receptor ligand as a novel method for delivering a SMAC mimetic drug for treating ovarian cancer. Br J Cancer 2013;109(9):2368–2377.
173. Garg G, Vangveravong S, Zeng C, Collins L, Hornick M, Hashim Y, Piwnica-Worms D, Powell MA, Mutch DG, Mach RH, Hawkins WG, Spitzer D. Conjugation to a SMAC mimetic potentiates sigma-2 ligand induced tumor cell death in ovarian cancer. Mol Cancer 2014;13:50–62.
174. Tu Z, Xu J, Jones LA, Li S, Dumstorff C, Vangveravong S, Chen DL, Wheeler KT, Welch MJ, Mach RH. Fluorine-18-labeled benzamide analogues for imaging the sigma2 receptor status of solid tumors with positron emission tomography. J Med Chem 2007;50(14):3194–3204.
175. Shoghi KI, Xu J, Su Y, He J, Rowland D, Yan Y, Garbow JR, Tu Z, Jones LA, Higashikubo R, Wheeler KT, Lubet RA, Mach RH, You M. Quantitative receptor-based imaging of tumor proliferation with the sigma-2 ligand [(18)F]ISO-1. PloS One 2013;8(9):e74188.
176. Dehdashti F, Laforest R, Gao F, Shoghi KI, Aft RL, Nussenbaum B, Kreisel FH, Bartlett NL, Cashen A, Wagner-Johnston N, Mach RH. Assessment of cellular proliferation in tumors by PET using 18F-ISO-1. J Nucl Med 2013;54(3):350–357.
177. Tu Z, Xu J, Jones LA, Li S, Zeng D, Kung MP, Kung HF, Mach RH. Radiosynthesis and biological evaluation of a promising sigma(2)-receptor ligand radiolabeled with fluorine-18 or iodine-125 as a PET/SPECT probe for imaging breast cancer. Appl Radiat Isot 2010;68(12):2268–2273.
178. Segal RA. Selectivity in neurotrophin signaling: Theme and variations. Annu Rev Neurosci 2003;26:299–330.
179. Schneider R, Schweiger M. A novel modular mosaic of cell adhesion motifs in the extracellular domains of the neurogenic trk and trkB tyrosine kinase receptors. Oncogene 1991;6(10):1807–1811.
180. Urfer R, Tsoulfas P, O'Connell L, Shelton DL, Parada LF, Presta LG. An immunoglobulin-like domain determines the specificity of neurotrophin receptors. EMBO J 1995;14(12):2795–2805.
181. Windisch JM, Marksteiner R, Schneider R. Nerve growth factor binding site on TrkA mapped to a single 24-amino acid leucine-rich motif. J Biol Chem 1995;270(47):28133–28138.
182. Huang EJ, Reichardt LF. Trk receptors: roles in neuronal signal transduction. Annual review of biochemistry 2003;72:609–642.
183. Yamashiro DJ, Liu XG, Lee CP, Nakagawara A, Ikegaki N, McGregor LM, Baylin SB, Brodeur GM. Expression and function of Trk-C in favourable human neuroblastomas. Eur J Cancer 1997;33(12):2054–2057.
184. Brodeur GM, Nakagawara A, Yamashiro DJ, Ikegaki N, Liu XG, Azar CG, Lee CP, Evans AE. Expression of TrkA, TrkB and TrkC in human neuroblastomas. J Neurooncol 1997;31(1–2):49–55.
185. Wang Y, Hagel C, Hamel W, Muller S, Kluwe L, Westphal M. Trk A, B, and C are commonly expressed in human astrocytes and astrocytic gliomas but not by human oligodendrocytes and oligodendroglioma. Acta Neuropathol 1998;96(4):357–364.
186. Kumar S, de Vellis J. Neurotrophin activates signal transduction in oligodendroglial cells: Expression of functional TrkC receptor isoforms. J Neurosci Res 1996;44(5):490–498.
187. McGregor LM, McCune BK, Graff JR, McDowell PR, Romans KE, Yancopoulos GD, Ball DW, Baylin SB, Nelkin BD. Roles of trk family neurotrophin receptors in medullary thyroid carcinoma development and progression. Proc Natl Acad Sci USA 1999;96(8):4540–4545.
188. Xu X, Tahan SR, Pasha TL, Zhang PJ. Expression of neurotrophin receptor Trk-C in nevi and melanomas. J Cutan Pathol 2003;30(5):318–322.
189. Blasco-Gutierrez MJ, Jose-Crespo IJ, Zozaya-Alvarez E, Ramos-Sanchez R, Garcia-Atares N. TrkC: A new predictive marker in breast cancer? Cancer Invest 2007;25(6):405–410.
190. Jin W, Kim GM, Kim MS, Lim MH, Yun C, Jeong J, Nam JS, Kim SJ. TrkC plays an essential role in breast tumor growth and metastasis. Carcinogenesis 2010;31(11):1939–1947.
191. Vaishnavi A, Le AT, Doebele RC. TRKing down an old oncogene in a new era of targeted therapy. Cancer Discov 2015;5(1):25–34.

192. Butowt R, von Bartheld CS. Sorting of internalized neurotrophins into an endocytic transcytosis pathway via the Golgi system: Ultrastructural analysis in retinal ganglion cells. J Neurosci 2001;21(22):8915–8930.

193. Chen D, Brahimi F, Angell Y, Li YC, Moscowicz J, Saragovi HU, Burgess K. Bivalent peptidomimetic ligands of TrkC are biased agonists and selectively induce neuritogenesis or potentiate neurotrophin-3 trophic signals. ACS Chem Biol 2009;4(9):769–781.

194. Ko E, Kamkaew A, Burgess K. Small molecule ligands for active targeting of TrkC-expressing tumor cells. ACS Med Chem Lett 2012;3(12):1008–1012.

195. Kamkaew A, Burgess K. Double-targeting using a TrkC ligand conjugated to dipyrrometheneboron difluoride (BODIPY) based photodynamic therapy (PDT) agent. J Med Chem 2013;56(19):7608–7614.

196. Kue CS, Kamkaew A, Lee HB, Chung LY, Kiew LV, Burgess K. Targeted PDT agent eradicates TrkC expressing tumors via photodynamic therapy (PDT). Mol Pharm 2015;12(1):212–222.

197. Zavada J, Zavadova Z, Pastorekova S, Ciampor F, Pastorek J, Zelnik V. Expression of MaTu-MN protein in human tumor cultures and in clinical specimens. Int J Cancer 1993;54(2):268–274.

198. Frost SC. Physiological functions of the alpha class of carbonic anhydrases. Subcell Biochem 2014;75:9–30.

199. Supuran CT. Carbonic anhydrases: Novel therapeutic applications for inhibitors and activators. Nat Rev Drug Discov 2008;7(2):168–181.

200. Opavsky R, Pastorekova S, Zelnik V, Gibadulinova A, Stanbridge EJ, Zavada J, Kettmann R, Pastorek J. Human MN/CA9 gene, a novel member of the carbonic anhydrase family: Structure and exon to protein domain relationships. Genomics 1996;33(3):480–487.

201. Hilvo M, Baranauskiene L, Salzano AM, Scaloni A, Matulis D, Innocenti A, Scozzafava A, Monti SM, Di Fiore A, De Simone G, Lindfors M, Janis J, Valjakka J, Pastorekova S, Pastorek J, Kulomaa MS, Nordlund HR, Supuran CT, Parkkila S. Biochemical characterization of CA IX, one of the most active carbonic anhydrase isozymes. J Biol Chem 2008;283(41):27799–27809.

202. Pastorekova S, Parkkila S, Parkkila AK, Opavsky R, Zelnik V, Saarnio J, Pastorek J. Carbonic anhydrase IX, MN/CA IX: Analysis of stomach complementary DNA sequence and expression in human and rat alimentary tracts. Gastroenterology 1997;112(2):398–408.

203. Proescholdt MA, Merrill MJ, Stoerr EM, Lohmeier A, Pohl F, Brawanski A. Function of carbonic anhydrase IX in glioblastoma multiforme. Neurooncology 2012;14(11):1357–1366.

204. Niemela AM, Hynninen P, Mecklin JP, Kuopio T, Kokko A, Aaltonen L, Parkkila AK, Pastorekova S, Pastorek J, Waheed A, Sly WS, Orntoft TF, Kruhoffer M, Haapasalo H, Parkkila S, Kivela AJ. Carbonic anhydrase IX is highly expressed in hereditary nonpolyposis colorectal cancer. Cancer Epidemiol Biomarkers Prev 2007;16(9):1760–1766.

205. Hussain SA, Ganesan R, Reynolds G, Gross L, Stevens A, Pastorek J, Murray PG, Perunovic B, Anwar MS, Billingham L, James ND, Spooner D, Poole CJ, Rea DW, Palmer DH. Hypoxia-regulated carbonic anhydrase IX expression is associated with poor survival in patients with invasive breast cancer. Br J Cancer 2007;96(1):104–109.

206. Chamie K, Klopfer P, Bevan P, Storkel S, Said J, Fall B, Belldegrun AS, Pantuck AJ. Carbonic anhydrase-IX score is a novel biomarker that predicts recurrence and survival for high-risk, nonmetastatic renal cell carcinoma: Data from the phase III ARISER clinical trial. Urol Oncol 2015;33(5):204.e25–e32.

207. Ivanov S, Liao SY, Ivanova A, Danilkovitch-Miagkova A, Tarasova N, Weirich G, Merrill MJ, Proescholdt MA, Oldfield EH, Lee J, Zavada J, Waheed A, Sly W, Lerman MI, Stanbridge EJ. Expression of hypoxia-inducible cell-surface transmembrane carbonic anhydrases in human cancer. Am J Pathol 2001;158(3):905–919.

208. Krall N, Pretto F, Decurtins W, Bernardes GJ, Supuran CT, Neri D. A small-molecule drug conjugate for the treatment of carbonic anhydrase IX expressing tumors. Angew ChemInt Ed Engl 2014;53(16):4231–4235.

209. Krall N, Pretto F, Neri D. A bivalent small molecule-drug conjugate directed against carbonic anhydrase IX can elicit complete tumour regression in mice. Chem Sci 2014;5(9):3640–3644.
210. Scheepers A, Joost HG, Schurmann A. The glucose transporter families SGLT and GLUT: Molecular basis of normal and aberrant function. JPEN J Parenter Enter Nutr 2004;28(5):364–371.
211. Wood IS, Trayhurn P. Glucose transporters (GLUT and SGLT): Expanded families of sugar transport proteins. Br J Nutr 2003;89(1):3–9.
212. Joost HG, Thorens B. The extended GLUT-family of sugar/polyol transport facilitators: Nomenclature, sequence characteristics, and potential function of its novel members (review). Mol Membr Biol 2001;18(4):247–256.
213. Yamamoto T, Seino Y, Fukumoto H, Koh G, Yano H, Inagaki N, Yamada Y, Inoue K, Manabe T, Imura H. Over-expression of facilitative glucose transporter genes in human cancer. Biochem Biophys Res Commun 1990;170(1):223–230.
214. Warburg O. On the origin of cancer cells. Science 1956;123(3191):309–314.
215. Younes M, Lechago LV, Somoano JR, Mosharaf M, Lechago J. Wide expression of the human erythrocyte glucose transporter Glut1 in human cancers. Cancer Res 1996;56(5):1164–1167.
216. Niculescu-Duvaz I. Glufosfamide (Baxter Oncology). Curr Opin Investig Drugs 2002;3(10):1527–1532.
217. Arafa HM. Possible contribution of beta-glucosidase and caspases in the cytotoxicity of glufosfamide in colon cancer cells. Eur J Pharmacol 2009;616(1–3):58–63.
218. Seker H, Bertram B, Burkle A, Kaina B, Pohl J, Koepsell H, Wiesser M. Mechanistic aspects of the cytotoxic activity of glufosfamide, a new tumour therapeutic agent. Br J Cancer 2000;82(3):629–634.
219. Becker R, Ritter A, Eichhorn U, Lips J, Bertram B, Wiessler M, Zdzienicka MZ, Kaina B. Induction of DNA breaks and apoptosis in crosslink-hypersensitive V79 cells by the cytostatic drug beta-D-glucosyl-ifosfamide mustard. Br J Cancer 2002;86(1):130–135.
220. Briasoulis E, Judson I, Pavlidis N, Beale P, Wanders J, Groot Y, Veerman G, Schuessler M, Niebch G, Siamopoulos K, Tzamakou E, Rammou D, Wolf L, Walker R, Hanauske A. Phase I trial of 6-hour infusion of glufosfamide, a new alkylating agent with potentially enhanced selectivity for tumors that overexpress transmembrane glucose transporters: A study of the European Organization for Research and Treatment of Cancer Early Clinical Studies Group. J Clin Oncol 2000;18(20):3535–3544.
221. Giaccone G, Smit EF, de Jonge M, Dansin E, Briasoulis E, Ardizzoni A, Douillard JY, Spaeth D, Lacombe D, Baron B, Bachmann P, Fumoleau P. Glufosfamide administered by 1-hour infusion as a second-line treatment for advanced non-small cell lung cancer; a phase II trial of the EORTC-New Drug Development Group. Eur J Cancer 2004;40(5):667–672.
222. Chiorean EG, Dragovich T, Hamm J, Langmuir VK, Kroll S, Jung DT, Colowick AB, Tidmarsh GF, Loehrer PJ. A phase 1 dose-escalation trial of glufosfamide in combination with gemcitabine in solid tumors including pancreatic adenocarcinoma. Cancer Chemother Pharmacol 2008;61(6):1019–1026.
223. van den Bent MJ, Grisold W, Frappaz D, Stupp R, Desir JP, Lesimple T, Dittrich C, de Jonge MJ, Brandes A, Frenay M, Carpentier AF, Chollet P, Oliveira J, Baron B, Lacombe D, Schuessler M, Fumoleau P. European Organization for Research and Treatment of Cancer (EORTC) open label phase II study on glufosfamide administered as a 60-minute infusion every 3 weeks in recurrent glioblastoma multiforme. Ann Oncol 2003;14(12):1732–1734.
224. Briasoulis E, Pavlidis N, Terret C, Bauer J, Fiedler W, Schoffski P, Raoul JL, Hess D, Selvais R, Lacombe D, Bachmann P, Fumoleau P. Glufosfamide administered using a 1-hour infusion given as first-line treatment for advanced pancreatic cancer. A phase II trial of the EORTC-new drug development group. Eur J Cancer 2003;39(16):2334–2340.
225. Dollner R, Dietz A, Kopun M, Helbig M, Wallner F, Granzow C. Ex vivo responsiveness of head and neck squamous cell carcinoma to glufosfamide, a novel alkylating agent. Anticancer Res 2004;24(5a):2947–2951.

226. Ciuleanu TE, Pavlovsky AV, Bodoky G, Garin AM, Langmuir VK, Kroll S, Tidmarsh GT. A randomised phase III trial of glufosfamide compared with best supportive care in metastatic pancreatic adenocarcinoma previously treated with gemcitabine. Eur J Cancer 2009;45(9):1589–1596.
227. Lin YS, Tungpradit R, Sinchaikul S, An FM, Liu DZ, Phutrakul S, Chen ST. Targeting the delivery of glycan-based paclitaxel prodrugs to cancer cells via glucose transporters. J Med Chem 2008;51(23):7428–7441.
228. Mikuni K, Nakanishi K, Hara K, Hara K, Iwatani W, Amano T, Nakamura K, Tsuchiya Y, Okumoto H, Mandai T. In vivo antitumor activity of novel water-soluble taxoids. Biol Pharm Bull 2008;31(6):1155–1158.
229. Liu DZ, Sinchaikul S, Reddy PV, Chang MY, Chen ST. Synthesis of 2′-paclitaxel methyl 2-glucopyranosyl succinate for specific targeted delivery to cancer cells. Bioorg Med Chem Lett 2007;17(3):617–620.
230. Reux B, Weber V, Galmier MJ, Borel M, Madesclaire M, Madelmont JC, Debiton E, Coudert P. Synthesis and cytotoxic properties of new fluorodeoxyglucose-coupled chlorambucil derivatives. Bioorg Med Chem 2008;16(9):5004–5020.
231. Miot-Noirault E, Reux B, Debiton E, Madelmont JC, Chezal JM, Coudert P, Weber V. Preclinical investigation of tolerance and antitumour activity of new fluorodeoxyglucose-coupled chlorambucil alkylating agents. Investig New Drugs 2011;29(3):424–433.
232. Cao J, Cui S, Li S, Du C, Tian J, Wan S, Qian Z, Gu Y, Chen WR, Wang G. Targeted cancer therapy with a 2-deoxyglucose-based adriamycin complex. Cancer Res 2013;73(4):1362–1373.
233. Lee HY, Kwon JT, Koh M, Cho MH, Park SB. Enhanced efficacy of 7-hydroxy-3-methoxycadalene via glycosylation in in vivo xenograft study. Bioorg Med Chem Lett 2007;17(22):6335–6339.
234. Goff RD, Thorson JS. Assessment of chemoselective neoglycosylation methods using chlorambucil as a model. J Med Chem 2010;53(22):8129–8139.
235. Goff RD, Thorson JS. Enhancement of cyclopamine via conjugation with nonmetabolic sugars. Org Lett 2012;14(10):2454–2457.
236. Oliveri V, Giuffrida ML, Vecchio G, Aiello C, Viale M. Gluconjugates of 8-hydroxyquinolines as potential anti-cancer prodrugs. Dalton Trans 2012;41(15):4530–4535.
237. Koehler KF, Helguero LA, Haldosen LA, Warner M, Gustafsson JA. Reflections on the discovery and significance of estrogen receptor beta. Endocr Rev 2005;26(3):465–478.
238. Zhu BT, Han GZ, Shim JY, Wen Y, Jiang XR. Quantitative structure-activity relationship of various endogenous estrogen metabolites for human estrogen receptor alpha and beta subtypes: Insights into the structural determinants favoring a differential subtype binding. Endocrinology 2006;147(9):4132–4150.
239. Harrington WR, Sheng S, Barnett DH, Petz LN, Katzenellenbogen JA, Katzenellenbogen BS. Activities of estrogen receptor alpha- and beta-selective ligands at diverse estrogen responsive gene sites mediating transactivation or transrepression. Mol Cell Endocrinol 2003;206(1–2):13–22.
240. Falk RT, Brinton LA, Dorgan JF, Fuhrman BJ, Veenstra TD, Xu X, Gierach GL. Relationship of serum estrogens and estrogen metabolites to postmenopausal breast cancer risk: A nested case-control study. Breast Cancer Res 2013;15(2):R34–47.
241. Santen RJ, Yue W, Wang JP. Estrogen metabolites and breast cancer. Steroids 2014.
242. Zafrani B, Aubriot MH, Mouret E, De Cremoux P, De Rycke Y, Nicolas A, Boudou E, Vincent-Salomon A, Magdelenat H, Sastre-Garau X. High sensitivity and specificity of immunohistochemistry for the detection of hormone receptors in breast carcinoma: Comparison with biochemical determination in a prospective study of 793 cases. Histopathology 2000;37(6):536–545.
243. Harvey JM, Clark GM, Osborne CK, Allred DC. Estrogen receptor status by immunohistochemistry is superior to the ligand-binding assay for predicting response to adjuvant endocrine therapy in breast cancer. J Clin Oncol 1999;17(5):1474–1481.
244. Hall JM, Couse JF, Korach KS. The multifaceted mechanisms of estradiol and estrogen receptor signaling. J Biol Chem 2001;276(40):36869–36872.

245. Ameller T, Legrand P, Marsaud V, Renoir JM. Drug delivery systems for oestrogenic hormones and antagonists: The need for selective targeting in estradiol-dependent cancers. J Steroid Biochem Mol Biol 2004;92(1–2):1–18.

246. Dao KL, Hanson RN. Targeting the estrogen receptor using steroid-therapeutic drug conjugates (hybrids). Bioconjug Chem 2012;23(11):2139–2158.

247. Devraj R, Barrett JF, Fernandez JA, Katzenellenbogen JA, Cushman M. Design, synthesis, and biological evaluation of ellipticine-estradiol conjugates. J Med Chem 1996;39(17):3367–3374.

248. Tsumura K, Suzuki A, Tsuzuki T, Tanimoto S, Kaneko H, Matsumura S, Imoto M, Umezawa K, Takahashi D, Toshima K. Molecular design, chemical synthesis, and biological evaluation of agents that selectively photo-degrade the transcription factor estrogen receptor-alpha. Org Biomol Chem 2011;9(18):6357–6366.

249. Khan EH, Ali H, Tian H, Rousseau J, Tessier G, Shafiullah, van Lier JE. Synthesis and biological activities of phthalocyanine-estradiol conjugates. Bioorg Med Chem Lett 2003;13(7):1287–1290.

250. van Lier JE, Kan G, Autenrieth D, Hulsinga E. Steroid-nucleosides. Cancer Treat Rep 1978;62(8):1251–1253.

251. Delbarre A, Oberlin R, Roques BP, Borgna JL, Rochefort H, Le Pecq JB, Jacquemin-Sablon A. Ellipticine derivatives with an affinity to the estrogen receptor, an approach to develop intercalating drugs with a specific effect on the hormone-dependent breast cancer. J Med Chem 1985;28(6):752–761.

252. Eisenbrand G, Berger MR, Fischer J, Schneider MR, Tang W, Zeller WJ. Development of more selective anti-cancer nitrosoureas. Anticancer Drug Des 1988;2(4):351–359.

253. Gupta A, Saha P, Descoteaux C, Leblanc V, Asselin E, Berube G. Design, synthesis and biological evaluation of estradiol-chlorambucil hybrids as anticancer agents. Bioorg Med Chem Lett 2010;20(5):1614–1618.

254. Liu C, Strobl JS, Bane S, Schilling JK, McCracken M, Chatterjee SK, Rahim-Bata R, Kingston DG. Design, synthesis, and bioactivities of steroid-linked taxol analogues as potential targeted drugs for prostate and breast cancer. J Nat Prod 2004;67(2):152–159.

255. Biersack B, Schobert R. Metallodrug conjugates with steroids and selective estrogen receptor modulators (SERM). Curr Med Chem 2009;16(18):2324–2337.

256. Hanson RN, Hua E, Hendricks JA, Labaree D, Hochberg RB. Synthesis and evaluation of 11beta-(4-substituted phenyl) estradiol analogs: Transition from estrogen receptor agonists to antagonists. Bioorg Med Chem 2012;20(12):3768–3780.

257. Hendricks JA, Hanson RN, Amolins M, Mihelcic JM, Blagg BS. Synthesis and preliminary evaluation steroidal antiestrogen-geldanamycin conjugates. Bioorg Med Chem Lett 2013;23(12):3635–3639.

258. Dao KL, Sawant RR, Hendricks JA, Ronga V, Torchilin VP, Hanson RN. Design, synthesis, and initial biological evaluation of a steroidal anti-estrogen-doxorubicin bioconjugate for targeting estrogen receptor-positive breast cancer cells. Bioconjug Chem 2012;23(4):785–795.

259. Kiesewetter DO, Kilbourn MR, Landvatter SW, Heiman DF, Katzenellenbogen JA, Welch MJ. Preparation of four fluorine-18-labeled estrogens and their selective uptakes in target tissues of immature rats. J Nucl Med 1984;25(11):1212–1221.

260. Sasaki M, Fukumura T, Kuwabara Y, Yoshida T, Nakagawa M, Ichiya Y, Masuda K. Biodistribution and breast tumor uptake of 16alpha-[18F]-fluoro-17beta-estradiol in rat. Ann Nucl Med 2000;14(2):127–130.

261. Seimbille Y, Rousseau J, Benard F, Morin C, Ali H, Avvakumov G, Hammond GL, van Lier JE. 18F-labeled difluoroestradiols: preparation and preclinical evaluation as estrogen receptor-binding radiopharmaceuticals. Steroids 2002;67(9):765–775.

262. Oliveira MC, Neto C, Ribeiro Morais G, Thiemann T. Steroid receptor ligands for breast cancer targeting: An insight into their potential role as PET imaging agents. Curr Med Chem 2013;20(2):222–245.

263. Turcotte E, Paquette M, Lavallee E, Langlois R, Dubreuil S, Senta H, Lecomte R, Guerin B, Benard F, van Lier J. Comparison of 4FMFES-PET with FES-PET in a phase II trial to detect estrogen receptor-positive breast cancer: Preliminary results. J Nucl Med 2012;53(1_MeetingAbstracts):281.

264. Hanson RN, Franke LA. Preparation and evaluation of 17 alpha-[125I]iodovinyl-11 beta-methoxyestradiol as a highly selective radioligand for tissues containing estrogen receptors: Concise communication. J Nucl Med 1984;25(9):998–1002.

265. Katzenellenbogen JA, McElvany KD, Senderoff SG, Carlson KE, Landvatter SW, Welch MJ. 16 alpha-[77Br]bromo-11 beta-methoxyestradiol-17 beta: A gamma-emitting estrogen imaging agent with high uptake and retention by target organs. J Nucl Med 1982;23(5):411–419.

266. VanBrocklin HF, Carlson KE, Katzenellenbogen JA, Welch MJ. 16 Beta.-([18F]fluoro)estrogens: Systematic investigation of a new series of fluorine-18-labeled estrogens as potential imaging agents for estrogen-receptor-positive breast tumors. J Med Chem 1993;36(11):1619–1629.

267. Jonson SD, Bonasera TA, Dehdashti F, Cristel ME, Katzenellenbogen JA, Welch MJ. Comparative breast tumor imaging and comparative in vitro metabolism of 16alpha-[18F]fluoroestradiol-17beta and 16beta-[18F]fluoromoxestrol in isolated hepatocytes. Nucl Med Biol 1999;26(1):123–130.

268. Dence CS, Napolitano E, Katzenellenbogen JA, Welch MJ. Carbon-11-labeled estrogens as potential imaging agents for breast tumors. Nucl Med Biol 1996;23(4):491–496.

269. Inoue T, Kim EE, Wallace S, Yang DJ, Wong FC, Bassa P, Cherif A, Delpassand E, Buzdar A, Podoloff DA. Positron emission tomography using [18F]fluorotamoxifen to evaluate therapeutic responses in patients with breast cancer: Preliminary study. Cancer Biother Radiopharm 1996;11(4):235–245.

270. McElvany KD, Katzenellenbogen JA, Shafer KE, Siegel BA, Senderoff SG, Welch MJ. 16 Alpha-[77Br]bromoestradiol: Dosimetry and preliminary clinical studies. J Nucl Med 1982;23(5):425–430.

271. Parent E, Katzenellenbogen, J, Welch, M. Preclinical evaluation of 16α-[76Br/77Br]-bromo-11β-methoxyestradiol as a selective radiotherapeutic agent in estrogen receptor positive tumors. Radiological Society of North America 2009 Scientific Assembly and Annual Meeting, November 29–December 4, 2009, Chicago, IL.

272. Tsai MJ, O'Malley BW. Molecular mechanisms of action of steroid/thyroid receptor superfamily members. Annu Rev Biochem 1994;63:451–486.

273. Clarke RB, Anderson E, Howell A. Steroid receptors in human breast cancer. Trends Endocrinol Metab 2004;15(7):316–323.

274. Clarke RB, Howell A, Potten CS, Anderson E. Dissociation between steroid receptor expression and cell proliferation in the human breast. Cancer Res 1997;57(22):4987–4991.

275. Balleine R, Mote P, Hunt SN, McGowan E, Clarke C. Progesterone receptors in normal and neoplastic breast. In: Ethier S, Ed. Endocrine Oncology, Contemporary Endocrinology. Humana Press Inc., Totowa, NJ; 2000. p 35–47.

276. Dehdashti F, McGuire AH, van Brocklin HF, Siegel BA, Andriole DP, Griffeth LK, Pomper MG, Katzenellenbogen JA, Welch MJ. Assessment of 21-[18F]fluoro-16 alpha-ethyl-19-norprogesterone as a positron-emitting radiopharmaceutical for the detection of progestin receptors in human breast carcinomas. J Nucl Med 1991;32(8):1532–1537.

277. Buckman BO, Bonasera TA, Kirschbaum KS, Welch MJ, Katzenellenbogen JA. Fluorine-18-labeled progestin 16 alpha, 17 alpha-dioxolanes: Development of high-affinity ligands for the progesterone receptor with high in vivo target site selectivity. J Med Chem 1995;38(2):328–337.

278. Dehdashti F, Laforest R, Gao F, Aft RL, Dence CS, Zhou D, Shoghi KI, Siegel BA, Katzenellenbogen JA, Welch MJ. Assessment of progesterone receptors in breast carcinoma by PET with 21–18F-fluoro-16alpha,17alpha-[(R)-(1′-alpha-furylmethylidene)dioxy]-19-norpregn- 4-ene-3,20-dione. J Nucl Med 2012;53(3):363–370.

279. Zhou HB, Lee JH, Mayne CG, Carlson KE, Katzenellenbogen JA. Imaging progesterone receptor in breast tumors: Synthesis and receptor binding affinity of fluoroalkyl-substituted analogues of tanaproget. J Med Chem 2010;53(8):3349–3360.

280. Lee JH, Zhou HB, Dence CS, Carlson KE, Welch MJ, Katzenellenbogen JA. Development of [F-18]fluorine-substituted Tanaproget as a progesterone receptor imaging agent for positron emission tomography. Bioconjug Chem 2010;21(6):1096–1104.

281. Dhyani MV, Satpati D, Korde A, Sarma HD, Kumar C, Banerjee S. Preparation and preliminary bioevaluation of 99mTc(CO)3–11beta-progesterone derivative prepared via click chemistry route. Nucl Med Biol 2010;37(8):997–1004.

282. McPhaul MJ. Androgen receptor mutations and androgen insensitivity. Mol Cell Endocrinol 2002;198(1–2):61–67.

283. Mooradian AD, Morley JE, Korenman SG. Biological actions of androgens. Endocr Rev 1987;8(1):1–28.

284. Labrie F, Luu-The V, Labrie C, Belanger A, Simard J, Lin SX, Pelletier G. Endocrine and intracrine sources of androgens in women: Inhibition of breast cancer and other roles of androgens and their precursor dehydroepiandrosterone. Endocr Rev 2003;24(2):152–182.

285. Marquis JC, Hillier SM, Dinaut AN, Rodrigues D, Mitra K, Essigmann JM, Croy RG. Disruption of gene expression and induction of apoptosis in prostate cancer cells by a DNA-damaging agent tethered to an androgen receptor ligand. Chem Biol 2005;12(7):779–787.

286. Itoh Y, Kitaguchi R, Ishikawa M, Naito M, Hashimoto Y. Design, synthesis and biological evaluation of nuclear receptor-degradation inducers. Bioorg Med Chem 2011;19(22):6768–6778.

287. Huxley M, Sanchez-Cano C, Browning MJ, Navarro-Ranninger C, Quiroga AG, Rodger A, Hannon MJ. An androgenic steroid delivery vector that imparts activity to a non-conventional platinum(II) metallo-drug. Dalton Trans 2010;39(47):11353–11364.

288. Sanchez-Cano C, Huxley M, Ducani C, Hamad AE, Browning MJ, Navarro-Ranninger C, Quiroga AG, Rodger A, Hannon MJ. Conjugation of testosterone modifies the interaction of monofunctional cationic platinum(II) complexes with DNA, causing significant alterations to the DNA helix. Dalton Trans 2010;39(47):11365–11374.

289. Cogan PS, Koch TH. Studies of targeting and intracellular trafficking of an anti-androgen doxorubicin-formaldehyde conjugate in PC-3 prostate cancer cells bearing androgen receptor-GFP chimera. J Med Chem 2004;47(23):5690–5699.

290. Gryder BE, Akbashev MJ, Rood MK, Raftery ED, Meyers WM, Dillard P, Khan S, Oyelere AK. Selectively targeting prostate cancer with antiandrogen equipped histone deacetylase inhibitors. ACS Chem Biol 2013;8(11):2550–2560.

291. Yang J, Bohl CE, Nair VA, Mustafa SM, Hong SS, Miller DD, Dalton JT. Preclinical pharmacology of a nonsteroidal ligand for androgen receptor-mediated imaging of prostate cancer. J Pharmacol Exp Therapeut 2006;317(1):402–408.

292. Marhefka CA, Gao W, Chung K, Kim J, He Y, Yin D, Bohl C, Dalton JT, Miller DD. Design, synthesis, and biological characterization of metabolically stable selective androgen receptor modulators. J Med Chem 2004;47(4):993–998.

293. Nair VA, Mustafa SM, Mohler ML, Fisher SJ, Dalton JT, Miller DD. Synthesis of novel iodo derived bicalutamide analogs. Tetrahedr Lett 2004;45(51):9475–9477.

294. Kortylewicz ZP, Mack E, Enke CA, Estes KA, Mosley RL, Baranowska-Kortylewicz J. Preclinical evaluation of investigational radiopharmaceutical RISAD-P intended for use as a diagnostic and molecular radiotherapy agent for prostate cancer. Prostate 2015;75(1):8–22.

295. Das T, Banerjee S, Samuel G, Bapat K, Subramanian S, Pillai MR, Venkatesh M. A novel 99mTc-labeled testosterone derivative as a potential agent for targeting androgen receptors. Bioorg Med Chem Lett 2006;16(22):5788–5792.

296. Collina S. New perspectives in cancer therapy: The biotin-antitumor molecule conjugates. Med Chem 2014;S1:004.

297. Luo S, Kansara VS, Zhu X, Mandava NK, Pal D, Mitra AK. Functional characterization of sodium-dependent multivitamin transporter in MDCK-MDR1 cells and its utilization as a target for drug delivery. Mol Pharm 2006;3(3):329–339.

298. Vadlapudi AD, Vadlapatla RK, Pal D, Mitra AK. Functional and molecular aspects of biotin uptake via SMVT in human corneal epithelial (HCEC) and retinal pigment epithelial (D407) cells. AAPS J 2012;14(4):832–842.
299. Russell-Jones G, McEwan J. Amplification of biotin-mediated targeting. Google Patents, 2006.
300. Chen S, Zhao X, Chen J, Chen J, Kuznetsova L, Wong SS, Ojima I. Mechanism-based tumor-targeting drug delivery system. Validation of efficient vitamin receptor-mediated endocytosis and drug release. Bioconjug Chem 2010;21(5):979–987.
301. Ibsen S, Zahavy E, Wrasdilo W, Berns M, Chan M, Esener S. A novel doxorubicin prodrug with controllable photolysis activation for cancer chemotherapy. Pharm Res 2010;27(9):1848–1860.
302. Maiti S, Park N, Han JH, Jeon HM, Lee JH, Bhuniya S, Kang C, Kim JS. Gemcitabine-coumarin-biotin conjugates: A target specific theranostic anticancer prodrug. J Am Chem Soc 2013;135(11):4567–4572.
303. Bhuniya S, Lee MH, Jeon HM, Han JH, Lee JH, Park N, Maiti S, Kang C, Kim JS. A fluorescence off-on reporter for real time monitoring of gemcitabine delivery to the cancer cells. Chem Commun 2013;49(64):7141–7143.
304. Plażuk D, Zakrzewski J, Salmain M, Błauż A, Rychlik B, Strzelczyk P, Bujacz A, Bujacz G. Ferrocene–biotin conjugates targeting cancer cells: Synthesis, interaction with avidin, cytotoxic properties and the crystal structure of the complex of avidin with a biotin–linker–ferrocene conjugate. Organometallics 2013;32(20):5774–5783.
305. Saha S, Majumdar R, Hussain A, Dighe RR, Chakravarty AR. Biotin-conjugated tumour-targeting photocytotoxic iron(III) complexes. Philos Trans A Math Phys Eng Sci 2013;371(1995):20120190.
306. Shi JF, Wu P, Jiang ZH, Wei XY. Synthesis and tumor cell growth inhibitory activity of biotinylated annonaceous acetogenins. Eur J Med Chem 2014;71:219–228.
307. Vineberg JG, Zuniga ES, Kamath A, Chen YJ, Seitz JD, Ojima I. Design, synthesis, and biological evaluations of tumor-targeting dual-warhead conjugates for a taxoid-camptothecin combination chemotherapy. J Med Chem 2014;57(13):5777–5791.
308. Vineberg JG, Wang T, Zuniga ES, Ojima I. Design, synthesis, and biological evaluation of theranostic vitamin-linker-taxoid conjugates. J Med Chem 2015;58(5):2406–2416.
309. Corti A, Curnis F, Arap W, Pasqualini R. The neovasculature homing motif NGR: More than meets the eye. Blood 2008;112(7):2628–2635.
310. Mate G, Kertesz I, Enyedi KN, Mezo G, Angyal J, Vasas N, Kis A, Szabo E, Emri M, Biro T, Galuska L, Trencsenyi G. In vivo imaging of Aminopeptidase N (CD13) receptors in experimental renal tumors using the novel radiotracer (68)Ga-NOTA-c(NGR). Eur J Pharm Sci 2015;69:61–71.
311. Curnis F, Arrigoni G, Sacchi A, Fischetti L, Arap W, Pasqualini R, Corti A. Differential binding of drugs containing the NGR motif to CD13 isoforms in tumor vessels, epithelia, and myeloid cells. Cancer Res 2002;62(3):867–874.
312. Corti A, Pastorino F, Curnis F, Arap W, Ponzoni M, Pasqualini R. Targeted drug delivery and penetration into solid tumors. Med Res Rev 2012;32(5):1078–1091.
313. Wang RE, Niu Y, Wu H, Hu Y, Cai J. Development of NGR-based anti-cancer agents for targeted therapeutics and imaging. Anticancer Agents Med Chem 2012;12(1):76–86.
314. Arap W, Pasqualini R, Ruoslahti E. Cancer treatment by targeted drug delivery to tumor vasculature in a mouse model. Science 1998;279(5349):377–380.
315. Colombo G, Curnis F, De Mori GM, Gasparri A, Longoni C, Sacchi A, Longhi R, Corti A. Structure-activity relationships of linear and cyclic peptides containing the NGR tumor-homing motif. J Biol Chem 2002;277(49):47891–47897.
316. Di Matteo P, Curnis F, Longhi R, Colombo G, Sacchi A, Crippa L, Protti MP, Ponzoni M, Toma S, Corti A. Immunogenic and structural properties of the Asn-Gly-Arg (NGR) tumor neovasculature-homing motif. Mol Immunol 2006;43(10):1509–1518.
317. Zhang Z, Hatta H, Tanabe K, Nishimoto S. A new class of 5-fluoro-2′-deoxyuridine prodrugs conjugated with a tumor-homing cyclic peptide CNGRC by ester linkers: Synthesis, reactivity, and tumor-cell-selective cytotoxicity. Pharm Res 2005;22(3):381–389.

318. Zhang Z, Hatta H, Ito T, Nishimoto S. Synthesis and photochemical properties of photoactivated antitumor prodrugs releasing 5-fluorouracil. Org Biomol Chem 2005;3(4):592–596.

319. Ndinguri MW, Solipuram R, Gambrell RP, Aggarwal S, Hammer RP. Peptide targeting of platinum anti-cancer drugs. Bioconjug Chem 2009;20(10):1869–1878.

320. Ma W, Wang Z, Yang W, Ma X, Kang F, Wang J. Biodistribution and SPECT imaging study of 99mTc labeling NGR peptide in nude mice bearing human HepG2 hepatoma. BioMed Res Int 2014;2014:6. doi:10.1155/2014/618096.

321. Chen K, Ma W, Li G, Wang J, Yang W, Yap LP, Hughes LD, Park R, Conti PS. Synthesis and evaluation of 64Cu-labeled monomeric and dimeric NGR peptides for MicroPET imaging of CD13 receptor expression. Mol Pharm 2013;10(1):417–427.

322. Zhang J, Lu X, Wan N, Hua Z, Wang Z, Huang H, Yang M, Wang F. 68Ga-DOTA-NGR as a novel molecular probe for APN-positive tumor imaging using MicroPET. Nucl Med Biol 2014;41(3):268–275.

323. Shao Y, Liang W, Kang F, Yang W, Ma X, Li G, Zong S, Chen K, Wang J. A direct comparison of tumor angiogenesis with (68)Ga-labeled NGR and RGD peptides in HT-1080 tumor xenografts using microPET imaging. Amino Acids 2014;46(10):2355–2364.

324. Pathuri G, Hedrick AF, Disch BC, Doan JT, Ihnat MA, Awasthi V, Gali H. Synthesis and evaluation of novel Tc-99m labeled probestin conjugates for imaging APN/CD13 expression in vivo. Bioconjug Chem 2012;23(1):115–124.

325. Desgrosellier JS, Cheresh DA. Integrins in cancer: Biological implications and therapeutic opportunities. Nat Rev Cancer 2010;10(1):9–22.

326. Kim JW, Lee HS. Tumor targeting by doxorubicin-RGD-4C peptide conjugate in an orthotopic mouse hepatoma model. Int J Mol Med 2004;14(4):529–535.

327. de Groot FM, Broxterman HJ, Adams HP, van Vliet A, Tesser GI, Elderkamp YW, Schraa AJ, Kok RJ, Molema G, Pinedo HM, Scheeren HW. Design, synthesis, and biological evaluation of a dual tumor-specific motive containing integrin-targeted plasmin-cleavable doxorubicin prodrug. Mol Cancer Ther 2002;1(11):901–911.

328. Janssen M, Oyen WJ, Massuger LF, Frielink C, Dijkgraaf I, Edwards DS, Radjopadhye M, Corstens FH, Boerman OC. Comparison of a monomeric and dimeric radiolabeled RGD-peptide for tumor targeting. Cancer Biother Radiopharm 2002;17(6):641–646.

329. Janssen ML, Oyen WJ, Dijkgraaf I, Massuger LF, Frielink C, Edwards DS, Rajopadhye M, Boonstra H, Corstens FH, Boerman OC. Tumor targeting with radiolabeled alpha(v)beta(3) integrin binding peptides in a nude mouse model. Cancer Res 2002;62(21):6146–6151.

330. Ryppa C, Mann-Steinberg H, Fichtner I, Weber H, Satchi-Fainaro R, Biniossek ML, Kratz F. In vitro and in vivo evaluation of doxorubicin conjugates with the divalent peptide E-[c(RGDfK)2] that targets integrin alphavbeta3. Bioconjug Chem 2008;19(7):1414–1422.

331. Chen X, Plasencia C, Hou Y, Neamati N. Synthesis and biological evaluation of dimeric RGD peptide-paclitaxel conjugate as a model for integrin-targeted drug delivery. J Med Chem 2005;48(4):1098–1106.

332. Cao Q, Li ZB, Chen K, Wu Z, He L, Neamati N, Chen X. Evaluation of biodistribution and anti-tumor effect of a dimeric RGD peptide-paclitaxel conjugate in mice with breast cancer. Eur J Nucl Med Mol Imaging 2008;35(8):1489–1498.

333. Colombo R, Mingozzi M, Belvisi L, Arosio D, Piarulli U, Carenini N, Perego P, Zaffaroni N, De Cesare M, Castiglioni V, Scanziani E, Gennari C. Synthesis and biological evaluation (in vitro and in vivo) of cyclic arginine-glycine-aspartate (RGD) peptidomimetic-paclitaxel conjugates targeting integrin alphaVbeta3. J Med Chem 2012;55(23):10460–10474.

334. Dal Pozzo A, Esposito E, Ni M, Muzi L, Pisano C, Bucci F, Vesci L, Castorina M, Penco S. Conjugates of a novel 7-substituted camptothecin with RGD-peptides as alpha(v)beta(3) integrin ligands: An approach to tumor-targeted therapy. Bioconjug Chem 2010;21(11):1956–1967.

335. Alloatti D, Giannini G, Vesci L, Castorina M, Pisano C, Badaloni E, Cabri W. Camptothecins in tumor homing via an RGD sequence mimetic. Bioorg Med Chem Lett 2012;22(20):6509–6512.

336. Li X, Hou J, Wang C, Liu X, He H, Xu P, Yang Z, Chen Z, Wu Y, Zhang L. Synthesis and biological evaluation of RGD-conjugated MEK1/2 kinase inhibitors for integrin-targeted cancer therapy. Molecules 2013;18(11):13957–13978.
337. Mukhopadhyay S, Barnes CM, Haskel A, Short SM, Barnes KR, Lippard SJ. Conjugated platinum(IV)-peptide complexes for targeting angiogenic tumor vasculature. Bioconjug Chem 2008;19(1):39–49.
338. Massaguer A, Gonzalez-Canto A, Escribano E, Barrabes S, Artigas G, Moreno V, Marchan V. Integrin-targeted delivery into cancer cells of a Pt(IV) pro-drug through conjugation to RGD-containing peptides. Dalton Trans 2015;44(1):202–212.
339. Buckley CD, Pilling D, Henriquez NV, Parsonage G, Threlfall K, Scheel-Toellner D, Simmons DL, Akbar AN, Lord JM, Salmon M. RGD peptides induce apoptosis by direct caspase-3 activation. Nature 1999;397(6719):534–539.
340. Li F, Liu J, Jas GS, Zhang J, Qin G, Xing J, Cotes C, Zhao H, Wang X, Diaz LA, Shi ZZ, Lee DY, Li KC, Li Z. Synthesis and evaluation of a near-infrared fluorescent non-peptidic bivalent integrin alpha(v)beta(3) antagonist for cancer imaging. Bioconjug Chem 2010;21(2):270–278.
341. Sundberg TB, Xavier RJ, Schreiber SL, Shamji AF. Small-molecule control of cytokine function: new opportunities for treating immune disorders. Curr Opin Chem Biol 2014;23:23–30.
342. Nakashima-Matsushita N, Homma T, Yu S, Matsuda T, Sunahara N, Nakamura T, Tsukano M, Ratnam M, Matsuyama T. Selective expression of folate receptor beta and its possible role in methotrexate transport in synovial macrophages from patients with rheumatoid arthritis. Arthritis Rheum 1999;42(8):1609–1616.
343. Paulos CM, Turk MJ, Breur GJ, Low PS. Folate receptor-mediated targeting of therapeutic and imaging agents to activated macrophages in rheumatoid arthritis. Adv Drug Deliv Rev 2004;56(8):1205–1217.
344. Yamaguchi T, Hirota K, Nagahama K, Ohkawa K, Takahashi T, Nomura T, Sakaguchi S. Control of immune responses by antigen-specific regulatory T cells expressing the folate receptor. Immunity 2007;27(1):145–159.
345. Matejuk A, Adlard K, Zamora A, Silverman M, Vandenbark AA, Offner H. 17 beta-estradiol inhibits cytokine, chemokine, and chemokine receptor mRNA expression in the central nervous system of female mice with experimental autoimmune encephalomyelitis. J Neurosci Res 2001;65(6):529–542.
346. Wang C, Dehghani B, Li Y, Kaler LJ, Proctor T, Vandenbark AA, Offner H. Membrane estrogen receptor regulates experimental autoimmune encephalomyelitis through up-regulation of programmed death 1. J Immunol 2009;182(5):3294–3303.
347. Siebels M, Rohrmann K, Oberneder R, Stahler M, Haseke N, Beck J, Hofmann R, Kindler M, Kloepfer P, Stief C. A clinical phase I/II trial with the monoclonal antibody cG250 (RENCAREX(R)) and interferon-alpha-2a in metastatic renal cell carcinoma patients. World J Urol 2011;29(1):121–126.
348. Ganesh T. Improved biochemical strategies for targeted delivery of taxoids. Bioorg Med Chem 2007;15(11):3597–3623.
349. Sievers EL, Senter PD. Antibody-drug conjugates in cancer therapy. Annu Rev Med 2013;64:15–29.
350. Heng BC, Cao T. Making cell-permeable antibodies (Transbody) through fusion of protein transduction domains (PTD) with single chain variable fragment (scFv) antibodies: Potential advantages over antibodies expressed within the intracellular environment (Intrabody). Med Hypotheses 2005;64(6):1105–1108.

Chin Siang Kue *obtained his MSc in Molecular Immunology (2011) at Korea University. He received Bright Spark scholarship from University of Malaya (UM), Malaysia, in 2013 to pursue his PhD. His current research interests are targeted cancer therapy and immunology.*

Anyanee Kamkaew *received her PhD (2015) from Texas A&M University (TAMU), USA. She is now a Postdoc researcher at University of Wisconsin, USA, studying synthesis of organic and biomolecules for intramolecular delivery and targeting.*

Kevin Burgess *obtained his PhD from University of Cambridge, UK. He was Assistant Professor at Rice University, USA before joining TAMU where he is currently Rachal Professor of Chemistry. His research interests include synthetic organic methods for preparing small molecules that bind to proteins for active targeting of tumors and disruption of PPIs.*

Lik Voon Kiew *received his doctorate from the UM (2008). He is currently a senior lecturer at the Department of Pharmacology, UM. His current research interests include the development and evaluation of cancer targeting drug carriers and photosensitizers.*

Lip Yong Chung *received his doctorate (1990) in Pharmacy from the University of Cardiff, UK. He is currently a Professor in Pharmaceutical Sciences, UM. His research interests include the design of bioactive molecules of pharmacological interest and the study of targeting biological systems.*

Hong Boon Lee *obtained her BA (1996) and PhD (2000) in Chemistry from University of Cambridge, UK. She conducted Postdoc research in Prof Kevin Burgess' group in TAMU. She is currently Senior Researcher at UM, with research interests in photodynamic therapy and drug delivery for cancer.*

Organic & Biomolecular Chemistry

PAPER

View Article Online
View Journal | View Issue

Published on 13 May 2016. Downloaded by Texas A & M University on 29/09/2016 19:53:27.

Cite this: *Org. Biomol. Chem.*, 2016, **14**, 5049

Anthranilic acid-containing cyclic tetrapeptides: at the crossroads of conformational rigidity and synthetic accessibility†

Dongyue Xin and Kevin Burgess*

Received 1st April 2016,
Accepted 29th April 2016

DOI: 10.1039/c6ob00693k

www.rsc.org/obc

Each amino acid in a peptide contributes three atom units to main-chains, hence natural cyclic peptides can be 9, 12, 15, …. *i.e.* 3*n* membered-rings, where *n* is the number of amino acids. Cyclic peptides that are 9 or 12-membered ring compounds tend to be hard to prepare because of strain, while their one amino acid homologs (15-membered cyclic pentapeptides) are not conformationally homogeneous unless constrained by strategically placed proline or D-amino acid residues. We hypothesized that replacing one genetically encoded amino acid in a cyclic tetrapeptide with a rigid β-amino acid would render peptidomimetic designs that rest at a useful crossroads between synthetic accessibility and conformational rigidity. Thus this research explored non-proline containing 13-membered ring peptides **1** featuring one anthranilic acid (*Anth*) residue. Twelve cyclic peptides of this type were prepared, and in doing so the viability of both solution- and solid-phase methods was demonstrated. The library produced contained a complete set of four diastereoisomers of the sequence **1aaf** (*i.e. cyclo*-AlaAlaPhe*Anth*). Without exception, these four diastereoisomers each adopted one predominant conformation in solution; basically these conformations feature amide *N*–*H* vectors puckering above and below the equatorial plane, and approximately oriented their *N*–*H* atoms towards the polar axis. Moreover, the shapes of these conformers varied in a logical and predictable way (NOE, temperature coefficient, D/H exchange, circular dichroism). Comparisons were made of the side-chain orientations presented by compounds **1aaa** in solution with ideal secondary structures and protein–protein interaction interfaces. Various **1aaa** stereoisomers in solution present side-chains in similar orientations to regular and inverse γ-turns, and to the most common β-turns (types I and II). Consistent with this, compounds **1aaa** have a tendency to mimic various turns and bends at protein–protein interfaces. Finally, proteolytic- and hydrolytic stabilities of the compounds at different pHs indicate they are robust relative to related linear peptides, and rates of permeability through an artificial membrane indicate their structures are conducive to cell permeability.

Introduction

Cyclization of linear peptides increases their proteolytic stabilities and rigidities. In ideal cases these structures will adopt only *one* preferred conformation; if that occurs, less entropy will be surrendered on interaction with biomolecular receptors, increasing the free energies for the interactions. Observation of a strongly preferred conformation in solution also makes it probable that the molecule will bind to the receptor in a similar conformation, compared to other situations in which the compound exists in several solution conformations. Moreover, exclusion of competing conformational states reduces possibilities for off-target binding.

Inconveniently, cyclic peptides composed of the 20 genetically encoded amino acids miss a "sweet spot" ring size where conformational homogeneity is attained without compromising ease of syntheses. Thus, cyclic tri-[1–4] **A** and tetra-peptides **B** [5–11] are notoriously difficult to prepare because they are constrained in 9- and 12-membered ring conformations. Analogs of cyclic tetrapeptides, like the 12-membered ring system **C**, may be more easily prepared but another problem arises: *cis*/*trans* amide bond equilibria introduces conformational heterogeneity.[12] Cyclic pentapeptides,[13–15] are easier to make than cyclic tri- or tetrapeptides[16] because their 15-membered rings

Department of Chemistry, Texas A & M University, Box 30012, College Station, TX 77842, USA. E-mail: burgess@tamu.edu

† Electronic supplementary information (ESI) available: Experimental procedures and spectroscopic data for all compounds; H/D exchange experiments and temperature coefficient measurements; procedures and results for conformational modeling with QMD and MacroModel, results of the overlays on turn structures, data of protein database mining and the procedure for QikProp calculations; procedures for stability studies and the PAMPA assay. See DOI: 10.1039/c6ob00693k

Published on 13 May 2016. Downloaded by Texas A & M University on 29/09/2016 19:53:27.

are less strained, but they tend to equilibrate between conformers **D** [1–5] containing β- and γ-turns. Certain states in the **D** [1–5] equilibrium can be favored if one of the amino acids has a D-configuration, especially D-Pro,[17] but most cyclic pentapeptides and higher homologs overall do not tend to be rigid unless further constrained (Fig. 1).[18,19]

Based on the observations above, there should be favored ring sizes in peptidomimetic design where non-genetically encoded residues replace one amino acid to give conformationally rigid 13- or 14-membered rings. Ghadiri and coworkers, for instance,[20,21] have used copper-mediated azide–alkyne cycloadditions to give the 13-membered rings **E** which were conformationally rigid.[22] In other illustrative work, Fairlie *et al.* substituted β-amino acids into cyclic tetrapeptides and found some 13-membered ring systems, including **F**[23] and **G**,[24] that could be prepared efficiently, and were conformationally rigid. However, that same work showed similar, but conformationally *heterogeneous*, 13-membered ring systems.[24]

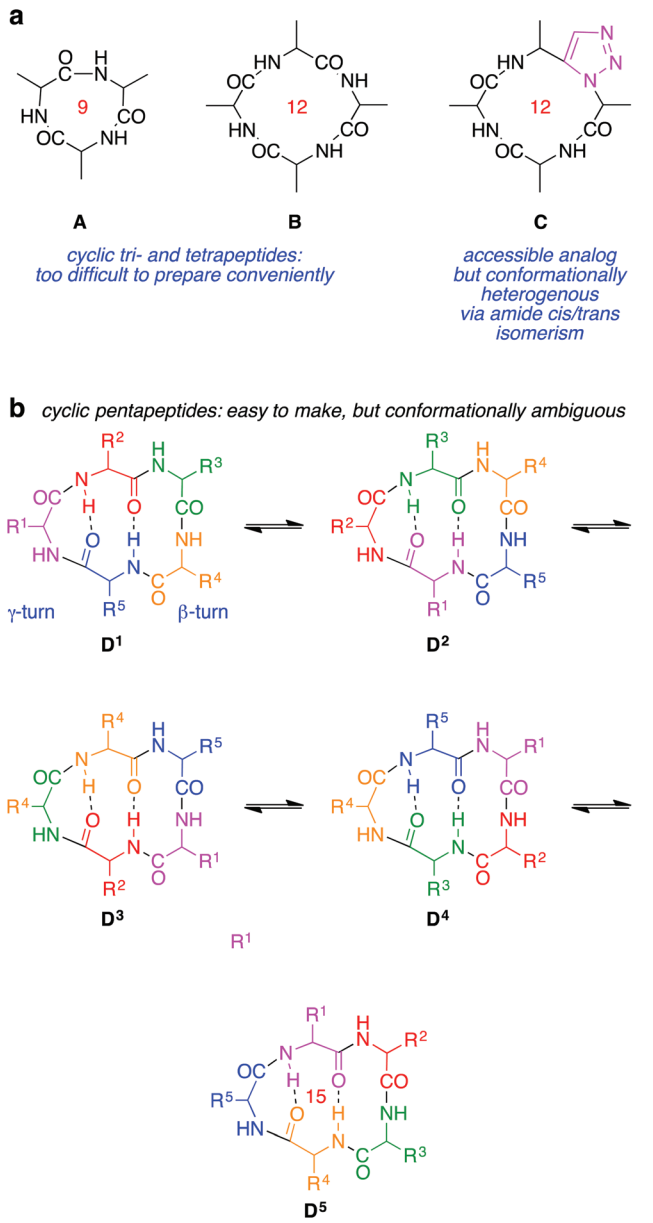

Fig. 1 (a) 12-Membered ring peptidic systems (*e.g.* cyclic tetrapeptides) are highly constrained and their conformations may be complicated by *cis-trans* isomerism. (b) Cyclic pentapeptides tend to equilibrate between similar states containing both γ and β-turns, *i.e.* they tend to be conformationally heterogeneous. (c) 13-Membered rings may give only one preferred conformer (*e.g.* **E**–**G**) but this issue has not previously been studied for systems containing the *Anth* residue (*e.g.* for **H** and **I**).

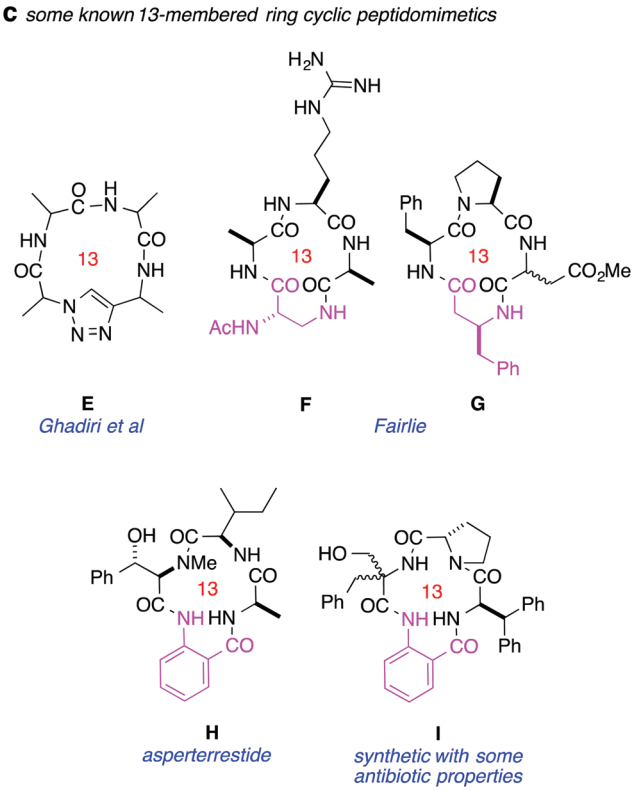

Fig. 1 *(Contd).*

Anthranilic acid is readily available and more rigid than most other β-amino acids. Several peptidic macrocycles containing anthranilic acid occur in Nature, most where this unit is one of five in a pentapeptide ring.[25–38] There are also numerous examples of similar hexapeptides and higher homologs incorporating anthranilic acid,[25,39–45] a few 10-membered tripeptide derivatives[46–48] and several cyclic systems containing the "*Anth*" residue and another non-encoded amino acid.[49–51] However, 13-membered ring systems containing this ubiquitous residue have been under-explored. Only one natural tetrapeptide **H** that features *Anth* in a 13-membered ring has been discovered,[52] and the only 13-membered cyclic peptide containing *Anth* that has been synthesized is compound **I**, prepared as part of a medicinal chemistry project.[53] To the best of our knowledge, neither **H** nor **I** have been studied in solution to determine their conformational biases.

We hypothesized compounds **1** could be prepared from readily available starting materials, and would be conformationally

 This journal is © The Royal Society of Chemistry 2016

Published on 13 May 2016. Downloaded by Texas A & M University on 29/09/2016 19:53:27.

rigid. This paper describes how those compounds were made, and the conformational biases of one complete set of enantiomers in this series. In the event the conformations of these molecules were shown to correlate with their chiral amino acid stereochemistries in a logical, easily understood, way that is useful for predicting the preferred shapes of these rigid scaffolds.

do these cyclic peptidomimetics occupy the sweet spot that combines synthetic accessibility and conformational homogeneity?

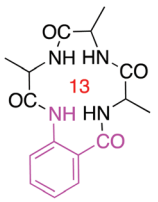

1
this work

Results and discussion

Syntheses *via* iterative precipitations

Couplings to anthranilic acid are not facile because the aromatic amine is deactivated *via* resonance. However, Scheme 1 describes how solution-phase syntheses of several compounds were achieved using a large excess of *Anth* and a high concentration of all agents; if high concentrations were not used then epimerization was competitive with product formation. Use of a relatively weak base (*N*-methyl morpholine) and of the superior, though more expensive, coupling additive HOAt,[54] was also beneficial in this step.

Early in this study we realized the physiochemical properties of peptides containing anthranilic acid facilitated their isolation. Thus, coupling three amino acids to the *Anth* unit gave products that precipitated from dichloromethane/hexanes with sufficient purities to use in the next steps. In fact, the only chromatography needed in the "Boc-approach" to the cyclic systems shown in Scheme 1 was to isolate the cyclized product. Serine and tyrosine residues in the compounds prepared were protected with benzyl groups. Glutamic acid side-chain protection was achieved using a *tert*-butyl ester, which withstands selective deprotection of the *N*-Boc functionality with 4 M HCl.[55]

Scheme S2 (ESI†) shows a similar solution-phase approach to the same types of products but using Cbz protected amino acids and *N*α-deprotection *via* hydrogenolysis. In one of these syntheses the first amino acid added was H-Glu(O^{t}Bu) where successive deprotection under acidic conditions, as in Scheme 1, might have eroded the yield of this product, but *N*-deprotection *via* hydrogenolysis circumvented this potential problem. A complementary *solid phase* Fmoc-approach was also established (Scheme S3, ESI†), based on 2-chloro-trityl polystyrene resin and involves cleavage from the support then cyclization in the final step.

Conformational analyses

One goal in this study was to elucidate the intrinsic conformational biases of the stereoisomeric scaffolds **1** with minimal perturbation from side-chain interactions. The ideal system to study might have been the simple peptide **1aaa** (or *cyclo*-AlaAlaAla*Anth*). However, there was insufficient dispersion of the ^{1}H NMR peaks in that particular compound to facilitate convenient conformational analyses. Consequently, we decided to

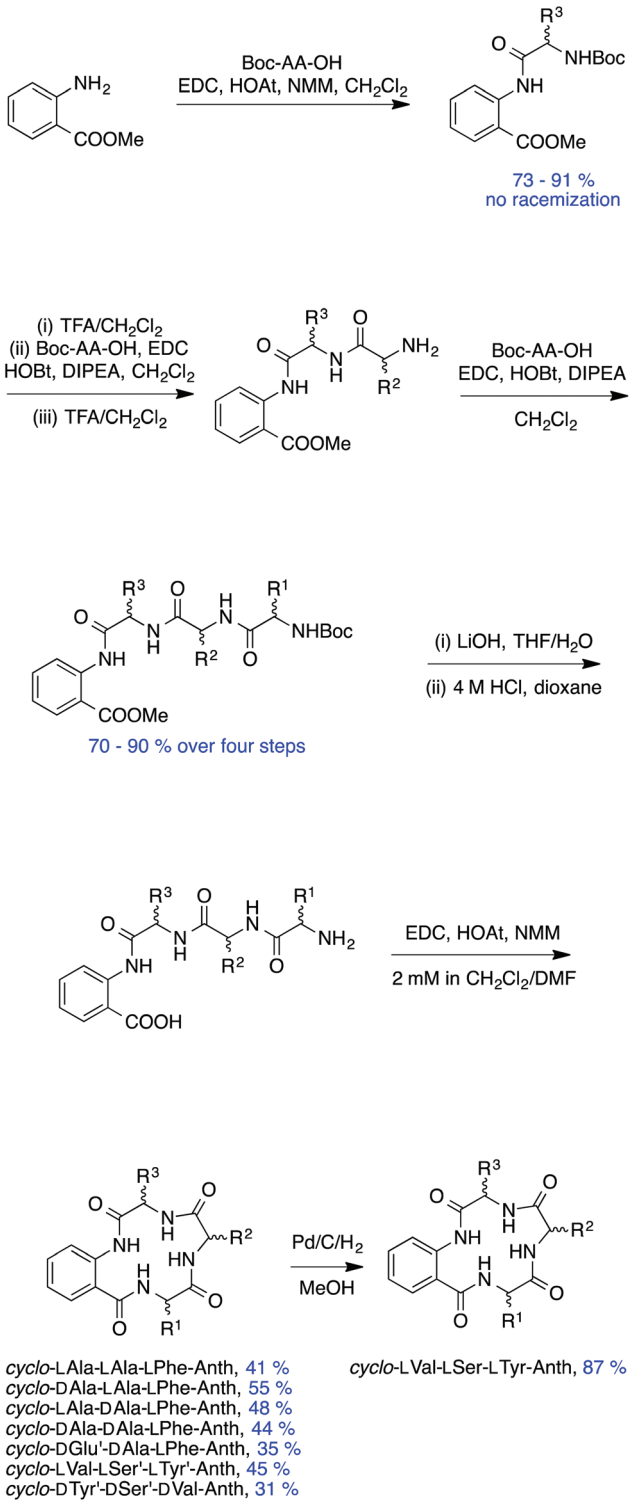

Scheme 1 Boc approach to products **1**.

Published on 13 May 2016. Downloaded by Texas A & M University on 29/09/2016 19:53:27.

study one enantiomeric series of the compounds **1aaf** (or *cyclo*-AlaAlaPhe*Anth*).

One-dimensional ^{1}H NMR of the **1aaf** series all showed sharp, resolved peaks for the side-chains and for the amide protons. All the amino acid amide *NH* resonances were split into doublets *via* coupling to the *CH* protons (see below, Table 1). These observations imply that the compounds do not equilibrate between different conformations on the NMR time-scale, and that in solution each exists predominantly in one form. Temperature coefficient data[56,57] and rates of H/D exchange[58,59] were also measured. Neither set of data were particularly informative, except that they indicate there are no "*endo*-cyclic" *H*-bonds, consistent with the conformations deduced from NMR and calculations that are described immediately below. NOE data were collected for all the compounds, and no *cis*-amide bonds were present (Cα*H*–Cα*H* cross-peaks absent).

Two methods were used to deduce the predominant conformations of compounds **1** in polar solvents. First, the molecules **1aaa** were simulated in a medium of dielectric 46.7 representing DMSO (and 80 representing water, see ESI†) using the quenched molecular dynamics (QMD) technique.[60,61] QMD simulations are valuable because they are not bias by NOE data which over-represents some conformations due to the NOE effect depends on $1/r^6$ distance relationships.[62] Moreover, QMD thoroughly explores possible local minima in a Boltzmann equilibrium. Second, and independently, NOE restraints *were* applied in a Macromodel[63] simulation of molecules **1aaf** in dielectric 46.7.

One conformational cluster (maximum RMSD of the Cα–Cβ coordinates 0.5 Å) arose from the QMD simulations of each of the **1aaa** stereoisomers, Fig. 2a (QMD simulated scaffold conformations are shown in black throughout this paper). The fact that >1000 conformers (all below 3 kcal mol^{-1} of the lowest energy one identified) *all* converged to one cluster emphatically indicates conformational rigidity. Comparison of the QMD-generated structures with the NOE data showed they are consistent. Similarly, the MacroModel simulations with NMR constraints also gave one predominant conformation for each **1aaf** stereoisomer, Fig. 2b (MacroModel simulated scaffold conformations involving NOE constraints are grey throughout). None of the $^{3}J_{NH\text{-}\alpha}$ coupling constants were above 9 Hz (see Table 1 below); only couplings >9 Hz are indicative of unambiguous calculated dihedral angles, hence none were used as constraints in the MacroModel calculations.

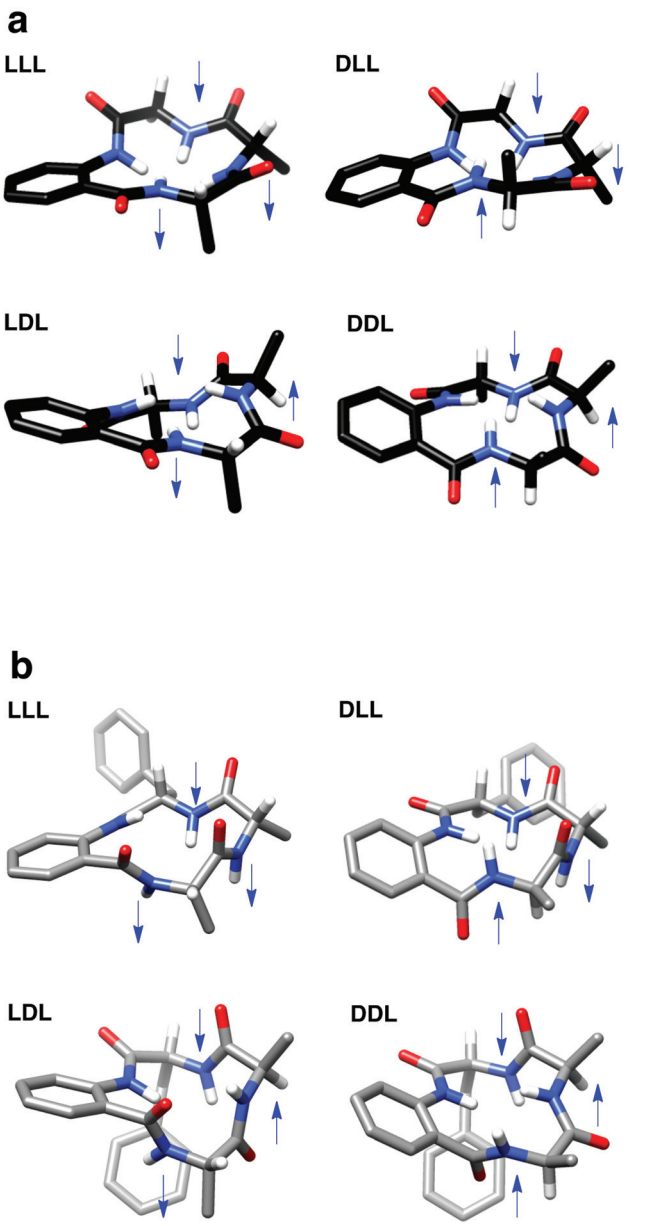

Fig. 2 Conformations simulated by: (a) QMD calculations for **1aaa** stereomers *without* NOE constraints; and, (b) MacroModel for **1aaf** stereomers with NOE constraints. The blue arrows approximate the orientation of the NH bond vectors to either pointing up or below the ring system.

Table 1 Comparison of experimentally observed $^{3}J_{NH\text{-}\alpha}$ coupling constants with those calculated using the NMR constrained structures simulated in Fig. 2b

	Ala(R^1)		Ala(R^2)		Phe (R^3)	
	Exp'l[a]	Calc.[b]	Exp'l[a]	Calc.[b]	Exp'l[a]	Calc.[b]
LLL	5.0	6.2–6.7	—	7.8–8.3	7.0	6.5–7.8
DLL	7.7	7.6–8.2	8.9	6.6–7.9	7.9	8.0–9.0
LDL	7.2	6.8–8.0	8.8	7.9–8.9	7.7	6.9–8.1
DDL	5.2	5.6–6.3	—	6.6–7.1	5.6	6.6–7.1

[a] Directly from NMR spectra. [b] Based on the structures simulated from the NOE data, and calculated using the Poulson form of the Karplus equation.[64]

Overlays of the conformations generated using the approaches described above, *i.e.* without and with NOE constraints, showed close agreement (RMSD 0.18–0.34 Å for the Cα–Cβ coordinates; Fig. 3). Moreover, even though the fit of these overlays was based on Cα–Cβ vectors, it is clear that the ring structures also are very similar.

 This journal is © The Royal Society of Chemistry 2016

Published on 13 May 2016. Downloaded by Texas A & M University on 29/09/2016 19:53:27.

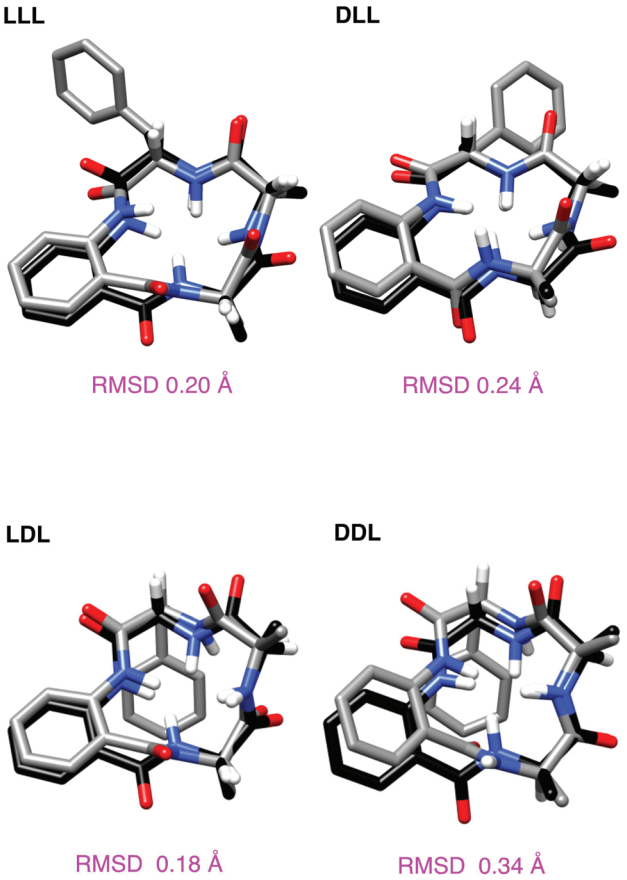

Fig. 3 Overlays of **1** simulated structures without (black, **1aaa**) and with (grey, **1aaf**) NOE constraints are within 0.18–0.34 Å based on 6 coordinates.

Comparisons of favored conformations for stereomers of **1** revealed a simple correlation. When drawn with the ring on the equator, and the *Anth* residue on the West, then L-amino acids point their *N–H* vectors South, while *N–H* vectors for D-amino acids are North-oriented, irrespective of the other amino acid stereochemistries. Thus the cyclic 13-membered ring scaffold is constrained to one highly predictable conformation per stereoisomer. This observation held for all the compounds prepared in this study based on similarities in NOE cross-peaks, *i.e.* for *cyclo*-DGlu′-DAla-LPhe-*Anth*, *cyclo*-LVal-LSer′-LTyr′-*Anth*, *cyclo*-DTyr′-DSer′-DVal-*Anth*, *cyclo*-LVal-LSer-LTyr-*Anth*, *cyclo*-LPhe-DAla-LPhe-*Anth*, *cyclo*-DPhe-LAla-LGlu′-*Anth*, *cyclo*-DPhe-LAla-LGlu-*Anth* (see ESI†); those observations imply the conformations are governed by the scaffold and the side-chain variables are less significant (Fig. 4).

Table 1 compares N*H*–Cα*H* coupling constants directly from NMR spectra with those calculated from the MacroModel simulations involving NOE constraints. In some cases the coupling was obscured, and in several cases the true *J*-values were marginally (by 1.2 Hz at most) outside the calculated range, but the rest were consistent with the values inferred from simulations.

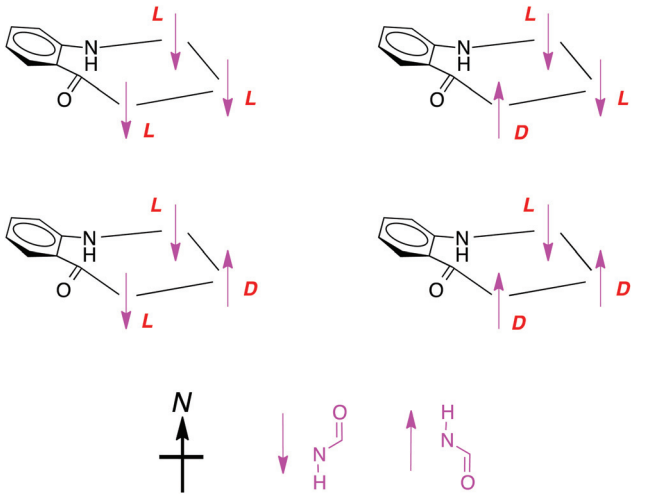

Fig. 4 "North south orientations" of the amide *N–H* vectors in stereomers of **1** correlate with the amino acid configurations. L-Amino acid *N–H* vectors point South, and while the D-isomers give North-aligned local *N–H* vector orientations, when drawn in the orientations shown.

Circular dichroism (CD) data for the **1aaf** stereomers are shown in Fig. 5 (solid lines). Unsurprisingly, significantly greater molar elipticities were observed for these compounds compared with related linear peptides (dotted lines), indicative of more conformational ordering in the cyclic systems. Moreover, there are logical trends in the data. For instance, the LLL-**1aaf** stereomer (red line) has negative maxima at *ca.* 195 and 215, and a maximum at *ca.* 230 nm. Substitution of two L-amino acids in LLL-**1aaf** giving DDL-**1aaf** is accompanied by near complete inversion of the CD maxima and minima. The two possible "intermediate" diastereomers, *i.e.* DLL-**1aaf** and LDL-**1aaf**, in which only one L-amino acid of LLL-**1aaf** is replaced, show shallower peak intensities. The CD spectrum of DLL-**1aaf** (green) is more closely related to that for LLL-**1aaf** (red) than it is to DDL-**1aaf** (purple), whereas for LDL-**1aaf** (blue) the inverse is true; this implies the amino acid opposite

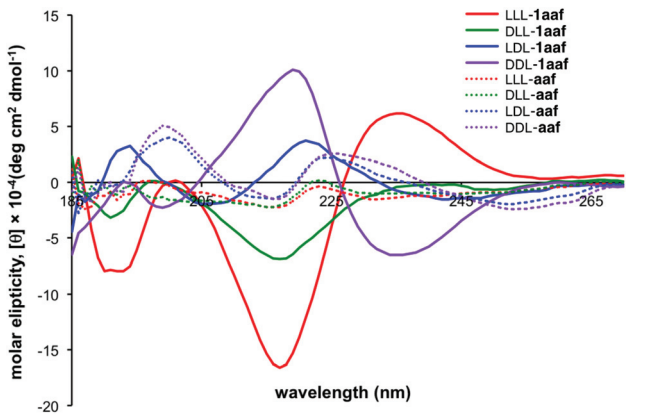

Fig. 5 CD spectra of compounds **1aaf** (solid lines) and closely related linear peptides (dashed lines).

Published on 13 May 2016. Downloaded by Texas A & M University on 29/09/2016 19:53:27.

the *Anth* residue in the cyclic scaffold has a more profound effect on the molar elipticity.

Comparisons of the *Anth*-cyclic peptidomimetics with peptide and protein structures

Exploring key orientations on secondary structures (EKOS)[65] facilitates comparison of all the favored QMD simulated conformers with all the common ideal secondary structures based on Cα–Cβ coordinates. For **1aaf** there was only one preferred conformer cluster for each stereomer. Not surprisingly, then, most stereomers matched on only one secondary structure, or none at all, *i.e.* they are not universal peptidomimetics.[66,67] One apparent exception was LLL-**1aaf** which gave an acceptable fit on γ- and type II β-turn conformations (Fig. 6); however, γ- and type II β-turn conformations have similar side-chain orientations that overlay well on each other (ESI Fig. S1b†). An inverse γ-turn matched reasonably well with LDL-**1aaf**, and DLL-**1aaf** overlaid closely with a type I β-turn.

Whereas, Fig. 6 depicts preferred overlays of select **1aaf** stereoisomers on ideal secondary structures, the EKO routine[68] facilitates matching QMD generated structures of **1aaa** with crystallized protein–protein interaction interfaces based on Cα–Cβ coordinates. Thus, preferred conformations of each stereomer were compared with around 160 000 protein–protein interfaces, and each match of RMSD <0.3 Å was analyzed in terms of what secondary structure type at the interface was implicated in the overlay. There were between 106–258 matches of <0.3 Å RMSD for each stereomer. The term "no secondary structure" is used here to describe situations in which the region overlaid did not contain any discernable secondary structure. "Turns" refers to a turn of any type (α, β, γ, δ) that has appropriate intrachain hydrogen bonds, while loops and turns without any intra-ring *H*-bonding interactions are classified as "bends". Fig. 7 shows

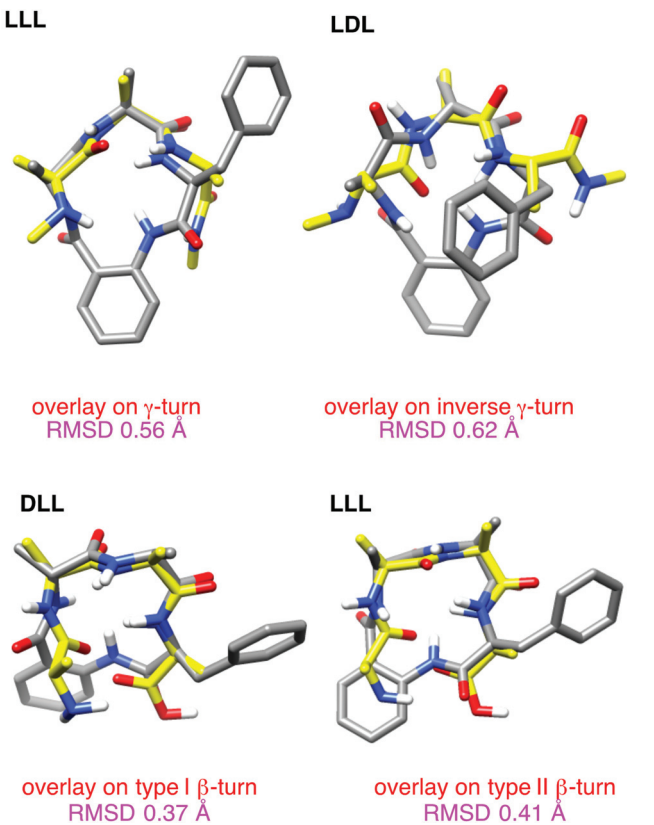

Fig. 6 Preferred conformations of select stereoisomers of **1aaf** overlaid on γ-, inverse γ-, type I β-, and type II β-turns. RMSD values indicated are for overlay of the side-chain Cα–Cβ vectors.

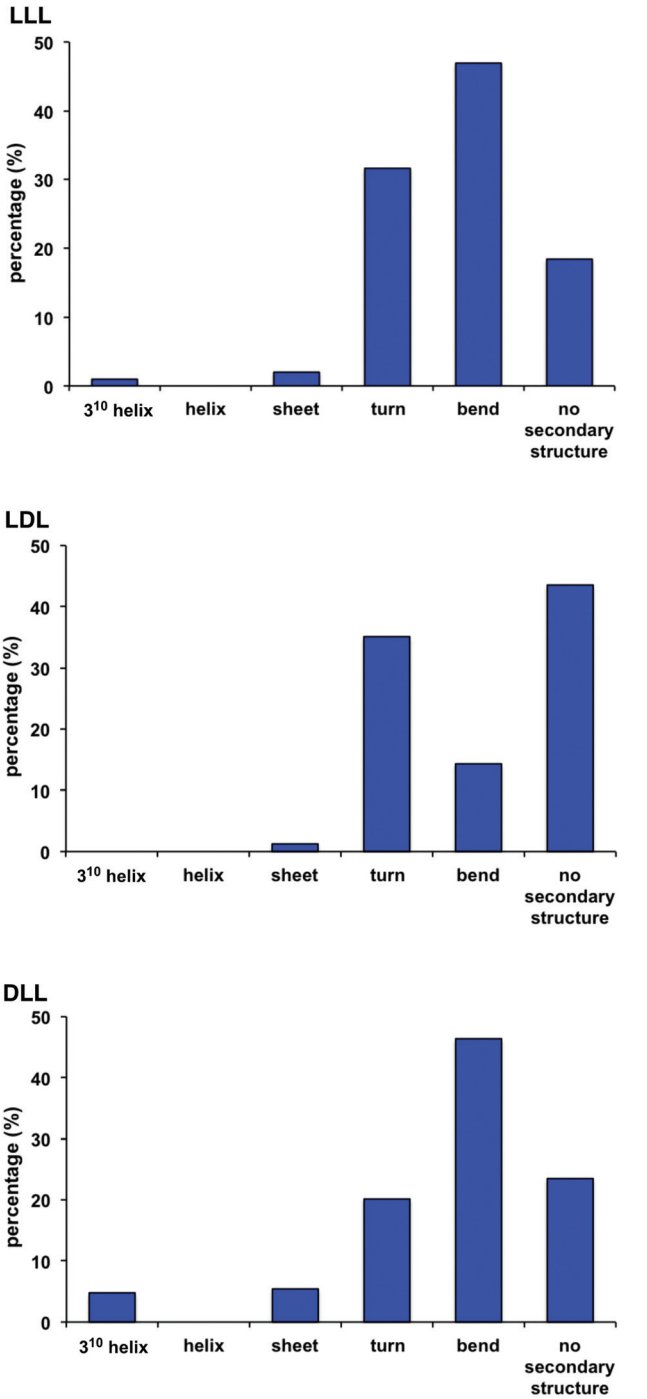

Fig. 7 Distribution of best overlays on PPI interface segments with respect to secondary structure for the stereomers featured in Fig. 6.

This journal is © The Royal Society of Chemistry 2016

Published on 13 May 2016. Downloaded by Texas A & M University on 29/09/2016 19:53:27.

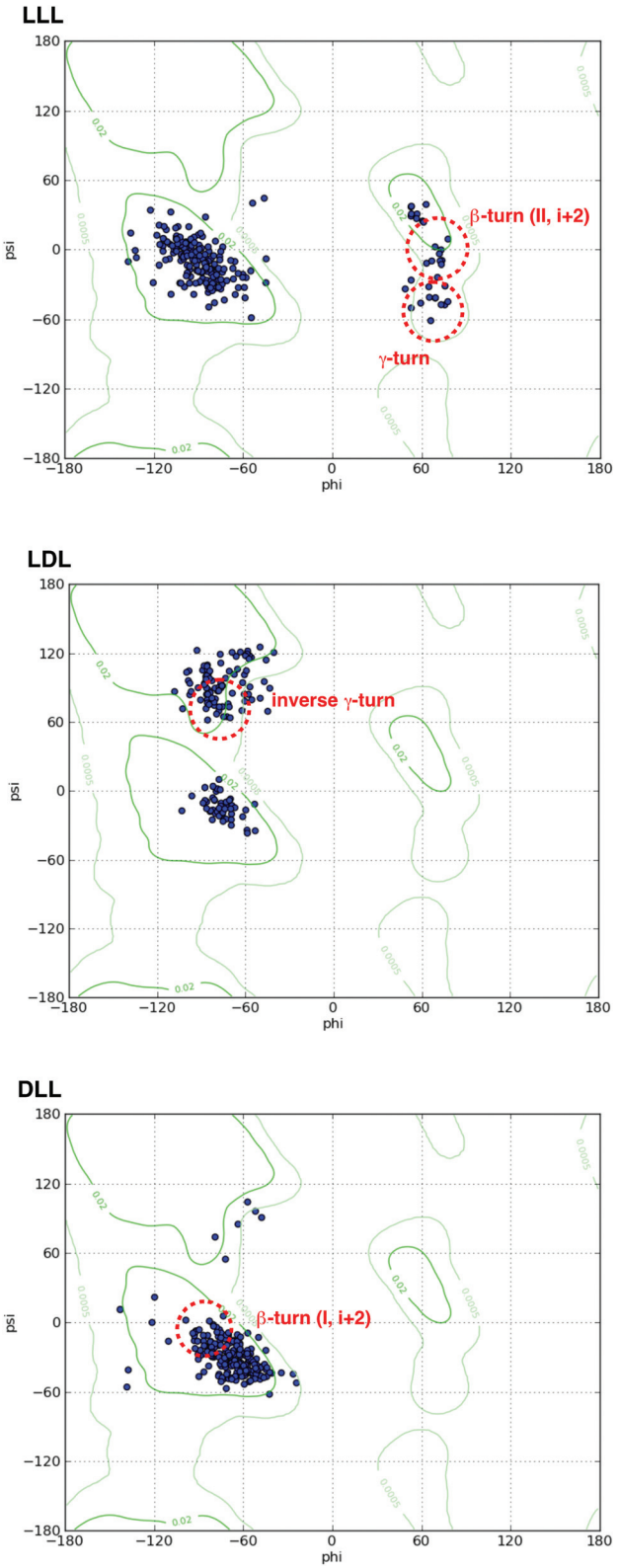

Fig. 8 Each dot on these plots is associated with a ϕ,ψ-bond vector of a protein interface region that overlaid closely with a preferred conformer of the **1aaa** stereomer indicated.

the distribution of overlays within those categories and some other secondary structures. Thus the preferred **1aaa** conformations are strongly bias towards turns and bends, consistent with the EKOS study presented in Fig. 6. Full data for all the **1aaa** stereomers are given in the ESI (Fig. S2†).

Finer detail of the secondary structure types that were overlaid in the EKO analysis of PPIs in the PDB is indicated by ϕ,ψ-angles, indicative of the type of secondary structure implicated. Fig. 8 shows select data for the stereomers featured in Fig. 6, and Fig. S3† shows the complete data set. Thus, the number of occurrences where LLL-**1aaa**, LDL-**1aaa**, and DLL-**1aaa** overlaid closely with γ-turns, type I β-turns, inverse γ- and type II β-turn conformations are consistent with the favored conformations predicted in Fig. 6.

Physiochemical properties

Table 2 shows how HPLC was used to monitor the stability of LLL-**1aaf** under aqueous conditions of pH 2,7, and 12, and, in separate experiments, the mixture of proteases called Pronase[69] that is used to extensively hydrolyze proteins in proteomics studies (any amide between two hydrophobic residues could be cleaved by this enzyme mixture). Under neutral or acidic conditions, and in the presence of Pronase, LLL-**1aaf** did not any significant cleavage. Only some cleavage was observed after extended expose to the aqueous pH12 conditions.

Predictions of cell permeability

Fig. 9 shows data calculated (QikProp)[70,71] for the polar surface area (PSA) and cell permeability of LLL-**1aaf**. The impli-

Table 2 Stabilities of LLL-**1aaf** under different pH conditions

	Conditions	$t_{1/2}$/h
pH stability of LLL-**1aaf**	pH 2.0[a]	>500
	pH 12.0[b]	240
	pH 7.4[c]	>500
LLL-**1aaf** linear LLL-**aaf**	Pronase[c]	No cleavage after 12 h
	Pronase[c]	1.5

[a] 10 mM HCl. [b] 10 mM NaOH. [c] PBS buffer. 20% MeOH was added in all cases to increase solubilities.

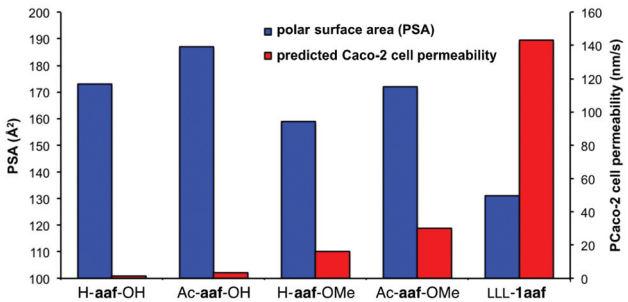

Fig. 9 Comparison of PSA (blue) and predicted Caco-2 cell permeabilities (red) for linear peptides based on **aaf** and a featured cyclic molecule **1aaf**.

Published on 13 May 2016. Downloaded by Texas A & M University on 29/09/2016 19:53:27.

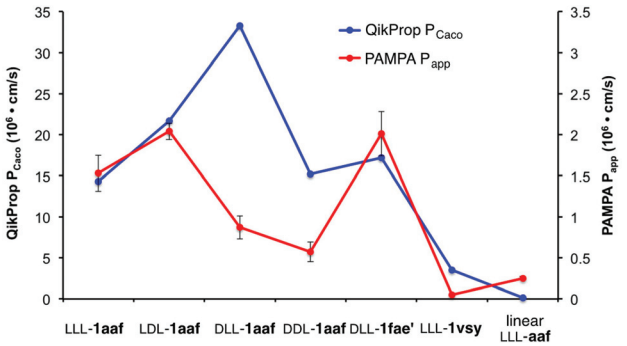

Fig. 10 Calculated cell permeability rates from QikProp (blue), and experimental data from PAMPA assays (red).

cations of this data are that LLL-**1aaf** has less PSA and a higher tendency to permeate into cells than closely related linear peptide controls. Polar surface areas <140 Å^2 are generally preferable for cell permeability.[72] Similarly, compounds with predicted PCaco-2 permeability rates >20 nm s^{-1} are usually cell permeable; data calculated for LLL-**1aaf** exceeds both expectations, and predict cell permeability.

The parallel artificial membrane permeability assay (PAMPA)[73–77] was used to obtain experimental data to compare with QikProp calculations (Fig. 10). In PAMPA assays, a polyvinyldifluoroethene membrane is coated with mixture of a lipophilic hydrocarbon (here dodecane) and lipids, then the rate of diffusion of test compounds from donor to acceptor wells are measured over a period of time to mimic passive diffusion into cells. There is no uniformly accepted cut-off value in PAMPA assays above which the compounds are considered to be cell permeable, mainly because there is some variance in the membrane composition used. However, the following illustrative data for cell permeable pharmaceuticals have been obtained by others using exactly the method described here[78] (P_{app} in 10^6 cm s^{-1}): testosterone (13), propranolol (10), warfarin (1.0), furosemide (0.16), methotrexate (0.016). These data may serve as a reference for the data collected and shown in Fig. 10. That data suggests compounds based on the **aaf** core will tend to be cell permeable. Membrane permeability was reduced for the compounds with more polar side-chains, **vsy**, and for the linear control, LLL-H-**aaf**-OH as expected. This assertion is supported by another study that suggests P_{app} of around 1×10^6 cm s^{-1} correlate with cell permeability.[79]

Others have noted[79] that data from PAMPA assays tends to be less than those from Caco2 assays, so the difference in the absolute values from QikProp (calculated Caco2 rates) and PAMPA are unsurprising. Moreover, there is a reasonable correlation between the relative rates in both sets of data (Fig. 10).

Conclusion

The *Anth* containing peptides featured in this study have a greater tendency towards conformational homogeneity than systems based on other β-amino acids related to **F** and **G**.[24] In view of this, and other observations outlined in the introduction, we suggest 13-membered systems based on the *Anth* residue are at a favorable point on the crossroads between ease of synthesis and conformational rigidity.

Predictability of conformational preferences for a set of cyclic peptidomimetics is an attractive feature of the systems studied here. It is possible that different side-chains to the ones in **1aaf** could perturb the predicted conformations, and this study does not encompass the special case of systems that contain Pro- or Gly-. Nevertheless, the data above clearly indicates strong intrinsic conformational biases of the scaffolds based on other amino acids. Moreover, stereochemistries of the scaffolds can be manipulated so that they orient their side-chains in ways that resemble the same orientation for regular and inverse γ-turns, and for the two most common β-turns (types I and II). Consistent with this, conformations of **1aaa** stereomers have a pronounced tendency to orient side-chains in ways that some turns and bends do at PPI interfaces.

Cyclic peptides containing only secondary amide bonds do not tend to be cell permeable.[80] In fact, making cyclic peptides cell permeable by inclusion of *N*-methyl groups is an area of interest in the contemporary literature.[81–83] Molecules **1** show promise as cell permeable molecules, even though they do not have tertiary amide *N*-methyl groups. We suggest this is because the favored conformers of **1** in solution orient their *N–H* vectors towards a central point, *i.e.* relatively insulated from the medium around the mimic.[84]

Overall, while tens of naturally occurring cyclic peptides containing *Anth* have been discovered, the potential of this simple residue in designs of conformationally rigid protein interface mimics has hitherto been under-appreciated.

Conflict of interest

The authors declare no competing financial interests.

Acknowledgements

Financial support for this project was provided by the National Institutes of Health (GM087981), the Robert A. Welch foundation (A-1121), DoD BCRP Breakthrough Award (BC141561), CPRIT (RP150559), and the High Impact Research (HIR) (UM.C/625/1/HIR/MOHE/MED/17 & UM.C/625/1/HIR/MOHE/MED/33) from the Ministry of Higher Education, Malaysia. We thank Dr Lisa M. Perez and Dr Howard Williams for useful discussions. TAMU/LBMS-Applications Laboratory provided mass spectrometric support. The NMR instrumentation at Texas A&M University was supported by a grant from the National Science Foundation (DBI-9970232) and the Texas A&M University System.

References

1 P. W. Dalsgaard, T. O. Larsen, K. Frydenvang and C. Christophersen, *J. Nat. Prod.*, 2004, **67**, 878–881.

 This journal is © The Royal Society of Chemistry 2016

Published on 13 May 2016. Downloaded by Texas A & M University on 29/09/2016 19:53:27.

2 G. Kartha, G. Ambady and P. V. Shankar, *Nature*, 1974, **247**, 204–205.
3 J. Zheng, Z. Xu, Y. Wang, K. Hong, P. Liu and W. Zhu, *J. Nat. Prod.*, 2010, **73**, 1133–1137.
4 B. Wels, J. A. W. Kruijtzer and R. M. J. Liskamp, *Org. Lett.*, 2002, **4**, 2173–2176.
5 Y. Takeuchi and G. R. Marshall, *J. Am. Chem. Soc.*, 1998, **120**, 5363–5372.
6 M. El Haddadi, F. Cavelier, E. Vives, A. Azmani, J. Verducci and J. Martinez, *J. Pept. Sci.*, 2000, **6**, 560–570.
7 E. Cini, C. B. Botta, M. Rodriquez and M. Taddei, *Tetrahedron Lett.*, 2009, **50**, 7159–7161.
8 M. Ngu-Schwemlein, Z. Zhou, T. Bowie and R. Eden, *J. Mol. Struct.*, 2003, **655**, 59–68.
9 W. D. F. Meutermans, G. T. Bourne, S. W. Golding, D. A. Horton, M. R. Campitelli, D. Craik, M. Scanlon and M. L. Smythe, *Org. Lett.*, 2003, **5**, 2711–2714.
10 D. A. Horton, G. T. Bourne, J. Coughlan, S. M. Kaiser, C. M. Jacobs, A. Jones, A. Ruehmann, J. Y. Turner and M. L. Smythe, *Org. Biomol. Chem.*, 2008, **6**, 1386–1395.
11 C. T. T. Wong, H. Y. Lam, T. Song, G. Chen and X. Li, *Angew. Chem., Int. Ed.*, 2013, **52**, 10212–10215.
12 W. S. Horne, C. A. Olsen, J. M. Beierle, A. Montero and M. R. Ghadiri, *Angew. Chem., Int. Ed.*, 2009, **48**, 4718–4724.
13 L. G. Pease and C. Watson, *J. Am. Chem. Soc.*, 1978, **100**, 1279–1286.
14 A. C. Bach II, A. A. Bothner-By and L. M. Gierasch, *J. Am. Chem. Soc.*, 1982, **104**, 572–576.
15 M. D. Bruch, J. H. Noggle and L. M. Gierasch, *J. Am. Chem. Soc.*, 1985, **107**, 1400–1407.
16 A. Ehrlich, H.-U. Heyne, R. Winter, M. Beyermann, H. Haber, L. A. Carpino and M. Bienert, *J. Org. Chem.*, 1996, **61**, 8831–8838.
17 H. Kessler and B. Kutscher, *Tetrahedron Lett.*, 1985, **26**, 177–180.
18 D. F. Mierke, M. Kurz and H. Kessler, *J. Am. Chem. Soc.*, 1994, **116**, 1042–1049.
19 R. Haubner, R. Gratias, B. Diefenbach, S. L. Goodman, A. Jonczyk and H. Kessler, *J. Am. Chem. Soc.*, 1996, **118**, 7461–7472.
20 A. Montero, J. M. Beierle, C. A. Olsen and M. R. Ghadiri, *J. Am. Chem. Soc.*, 2009, **131**, 3033–3041.
21 C. A. Olsen, A. Montero, L. J. Leman and M. R. Ghadiri, *ACS Med. Chem. Lett.*, 2012, **3**, 749–753.
22 J. M. Beierle, W. S. Horne, J. H. van Maarseveen, B. Waser, J. C. Reubi and M. R. Ghadiri, *Angew. Chem., Int. Ed.*, 2009, **48**, 4725–4729.
23 H. N. Hoang, R. W. Driver, R. L. Beyer, A. K. Malde, G. T. Le, G. Abbenante, A. E. Mark and D. P. Fairlie, *Angew. Chem., Int. Ed.*, 2011, **50**, 11107–11111.
24 M. Glenn, M. Kelso, J. Tyndall and D. Fairlie, *J. Am. Chem. Soc.*, 2003, **125**, 640–6411.
25 Y. Igarashi, T. Hanafusa, F. Gohda, S. Peterson and G. Bills, *Mycology*, 2014, **5**, 102–109.
26 Y. Hamada, K. Nakao and T. Shioiri, *Pept. Chem.*, 1988, 351–354.
27 R. Kobayashi, Y. Samejima, S. Nakajima, K. Kawai and S. Udagawa, *Chem. Pharm. Bull.*, 1987, **35**, 1347–1352.
28 G. Schmeda-Hirschmann, E. Hormazabal, J. A. Rodriguez and C. Theoduloz, *Z. Naturforsch., C: J. Biosci.*, 2008, **63**, 383–388.
29 Y.-G. Zhang, X.-K. Xia, W.-P. Yuan, X. Liu, M.-S. Zhang, X.-M. Meng, X.-J. Wang and C.-H. Liu, *Z. Kristallogr. - New Cryst. Struct.*, 2010, **225**, 236–238.
30 M. Yamazaki, Y. Horie, K. Bae, Y. Maebayashi, Y. Jisai and H. Fujimoto, *Chem. Pharm. Bull.*, 1987, **35**, 2122–2124.
31 O. Convert, J. P. Mazaleyrat, M. Wakselman, I. Morize and M. Reboud-Ravaux, *Biopolymers*, 1990, **30**, 583–591.
32 P. Lewer, P. R. Graupner, D. R. Hahn, L. L. Karr, D. O. Duebelbeis, J. M. Lira, P. B. Anzeveno, S. C. Fields, J. R. Gilbert and C. Pearce, *J. Nat. Prod.*, 2006, **69**, 1506–1510.
33 Y. Zhang, S. Liu, H. Liu, X. Liu and Y. Che, *J. Nat. Prod.*, 2009, **72**, 1364–1367.
34 L.-N. Zhou, H.-Q. Gao, S.-X. Cai, T.-J. Zhu, Q.-Q. Gu and D.-H. Li, *Helv. Chim. Acta*, 2011, **94**, 1065–1070.
35 M. Chen, C.-L. Shao, X.-M. Fu, C.-J. Kong, Z.-G. She and C.-Y. Wang, *J. Nat. Prod.*, 2014, **77**, 1601–1606.
36 C.-Y. Mang, Y. Zhao, H.-F. Li, H. Lan, Y. Yan and M.-H. Yang, *Mol. Phys.*, 2015, **113**, 104–112.
37 J. Peng, H. Gao, X. Zhang, S. Wang, C. Wu, Q. Gu, P. Guo, T. Zhu and D. Li, *J. Nat. Prod.*, 2014, **77**, 2218–2223.
38 Y. Masuda, R. Tanaka, K. Kai, A. Ganesan and T. Doi, *J. Org. Chem.*, 2014, **79**, 7844–7853.
39 J. P. Mazaleyrat, M. Reboud-Ravaux and M. Wakselman, *Int. J. Pept. Protein Res.*, 1987, **30**, 622–633.
40 N. Boggetto, A. C. Vilain, J. J. Montagne, M. Reboud-Ravaux, J. P. Mazaleyrat, J. Xie and M. Wakselman, *Bull. Soc. Chim. Fr.*, 1994, **131**, 152–166.
41 K. H. Kumar, P. Boja and S. L. Belagali, *Indian J. Heterocycl. Chem.*, 2002, **12**, 149–152.
42 K. Kai, H. Yoshikawa, Y.-H. Kuo, K. Akiyama and H. Hayashi, *Biosci., Biotechnol., Biochem.*, 2010, **74**, 1309–1311.
43 J. Zheng, H. Zhu, K. Hong, Y. Wang, P. Liu, X. Wang, X. Peng and W. Zhu, *Org. Lett.*, 2009, **11**, 5262–5265.
44 Y.-H. Kuo, K. Kai, K. Akiyama and H. Hayashi, *Tetrahedron Lett.*, 2012, **53**, 429–431.
45 J. P. Mazaleyrat, M. Reboud-Ravaux, J. J. Montagne, O. Convert and M. Wakselman, *Colloq. INSERM*, 1989, **174**, 333–336.
46 S. Cerrini, E. Gavuzzo, G. Lucente and F. Pinnen, *Int. J. Pept. Protein Res.*, 1988, **31**, 447–453.
47 S. Cerrini, E. Gavuzzo, G. Lucente, F. Pinnen and G. Zanotti, *Int. J. Pept. Protein Res.*, 1989, **34**, 6–13.
48 F. Pinnen, A. Di Muro, G. Zanotti and G. Lucente, *Int. J. Pept. Protein Res.*, 1987, **30**, 388–396.
49 M. Feigel and G. Lugert, *Liebigs Ann. Chem.*, 1989, 1089–1092.
50 M. Akazome, M. Enzu, K. Takagi and S. Matsumoto, *Chirality*, 2011, **23**, 568–573.

Published on 13 May 2016. Downloaded by Texas A & M University on 29/09/2016 19:53:27.

51 J. Xu, S. Zhao and X. Yang, *Nat. Prod. Res.*, 2014, **28**, 994–997.
52 F. He, J. Bao, X.-Y. Zhang, Z.-C. Tu, Y.-M. Shi and S.-H. Qi, *J. Nat. Prod.*, 2013, **76**, 1182–1186.
53 C. N. Eid, T. I. Nicas, D. L. Mullen, R. J. Loncharich and J. W. Paschal, *Bioorg. Med. Chem. Lett.*, 1997, **7**, 2087–2092.
54 L. A. Carpino, *J. Am. Chem. Soc.*, 1993, **115**, 4397–4398.
55 G. Han, M. Tamaki and V. J. Hruby, *J. Pept. Res.*, 2001, **58**, 338–341.
56 N. J. Baxter and M. P. Williamson, *J. Biomol. NMR*, 1997, **9**, 359–369.
57 T. Cierpicki and J. Otlewski, *J. Biomol. NMR*, 2001, **21**, 249–261.
58 H. Lingard, J. T. Han, A. L. Thompson, I. K. H. Leung, R. T. W. Scott, S. Thompson and A. D. Hamilton, *Angew. Chem., Int. Ed.*, 2014, **53**, 3650–3653.
59 L. R. Steffel, T. J. Cashman, M. H. Reutershan and B. R. Linton, *J. Am. Chem. Soc.*, 2007, **129**, 12956–12957.
60 B. M. Pettitt, T. Matsunaga, F. Al-Obeidi, C. Gehrig, V. J. Hruby and M. Karplus, *Biophys. J.*, 1991, **60**, 1540–1544.
61 S. D. O'Connor, P. E. Smith, F. Al-Obeidi and B. M. Pettitt, *J. Med. Chem.*, 1992, **35**, 2870–2881.
62 T. D. W. Claridge, *High-Resolution NMR Techniques in Organic Chemistry*, Pergamon, Oxford, 1999.
63 F. Mohamadi, N. G. J. Richards, W. C. Guida, R. Liskamp, M. Lipton, C. Caufield, G. Chang, T. Hendrickson and W. C. Still, *J. Comput. Chem.*, 1990, **11**, 440–467.
64 S. Ludvigsen, K. V. Andersen and F. M. Poulsen, *J. Mol. Biol.*, 1991, **217**, 731–736.
65 D. Xin, E. Ko, L. M. Perez, T. R. Ioerger and K. Burgess, *Org. Biomol. Chem.*, 2013, **11**, 7789–7801.
66 E. Ko, J. Liu, L. M. Perez, G. Lu, A. Schaefer and K. Burgess, *J. Am. Chem. Soc.*, 2011, **133**, 462–477.
67 E. Ko, J. Liu and K. Burgess, *Chem. Soc. Rev.*, 2011, **40**, 4411–4421.
68 E. Ko, A. Raghuraman, L. M. Perez, T. R. Ioerger and K. Burgess, *J. Am. Chem. Soc.*, 2013, **135**, 167–173.
69 L. Jurasek, P. Johnson, R. W. Olafson and L. B. Smillie, *Can. J. Biochem.*, 1971, **49**, 1195–1201.
70 W. L. Jorgensen and E. M. Duffy, *Bioorg. Med. Chem. Lett.*, 2000, **10**, 1155–1158.
71 E. M. Duffy and W. L. Jorgensen, *J. Am. Chem. Soc.*, 2000, **122**, 2878–2888.
72 D. F. Veber, S. R. Johnson, H.-Y. Cheng, B. R. Smith, K. W. Ward and K. D. Kopple, *J. Med. Chem.*, 2002, **45**, 2615–2623.
73 M. Kansy, F. Senner and K. Gubernator, *J. Med. Chem.*, 1998, **41**, 1007–1010.
74 K. Sugano, H. Hamada, M. Machida and H. Ushio, *J. Biomol. Screening*, 2001, **6**, 189–196.
75 F. Wohnsland and B. Faller, *J. Med. Chem.*, 2001, **44**, 923–930.
76 E. H. Kerns, L. Di, S. Petusky, M. Farris, R. Ley and P. Jupp, *J. Pharm. Sci.*, 2004, **93**, 1440–1453.
77 M. Fujikawa, R. Ano, K. Nakao, R. Shimizu and M. Akamatsu, *Bioorg. Med. Chem.*, 2005, **13**, 4721–4732.
78 E. Millipore, *Non-cell-based Assays for Drug Transport*, http://www.emdmillipore.com/US/en/product/Non-cell-based-Assays-for-Drug-Transport,MM_NF-C7702-documentation.
79 Z. S. Teksin, P. R. Seo and J. E. Polli, *AAPS J.*, 2010, **12**, 238–241.
80 A. K. Yudin, *Chem. Sci.*, 2015, **6**, 30–49.
81 E. Biron, J. Chatterjee, O. Ovadia, D. Langenegger, J. Brueggen, D. Hoyer, H. A. Schmid, R. Jelnick, C. Gilon, A. Hoffman and H. Kessler, *Angew. Chem., Int. Ed.*, 2008, **47**, 2595–2599.
82 T. R. White, C. M. Renzelman, A. C. Rand, T. Rezai, C. M. McEwen, V. M. Gelev, R. A. Turner, R. G. Linington, S. S. F. Leung, A. S. Kalgutkar, J. N. Bauman, Y. Zhang, S. Liras, D. A. Price, A. M. Mathiowetz, M. P. Jacobson and R. S. Lokey, *Nat. Chem. Biol.*, 2011, **7**, 810–817.
83 W. M. Hewitt, S. S. F. Leung, C. R. Pye, A. R. Ponkey, M. Bednarek, M. P. Jacobson and R. S. Lokey, *J. Am. Chem. Soc.*, 2015, **137**, 715–721.
84 T. Rezai, B. Yu, G. L. Millhauser, M. P. Jacobson and R. S. Lokey, *J. Am. Chem. Soc.*, 2006, **128**, 2510–2511.

 This journal is © The Royal Society of Chemistry 2016

JOC The Journal of Organic Chemistry

Note

pubs.acs.org/joc

Heterogeneous Phase Transfer Catalysis in Solid Phase Syntheses of *Anth*-Cyclic Tetrapeptides

Dongyue Xin,[†] Jian Yuan,[‡] Kwok-Yin Wong,[‡] and Kevin Burgess*[,†]

[†]Department of Chemistry, Texas A & M University, Box 30012, College Station, Texas 77842, United States

[‡]Department of Applied Biology and Chemical Technology and the State Key Laboratory of Chirosciences, The Hong Kong Polytechnic University, Hunghom, Kowloon, Hong Kong, P. R. China

Supporting Information

ABSTRACT: This study features solid phase syntheses of cyclic tetrapeptides containing anthranilic acid (*Anth*) on relatively inexpensive resins derived from polystyrene. It proved to be difficult to hydrolyze a supported *Anth*-methyl ester *unless* a phase transfer catalyst was added to facilitate transport of hydroxide into the swollen hydrophobic gel state of the resin. We suggest this may be an under-appreciated strategy for improving syntheses on polystyrene supports.

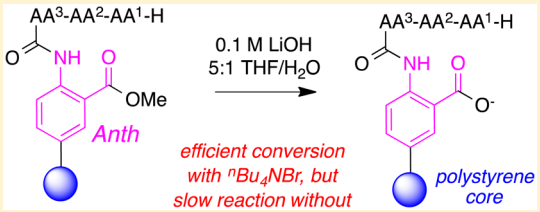

Tetraalkylammonium salts are widely used for liquid−liquid phase transfer catalysis,[1,2] but not to ferry reagents across a *solid*−liquid interface. We came across a useful example of this kind of heterogeneous phase transfer catalysis when developing a route to the 13-ring cyclic tetrapeptides **1** on a polystyrene-based support.

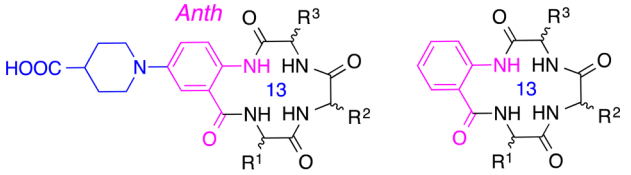

Solution phase access tp the *Anth*-containing cyclic tetrapeptides **A** has recently been developed in our laboratories,[3] but that unfunctionalized *Anth*-residue does not have a functional group to enable attachment to a solid phase. Consequently, the first task in this study was to make a modified anthranilic acid (fragment in blue for structure **1**). Use of piperidine-4-carboxylic acid as a nucleophile in SNAr displacement of fluoride from methyl 5-fluoro-2-nitrobenzoate gave the linked system **2** (Scheme 1).[4] It was important to use a *methyl* benzoate rather than another ester (e.g., allyl) because pilot reactions showed coupling onto methyl anthranilates were significantly easier than if a larger ester were used (see Supporting Information, Reaction S1). Hydrogenation of the nitro-group and then reaction with Fmoc-Cl gave **3**. *N*-Protected amino acid **3** was used as a nucleophile to displace chloride from chlorotrityl polystyrene resin to give the corresponding supported diester (Scheme 2). Substoichiometric amounts of acid **3** were used relative to the available loading sites on the resin, and any unreacted electrophilic centers on the polymer were capped as indicated. Quantitative UV-detection of Fmoc-cleavage products[5,6] indicated the loading of the resin with **3** was 0.2 mmol/g. Thus, this strategy conserved

Scheme 1. Synthesis of a Modified Anthranilic Acid Derivative

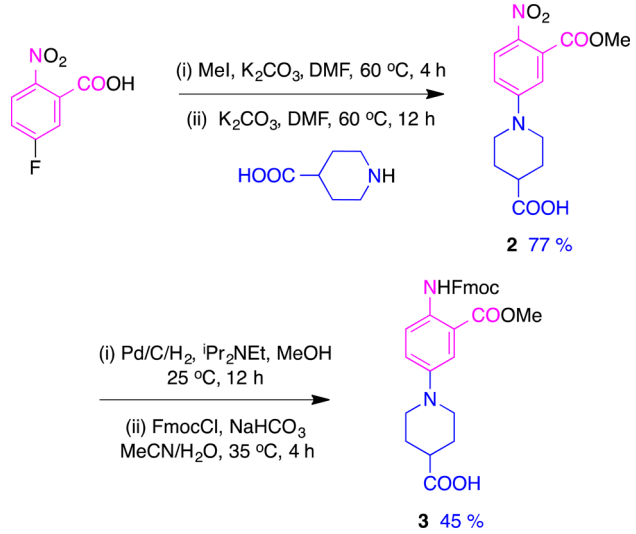

the most valuable component (**3**) and reduced the loading of the resin to levels that are conducive to intramolecular cyclization over intermolecular processes.[7,8] Conventional couplings for Fmoc-based amino acids led to the linear precursor **B** that may be represented as H-Glu(ᵗBu)-Phe-Ile-*Anth*'.

Table 1 outlines some of the attempts that were made to achieve the methyl ester hydrolysis of the supported linear peptide (see Supporting Information for all the conditions attempted). Cleavage of the products from the resin under mildly acidic conditions enabled the degree of conversion of the

Received: June 20, 2016
Published: August 23, 2016

ACS Publications © 2016 American Chemical Society

DOI: 10.1021/acs.joc.6b01475
J. Org. Chem. 2016, 81, 8077−8081

Scheme 2. Solid Phase Syntheses of Linear *Anth*-Containing Peptides

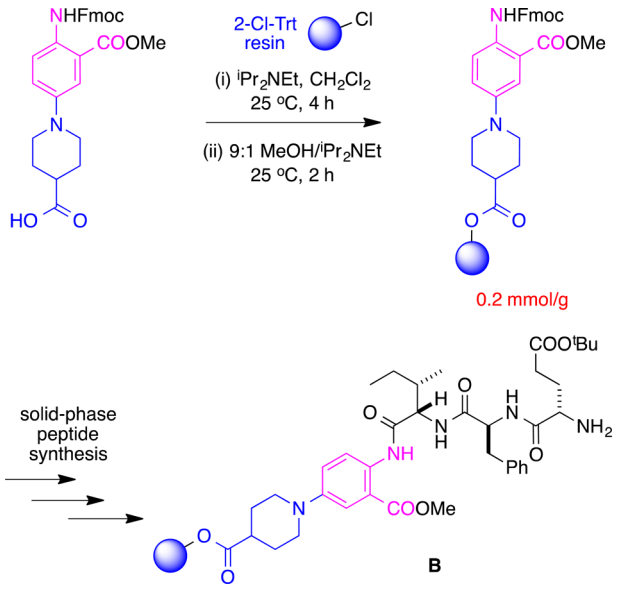

methyl ester to the side-chain-protected linear peptide **4e′fi** {*ie* the linear peptide containing Glu(^{t}Bu), Phe, and Ile } to be analyzed by HPLC.

Entries 1−4 in Table 1 show there was poor conversion to the desired product **4** even after an extended time (12 h); this is consistent with others who found it necessary to use 72 h to obtain a reasonable conversion of a polystyrene-supported methyl ester to the corresponding carboxylic acid.[9] In THF/MeOH (entry 5) the reaction was faster, but the product purity was compromised (two significant byproducts by HPLC, one of these was from hydrolysis of the ^{t}Bu-ester as concluded from LC-MS). However, the reaction rate increased dramatically when tetra-*n*-butyl ammonium bromide was added to the THF/H_2O conditions (entry 6), so much, in fact, that the hydrolysis was complete in 1 h (entry 7). At 1 h of reaction time, the less hydrophobic salts Et_4NBr and $BnNEt_3Cl$ gave much less conversion than nBu_4NBr (entries 8 and 9). Tetra-*n*-hexyl ammonium bromide gave only marginally less conversion than nBu_4NBr (compare entries 7 and 10), which was slightly more efficient than cetrimonium bromide, ($^nC_{16}H_{33}$)N-(CH_3)$_3$Br (entry 11), and triphenyl phosphonium salts gave very poor conversion (entries 12 and 13). Overall, these data indicate symmetrical long-chain tetraalkyl ammonium salts are preferred, and unsymmetrical analogs are marginally inferior. Phenyl phosphonium salts are ineffective for the featured reaction, and cations having several aromatic rings do not appear to be able to permeate into the resin effectively.

Table 2 shows hydrolysis product *purities* at 100% conversion when the optimized conditions were used (*nb*, Table 1 is different because it shows *conversions*). Little variation in the product purities was observed as the constituent amino acids were varied between combinations of Ile (**i**), Phe (**f**), Glu(^{t}Bu) (**e′**), Val (**v**), Ala (**a**), Ser(^{t}Bu) (**s′**), Tyr(^{t}Bu) (**y′**), Arg(Pbf) (**r′**), Cys(Acm) (**c′**), and His(Tr) (**h′**). NMR analysis of the crude material after cleavage of **4e′fi** indicated that the carboxylate was paired with a tetra-*n*-butyl ammonium cation. Throughout, there was no evidence of cleavage of *tert*-butyl side-chain esters, and premature (*ie* in the base-mediated step)

Table 1. Phase Transfer Catalysts and Methyl Ester Hydrolysis on Polystyrene Beads

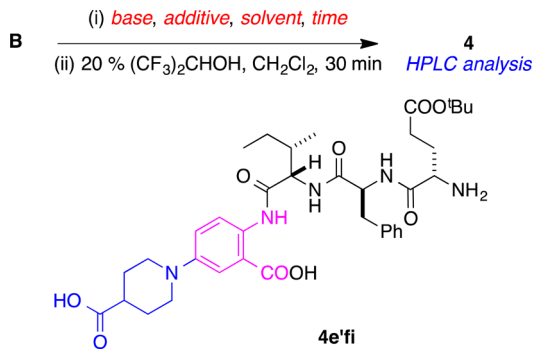

entry	base (concn/M)	solvent (ratio)	time (h)	additive	conversion (%)
1	LiOH (0.1)	THF/H_2O (5:1)	12	–	40
2	LiOH (0.2)	THF/H_2O (5:1)[a]	12	–	30
3	KOH (0.2)	THF/H_2O (10:1)	12	–	15
4	LiOH (0.1)	THF/H_2O (2:1)	12	–	8
5	LiOH (0.1)	THF/MeOH (5:1)	12	–	80[b]
6	LiOH (0.1)	THF/H_2O (5:1)	12	$^nBu_4NBr$	>95
7	**LiOH (0.1)**	**THF/H_2O (5:1)**	**1**	**$^nBu_4NBr$**	**>95**
8	LiOH (0.1)	THF/H_2O (5:1)	1	Et_4NBr	25
9	LiOH (0.1)	THF/H_2O (5:1)	1	$BnNEt_3Cl$	42
10	LiOH (0.1)	THF/H_2O (5:1)	1	Hex_4NBr	89
11	LiOH (0.1)	THF/H_2O (5:1)	1	($^nC_{16}H_{33}$) $N(CH_3)_3Br$	65
12	LiOH (0.1)	THF/H_2O (5:1)	1	Ph_4PBr	5
13	LiOH (0.1)	THF/H_2O (5:1)	1	Ph_3PEtBr	6

[a]Two phases. [b]Impurities identified by HPLC.

cleavage of the ester link from the trityl polystyrene was not observed by HPLC.

Cyclization of tetrapeptide precursors to relatively small, and therefore strained, 13-membered rings is a difficult transformation, and much optimization was required to achieve this for the supported intermediates **C**. For instance, when HATU (1-[bis(dimethylamino)methylene]-1*H*-1,2,3-triazolo[4,5-*b*]-pyridinium 3-oxid hexafluorophosphate)[10,11] was used the predominant product was the tetramethylguanidine.

After experimenting with 35 sets of reagents and conditions (see Supporting Information Table S2) those indicated in Table 3 were selected. In practice, it is important to follow a "staged" coupling procedure wherein (i) the acid is activated using DCC/HOAt and *N*-methyl morpholine (NMM) for 2 h; (ii) the coupling agents and byproducts that are in solution are washed away; (iii) the resin is resuspended in NMM/DMF for 48 h to allow the cyclization to proceed in an environment that does not contain byproducts and excess reagents from the activation step; and (iv) operations (i)−(iii) are repeated. If the excess coupling agents were not removed in step (ii) then significant amounts of linear *N*-terminal guanidines formed.

DOI: 10.1021/acs.joc.6b01475
J. Org. Chem. 2016, 81, 8077−8081

Table 2. Efficient Methyl Ester Hydrolysis on a Polystyrene Support

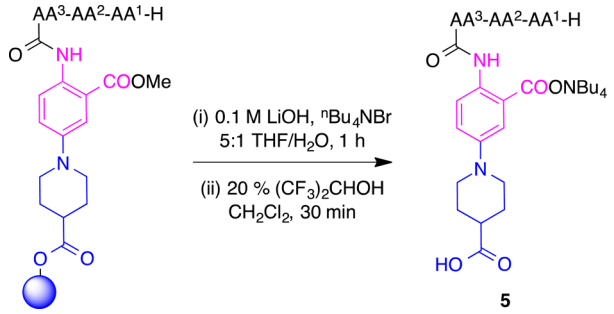

5

entry	sequence	HPLC purity (%)
1	LLL-**4e′fi**	92
2	LLL-**4aaf**	95
3	LLL-**4vs′y′**	91
4	DDL-**4y′s′v**	89
5	DDL-**4e′af**	86
6	DLL-**4fae′**	90
7	LLD-**4ar′c′**	83
8	DDL-**4h′e′c′**	81

Table 3. Formation of the Featured *Anth*-Containing Cyclic Tetrapeptides 1

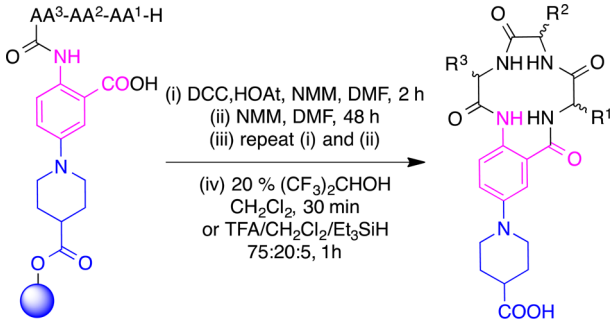

1

entry	sequence	HPLC purity (%)	isolated yield (%)
1[a]	LLL-**1vsy**	81	45
2[a]	DDL-**1ysv**	87	35
3[a]	DDL-**1eaf**	82	41
4[a]	DLL-**1fae**	76	39
5[b]	LLD-**1ar′c′**	71	31
6[b]	DDL-**1h′e′c′**	75	29

[a]Final step: TFA-based cleavage. [b]Final step: HFIP-based.

Staged couplings of this kind are at least uncommon in the literature.

Overall, the above procedure to obtain the cyclic tetrapeptides was difficult, probably because the desired cyclization reaction is only slightly more favorable than several possible competing processes. Nevertheless, Table 3 lists the products that were isolated under the optimized conditions, without (TFA-based conditions) or with (1,1,1,3,3,3-hexafluoropropanol, HFIP)[12] side-chain protection.

In conclusion, tetra-*n*-butylammonium bromide was pivotal in the supported methyl ester hydrolyses described here. Use of ammonium salts in solid phase syntheses is rare; examples we found include $^{n}Bu_4NI$/18-crown-6 in loading a sodium alkoxide onto a bromomethylene polystyrene resin,[13] $Me_4NHB(OAc)_3$ in a reductive amination,[14] $^{n}Bu_4NOH$ featuring a TOSMIC reaction,[15] $^{n}Bu_4NOH$ as a base in a cyclization reaction,[16] $^{n}Bu_4NIO_4$ in an oxidation reaction,[17] and in an electrolysis of a supported substrate.[18] Optimization of the conditions for the hydrolysis greatly facilitated synthesis of the strained cyclic tetrapeptides **1**, and we suggested that similar strategies warrant wider consideration in optimization of reactions on polystyrene supports.

EXPERIMENTAL SECTION

General Procedures. All solution phase reactions were carried out under an inert atmosphere (nitrogen or argon where stated). Glassware for anhydrous reactions was dried in an oven at 140 °C for a minimum of 6 h prior to use. Solid phase syntheses were carried out in plastic fritted syringes. Dry solvents were obtained by passing the previously degassed solvents through activated alumina columns. Yields refer to chromatographically and spectroscopically (^{1}H NMR) homogeneous materials, unless otherwise stated. Reagents were purchased at a high commercial quality (typically 97% or higher) and used without further purification. Analytical thin layer chromatography (TLC) was carried out on Merck silica gel plates with QF-254 indicator and visualized by UV. Flash column chromatography was performed using silica gel (230−400 mesh). ^{1}H and ^{13}C spectra were recorded on a 400 MHz spectrometer and were calibrated using residual nondeuterated solvent as an internal reference. The following abbreviations or combinations thereof were used to explain the multiplicities: s = singlet, d = doublet, t = triplet, q = quartet, m = multiplet, p = pentet, br = broad singlet, dd = doublet of doublet. Melting points were recorded on an automated melting point apparatus and are uncorrected. All of the HPLC analyses were carried out with UV detection monitored at 254 nm. Analytical reversed-phase HPLC analyses were performed with a 250 mm × 4.6 mm C-18 column using gradient conditions (10−90% acetonitrile in water, flow rate = 0.75 mL/min, injection volume = 30 μL).

General Procedure for the Syntheses of 3. MeI (1.25 mL, 20 mmol) was added dropwise to a mixture of 5-fluoro-2-nitrobenzoic acid (3.70 g, 20 mmol) and K_2CO_3 (2.76 g, 20 mmol) in 100 mL of DMF at room temperature. The mixture was stirred at 60 °C for 4 h under N_2. Then K_2CO_3 (6.90 g, 50 mmol) was added, followed by the addition of piperidine-4-carboxylic acid (3.10 g, 24 mmol) in one portion. The mixture was further stirred at 60 °C under N_2 for 12 h. The reaction mixture was cooled to room temperature, and DMF was removed under vacuum. 1 M $KHSO_4$ aqueous solution was added slowly while stirring to acidify the crude mixture until the pH was adjusted to 3−4. The precipitated yellow solid product was filtered and washed with water (20 mL × 3) and then with CH_2Cl_2 (5 mL × 2). After drying, compound **2** was obtained as a yellow solid (4.74 g, 77% yield).

To a solution of **2** (3.08 g, 10 mmol) and DIPEA (1.71 mL, 10 mmol) in methanol (100 mL, 0.1 M) under nitrogen was added 10 wt % Pd/C (1.02 g, 0.1 equiv. Pd). The reaction was placed under an atmosphere of hydrogen (1 atm, balloon) for 12 h. After the reaction finished, the flask was purged with N_2. The reaction mixture was filtered over a Celite pad and concentrated to afford the product. The product was dissolved in 100 mL of MeCN/H_2O (1:1 mixture), and $NaHCO_3$ (1.68 g, 20 mmol) was added. The mixture was stirred at room temperature for 5 min followed by the addition of Fmoc-Cl (3.88 g, 15 mmol) in one portion. The mixture was stirred at 35 °C for 4 h, and the mixture was concentrated under vacuum to remove MeCN. 0.1 M aqueous HCl was added to adjust the pH of the mixture to 3−4, and the solution was extracted with chloroform (50 mL × 5). The combined organic phase was dried over $MgSO_4$, filtered, and concentrated under vacuum to give the crude product. The crude material was purified with flash chromatography (1% MeOH in CH_2Cl_2 to 3% MeOH in CH_2Cl_2) to give the pure product as a white solid (2.2 g, 44%).

*1-(3-(Methoxycarbonyl)-4-nitrophenyl)piperidine-4-carboxylic Acid (**2**).* Yellow solid, 4.74 g, 77%; mp = 214.9−216.0 °C; ^{1}H NMR (400 MHz, DMSO) δ 7.99 (d, J = 9.1 Hz, 1H), 7.15−7.04 (m, 2H), 4.04−3.97 (m, 2H), 3.83 (s, 3H), 3.19−3.10 (m, 2H), 2.64−2.53 (m,

DOI: 10.1021/acs.joc.6b01475
J. Org. Chem. 2016, 81, 8077−8081

1H), 1.98−1.87 (m, 2H), 1.62−1.52 (m, 2H); ^{13}C NMR (101 MHz, DMSO) δ 175.9, 167.6, 153.9, 133.7, 132.5, 127.5, 113.8, 112.1, 53.3, 46.5, 27.6; HRMS (ESI-TOF) m/z calcd for $C_{14}H_{15}N_2O_6$ $(M-H)^-$ 307.0930; found 307.0933.

*1-(4-((((9H-Fluoren-9-yl)methoxy)carbonyl)amino)-3-(methoxycarbonyl)phenyl)piperidine-4-carboxylic Acid (**3**).* White solid, 2.2 g, 44%; mp = 194.8−195.8 °C; ^{1}H NMR (400 MHz, DMSO) δ 9.80 (s, 1H), 7.92 (d, J = 7.5 Hz, 2H), 7.79 (d, J = 8.5 Hz, 1H), 7.70 (d, J = 7.4 Hz, 2H), 7.49−7.41 (m, 2H), 7.39−7.28 (m, 3H), 7.24 (dd, J = 9.1, 2.6 Hz, 1H), 4.46 (d, J = 6.8 Hz, 2H), 4.32 (t, J = 6.7 Hz, 1H), 3.83 (s, 3H), 3.63−3.54 (m, 2H), 2.83−2.66 (m, 2H), 2.43−2.36 (m, 1H), 1.96−1.88 (m, 2H), 1.69−1.62 (m, 2H); ^{13}C NMR (101 MHz, DMSO) δ 176.3, 168.1, 153.7, 147.1, 144.2, 141.2, 131.8, 128.2, 127.6, 125.5, 122.7, 122.3, 120.6, 119.1, 117.1, 66.5, 52.8, 48.9, 47.0, 28.0; HRMS (ESI-TOF) m/z calcd for $C_{29}H_{27}N_2O_6$ $(M-H)^-$ 499.1869; found 499.1875.

Solid Phase Synthesis of Cyclic Peptides 1. *Loading of Linker onto 2-Cl-Trityl Resin.* 2-Cl-Trt resin (200 mg, 1.4 mequiv/g) was shaken with anhydrous CH_2Cl_2 (4 mL) in a fritted syringe for 30 min. Then the CH_2Cl_2 was removed, and a mixture of **3** (22 mg, 0.044 mmol) and DIPEA (68 μL, 0.4 mmol) in CH_2Cl_2 (2 mL) was added into the syringe, followed by shaking at room temperature for 12 h. The remaining reactive site was blocked with MeOH/DIPEA (9:1 v/v) for 30 min, and the beads were washed with CH_2Cl_2 3 times, MeOH, and then DMF 3 times.

Coupling with Amino Acids and Fmoc Deprotection. Fmoc protection groups were deprotected by treating the bead with 20% piperidine in DMF for 1 min, followed by the second treatment with 20% piperidine in DMF for 15 min. The beads were washed with DMF 6 times after the second treatment.

Coupling reactions with the first amino acids were carried out twice with 5 equiv of Fmoc amino acid, 5 equiv of HATU, and 10 equiv of NMM at 0.6 M concentration in DMF for 1 h. For the other coupling reactions, 3 equiv of Fmoc amino acid, 3 equiv of HBTU, and 6 equiv of DIPEA were used at 0.2 M concentration in DMF for 1 h at room temperature. The beads were washed with DMF 6 times after the coupling reaction, and a few beads were subjected to a chloranil test (for the first coupling reaction) or Kaiser test (for the other coupling reactions) to confirm the completion of the coupling reaction.

Methyl Ester Hydrolysis. After the last Fmoc deprotection step, the resin was washed with DMF 3 times, MeOH 2 times, and THF 3 times. A mixture of THF/0.5 M LiOH aqueous solution (5:1) and 3 equiv of ^{n}Bu$_4$NBr was added to the resin, and the mixture was shaken at room temperature for 1 h. The beads were washed with THF 3 times, MeOH 2 times, and DMF 3 times. The materials on a small sample of beads were cleaved with the method described in Cleavage From Solid Support Method 1 and analyzed by reversed-phase HPLC for purity.

Cleavage from Solid Support Method 1. The peptide was cleaved off the bead by treating the beads with HFIP/CH_2Cl_2 (1:4 v/v) for 30 min at room temperature. After filtration, the solvents were removed under vacuum, and the crude material was dried under high vacuum to give the crude product. The crude material was analyzed by reversed-phase analytical HPLC for its purity.

Cleavage from Solid Support Method 2. The peptide was cleaved off the bead by treating the beads with TFA/CH_2Cl_2/Et_3SiH (75:20:5) for 1 h at room temperature. After filtration, the solvents were removed under vacuum and the crude material was dried under high vacuum to give the crude product. The crude material was analyzed by reversed-phase analytical HPLC for its purity.

On-Bead Cyclization. The deprotected linear peptide on resin was activated with 3 equiv of DCC, 3 equiv of HOAt, and 6 equiv of NMM at 0.06 M concentration in DMF at room temperature for 2 h to give the HOAt ester of the linear peptide. Then the beads were filtered and shaken with 6 equiv of NMM at 0.06 M concentration in DMF at room temperature for 48 h to enable the cyclization of the activated linear peptides. The activation−cyclization cycle was repeated, and then the material on the bead was cleaved with the method described in Cleavage From Solid Support Method 1 for protected cyclic peptides and Cleavage From Solid Support Method 2 for deprotected cyclic peptides and analyzed by reversed-phase HPLC for purity. The crude product was purified with reversed-phase prep-HPLC (10%−50% MeCN/water containing 0.1% TFA), and the fractions containing the product were lyophilized to give the pure product as white solids.

*1-((3S,6S,9S)-3-(4-Hydroxybenzyl)-6-(hydroxymethyl)-9-isopropyl-2,5,8,11-tetraoxo-2,3,4,5,6,7,8,9,10,11-decahydro-1H-benzo[k][1,4,7,10]tetraazacyclotridecin-13-yl)piperidine-4-carboxylic Acid (LLL-**1vsy**).* White amorphous solid, 10.7 mg, 45%; ^{1}H NMR (400 MHz, DMSO) δ 9.16 (s, 1H), 8.73 (d, J = 7.0 Hz, 1H), 8.44 (d, J = 5.8 Hz, 1H), 8.09 (d, J = 9.0 Hz, 1H), 7.15−6.92 (m, 5H), 6.63 (d, J = 8.4 Hz, 2H), 4.39−4.30 (m, 1H), 3.97−3.90 (m, 1H), 3.68−3.53 (m, 5H), 3.16−3.07 (m, 1H), 2.94−2.74 (m, 3H), 2.46−2.36 (m, 1H), 2.07−1.86 (m, 3H), 1.80−1.59 (m, 2H), 1.05 (d, J = 6.6 Hz, 3H), 0.93 (d, J = 6.6 Hz, 3H); ^{13}C NMR (101 MHz, DMSO) δ 176.3, 171.0, 170.9, 170.2, 169.1, 158.7, 156.0, 130.9, 129.4, 129.1, 127.3, 122.3, 118.8, 115.5, 115.3, 64.3, 61.2, 56.8, 55.3, 49.9, 49.3, 33.8, 28.6, 27.9, 20.8, 19.5; HRMS (ESI-TOF) m/z calcd for $C_{30}H_{38}N_5O_8$ $(M+H)^+$ 596.2720; found 596.2734.

*1-((3S,6R,9R)-9-(4-Hydroxybenzyl)-6-(hydroxymethyl)-3-isopropyl-2,5,8,11-tetraoxo-2,3,4,5,6,7,8,9,10,11-decahydro-1H-benzo[k][1,4,7,10]tetraazacyclotridecin-13-yl)piperidine-4-carboxylic Acid (DDL-**1ysv**).* White amorphous solid, 8.3 mg, 35%; ^{1}H NMR (400 MHz, DMSO) δ 9.04 (s, 1H), 8.85 (d, J = 4.9 Hz, 1H), 8.27 (d, J = 5.7 Hz, 1H), 8.14 (d, J = 9.0 Hz, 1H), 7.25 (d, J = 8.5 Hz, 1H), 7.13−7.00 (m, 3H), 6.78 (s, 1H), 6.70 (d, J = 8.4 Hz, 2H), 4.59−4.49 (m, 1H), 4.05−3.94 (m, 1H), 3.74−3.52 (m, 4H), 3.28 (dd, J = 10.0, 4.9 Hz, 1H), 2.93−2.86 (m, 2H), 2.86−2.73 (m, 2H), 2.45−2.40 (m, 1H), 2.07−1.86 (m, 3H), 1.77−1.59 (m, 2H), 1.02 (d, J = 6.7 Hz, 3H), 0.99 (d, J = 6.7 Hz, 3H); ^{13}C NMR (101 MHz, DMSO) δ 176.2, 172.0, 171.3, 169.7, 169.5, 158.7, 156.6, 130.5, 127.7, 127.0, 121.9, 118.8, 117.6, 115.5, 114.7, 63.1, 60.7, 59.7, 54.1, 49.4, 49.0, 35.3, 29.2, 27.7, 27.6, 19.8, 19.6; HRMS (ESI-TOF) m/z calcd for $C_{30}H_{38}N_5O_8$ $(M+H)^+$ 596.2720; found 596.2695.

*1-((3S,6R,9R)-3-Benzyl-9-(2-carboxyethyl)-6-methyl-2,5,8,11-tetraoxo-2,3,4,5,6,7,8,9,10,11-decahydro-1H-benzo[k][1,4,7,10]tetraazacyclotridecin-13-yl)piperidine-4-carboxylic Acid (DDL-**1eaf**).* White amorphous solid, 9.7 mg, 41%; ^{1}H NMR (400 MHz, DMSO) δ 9.23 (s, 1H), 8.99 (d, J = 6.0 Hz, 1H), 8.44 (d, J = 5.2 Hz, 1H), 8.11 (d, J = 9.7 Hz, 1H), 7.70 (d, J = 8.8 Hz, 1H), 7.37−7.15 (m, 5H), 7.10−7.05 (m, 2H), 4.53−4.46 (m, 1H), 4.28−4.16 (m, 1H), 4.03−3.94 (m, 1H), 3.67−3.59 (m, 2H), 3.05−2.94 (m, 2H), 2.86−2.77 (m, 2H), 2.47−2.35 (m, 3H), 2.07−1.77 (m, 4H), 1.77−1.60 (m, 2H), 1.05 (d, J = 6.6 Hz, 3H); ^{13}C NMR (101 MHz, DMSO) δ 176.3, 174.3, 172.3, 171.4, 169.9, 169.7, 138.4, 129.4, 128.7, 127.4, 126.9, 121.7, 119.4, 118.5, 115.3, 58.3, 57.4, 55.3, 49.2, 49.1, 47.9, 36.8, 30.8, 27.9, 25.5, 17.4; HRMS (ESI-TOF) m/z calcd for $C_{30}H_{36}N_5O_8$ $(M+H)^+$ 594.2564; found 594.2583.

*1-((3S,6S,9R)-9-Benzyl-3-(2-carboxyethyl)-6-methyl-2,5,8,11-tetraoxo-2,3,4,5,6,7,8,9,10,11-decahydro-1H-benzo[k][1,4,7,10]tetraazacyclotridecin-13-yl)piperidine-4-carboxylic Acid (DLL-**1fae**).* White amorphous solid, 9.3 mg, 39%; ^{1}H NMR (400 MHz, DMSO) δ 9.19 (d, J = 8.0 Hz, 1H), 9.07 (s, 1H), 8.44 (d, J = 7.2 Hz, 1H), 7.85 (d, J = 8.9 Hz, 1H), 7.69 (d, J = 9.3 Hz, 1H), 7.37−7.14 (m, 5H), 7.06−6.91 (m, 1H), 6.60 (d, J = 2.5 Hz, 1H), 4.51−4.37 (m, 1H), 4.36−4.29 (m, 1H), 4.17−4.09 (m, 1H), 3.58−3.50 (m, 2H), 3.13 (dd, J = 13.7, 5.6 Hz, 1H), 2.99 (dd, J = 13.2, 9.2 Hz, 1H), 2.80−2.70 (m, 2H), 2.46−2.39 (m, 1H), 2.31−2.25 (m, 2H), 2.15−2.01 (m, 1H), 1.95−1.79 (m, 3H), 1.72−1.58 (m, 2H), 1.27 (d, J = 8.0 Hz, 3H); ^{13}C NMR (101 MHz, DMSO) δ 176.3, 174.3, 172.3, 170.2, 169.8, 169.4, 139.0, 129.9, 128.6, 126.7, 126.1, 123.0, 122.7, 118.3, 114.5, 62.2, 56.1, 55.5, 54.0, 50.7, 48.6, 34.9, 30.7, 27.8, 26.3, 17.7; HRMS (ESI-TOF) m/z calcd for $C_{30}H_{35}N_5O_8Na$ $(M+Na)^+$ 616.2383; found 616.2367.

*1-((3S,6S,9S)-3-(((Acetamidomethyl)thio)methyl)-9-methyl-2,5,8,11-tetraoxo-6-(3-(3-((2,2,4,6,7-pentamethyl-2,3-dihydrobenzofuran-5-yl)sulfonyl)guanidino)propyl)-2,3,4,5,6,7,8,9,10,11-decahydro-1H-benzo[k][1,4,7,10]tetraazacyclotridecin-13-yl)piperidine-4-carboxylic Acid (LLD-**1ar′c′**).* White amorphous solid, 11.1 mg, 31%; ^{1}H NMR (400 MHz, DMSO) δ 9.35 (s, 1H), 8.99 (d, J = 5.2 Hz, 1H), 8.58−8.51 (m, 2H), 8.10 (d, J = 8.9 Hz, 1H), 7.47 (d, J = 8.7 Hz, 1H), 7.13−7.07 (m, 2H), 6.88−6.30 (m, 4H), 4.48−4.40 (m, 1H), 4.31−4.18 (m, 2H),

DOI: 10.1021/acs.joc.6b01475
J. Org. Chem. 2016, 81, 8077−8081

4.18−4.08 (m, 1H), 4.01−3.95 (m, 1H), 3.10−3.01 (m, 2H), 2.99−2.91 (m, 4H), 2.82 (t, J = 11.2 Hz, 2H), 2.48 (s, 3H), 2.43 (s, 3H), 2.02 (s, 3H), 1.97−1.88 (m, 3H), 1.86−1.78 (m, 4H), 1.73−1.65 (m, 2H), 1.61−1.39 (m, 10H), 1.36 (d, J = 7.3 Hz, 3H); ^{13}C NMR (101 MHz, DMSO) δ 176.2, 173.4, 172.2, 169.9, 169.5, 168.9, 158.8, 157.9, 156.5, 137.7, 131.9, 127.1, 124.8, 121.9, 118.8, 116.7, 115.5, 86.8, 57.1, 53.8, 52.3, 49.4, 49.2, 42.9, 41.3, 31.8, 29.4, 28.8, 27.8, 25.9, 23.0, 19.4, 18.0, 16.2, 12.7; HRMS (ESI-TOF) m/z calcd for $C_{41}H_{58}N_9O_{10}S_2$ $(M + H)^+$ 900.3748; found 900.3719.

*1-((3R,6R,9R)-3-(((Acetamidomethyl)thio)methyl)-6-(3-(tert-butoxy)-3-oxopropyl)-2,5,8,11-tetraoxo-9-((1-trityl-1H-imidazol-4-yl)methyl)-2,3,4,5,6,7,8,9,10,11-decahydro-1H-benzo[k][1,4,7,10]tetraazacyclotridecin-13-yl)piperidine-4-carboxylic aAcid (DDL-**1h′e′c′**).* White amorphous solid, 11.4 mg, 29%; ^{1}H NMR (400 MHz, DMSO) δ 9.18 (s, 1H), 8.96 (d, J = 5.6 Hz, 1H), 8.80 (s, 1H), 8.73 (d, J = 5.1 Hz, 1H), 8.52 (t, J = 6.2 Hz, 1H), 8.08 (d, J = 9.1 Hz, 1H), 7.63 (d, J = 8.6 Hz, 1H), 7.51−7.39 (m, 9H), 7.34−6.95 (m, 9H), 4.49−4.40 (m, 1H), 4.39−4.33 (m, 1H), 4.28−4.19 (m, 3H), 3.59−3.49 (m, 2H), 3.20−3.11 (m, 2H), 3.03−2.92 (m, 2H), 2.81−2.69 (m, 2H), 2.43−2.32 (m, 1H), 2.11−2.01 (m, 2H), 1.93−1.75 (m, 5H), 1.77−1.55 (m, 4H), 1.35 (s, 9H); ^{13}C NMR (101 MHz, DMSO) δ 176.2, 171.9, 171.6, 170.9, 169.9, 169.5, 168.8, 158.7, 158.4, 148.2, 140.7, 137.3, 129.8, 129.2, 129.1, 128.2, 128.0, 127.1, 121.8, 118.5, 115.2, 80.1, 77.9, 57.0, 56.8, 52.1, 49.0, 48.9, 41.3, 31.6, 28.2, 28.0, 27.0, 23.0; HRMS (ESI-TOF) m/z calcd for $C_{53}H_{61}N_8O_9S$ $(M + H)^+$ 985.4282; found 985.4306.

A tetramethylguanidine side-product was formed when 3.0 equiv of HATU were used as the coupling reagent. The side-product was cleaved from the bead with Cleavage From Solid Support Method 2.

1-(3-Carboxy-4-((5S,8S,11S)-3-(Dimethylamino)-11-(4-hydroxybenzyl)-8-(hydroxymethyl)-5-isopropyl-2-methyl-6,9-dioxo-2,4,7,10-tetraazadodec-3-en-12-amido)phenyl)piperidine-4-carboxylic Acid. ^{1}H NMR (400 MHz, DMSO) δ 10.90 (s, 1H), 9.15 (s, 1H), 8.39 (d, J = 7.4 Hz, 1H), 8.32 (d, J = 8.0 Hz, 1H), 8.25 (d, J = 9.1 Hz, 1H), 7.45 (d, J = 2.92 Hz, 1H), 7.40 (d, J = 7.2 Hz, 1H), 7.24 (dd, J = 9.2, 3.0 Hz, 1H), 7.04−6.98 (m, 2H), 6.64−6.59 (m, 2H), 4.54−4.29 (m, 2H), 3.89−3.83 (m, 1H), 3.71−3.62 (m, 1H), 3.61−3.53 (m, 3H), 3.04−2.67 (m, 16H), 2.44−2.36 (m, 1H), 2.08−2.00 (m, 1H), 1.96−1.88 (m, 2H), 1.71−1.60 (m, 2H), 0.97 (d, J = 6.8 Hz, 3H), 0.89 (d, J = 6.8 Hz, 3H); ^{13}C NMR (101 MHz, DMSO) δ 176.3, 170.3, 170.2, 169.6, 161.9, 156.3, 147.0, 132.5, 130.4, 130.3, 127.9, 122.4, 122.0, 118.6, 117.5, 115.5, 63.6, 62.0, 56.7, 55.2, 48.8, 36.8, 31.3, 31.0, 28.0, 19.2, 18.9; HRMS (ESI-TOF) m/z calcd for $C_{35}H_{50}N_7O_9$ $(M + H)^+$ 712.3670; found 712.3647.

■ ASSOCIATED CONTENT

Supporting Information

The Supporting Information is available free of charge on the ACS Publications website at DOI: 10.1021/acs.joc.6b01475.

Copies of ^{1}H NMR, ^{13}C NMR, and HPLCs for selected intermediate and all final compounds **1**; conditions tried for the optimization of methyl ester hydrolysis and on-bead cyclization (PDF)

■ AUTHOR INFORMATION

Corresponding Author

*E-mail: burgess@tamu.edu.

Notes

The authors declare no competing financial interest.

■ ACKNOWLEDGMENTS

Financial support for this project was provided by The Robert A. Welch Foundation (A-1121), DoD BCRP Breakthrough Award (BC141561), The National Science Foundation (1608009) and CPRIT (RP150559). The NMR instrumentation at Texas A&M University was supported by a grant from the National Science Foundation (DBI-9970232) and the Texas A&M University System. KYW acknowledges the support from the Innovation and Technology Commission and the Hong Kong Polytechnic University. JY acknowledges the support from the Research Committee of the Hong Kong Polytechnic University for a travelling grant to the United States.

■ REFERENCES

(1) Sasson, Y., Neumann, R., Eds. *Handbook of Phase Transfer Catalysis*; Blackie Academic and Professional: 1997.

(2) Starks, C. M., Liotta, C. L., Halpern, M., Eds. *Phase-Transfer Catalysis: Fundamentals, Applications, and Industrial Perspectives*; Springer-Science: 1994.

(3) Xin, D.; Burgess, K. *Org. Biomol. Chem.* **2016**, *14*, 5049.

(4) Rudolph, J.; Esler, W. P.; O'Connor, S.; Coish, P. D. G.; Wickens, P. L.; Brands, M.; Bierer, D. E.; Bloomquist, B. T.; Bondar, G.; Chen, L.; Chuang, C.-Y.; Claus, T. H.; Fathi, Z.; Fu, W.; Khire, U. R.; Kristie, J. A.; Liu, X.-G.; Lowe, D. B.; McClure, A. C.; Michels, M.; Ortiz, A. A.; Ramsden, P. D.; Schoenleber, R. W.; Shelekhin, T. E.; Vakalopoulos, A.; Tang, W.; Wang, L.; Yi, L.; Gardell, S. J.; Livingston, J. N.; Sweet, L. J.; Bullock, W. H. *J. Med. Chem.* **2007**, *50*, 5202−5216.

(5) Fields, G. B.; Noble, R. L. *Int. J. Pept. Protein Res.* **1990**, *35*, 161−214.

(6) Atherton, E.; Sheppard, R. C. *Solid Phase Peptide Synthesis, A Practical Approach*; IRL Press: Oxford, 1989.

(7) Alsina, J.; Rabanal, F.; Chiva, C.; Giralt, E.; Albericio, F. *Tetrahedron* **1998**, *54*, 10125−10152.

(8) Mazur, S.; Jayalekshmy, P. *J. Am. Chem. Soc.* **1979**, *101*, 677−683.

(9) Johansson, P.-O.; Chen, Y.; Belfrage, A. K.; Blackman, M. J.; Kvarnstroem, I.; Jansson, K.; Vrang, L.; Hamelink, E.; Hallberg, A.; Rosenquist, A.; Samuelsson, B. *J. Med. Chem.* **2004**, *47*, 3353−3366.

(10) Carpino, L. A.; El-Faham, A. *J. Org. Chem.* **1994**, *59*, 695−698.

(11) Carpino, L. A.; Imazumi, H.; El-Faham, A.; Ferrer, F. J.; Zhang, C.; Lee, Y.; Foxman, B. M.; Henklein, P.; Hanay, C.; Mügge, C.; Wenschuh, H.; Klose, J.; Beyermann, M.; Bienert, M. *Angew. Chem., Int. Ed.* **2002**, *41*, 441−445.

(12) Bollhagen, R.; Schmiedberger, M.; Barlos, K.; Grell, E. *J. Chem. Soc., Chem. Commun.* **1994**, 2559−2560.

(13) Lee, C. E.; Kick, E. K.; Ellman, J. A. *J. Am. Chem. Soc.* **1998**, *120*, 9735−9747.

(14) Estep, K. G.; Neipp, C. E.; Stramiello, L. M. S.; Adam, M. D.; Robinson, S.; Roskamp, E. J. *J. Org. Chem.* **1998**, *63*, 5300−5301.

(15) Kulkarni, B. A.; Ganesan, A. *Tetrahedron Lett.* **1999**, *40*, 5633−5636.

(16) Kulkarni, B. A.; Ganesan, A. *Tetrahedron Lett.* **1998**, *39*, 4369−4372.

(17) Cosstick, R.; Vyle, J. S. *Tetrahedron Lett.* **1989**, *30*, 4693−4696.

(18) Scheuerman, R. A.; Tumelty, D. *Tetrahedron Lett.* **2000**, *41*, 6531−6535.

DOI: 10.1021/acs.joc.6b01475
J. Org. Chem. 2016, 81, 8077−8081